

**NANO-PARTICLES MODIFIED GLASSY CARBON  
ELECTRODES IN THE TRACE DETECTION OF ARSENIC AND  
SOME MICROPOLLUTANTS**

**A THESIS SUBMITTED IN PARTIAL FULFILLMENT OF THE  
REQUIREMENTS FOR THE DEGREE OF DOCTOR OF  
PHILOSOPHY**

**J. LALMALSAWMI**

MZU REGISTRATION NUMBER : 3992 OF 2009-10

PH.D REGISTRATION NUMBER : MZU/PH.D/846 OF 21.04.2016



**DEPARTMENT OF CHEMISTRY  
SCHOOL OF PHYSICAL SCIENCES  
SEPTEMBER, 2021**

**NANO-PARTICLES MODIFIED GLASSY CARBON ELECTRODES IN THE  
TRACE DETECTION OF ARSENIC AND SOME  
MICROPOLLUTANTS**

**BY**

**J. LALMALSAWMI**

**Department of Chemistry**

**Under the supervision of**

**Prof. Diwakar Tiwari**

**Submitted**

**In partial fulfillment of the requirement of the Degree of Doctor of Philosophy  
in Chemistry of Mizoram University, Aizawl.**



**MIZORAM UNIVERSITY**  
**Department of Chemistry**  
(A DST-FIST Supported Department)  
Tanhril, Aizawl, Mizoram. PIN: 796004

---

*Prof. Diwakar Tiwari, Dean (SPS)*

**Thesis Certificate**

This is hereby certified that the research work for the dissertation entitled “*Nano-Particles Modified Glassy Carbon Electrodes in the Trace Detection of Arsenic and Some Micropollutants*” submitted by **J. Lalmalsawmi** to Mizoram University, Tanhril, Aizawl, for the award of the Degree of Doctor of Philosophy in Chemistry is *bona fide* record of the research work carried by under my supervision. The contents of this dissertation, in full or in parts, have not been submitted to any other Institute or University for the award of any degree or diploma.

Tanhril, Aizawl  
Date : 30.09.2021

(DIWAKAR TIWARI)  
Supervisor

**Declaration**  
**Mizoram University**  
**September, 2021**

I, J. Lalmalsawmi, hereby declare that the subject matter of this thesis is the record of work done by me, that the contents of this thesis did not form the basis of the award of any previous degree to me or to the best of my knowledge to anybody else, and that the thesis has not been submitted by me for any research degree in any other University/Institute.

This is being submitted to the Mizoram University for the degree of Doctor of Philosophy in Chemistry.

(J.LALMALSAWMI)  
Candidate

(Prof. MUTHUKUMARAN, R.)  
Head

(Prof. DIWAKAR TIWARI)  
Supervisor



## ACKNOWLEDGEMENT

First of all, I thank Almighty God for blessing me with health, strength, and knowledge to accomplish this work. Without his grace and mercy, this work would not have been possible.

It gives me great pleasure to express my heartfelt appreciation to my mentor and supervisor, *Prof. Diwakar Tiwari*, Department of Chemistry, Mizoram University. His dedication, genuine interest, and, most of all, his overwhelming attitude to assist his students had been solely responsible for the completion of my work. He is always ready to provide a fresh perspective and scholarly advice during my entire tenure. I admire his timely advice, scrutiny, and scientific approach, which have greatly aided me in completing this work.

I sincerely thank and give respect to *Prof. Muthukumaran, R.*, Head, Department of Chemistry, MZU, and other faculty members viz., *Dr. Zodinpuia Pachuau*, *Dr. N. Mohondas Singh*, *Dr. Ved Prakash Singh*, and *Dr. A. Bimolini Devi*, for their constant encouragement and useful advice they have offered me throughout my academic career in the University.

My heartfelt thanks go to *Dr. Lalhmunsiamia* for his incentive and helpful suggestions in completing my research works.

I am grateful for the close cooperation and support I received from all of my colleagues in the Department of Chemistry. I'd like to thank *Mr. R. Malsawmdawgnzela*, *Ms. Ngainunsiami*, *Mr. CVL Hmingmawia*, *Mr. Levia Lalthazuala*, *Mr. Ricky Lalawmpuia*, *Mr. Sarikokba*, and *Mr. Himangshu Dihingia* for assisting me with my laboratory work, as well as for the transportation they provided

me both inside and outside of campus, which I can't forget to mention. I owe a deep sense of gratitude to the assistance of *Mr. Brojendro Singh Shagolsem*, Sr. Laboratory Technician, and *Mr. John Vanlalhraia*, Technical Assistant, Chemistry Department.

It is my privilege to thank my parents and all of my family members for their love and support during my tenure for the degree, as well as their comforts and prayers; I can't repay them entirely, but I thank and appreciate them from the bottom of my heart.

(J. LALMALSAWMI)

## **CONTENTS**

Title of the Thesis

Certificate

Declaration of the Candidate

Acknowledgements

Table of Contents

List of Figures

List of Tables

## **CHAPTER 1**

<b>1. INTRODUCTION</b>	<b>1</b>
<b>1.1. BACKGROUND</b>	<b>1</b>
<b>1.2. FATE AND TOXICITY OF POLLUTANTS</b>	<b>4</b>
1.2.1. Arsenic	5
1.2.2. Lead	6
1.2.3. Cadmium	8
1.2.4. Sulfamethoxazole	10
1.2.5. Sulfamethazine	12
<b>1.3. REVIEW OF LITERATURE</b>	<b>14</b>
<b>1.4. SCOPE OF PRESENT INVESTIGATION</b>	<b>23</b>

## **CHAPTER 2**

<b>2. METHODOLOGY</b>	25
<b>2.1. CLAY SAMPLE AND REAL WATER SAMPLES</b>	25
<b>2.2. CHEMICALS AND APPARATUS</b>	26
<b>2.3. INSTRUMENTS</b>	30
<b>2.4. ELECTROCHEMICAL TECHNIQUES</b>	31
2.4.1. Electrochemical impedance spectroscopy	31
2.4.2. Cyclic voltammetry and linear sweep voltammetry	33
2.4.3. Differential pulse voltammetry	34
<b>2.5. PREPARATION OF MATERIALS</b>	35
2.5.1. Leaf extract of <i>Persea americana</i>	35
2.5.2. Phytochemical screening	35
2.5.3. Synthesis of nanoparticles	37
2.5.4. Synthesis of nanocomposite materials	37
<b>2.6. CHARACTERIZATION OF MATERIALS</b>	38
<b>2.7. FABRICATION OF MODIFIED ELECTRODES</b>	39
<b>2.8. ELECTROCHEMICAL PROCEDURES</b>	40
2.8.1. Electrochemical characterization of electrodes	40
2.8.2. Electrochemical detection of pollutants	41

## CHAPTER 3

<b>3. RESULTS AND DISCUSSION</b>	42
<b>3.1. CHARACTERIZATION OF MATERIALS</b>	42
3.1.1. Phytochemical studies of <i>Persea americana</i> leaf extract	42
3.1.2. UV-Vis spectroscopic analysis of nanoparticles	43
3.1.3. Fourier transform infra-red (FT-IR) spectroscopy	45
3.1.4. Surface morphological studies of materials	47
<b>3.2. ELECTROCHEMICAL STUDIES USING CARBON PASTE ELECTRODES</b>	54
3.2.1. Scan rate studies using cyclic voltammetry	54
3.2.2. Electrochemical impedance spectroscopic (EIS) studies	59
<b>3.3. ELECTROCHEMICAL DETECTION OF As(III)</b>	61
3.3.1. Cyclic voltametric studies of As(III)	61
3.3.2. pH dependence studies on detection of As(III)	63
3.3.3. Concentration studies and calibration of As(III) detection	65
3.3.4. Effect of co-existing ions	68
3.3.5. Studies in real water sample	69
3.3.6. Conclusion	73
<b>3.4. ELECTROCHEMICAL STUDIES USING GLASSY CARBON ELECTRODES</b>	74
3.4.1. Scan rate studies with cyclic voltammetry	74
3.4.2. Electrochemical impedance spectroscopic (EIS) studies	80

<b>3.5 ELECTROCHEMICAL DETECTION OF Pb(II)</b>	82
3.5.1. Electrochemical studies of Pb(II) using cyclic voltammetry	82
3.5.2. pH dependence studies on detection of Pb(II)	84
3.5.3. Electroanalytical performance of modified electrode for Pb(II)	86
3.5.4. Optimization of electrochemical parameters	87
3.2.4. Concentration dependence studies and calibration	90
3.2.5. Effect of co-existing ions	94
3.2.6. Studies in real water samples	95
3.2.7. Conclusion	100
<b>3.6. SINGLE AND SIMULTANEOUS ELECTROCHEMICAL DETECTION OF Cd(II) AND Pb(II)</b>	101
3.6.1. Electrochemical studies of Cd(II) and Pb(II) using cyclic voltammetry	101
3.6.2. pH dependence studies on detection of Cd(II) and Pb(II)	103
3.6.3. Electroanalytical performance of modified electrode for Cd(II) and Pb(II)	106
3.6.4. Optimization of electrochemical parameters	107
3.6.5. Concentration dependence studies and calibration for single species	109
3.6.6. Concentration studies and calibration for simultaneous detection	113
3.6.7. Effect of co-existing ions	117
3.6.8. Studies on real water sample	119
3.6.9. Conclusion	123

<b>3.7. ELECTROCHEMICAL DETECTION OF SULFAMETHOXAZOLE</b>	<b>124</b>
3.7.1. Electrochemical studies of sulfamethoxazole using cyclic voltammetry	124
3.7.2. Electroanalytical performance of modified electrodes for sulfamethoxazole	126
3.7.3. pH dependence studies on detection of sulfamethoxazole	126
3.7.4. Optimization of electrochemical parameters	130
3.7.5. Concentration dependence studies and calibration	132
3.7.6. Effect of co-existing ions	137
3.7.7. Studies in real water samples	139
3.7.8. Conclusion	143
 <b>3.8. ELECTROCHEMICAL DETECTION OF SULFAMETHAZINE</b>	 <b>144</b>
3.8.1. Electrochemical studies of sulfamethazine using cyclic voltammetry	144
3.8.2. Electroanalytical performance of modified electrodes for sulfamethazine	145
3.8.3. pH dependence studies on detection of sulfamethazine	146
3.8.4. Optimization of electrochemical parameters	149
3.8.5. Concentration dependence studies and calibration	151
3.8.6. Effect of co-existing ions	156
3.8.7. Studies in real water samples	157
3.8.8. Conclusion	161

## **CHAPTER 4**

<b>4. CONCLUSIONS</b>	162
-----------------------	-----

<b>REFERENCES</b>	169
-------------------	-----

### **BRIEF BIODATA OF THE CANDIDATE**

### **PARTICULARS OF THE CANDIDATE**

### **LIST OF PUBLICATIONS**

### **PUBLISHED JOURNAL PAPERS**

### **LIST OF FIGURES**

<b>Figure</b>	<b>Page No.</b>
<b>1.1.</b> Structure of Sulfamethoxazole	10
<b>1.2.</b> Structure of Sulfamethazine	12
<b>2.1.</b> Nyquist impedance plot for an electrochemical system. Regions of mass-transfer and kinetic control are found at low and high frequencies, respectively.	33
<b>3.1.</b> UV-Vis spectra of (a) Ag precursor solution, <i>Persea americana</i> leaf extract and Ag nanoparticle solution (2.0 mmol/L); and (b) Au nanoparticle solution, <i>Persea Americana</i> leaf extract and Au <sup>3+</sup> precursor solutions (2.0 mmol/L) [Inset: Colloidal solution of gold nanoparticles].	44
<b>3.2.</b> FT-IR spectra of pristine bentonite and nanocomposite materials (TCBN, Ag(NP)/TCBN and Au(NP)/TCBN).	46
<b>3.3.</b> Scanning electron micrographs (SEM) of (a & b) bare glassy carbon sheet;	48



(c) pristine bentonite coated glassy carbon sheet; (d) silane grafted bentonite (TCBN) coated glassy carbon sheet; (e) Ag(NP)/TCBN coated glassy carbon sheet; and (f) Au(NP)/TCBN coated glassy carbon sheet.	
<b>3.4.</b> EDX elemental mapping for the (a) pristine bentonite (BN); (b) TCBN Composite; (c) Ag(NP)/TCBN; and (d) Au(NP)/TCBN coated glassy carbon sheets.	50
<b>3.5.</b> TEM micrographs of (a) Ag(NP)/TCBN; and (b) Au(NP)/TCBN materials and the d-spacings of (c) Ag(NP)/TCBN; and (d) Au(NP)/TCBN materials.	51
<b>3.6.</b> 3D-AFM images of (a) Ag(NP)/TCBN; (b) Au(NP)/TCBN coated carbon sheets and surface roughness of (c) Ag(NP)/TCBN; and (d) Au(NP)/TCBN coated carbon sheets.	53
<b>3.7.</b> Effect of potential and scan rates on the redox behavior of 0.001 mol/L $\text{Fe}(\text{CN})_6^{3-}/\text{Fe}(\text{CN})_6^{4-}$ using (a) CPE; (b) BN/CPE; and (c) TCBN/CPE working electrodes.	55
<b>3.8.</b> Linear plots of $v^{1/2}$ against oxidative peak current ( $I_p$ ) of 0.001 mol/L $\text{Fe}(\text{CN})_6^{3-}/\text{Fe}(\text{CN})_6^{4-}$ obtained using various carbon paste electrodes.	58
<b>3.9.</b> EIS Nyquist plots (circles) obtained for the $\text{Fe}(\text{CN})_6^{3-}/\text{Fe}(\text{CN})_6^{4-}$ (0.1 mol/L KCl solution) and the fitted line for equivalent circuit (Continuous line) obtained with (a) bare CPE; and (b) TCBN/CPE [Inset: Fitted equivalent circuit].	60
<b>3.10.</b> Cyclic voltammograms of As(III) (30.0 $\mu\text{g/L}$ ) in 0.1 mol/L KCl (pH 2.0) background electrolytes employing the CPE, BN/CPE, and TCBN/CPE.	63
<b>3.11.</b> Cyclic voltammograms of 30.0 $\mu\text{g/L}$ As(III) (0.1 mol/L KCl) as a	64

function of solution pH (2.0 to 9.0) employing the TCBN/CPE.

**3.12.** (a) LSV voltammograms of arsenic (III) at different concentrations 66  
of As(III) (0.5 to 20.0  $\mu\text{g/L}$ ) using the 0.1 mol/L KCl (pH 2.0) and  
employing the TCBN/CPE; and (b) Calibration plot of peak current ( $I_p$ ) vs  
concentration of As(III).

**3.13.** Effect of various co-existing ions (150.0  $\mu\text{g/L}$ ) in the detection of 28.2 69  
 $\mu\text{g/L}$  As(III) in 0.1 mol/L KCl (pH 2.0) background electrolyte.

**3.14.** (a) LSV voltammograms of river water samples as spiked with 72  
various concentrations of As(III) (0.5 to 15.0  $\mu\text{g/L}$ ) at pH 2.0 in 0.1 mol/L KCl  
background electrolyte; and (b) Calibration plot of obtained between the peak  
current ( $I_p$ ) vs concentration of As(III).

**3.15 (a-e).** Effect of potential scan rate on the redox behavior of 0.001 mol/L 75  
 $\text{Fe}(\text{CN})_6^{3-}/\text{Fe}(\text{CN})_6^{4-}$  (0.1 mol/L KCl solution; pH 6.1) at (a) GCE;  
(b) BN/GCE; (c) TCBN/GCE; (d) Ag(NP)/TCBN/GCE; and  
(e) Au(NP)/TCBN/GCE working electrodes.

**3.16.** Linear plots of  $v^{1/2}$  against oxidative peak current ( $I_p$ ) obtained for the 79  
0.001 mol/L  $\text{Fe}(\text{CN})_6^{3-}/\text{Fe}(\text{CN})_6^{4-}$  (in 0.1 mol/L KCl solution; pH 6.1) using  
bare glassy carbon electrode and various fabricated glassy carbon electrodes.

**3.17.** EIS Nyquist plots (circles) obtained for the  $\text{Fe}(\text{CN})_6^{3-}/\text{Fe}(\text{CN})_6^{4-}$  81  
(0.1 mol/L KCl solution) and the fitted line for equivalent circuit  
(continuous line) obtained with (a) bare GCE and (b) BN/GCE  
(c) TCBN/GCE (d) Ag(NP)TCBN/GCE and (e) Au(NP)TCBN/GCE  
[Inset: Fitted equivalent circuit].

<b>3.18.</b> Cyclic voltammograms of 5.0 mg/L Pb(II) in acetate buffer (pH 4.0) using the bare GCE, BN/GCE, TCBN/GCE and Au(NP)/TCBN/ GCE at scan rate 100 mV/s.	84
<b>3.19.</b> Cyclic voltammograms of 1.0 mg/L Pb(II) (in 0.1 mol/L Acetate buffer) at varying pH of 3.6 to 7.0 using scate rate 100 mV/s.	85
<b>3.20.</b> pH dependence of oxidative peak current ( $I_p$ ) of 1.0 mg/L Pb(II) at Au(NP)/TCBN/GCE .	86
<b>3.21 (a-b).</b> Effects of (a) deposition potential; and (b) deposition time for the anodic peak current for the Au(NP)/TCBN/GCE in 0.1 mol/L acetate buffer, 50.0 $\mu\text{g/L}$ Pb(II) solution (Other conditions: pH = 4.0, pulse amplitude = 50 mV, frequency = 10 Hz, pulse increment = 10 mV).	89
<b>3.22 (a-b).</b> (a) DPASV voltammograms recorded with Au(NP)/TCBN/GCE (vs. Ag/AgCl) at increasing Pb(II) concentrations at a range of 1.0-60.0 $\mu\text{g/L}$ . (pH = 4.0 acetate buffer, deposition potential = -1.0 V, accumulation time = 180 s, pulse amplitude = 50 mV, frequency = 10 Hz, pulse increment = 10 mV) (b) Calibration line for anodic peak current ( $I_p$ ) vs Pb(II) concentration.	92
<b>3.23.</b> Bar graph for the DPASV current signal of 30.0 $\mu\text{g/L}$ Pb(II) at Au(NP)/TCBN/GCE in the presence of 300.0 $\mu\text{g/L}$ other co-existing cations (pH = 4.0 acetate buffer, deposition potential = -1.0 V, accumulation time = 180 s, pulse amplitude = 50 mV, frequency = 10 Hz, pulse increment = 10 mV).	95
<b>3.24.</b> DPASV for (a) river and (b) spring water samples spiked with 5.0,	98

10.0 and 15.0  $\mu\text{g/L}$  Pb(II) (pH = 4.0 acetate buffer, deposition potential = -1.0 V, accumulation time = 180 s, pulse amplitude = 50 mV, frequency = 10 Hz, pulse increment = 10 mV).

**3.25 (a-b).** Cyclic voltammograms of 5.0 mg/L (a) Cd(II) and (b) Pb(II) 102

in 0.1 mol/L acetate buffer (pH 4.0) at bare GCE, BN/GCE, TCBN/GCE and Ag(NP)/TCBN/GCE electrodes at the scan rate 100 mV/s.

**3.26 (a-d).** Effect of pH on cyclic voltammograms of 1.0 mg/L (0.1 mol/L 104

acetate buffer) (a) Cd(II); and (b) Pb(II) and change in intensity of oxidative peak currents of (c) Cd(II); and (d) Pb(II) as a function of pH .

**3.27 (a-b).** Effect of (a) accumulation potential; and (b) deposition/ 109

accumulation time on anodic peak current for 50.0  $\mu\text{g/L}$  Cd(II) and Pb(II) in 0.1 mol/L acetate buffer (pH 4.5) (Other conditions: pulse amplitude = 50 mV, pulse increment = 10 mV and pulse width = 50 ms).

**3.28.** DPASV curves obtained for (a) Cd(II) ; and (b) Pb(II) using the 111

Ag(NP)/TCBN/GCE electrode (Acetate buffer: 0.1 mol/L; pH: 4.5);

Calibration curves obtained for (c) Cd(II); and (d) Pb(II) detection

[Other conditions: pulse amplitude = 50 mV, pulse increment = 10 mV and pulse width = 50 ms).

**3.29 (a-b).** (a) DPASV for simultaneous detection of Cd(II) and Pb(II) 115

at 5.0-60.0  $\mu\text{g/L}$  concentration range (b) Calibration plot of Cd(II) and

Pb(II) (Other conditions: pulse amplitude = 50 mV, pulse increment = 10 mV and pulse width = 50 ms).

**3.30.** Effect of various interfering ions on the detection of 50.0  $\mu\text{g/L}$  of 119

Cd(II) and Pb(II) using the DPASV measurements at pH 4.5 (0.1 mol/L acetate buffer) in the absence and presence of 500.0 µg/L of each co-existing ion ((Hg(II), Zn(II), Ca(II), Cu(II), Fe(II) and Mn(II)).

**3.31.** DPASV graphs obtained for various concentrations of Cd(II) and Pb(II) in real water sample (spring) using Ag(NP)/TCBN/GCE electrode. 121

**3.32.** Cyclic voltammograms of 50.0 mg/L SMX using the bare glassy carbon electrode and various fabricated glassy carbon electrodes [Background electrolytes: 0.1 mol/L KCl, Acetate buffer: pH 4.0]. 125

**3.33.** Distribution of various species of SMX as a function of pH. 127

**3.34 (a-c).** DPASV graphs of 20.0 mg/L SMZ at different pH values obtained with (a) Ag(NP)/TCBN/GCE; (b) Au(NP)/TCBN/GCE; and (c) Plots of peak current ( $I_p$ ) values as a function of pH. (Other conditions; pulse amplitude = 50 mV, pulse increment = 10 mV and pulse width = 50 ms). 128

**3.35 (a-b).** Plots of peak currents of 20.0 mg/L SMX (0.1 mol/L KCl in acetate buffer pH: 4.0) as a function of (a) deposition potentials (V); and (b) deposition times (s). (Other conditions: pulse amplitude = 50 mV, pulse increment = 10 mV and pulse width = 50 ms). 131

**3.36 (a-d).** DPASV of SMX solutions (0.25 to 30.00 mg/L) (Background electrolytes: 0.1 mol/L KCl (Acetate buffer; pH 4)) obtained at (a) Ag(NP)/TCBN/GCE; and (b) Au(NP)/TCBN/GCE. Calibration lines obtained between  $I_p$  vs Concentration of SMX at (c) Ag(NP)/TCBN/GCE; and (d) Au(NP)/TCBN/GCE (Other conditions: deposition potential = -1.2 V, deposition time = 210 s, pulse amplitude = 50 mV, pulse increment 134

= 10 mV and pulse width = 50 ms).

**3.37.** Effect of co-existing ions (1.0 mg/L) on peak current of 0.5 mg/L 138

SMX (Background electrolytes: 0.1 mol/L KCl (Acetate buffer; pH 4))

using Ag(NP)/TCBN/GCE and Au(NP)/TCBN/GCE (Other conditions:

deposition potential = -1.2 V, deposition time = 210 s, pulse amplitude

= 50 mV, pulse increment = 10 mV and pulse width = 50 ms).

**3.38.** Linear calibration curves obtained between peak current ( $I_p$ ) and 142

spiked SMX concentrations at Ag(NP)/TCBN/GCE and Au(NP)/TCBN/GCE

in a real water sample.

**3.39.** Cyclic voltammograms of 50.0 mg/L SMZ (in 0.1 mol/L KCl + Acetate 143

buffer, pH 4.0) at 100 mV/s obtained with GCE and modified GCEs.

**3.40.** Distribution graph of different species of SMZ as a function of pH. 147

**3.41.** DPASV graphs of 20.0 mg/L SMZ (0.1 mol/L KCl + acetate buffer 147

pH 4.0) at different pH values obtained with (a) Ag(NP)/TCBN/GCE;

(b) Au(NP)/TCBN/GCE; and (c) Plots of peak current ( $I_p$ ) values as a function

of pH (Other conditions: pulse amplitude = 50 mV, pulse increment = 10 mV

and pulse width = 50 ms).

**3.42 (a-b).** Optimization of accumulation step with change in (a) deposition 150

potential and (b) deposition time at Ag(NP)/TCBN/GCE and

(b) Au(NP)/TCBN/GCE in 20.0 mg/L SMZ (0.1 mol/L KCl + acetate buffer

pH 4.0). (Other conditions: pulse amplitude = 50 mV, pulse increment =

10 mV and pulse width = 50 ms).

**3.43 (a-d).** Differential pulse voltammograms of SMZ solutions (0.25 to 152

30.0 mg/L) (Background electrolytes: 0.1 mol/L KCl (Acetate buffer; pH 4.0) obtained at (a) Ag(NP)/TCBN/GCE; and (b) Au(NP)/TCBN/GCE. Calibration line obtained between  $I_p$  vs Concentration of sulfamethazine at (c) Ag(NP)/TCBN/GCE (d) Au(NP)/TCBN/GCE (Other conditions: deposition potential = -1.2 V, deposition time = 180 s, pulse amplitude = 50 mV, pulse increment = 10 mV and pulse width = 50 ms).

**3.44.** Effect of co-existing ions (1.00 mg/L) on peak current of 0.5 mg/L sulfamethazine using Ag(NP)/TCBN/GCE in 0.1 mol/L KCl + Acetate buffer; pH 4.0) (Other conditions: deposition time = 180 s, pulse amplitude = 50 mV, pulse increment = 10 mV and pulse width = 50 ms). 157

**3.45.** Linear calibration curves obtained between peak current ( $I_p$ ) and spiked SMZ concentration at Ag(NP)/TCBN/GCE and Au(NP)/TCBN/GCE in a real water sample. 160

## LIST OF TABLES

<b>Table</b>	<b>Page no.</b>
<b>2.1.</b> GPS locations of various water samples collected.	26
<b>2.2.</b> Details of various chemicals used for complete experimental works.	27
<b>3.1.</b> Qualitative phytochemical analysis of leaf extract of <i>Persea americana</i> leaves.	43
<b>3.2.</b> Calculated electroactive surface area of fabricated carbon paste electrodes.	58
<b>3.3.</b> EIS parameters estimated from the fitted electrical circuit model of the Nyquist plots of carbon paste working electrodes.	60
<b>3.4.</b> Comparison of LOD for As(III) detection obtained with previous reported materials.	67
<b>3.5.</b> Various physco-chemical parametric analyses of Tlawng river water	71
<b>3.6.</b> Calculated electroactive surface area of various fabricated glassy carbon electrodes.	79
<b>3.7.</b> EIS parameters estimated from the fitted electrical circuit model of the Nyquist plots of various glassy carbon working electrodes.	81
<b>3.8.</b> Electrochemical detection of Pb(II) using different electrode materials.	93
<b>3.9.</b> Stability and repeatability test for Au(NP)/TCBN/GCE electrode in the detection of 50.0 µg/L Pb(II) solution.	94
<b>3.10.</b> Analysis of water quality for different parameters.	97
<b>3.11.</b> Determination of Pb(II) in real water samples using Au(NP)/TCBN/GCE.	99



<b>3.12.</b> Comparison of the present work with other recent reports for simultaneous detection of Cd(II) and Pb(II) on the basis of LOD values.	116
<b>3.13.</b> Stability and repeatability tests using the Ag(NP)/TCBN/GCE in the detection of 50.0 µg/L Cd(II) and Pb(II) (Acetate buffer: 0.1 mol/L; pH: 4.5).	117
<b>3.14.</b> Analysis of water quality for different parameters.	120
<b>3.15.</b> Determination of Cd(II) and Pb(II) in spring water using DPASV technique.	122
<b>3.16.</b> Comparative table of various modified electrodes employed for SMX determination.	135
<b>3.17.</b> Stability and repeatability test for Ag(NP)/TCBN/GCE and Au(NP)/TCBN/GCE in 20.0 mg/L SMX solution (pH 4.0).	137
<b>3.18.</b> Analysis of water quality for different parameters.	139
<b>3.19.</b> Determination of SMX in real water samples using the Ag(NP)/TCBN/GCE and Au(NP)/TCBN/GCE [Background electrolytes: 0.1 mol/L KCl (Acetate buffer; pH 4.0)].	141
<b>3.20.</b> Comparison of present work with other modified electrodes employed for SMZ and other sulfonamide detection.	155
<b>3.21.</b> Stability and repeatability test for Ag(NP)/TCBN/GCE and Au(NP)/TCBN/GCE in 20.0 mg/L SMZ solution (pH 4.0).	156
<b>3.22.</b> Analysis of water quality for different parameters.	159
<b>3.23.</b> Determination of SMZ in real water sample.	160
<b>4.1.</b> Comparison of LOD values of various pollutants obtained with modified electrodes and MCL values given by WHO and US-EPA guidelines.	168

# **CHAPTER 1**

## **INTRODUCTION**

## **1. INTRODUCTION**

### **1.1. BACKGROUND**

Water is one of the most important resources, and its continuous exploitation to meet human needs for economic and social developments, as well as its crisis caused by climate change, has resulted in ever-increasing environmental impacts. The majority of human activities that utilize water generate wastewater. Therefore, as the global demand for water rises, so does the amount of wastewater produced and the pollution load simultaneously increased. Globally, the amount of wastewater produced and its overall pollution stockpile are rising primarily because of population growth, accelerated urban growth, and economic development. It is estimated that water consumption in industries alone accounts for 19% of total global water consumption (Ritchie and Roster, 2017). Water usage by industries in Europe and North America was 50% in 2009, compared to 4-12% in developing countries. This fraction is projected to increase by a factor of five in rapidly developing countries over the next 10-20 years (UNESCO, 2017). Water bodies like rivers, seas, lakes, ponds etc. faced serious environmental problems due to its multiple uses, including drinking, food, hydropower, navigation, irrigation, industries and recreation. Additionally, the municipal/industrial wastewater discharge with varying degrees of treatment poses additional pollutant load to the aquatic environment. Pollutants released into water bodies seemingly harm the marine life and make natural water supplies unsafe for drinking as well (Bhatnagar and Sillanpää, 2010). Untreated or partially treated wastewaters as originated from various sources flows back into natural water bodies. This led to approximately 1.8 billion people likely to drink feces-contaminated water, putting them at risk of contracting water-borne diseases like cholera, dysentery, typhoid, etc. (UN, 2011). More than 80% of the World's wastewater and more than 95% in some least developed countries wastewater is released into the environment as untreated (UNESCO, 2017).

Many manufacturing industries are responsible for contamination of various heavy metal toxic ions in water bodies. Although many heavy metals are reported to be essential at trace concentrations, however, an elevated amount of intake resulted a

negative effect on living organisms. Heavy metals such as cadmium, chromium, copper, lead, or metalloid arsenic, among others, are frequently found in industrial waste/effluent waters, posing a serious threat to the aquatic ecosystem and health risks to humans (Cui *et al.*, 2015). Wastes from metal plating, mining operations, tanneries, and other industrial effluents are particularly responsible for heavy metal pollution to water bodies (Ali *et al.*, 2019). The agricultural sector is also a big contributor to water pollution. An excessive uses of fertilizers in farmlands can also lead to the accumulation of various toxic chemicals, which eventually contaminating the soil and aquatic environment (Kokoszka *et al.*, 2021). Moreover, in recent years, there is a tremendous increase in the use of synthetic chemicals such as hormones, pharmaceuticals, and personal care products, which are known to be emerging water pollutants since these chemicals are very persistent and the municipal waste contains high levels of these pollutants. Many of the pharmaceuticals are used in animal husbandry, and the overexploitation of these chemicals, particularly the antibiotics lead to serious environmental impacts (Haller *et al.*, 2002).

The deleterious water quality around the globe is forcing the researchers to adopt the newer and advanced treatment technologies for reclamation of wastewater. The management of wastewater is inextricably linked to the availability of safe and sufficient water supplies. In most cities, wastewater is collected and treated, however, the treatment efficiency varies depending on the system used. It is known that most of the potential water pollutants are quite persistent and tend to escape from the conventional treatment plants and enter into the natural aquatic systems which may further enter back to the food chain (Liu *et al.*, 2018). Therefore, new challenges arise for proper waste treatments and proper monitoring of the water qualities. Initiatives to achieve this goal are emerging up around the globe, and a major challenge arises when it comes to partially or inadequately treated water for release or reuse (Ragab *et al.*, 2021). As a result, wastewater management systems that can enable reuse and reclamation of contaminated water is very crucial (Bouwer, 2000). Likewise, the detection and measurement of various water pollutants at lower levels in water bodies is indispensable, hence researchers have given great heed to the development of

simple, accurate, and ultra-sensitive techniques for analyzing water quality at various sources.

Various advanced and sophisticated techniques *viz.*, inductively coupled plasma mass spectrometry or optical emission spectrometry (ICP-MS/ OES) (Dai *et al.*, 2012; Luis *et al.*, 2015) high performance liquid chromatography (HPLC) (Teshima *et al.*, 2003), hydride generation atomic absorption spectrometry and emission spectrometry (HG-AAS/AES) (Zhu *et al.*, 2006; Pohl, 2009), neutron activation analysis (NAA) (Hung *et al.*, 2004), atomic fluorescence spectrometry (AFS) (Marschner *et al.*, 2016) etc. are found to be accurate and sensitive techniques for determination of heavy metals and various organic compounds at trace levels. However, these laboratory-based techniques are sophisticated in their instrumentation, expensive in operation, time-consuming, non-portable and required skilled personnel for proper operation. This restricts its wider implications in real and possible *on-site* applications (Bhanjana *et al.*, 2018; Xu *et al.*, 2020). Therefore, the attention is towards the development of handy, robust, accurate, easy to operate and most importantly miniaturized portable devices which could be utilized even at remote places. Many handy and user-friendly heavy metal testing kits are available, but the low permissible limit of the toxic heavy metals makes it difficult to utilize for reliable on-site low-level analysis (Melamed, 2005). Therefore, challenges are lying in the device development for efficient on-site detection. However, electrochemical techniques have drawn much attention for on-site detection due to its portability, sensitivity, cost effectiveness and easier handling (Ghoreishi *et al.*, 2012). Moreover, many recent reviews suggested that electrochemical methods are known to be the most promising methods for field applications/implications (Cavicchioli *et al.*, 2004; Liu and Huang, 2014; Mays and Hussam, 2009). The development of electrochemical sensing devices deals with the modification of electrodes with newer and advanced materials that are designed to acquire the desired selectivity and sensitivity for the target analyte. Hence, this area of research has received momentum during last couple of decades and introduced variety of novel materials which have shown enhanced sensitivity towards the target ions/or compounds, ranging from metal nanoparticles, nanocomposites, polymers to biological composites obtained from DNA, enzymes, proteins, chitosan etc. The

choice of materials in the fabrication of electrodes, optimization of the electrochemical methods and pre-treatment of water samples are major concerns that need to be studied adequately for ultimate device development. In this context, various reports have shown that incorporation of engineered materials to the electrode as a film and adopted the electrochemical stripping voltammetry as one of the most simple and effective procedures for low level detection of arsenic (Luong *et al.*, 2014). Moreover, the rapid advancement in nanotechnology with nanomaterials/nanocomposites helped to further progress the performance of sensors concerning the detection limit, reproducibility and selectivity of miniaturized device development.

## **1.2. FATE AND TOXICITY OF POLLUTANTS**

Heavy metal contamination of aquatic environment is steadily increasing as a result of fast-growing industrialization and urbanization. It is known that heavy metals are non-biodegradable and their gradual build-up in the water bodies cause many toxic effects to the living organisms. Not only the adverse and detrimental impacts on aquatic life, these contaminants are long persistence in biological systems, accumulation in the environment through the food chain and occupational dangers are known impacts to the environment. In addition to the heavy metal pollution, contamination of aquatic environments by micro-pollutants, particularly hormones, pharmaceuticals, and personal care products, has recently been identified as newer but serious environmental concerns and are referred as ‘emerging’ water pollutants. These are associated with high persistency, low biodegradability and toxicity to aquatic life. Further, these micro-pollutants are increased significantly in the wastewater treatment plant (WWTP) effluents, surface water, sewage water, ground water or in the drinking water system. Hence, these micro-pollutants are found problematic in aquatic ecosystem and potential threat to the human health. The sources, toxic effects and health risks of several heavy metal toxic ions and the micro-pollutants are briefly described in the following sections.

### 1.2.1. Arsenic

Arsenic is a ubiquitous metalloid widely distributed in air, soil, and water. Among the prominent heavy metal toxic ions, arsenic is one of the most toxic element, posing serious threats to the lives of millions of people worldwide (Tang *et al.*, 2014). Although natural sources like arsenopyrites, realgar, lollingites, etc. are mainly responsible for the contamination of the aquatic environment; however, the vital source in most places is due to the anthropogenic activities. Agriculture, mining, and some industrial activities are leading to the enhanced arsenic contamination (Sullivan *et al.*, 2021). Arsenic is widely used in several insecticides, pesticides, wood preservatives, paints, alloys, etc. (Luong *et al.*, 2014). The toxicological, physiological, and geochemical behavior of arsenic largely depends on the oxidation states and chemical nature of arsenic. Humans are exposed to arsenic by several means but mainly through inhalation, skin contact (penetration), and intake of arsenic contaminated waters (Liu and Wei, 2008). Drinking arsenic-contaminated groundwater has caused widespread health problems in several countries. Bangladesh, China, Taiwan, Chile, Argentina, India (mainly West Bengal), Mexico, and the United States of America are the countries that are greatly affected by arsenic contamination (Luong *et al.*, 2014). A rough estimate indicated that more than 100 million people are affected by arsenic poisoning (Cornejo *et al.*, 2008). The United States Environmental Protection Agency (US-EPA) and World Health Organization (WHO) recommend 10 µg/L as the maximum permissible level of arsenic in drinking water (Karim, 2000). However, the levels of arsenic in groundwaters of many places in Thailand, Taiwan, India (West Bengal), and Bangladesh is significantly high and observed to be higher than 50 µg/L in some places (Kumar *et al.*, 2016). In natural water, arsenic exists both as inorganic arsenic (arsenite ( $\text{H}_3\text{AsO}_3$ ) i.e., As(III) and ( $\text{H}_3\text{AsO}_4$ ) arsenate i.e., As(V)) and organic forms of arsenic (dimethylarsinic acid and monomethylarsonic acid). The adverse effects of arsenic on human health varies with its oxidation state or its species. As(III) is found to be more toxic having higher mobility than the As(V). Further, studies showed that As(III) is 20-30 fold more harmful than As(V) (Sigdel *et al.*, 2016) hence, poses serious health concerns.

As(III) showed a high affinity to bind to sulfhydryl (-SH) group of some enzymes, thus interrupting the biological functions leading to oxidative stress whereas As(V) mimics the phosphate and disturb the ATP (adenosine triphosphate) production (Aposhian and Aposhian, 2006). The toxicity of arsenic also depends on the dose, rate, and duration of exposure. Chronic exposure through drinking arsenic-contaminated water leads to hyperkeratosis, skin cancer, and a high risk of bladder, lung, liver, prostate cancer, and kidney failure (Haider *et al.*, 2014). Moreover, the acute symptomatic ailments *viz.*, diarrhea, nausea, vomiting, abdominal and muscular pain, etc., are also reported with high-level ingestion of arsenic even with limited time of exposure (Mohan and Pittman, 2007; Tiwari and Lee, 2012). According to an assessment by the United States National Academy of Science and the United States National Research Council indicated that even at 3 µg/L of arsenic, the risk of bladder and lung cancer is between four and seven deaths per 10,000 persons, while at 10 µg/L, it is 12-23 deaths per 10,000 persons (NRC, 2001). Hence, Inorganic arsenic species are classified as Group 1 carcinogen (carcinogenic to humans), classified by the IARC (International Agency for Research on Cancer) (IARC, 2018).

### **1.2.2. Lead**

Lead is a ubiquitous, highly toxic element on the earth's crust and it is widely distributed in various segment of environment (Mahaffey, 1990). Various industrial applications have further contributed for elevated level of lead contamination in the environment including the water bodies. It possesses significant qualities, including softness, ductility, weak conductivity, malleability, and corrosion resistance, which makes it difficult to completely abandon the various industrial applications (Duzgoren-Aydin, 2007; Wani *et al.*, 2015). Humans get exposed to lead primarily through occupations related to lead, such as lead smelting and combustion, pottery, boat building, lead-based painting, lead-containing pipes, battery recycling, grids, the arms industry, pigments, book printing etc. (Duzgoren-Aydin, 2007; Wani *et al.*, 2015). Although, the revised guidelines restricted broadly the use of lead in many countries, nevertheless it is used in a variety of industries such as vehicle maintenance, battery



manufacture, and smelting, recycling, refining, etc. Hence, these sources are contributing significantly to pollute the natural environment. To a certain extent, the accumulation of harmful heavy metals in soil will not only cause soil degradation and a decline in crop yield and quality, but it will also pollute the surface and groundwater through rainwater, potentially poisoning plants or endangering human lives through the food chain (Shao *et al.*, 2020). Furthermore, due to atmospheric deposition from industries and automotive emissions, it is one of the most prevalent trace metal pollutants in urban soils (Guirado *et al.*, 2021). The metals that build up in the soil can have a deleterious impact on its fertility. They can also be exceedingly persistent, both in the soil and in plants and thus enter the food chain through consumption of crops grown in polluted areas (Biswas *et al.*, 2020). Waste streams from battery manufacture, acid metal plating, and finishing, ammunition, tetraethyl lead manufacture, ceramic and glass industries printing, painting, dying, etc. are all additional sources of lead contaminating the environment (An *et al.*, 2001; Li *et al.*, 2002). Hence, high levels of lead contamination in soil, ground water, plants, and aquatic life become a major global environmental problem (Lee *et al.*, 2015; Lormphongs *et al.*, 2003).

Lead poisoning showed a serious health concern for both humans and animals. Its toxicity afflicts the nervous system both in children and adults. Children are more vulnerable towards lead toxicity than adults due to their softer tissues (both internal and exterior) compared to the adults, and affects their brain and nervous system development (Edokpayi *et al.*, 2015). Even low levels of lead causes behavioral symptoms *viz.*, learning deficiencies, and decreased IQ (intelligence quotient) in infants and young children and even causes mental retardation if it exists in the body fluid at high levels (Rubin *et al.*, 2008; Zhang *et al.*, 2006). Long-term lead exposure is linked to anemia and an increase in blood pressure, particularly in the elderly and middle-aged people. Memory loss, neurological abnormalities, muscle paralysis, and irritability are all the symptoms of lead poisoning (Yang *et al.*, 2010). Furthermore, lead is seemingly accumulated to the bones and kidneys, causing adverse impact to the neurological system and renal function even at low level exposure (Lin *et al.*, 2003). Chronic lead exposure results in miscarriage in pregnant women and reduced male fertility (Sokol and Berman, 1991).

Therefore, because of its acute toxicity, the World Health Organization (WHO) and United States Environmental Protection Agency (US EPA) mandated a maximum acceptable concentration in drinking water as low as 10 µg/L and 15 µg/L, respectively (Hakonen and Strömberg, 2018) . The Bureau of Indian Standards have also set permissible limits for Pb(II) in drinking water and wastewater at 0.015 mg/L and 0.1 mg/L, respectively (Pandey *et al.*, 2015). Based on the Centers for Disease Control and Prevention (CDCP), the maximum acceptable concentration for lead in blood is 10 µg/dL (CDCP, 1991; Gilbert and Weiss, 2006).

### **1.2.3. Cadmium**

Cadmium (Cd) is a non-essential transition metal and similar to arsenic, lead, mercury, and chromium, it has no physiological function and is frequently regarded as a potential toxin (Friberg *et al.*, 2019; Sinicropi *et al.*, 2010). The increase in cadmium concentrations in various segment of environment (atmosphere, soil, and water) is due to the natural processes such as volcanic activity, the gradual erosion and abrasion of rocks and soils, forest fires etc. In addition, the industrial activities are having greater role in the increase of cadmium levels in the environment (Rahimzadeh *et al.*, 2017). Copper and nickel smelting and refining, fossil fuel burning, and use of phosphate fertilizers are all anthropogenic sources of cadmium, contaminating the environment. It is also used in nickel-cadmium batteries, paint pigments, electroplating, and the manufacture of polyvinyl chloride plastics (Genchi *et al.*, 2020). Cadmium occurred as a contaminant in nonferrous metal smelters and electronic waste recycling. The mine processing units for the extraction of zinc, lead, and copper contributes the emission of cadmium into the atmosphere, contaminating soil as well (Casado *et al.*, 2008). Cadmium is linked to zinc, and is usually recovered as zinc byproducts during smelting and refining processes, thus, the majority of cadmium produced today comes from zinc ores where the levels are typically around 0.03 to 9.0 wt% of zinc concentrations (Indian Bureau of Mines, 2016).

Exposure to cadmium or cadmium compounds is hazardous to human health. Cadmium can be absorbed in large amounts from contaminated water, food, and air. Absorption by inhalation is through the respiratory tract that occurs at lesser extent except for heavy smokers and exposed occupational workers. Much of the health risks are associated with intake of food items contaminated with cadmium which affects the gastro-intestinal system. However, the exposure of cadmium through skin absorption is quite uncommon (Bernard, 2008). The majority of cadmium that enters into the body through food comes from terrestrial sources. This means plants grown on contaminated soil or meat from animals that ate the contaminated soil-grown plants. Therefore, the reference dose for cadmium in drinking water is 0.0005 µg/L per day and according to Food and agriculture Organization (FAO) or WHO guidelines, the maximum amount of cadmium allowed in rice is 0.2 mg/kg (Zazouli *et al.*, 2008). Further, the ingested cadmium is transported to the bloodstream through erythrocytes and albumin, where it accumulates in the kidneys, liver, and gut (Satarug, 2018; Tinkov *et al.*, 2018). The acute (short-term) effects of cadmium are through inhalation only. This causes the lung-related problems, such as pulmonary inflammation (Goel *et al.*, 2006). Lung, breast, prostate, pancreas, urinary bladder, and nasopharynx cancers are due to the occupational or environmental cadmium exposure (Mezynska and Brzóska, 2018). Cadmium is a developmental toxin, causing prenatal deformities and risks in kidney development (Liu *et al.*, 2019). Human studies have revealed a link between cadmium exposure and an increased risk of lung cancer; however, these studies are inconclusive due to influencing variables but animals-based studies reveal that long-term inhalation exposure to cadmium causes lung cancer in animals (IARC, 1993).

Levels of cadmium in some natural freshwaters of Australia are ranged from 0.01 µg/L to 0.4 µg/L (Hart, 2017). Indian Standard Institutions suggest a maximum concentration of cadmium 2.0 mg/L for the discharge of cadmium-containing effluents on inland surface waters (ISI, 1981). Moreover, cadmium is classified as a Group B1 carcinogen by EPA and WHO and EPA suggested a maximum permissible level of cadmium in drinking water as 5 µg/L and 3 µg/L, respectively. According to national and international regulatory bodies, total cadmium concentrations in raw water supplies is recommended to be not more than 0.01 ppm (EPA, 1980; WHO, 1971).

#### 1.2.4. Sulfamethoxazole (SMX)

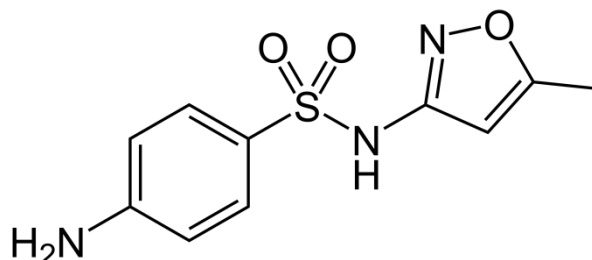


**Figure 1.1:** Structure of Sulfamethoxazole

Pharmaceuticals such as antibiotics, antimicrobials, etc. are often used medications for treating infectious diseases in humans, as well as in livestock or even as growth promoters in agricultural sectors (Petrie *et al.*, 2015). According to a recent report, the annual usage of non-prescribed drugs in the United Kingdom and Poland alone are 152 and 83 tons, respectively (Kwarciak-Kozłowska, 2019). It is known fact that a substantial portion of drugs, i.e., *Ca* 95% of the administered drugs in human and veterinary is not metabolized completely and therefore excreted out as unmetabolized or even in active forms (Negreanu *et al.*, 2012). The discharged residues of wastewater effluents from hospitals, agricultural sites, and veterinary farms enter into the surface waters, causing deterioration of the water qualities. Moreover, most of the pharmaceuticals including antibiotic compounds are having the persistence nature and are not entirely removed in the wastewater treatment plants hence, enter into the water bodies and contaminating the surface and groundwater followed by soil (Anekwe *et al.*, 2017; Levy and Marshall, 2005; Rizzo *et al.*, 2013). This persistent nature of pharmaceuticals imposed with high risks of bioaccumulation and even contribute to microbial antibiotic resistance in human (Quesada *et al.*, 2019).

Sulfamethoxazole (SMX) is a persistent antibiotic drug compound and often detected in the groundwater, surface water, wastewater sludge, streams etc. (Johnson *et al.*, 2015; Petrie *et al.*, 2015; Radović *et al.*, 2015). The drug is employed as antibiotics/antimicrobials to treat various infections in the urinary tract and respiratory

systems (Gong and Chu, 2016). It tops the US Geological Survey list of 30 most frequently perceived pharmaceuticals in wastewater (Zhu *et al.*, 2017). Sulfamethoxazole detected in various water bodies which is well documented and according to UNESCO and Helsinki Commission (HELCOM) report, concentrations reaching 10 mg/L as detected in river water samples in Germany (Vieno *et al.*, 2017). Sulfamethoxazole is detected in sludge and fish samples as well (Nielsen and Bandosz, 2016). The toxic effects of sulfamethoxazole are more chronic than being fatal. It is reported that antibiotic resistance among microbial populations is stimulated within the time frame of sulfamethoxazole degradation in the natural environment (Ferrari *et al.*, 2004; Patrolecco *et al.*, 2018). Furthermore, the excessive application of antibiotics in agriculture disturbs the mediation of nitrogen among microbes in soil and some antibiotics including sulphonamides inhibits the denitrification process in wastewater treatment plants (Laverman *et al.*, 2015). Sulfamethoxazole is one of the most commonly prescribed and used sulfonamide antibiotics in both human and veterinary medicine, with 15-25 percent of it excreted as such, resulting in its ubiquitous existence in aquatic ecosystems (Carvalho and Santos, 2016; Radke *et al.*, 2009). Hence, the use of these drugs in animals and human therapies is linked to the emergence of antibiotic-resistant bacteria, causing widespread public concern (Almeida *et al.*, 2011). Infection of humans by bacteria that are resistant to the drug would pose a serious health risk (Almeida *et al.*, 2013). Drug residues in foods like milk and meat are linked to allergic reactions, antibiotic resistance, and even enhanced risk of cancer (He and Chen, 2016). As a result, the European Union prescribed a maximum residue limits for total sulfonamides in milk, and other consumable products to 100 µg/kg (Centi *et al.*, 2010; Conzuelo *et al.*, 2013).

### 1.2.5. Sulfamethazine

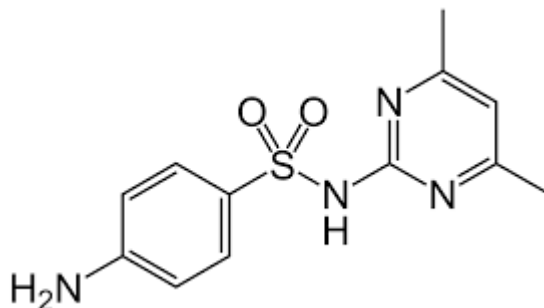


**Figure 1.2:** Structure of Sulfamethazine

Sulfamethazine (SMZ) is another antibiotic drug of the sulfonamide family or commonly known as sulfa-drug. It is an antibacterial drug mostly prescribed for the treatment of veterinary of livestock ailments such as respiratory tract and gastrointestinal diseases and also as growth promoters (de Zayas-Blanco *et al.*, 2004; Holland Deborah and Katz, 1991). Sulfamethazine inhibits the production of dihydrofolic acid which works against a variety of Gram-positive and Gram-negative bacteria (Richards *et al.*, 2011). It is noted that approximately 90% of ingested sulfamethazine is excreted by humans and livestock and through the wastewater it reaches to the wastewater treatment plants. Further, since the sulfamethazine is a hydrophilic chemical that is poorly degraded by microorganisms in the wastewater treatment plants hence, it discharged through the effluent of the treated wastewater treatment plants and entering into the water bodies. This resulted an elevated level of sulfamethazine in the water bodies ranging from ng/L to µg/L (Tang and Wang, 2019; Wen *et al.*, 2018). If livestock receive abusive antibiotic-based treatments without the safety guidelines, unwanted residues may persist in the animals. These residues also have an impact on milk-production and egg-laying animals and the presence of antibiotic residues in milk, eggs, and meat is a public health concern due to the development of drug resistance in gut bacteria populations (Premarathne *et al.*, 2017). It was reported earlier that milk has elevated concentrations of these sulfa drugs (Agarwal, 1992). Furthermore, long-term agricultural activities, including livestock

effluent, manure, and manure-fertilized crops contributed to the widespread occurrence of sulfamethazine in farmlands (Conde-Cid *et al.*, 2019). Through surface runoff/leaching, the sulfamethazine is readily reintroduced into ground and drinking waters, surface water, and eventually entire aquatic ecosystems (Davis *et al.*, 2006). For example, groundwater samples obtained from six different locations near Confined Animal Feeding Operation (CAFO) in Weiser, Idaho, USA is contained with elevated level of sulfamethazine (0.076 – 0.22 µg/L) (Batt *et al.*, 2006). Antibiotics, as well as antibiotic resistance genes, are widespread on fields and pastures when manure slurry is utilized as fertilizer. Due to its high mobility and water solubility, it has been identified in a wide range of environmental matrices, with concentrations as high as 20 mg/kg in animal feces, 323 ng/L in water, and 15 g/kg in agricultural soils (Xu *et al.*, 2007; Gaw *et al.*, 2014; Larsbo *et al.*, 2008). However, the concentrations of antibiotics and fate in manure and soil are less known (D'Alessio *et al.*, 2019). Assessing the role of contaminated manure in the transmission of antibiotic drugs and their accompanying resistance genes into the environment, as well as the risk of water and food contamination through this pathway, is critical area to be explored for greater understanding. Since sulfamethazine is one of the most extensively used sulfonamide medicine, hence, there are concerns for microbes developing resistance to sulfamethazine, rendering these medications ineffective in treating humans, which can cause resistance and allergic reactions (mostly skin rashes) (Han *et al.*, 2013). Studies in mice and rats are reported in the early '90s by National Centre for Toxicology Research, and it is demonstrated that high doses of sulfamethazine in the diet caused antithyroid activity that led to TSH (thyroid stimulating hormone) overproduction and tumor formation. Thyroid hypertrophy and follicular cell hyperplasia are observed in the thyroid glands of rats and mice given high doses of sulfamethazine (Poirier *et al.*, 1999).

### 1.3. REVIEW OF LITERATURE

Accurate, sensitive/efficient, and cost-effective analytical detection systems received greater attention in the recent past for the sensing of emerging water pollutants in the aquatic environment. In a line, the 'electrochemical sensors' play a crucial role since they provide versatile and promising miniature devices which are useful in several trace level detection of water pollutants. A "chemical sensor is a small device that, as the result of a chemical interaction or process between the analyte and the sensor device, transforms chemical, or biochemical information of a quantitative or qualitative type into an analytically useful signal" (Stetter *et al.*, 2003). Electrochemical sensors are also said to be appealing because of their high sensitivity, ease of experimentation, and low input cost (Mousty, 2004). Moreover, recent reviews suggested that electrochemical methods are known to be the most promising tools for field applications/implications (Liu *et al.*, 2013; Zaib *et al.*, 2015; Xu *et al.*, 2010). Electrochemical sensor development involves substituting electrodes with newer and more advanced materials to achieve the appropriate selectivity and sensitivity for the target analyte (Carrera *et al.*, 2017). As a result, this field of research has proliferated in recent decades, introducing a variety of innovative and advanced materials with increased sensitivity to pollutants including the arsenic. The selection of materials for electrode fabrication, the optimization of electrochemical procedures, and the pre-treatment of water samples are all key considerations that must be thoroughly investigated before the ultimate device developments. The role of clay materials is unique due to its wide variety of intriguing features (physical and chemical stability, high ion exchange capacity in a micro-structured environment, hydrophilic character, etc.), possibly be useful electrochemical interface materials to be explored for efficient and selective detection of several trace analytes in aqueous wastes (Mhammedi *et al.*, 2009; Gomez *et al.*, 2011; Lalmalsawmi *et al.*, 2020b; de-Almeida *et al.*, 2020).

Clay materials are hydrous layered aluminosilicates with very fine particle sizes (Park *et al.*, 2011) usually composed of mixtures of fine-grained clay minerals and clay-sized crystals of other minerals such as quartz, carbonate, and metal oxides. With a few exceptions, the crystal structure is made up of sheets (hence the term sheet clay minerals or phyllosilicates) firmly aligned in structural layers and each layer may



contain 2-4 sheets. Tetrahedral  $[\text{SiO}_4]^{4-}$  and octahedral  $[\text{AlO}_3(\text{OH})_3]^{6-}$  are the main structural frameworks of the sheets and based on the ratio of these constituents, the clays are classified into several groups. Clays invariably contain exchangeable cations and anions lying within the interspace of phyllosilicate sheets. The prominent cations and anions are  $\text{Ca}^{2+}$ ,  $\text{Mg}^{2+}$ ,  $\text{H}^+$ ,  $\text{K}^+$ ,  $\text{NH}_4^+$ ,  $\text{Na}^+$  and  $\text{SO}_4^{2-}$ ,  $\text{Cl}^-$ ,  $\text{PO}_4^{3-}$ ,  $\text{NO}_3^-$ , respectively. These ions are exchanged with other cations or anions energetically without changing the basic structure of clay minerals (Bhattacharyya and Gupta, 2008). The introduction of cationic surfactant molecules within the interspace by exchange process enables a significant increase in basal spacing of clay sheets (Tangaraj *et al.*, 2017). The properties of clay minerals could also be changed from highly hydrophilic/lyophobic to increasingly hydrophobic/lipophilic/organophilic. These modified hybrid materials are found to be effective in the attenuation of organic pollutants having low or no-polarity (Lee and Tiwari, 2012; Park *et al.*, 2011). Clays might thus be utilized in constructing electrochemically active nanostructured materials with greater sensitivity to the target pollutant species due to its ease of modification and accurate functionalization with desirable components.

Literature survey reveals that the clay modified electrodes is an attractive research area since these are introduced in electrochemistry during 1983 by Ghosh and Bard (Ghosh and Bard, 1984). Clay minerals are reported to be promising in the extension of electrochemical sensors and biosensors, because of its high specific area, swelling and porosity properties, good catalytic support, thermal and mechanical stabilities as well as low input cost (Mousty, 2004; Navrátilová and Kula, 2003; Zen and Kumar, 2004). Despite of these attractive properties, pristine clay minerals suffered extensively from poor selectivity which restricted the adsorption capacities for many water pollutants. These limitations could be overcome by the functionalization of clay with specific organic groups, leading to organo-inorgano hybrid materials. These materials show enhanced selectivity, or sensitivity as employed in the form of thin films onto an electrode surface (in a similar way as sol-gel-derived organic-inorganic hybrids introduced) (Collinson, 2002; Thanhmingliana *et al.*, 2015a; Thanhmingliana and Tiwari, 2015b). In a line, Cameroonian smectite clay was grafted with trimethylpropylammonium groups and the resulting organoclay deposited as a thin film onto a glassy carbon electrode (GCE) surface and employed

in the trace and simultaneous detection of ascorbic and uric acids from aqueous solutions (Mbougouen *et al.*, 2011). Similarly, a natural Cameroonian smectite-type clay was exchanged with cationic surfactants *viz.*, cetyltrimethylammonium (CTA) and di-dodecyl dimethyl ammonium (DDA). The organo-modified clays were then employed to obtain thin film formation onto the glassy carbon electrode and hence, intended to introduce in the trace detection of herbicide mesotrione using the square wave voltammetry (Wagheu *et al.*, 2013). The detection limit of the method was obtained to be 0.26  $\mu\text{M}$  for the mesotrione. Smectite was partially exchanged with tetrabutylammonium ions (TBA) and subsequently impregnated onto the glassy carbon electrode. The modified electrode was applied for the pre-concentration electroanalysis of various heavy metal toxic ions *viz.*, cadmium, lead, and copper (Maghear *et al.*, 2014).  $\text{Fe}(\text{dmbpy})_3^{2+}$  (where dmbpy is 4,4'-dimethyl-2,2'-bipyridine) was immobilized with the bentonite clay, forming a thin film onto a glassy carbon electrode. The modified electrode was introduced in the cyclic voltammetric studies and showed a characteristic redox behavior of immobilized  $\text{Fe}(\text{dmbpy})_3^{2+/3+}$ . Further, this caused to enhance significantly the anodic current in the oxidation of isoniazid (antibiotic drug) and enabled in trace detection of isoniazid from aqueous solutions (Azad *et al.*, 2014). The recent advances in the modified-clay and its electrochemical implications in the sensor or biosensor development is well demonstrated elsewhere (Mousty, 2004; Lalmalsawmi *et al.*, 2020b). Tiwari and co-workers intensively studied the modifications of variety of clay materials (Bentonite and locally collected clay) with hexadecyltrimethylammonium bromide (HDTMA) or Al-HDTMA i.e., organic– or inorganic-organic modifications. Further, these materials were utilized in the modifications of carbon paste electrodes and the modified electrodes were employed in the efficient low-level detection of As(III), As(V), Pb(II) and Cd(II) from aqueous solutions. The selectivity of the method was enabled with the real water matrix treatment as spiked with the respective pollutants (Tiwari *et al.*, 2017; Tiwari *et al.*, 2016; Lalmalsawmi *et al.*, 2020a; Lee *et al.*, 2016). Two types of granular electrodes modified with the (cetyltrimethyl ammonium bromide modified bentonite (CTAB-bent) and hydroxy-aluminum pillared organic bentonite (OH-Al-CTAB-bent)) were fabricated to form a three-dimensional (3-D) electrode system. The prepared electrodes were utilized to dispose/treat the pulp and paper in secondary wastewater

of paper mills (Chu *et al.*, 2016). Abdulla *et al.*, have fabricated clay-modified platinum electrodes (CMEs) using naturally occurring Jordanian silicates, kaolinite, and montmorillonite. The modified electrodes are then used for the selective and sensitive determination of Cu(II) and Hg(II) at ultra-trace levels. The modified electrodes showed a remarkable selectivity and sensitivity for heavy metal ions in natural water (Abdulla *et al.*, 2009).

### **Electrochemical detection of arsenic**

Electrochemical methods are developed and suggested to be efficient at low-level detection of arsenic (Guo *et al.*, 2017). A stripping voltammetric analysis of As(III) was conducted using a vibrating, gold microwire electrode. The arsenic detection was performed by the adsorptive deposition of  $\text{H}_3\text{AsO}_3^0$  at an applied cathodic potential to obtain the reduction current which occurred due to the reduction of As(III) to As(0) and studied at a wide pH range 7-12 (Gibbon-Walsh *et al.*, 2010). Exfoliated graphite electrode was used to deposit the bismuth film at potential -600 mV and further this working electrode was utilized in a square wave anodic stripping voltammetric determination of As(III) studied at pH 6.0. The method revealed a very low detection limit of As(III) i.e., 5  $\mu\text{g/L}$ , and the detection was not hampered in presence of several cations excluding Cu(II) (Ndlovu *et al.*, 2012). Similarly, reduced graphene oxide-lead dioxide was obtained *in situ* using the EGO (exfoliated graphene oxide) coated electrode surface. The electrode was sensitive to detect the low-level arsenic at a wide range of pH 2-11 with the detection limit of 1 nM (Ramesha and Sampath, 2011). The carbon nanotubes and polymeric resins modified carbon paste electrode was utilized in the voltammetric (cathodic stripping) low-level determination of arsenic in sugarcane brandy samples (Teixeira *et al.*, 2014). Similarly, the cobalt oxide nanoparticles deposited glassy carbon electrode was developed and this modified electrode was employed in the detection of As(III) in the cyclic voltammetric and hydrodynamic amperometry studies at a wide pH region 5-11. It was also demonstrated that the effect of several interfering reducing compounds could not affect the detection of arsenic from aqueous solutions (Salimi *et al.*, 2008). In a line, GCE

modified with SWCNTs (single-walled carbon nanotubes) and -SH groups using mercaptoethylamine was developed and found that introduced -SH group was highly sensitive towards As(III) in an electrochemical determination (Liu and Wei, 2008). Based on the sequential injection/anodic stripping voltammetry using a long-lasting gold-modified screen-printed carbon electrode was prepared at 0.5 V vs Ag/AgCl. Further, the electrode was employed in the determination of As(III) in a wide concentration range of 1-100  $\mu\text{g/L}$  (Punrat *et al.*, 2013). Electro reduced graphene oxide (ERGO)-Au nanoparticles composite film was electrodeposited onto a glassy carbon electrode using cyclic voltammetry. The electrode was then utilized in the trace determination of As(III) in 0.20 mol/L HCl by the anodic stripping voltammetry. Reasonably a good linearity was achieved for the As(III) determination in the concentration range 0.01 to 5.0  $\mu\text{M}$  (Liu *et al.*, 2013). The nanocomposite (NC) modified electrodes developed by depositing of Au and  $\text{Fe}_3\text{O}_4$  nanoparticles on the glassy carbon electrode by the simple drop-casting method was conducted by the voltammetric studies for arsenic detection and showed that synthesized NC's deposited on the electrode showed a good affinity towards As(III) species (Toor *et al.*, 2015). Gold nanoparticles electrodeposited on glassy carbon electrode in 0.5 mol/L  $\text{H}_2\text{SO}_4$  examined by different voltammetric studies showed a limit of detection (LOD) of 0.9  $\mu\text{g/L}$  at the optimized parameters. Moreover, the developed sensor is found to show no interfering effects due to the ionic copper which was the most potential obstructing ionic species in ionic As(III) detection (Radhakrishnan *et al.*, 2015). A glassy carbon electrode fabricated with nano Au-crystal violet (CRV) film and indium tin oxide (ITO) were employed for the detection of arsenic in various water samples that detected the arsenic with very low detection limits as 0.20  $\mu\text{mol/L}$  for laboratory water samples (Muniyandi *et al.*, 2011). Several other studies have focused on the use of gold nanoparticles or composite modified electrodes in the detection of As(III) at low levels which was demonstrated by the varying concentration ranges and detection limits (Domínguez-González *et al.*, 2013; He *et al.*, 2007; Huang and Chen, 2013; Song and Swain, 2007; Li *et al.*, 2012).

On the other hand, As(V) was shown non-electroactive species, hence its detection is mostly carried out indirectly as first reducing it to +3 state using the strong reducing agents followed by As(III) was detected; the total arsenic was accordingly

detected. Ruthenium oxide nanoparticles have shown greater affinity towards As(III) and As(V) due to surface complexation (Kim *et al.*, 2013). Hence, the detection of arsenic was carried using the ruthenium bipyridine-graphene oxide ( $[\text{Ru}(\text{bpy})_3]^{2+}$ -GO) nanocomposite material. The nanocomposite material was synthesized by the wet complexation process and the screen-printed electrode (SPE) was modified with nanocomposite. The modified electrode depicted three oxidative peaks at the potential of 0.38, 0.67 and 0.97 V (vs Ag/AgCl) which corresponded to the outer and inner oxidation of As(0) to As(III) and then As(III) to As(V). The modified SPE was introduced in the differential pulse voltammetry in the simultaneous detection of As(III) and As(V) with the sensitivity and LOD of 33.07  $\mu\text{A}/\mu\text{M}$  and 21 nM (for As(III)) and 21.21  $\mu\text{A}/\mu\text{M}$  and 34 nM (for As(V)), respectively (Gumpu *et al.*, 2018). Similarly, the europium doped magnetic graphene oxide-Au(NP)-multiwalled carbon nanotube nanohybrid (Eu-MGO/Au@MWCNT) modified pencil graphite electrode, was fabricated for the simultaneous trace detection of As(III) and As(V) using the square wave stripping voltammetry. The LOD was found to be 0.27 and 0.99  $\mu\text{g}/\text{L}$  for the As(III) and As(V), respectively (Roy *et al.*, 2016). The CoOOH nanoflakes modified GCE was utilized in the detection of As(V) at pH 4.0 (acetate buffer) in the chronoamperometric method. The results showed that a fairly good linear relationship was obtained between the chronoamperometric intensity against the logarithm of As(V) concentration within the concentration range of 0.1-200  $\mu\text{g}/\text{L}$ . The LOD was found to be 56.1 ng/L and the method has shown greater selectivity towards several cations and anions (Wen *et al.*, 2019).

## Electrochemical detection of lead and cadmium

Similar to arsenic, a large variety of chemically modified electrodes are employed for sensitive detection of Pb(II) and Cd(II) in aqueous media. Several voltametric methods are proposed which include both organic and inorganic materials (Promphet *et al.*, 2016; Wang *et al.*, 2014). In recent years, due to advances in nanotechnology, various nanomaterials are utilized for sensing purposes (Li *et al.*, 2013). The carbon-based nanomaterials such as graphene, carbon nanotubes, graphitic nano-compounds, graphene oxide or reduced graphene oxide, etc. are commonly utilized in the fabrication of electrodes (Raril *et al.*, 2020; Lu *et al.*, 2021; Lv *et al.*, 2013; Yang *et al.*, 2020). The nanostructured graphene and multiwalled carbon nanotube were used to modify the glassy carbon electrode, which was then used in the low-level detection of Cd(II) using differential pulse anodic stripping voltammetry (DPASV). According to a comparative study, the graphene-modified electrode showed a very low LOD value of 3.5 ng/L for Cd(II) detection (Wu *et al.*, 2014). Multiwalled carbon nanotube (MWCNT) further modified with  $\beta$ -cyclodextrin by physical/or chemical attachment was used for modifying screen-printed electrode (SPE) and used to detect lead in drinking water samples. The sensitivity and LOD was found to be 98 nA/ppb and 0.9 ppb, respectively. Further, the repeated use of electrode was conducted with the physically modified electrode surface and 90% reproducibility was achieved (Alam *et al.*, 2019). Recently, a new electrochemical approach for anodic stripping voltammetric detection of lead ion in cosmetics and blood serum was introduced, based on a high index facet (HIF) silver nanoflower modified glassy carbon electrode (AgNF@GCE). A low detection limit of 0.74  $\mu\text{g/L}$  was achieved in a linear concentration range of 10-700  $\mu\text{g/L}$  by making use of the unique surface feature of the HIF silver nanoparticles (Swetha *et al.*, 2020). Cadmium and lead are detected simultaneously from a single pollutant source. MWCNT modified with bismuth oxychloride particle (BiOCl/MWCNT) cast glassy carbon electrode was used to detect Pb(II) and Cd(II) using square wave anodic stripping voltammetry and LOD of 4.0  $\mu\text{g/L}$  for Cd(II) and 1.9  $\mu\text{g/L}$  for Pb(II) was achieved when accumulated for 120 s at pH 4.0 and at applied potential of -1.20 V (Cеровac *et al.*, 2015). The carbon nanomaterials, graphene and/or graphene oxide were used in combination with other

materials and coated/casted on the glassy carbon electrode for increased conductivity and electro catalyzed reactions (Baghayeri *et al.*, 2018; Dahaghin *et al.*, 2017). Poly(amidoamine) dendrimer functionalized magnetic graphene oxide (GO-Fe<sub>3</sub>O<sub>4</sub>-PAMAM) and graphene oxide (GO@Fe<sub>3</sub>O<sub>4</sub>) modified with benzothiazole-2-carboxaldehyde (2-CBT) were introduced to the electrode surface and employed to detect lead and cadmium in aqueous solution by SWASV technique. LOD of 0.13 µg/L and 0.07 µg/L was achieved at GO-Fe<sub>3</sub>O<sub>4</sub>-PAMAM/GCE for Pb(II) and Cd(II), respectively, whereas 0.02 µg/L and 0.03 µg/L were obtained at the GO@Fe<sub>3</sub>O<sub>4</sub>/2-BT surface for Pb(II) and Cd(II), respectively.

### **Electrochemical detection of pharmaceuticals (sulfonamides)**

Several nanomaterials were employed for the detection of various antibiotic drugs in aqueous solutions (Yang *et al.*, 2019; Wang *et al.*, 2021). Sulfonamides are widely used antibiotics however, scanty of work is conducted for the low-level detection of these pharmaceutical compounds using the electrochemical methods. These micro-pollutants were electrochemically oxidized at the amino (-NH<sub>2</sub>) group or reduced at -SO<sub>2</sub><sup>2-</sup> group. The reduction depends on the R group, the oxidation is however, almost unchanged with change in the R group. As a result, the structure of the sulfonamide is important in reduction, but not in oxidation (Braga *et al.*, 2010). In electrochemical method, the different sulfonamides were thus, detected by single/individual measurements. Nanoparticles and carbon nanotubes, mostly MWCNT were found to be valuable means of achieving efficient sensor platform for antibiotics (Yari and Shams, 2018; Chen *et al.*, 2018; Arvand *et al.*, 2011). Polymer modified electrodes such as poly-1,5-diaminonaphthalene (p-DAN) modified glassy carbon electrode (GCE) was used to demonstrate sulfamethazine detection in a linear response at the concentration range of 0.5–150 mM using square wave voltammetry (SWV). The results indicated that the detection limit of sulfamethazine was 0.05 nM with the sensitivity of 0.085 mA/moL (Chasta and Goyal, 2015). Similarly, screen printing electrode (SPE) modified with conducting polymer nanocomposite containing poly(3,4-ethylenedioxythiophene) (PEDOT) and MnO<sub>2</sub> showed much enhanced

electrochemical activity over the bare electrode for sulfamethazine determination. The sensitivity and detection limits ( $S/N=3$ ) were found to be  $0.115 \mu\text{A/mol}$  and  $0.16 \mu\text{M}$ , respectively at a wide linear response i.e., from  $1.0 \mu\text{M}$  to  $500 \mu\text{M}$ .

Therefore, the current research specifically aims to obtain the novel composite materials precursor to the natural bentonite clay and trichloro(octadecyl) silane. The silane grafted bentonite possesses enhanced physico-chemical properties showed enhanced organophilic nature as well higher affinity towards the oxyanions including As(III). Moreover, the silane grafted bentonite possessed with enhanced mechanical strength as well high settling capacity. Further, the nanocomposite solid was decorated with the silver and gold nanoparticles as obtained by the greener route utilizing the *Persea americana* (Avocado) leaf extracts. The nanocomposite solids are extensively employed for the electrochemical trace detection of heavy metal toxic ions viz., As(III), Cd(II) and Pb(II) along with the emerging pharmaceuticals including the sulfamethoxazole and sulfamethazine from aqueous solutions. Further, the real matrix studies further enable the possible implications of the method for miniaturized device development.



#### 1.4. SCOPE OF PRESENT INVESTIGATION

The contamination of aquatic environment with variety of pollutants including the heavy metal toxic ions and micro-pollutants has received a greater attention in recent time. The level of contaminants is reaching to the alarming level hence, serious threat to the humans and aquatic life. Although, the sensitive and efficient detection systems are available for the detection of these pollutants water bodies however, the instruments are having high input cost, sophisticated in instrumentation, needs skilled operator and most importantly the off-site monitoring is only possible i.e., the laboratory-based analyses. This restricted the greater applications of these instruments. Therefore, there is a greater demand of miniaturized, robust and less expensive devices which could easily be introduced for trace detection of several water pollutants at on site only. The electrochemical technologies are now acknowledged as potential instruments for meeting the needs since these are inexpensive, portable, and quick in analyzing the analytes making it potential alternatives for sensitive and efficient detection of heavy metal toxic ions and other micropollutants as well. These electroanalytical approaches entailed applying varying potentials to analyte solutions and recording the current response of the redox process occurring at the working electrode and solution interface. Chemical alteration of the working electrode to improve the detection signal has gained more attention in recent time. Thus, the specific aim of this study is to develop a versatile, robust, and efficient electrochemical sensor for the trace to sub-trace level detection of As(III), Cd(II), Pb(II) and some of the emerging pollutants viz., sulfamethoxazole and sulfamethazine from an aquatic environment. The sensor is to be developed by employing carbon-based electrodes, possibly modified carbon paste electrodes, and the modified glassy carbon electrodes which are easily be fabricated and be reused in the electrochemical sensing of the pollutants. Bentonite is utilized as substrate material for the development of nanostructured materials. Trichloro(octadecyl) silane is grafted with bentonite and decorated with silver and gold nanoparticles. The nanoparticles of silver and gold are obtained by the greener synthetic route using the *Persea americana* (Avocado) leaf extracts. The nanocomposite materials showed enhanced electroactive affinity hence, possibly show fairly good sensing platform for variety of water pollutants viz., As(III),

Cd(II), Pb(II), or even micro-pollutants like sulfamethoxazole and sulfamethazine. The detection of these pollutants at trace to sub trace level enhances the applicability of method. Further, the practical applicability of the method is assessed in real-water samples as collected from different parts of Aizawl City, India.

# **CHAPTER 2**

## **METHODOLOGY**

## **2. METHODOLOGY**

### **2.1. CLAY SAMPLE AND REAL WATER SAMPLES**

The raw bentonite clay, used as the substrate material for nanocomposite preparation was obtained from a mine located near Bhuj, Gujarat, India. Real water samples utilized for real matrix studies were collected from five different locations in Aizawl City, Mizoram, India. The detailed description of each location (including Global position system) is presented in Table 2.1. The sources of water samples are river, spring, and surface run-off waters. Prior to utilize these samples, it was filtered with Whatman filter paper (pore size 20  $\mu\text{m}$ ) and subjected for quality assessment. Various physico-chemical parametric studies were conducted for these water samples. The water quality using multi-parameters *viz.*, pH, conductivity, resistivity, salinity, oxidation-reduction potential, and total dissolved solids were measured using multiparameter instruments. The samples were also analysed for various elements present as impurity using the AAS (Atomic Absorption Spectrometer) instrument. The NPOC (Non-purgeable Organic Carbon) and IC (inorganic carbon) are obtained using the TOC analyser. The 0.1 mol/L KCl or acetate buffer solutions were prepared using the collected water samples whose pH was then adjusted. Further, this solution was spiked with standard solutions of As(III), Cd(II), Pb(II), sulfamethoxazole, and sulfamethazine pollutants for electrochemical detection in the collected samples. However, the other studies were conducted using the purified water.

**Table 2.1.** GPS locations of various water samples collected.

<b>Locations</b>	<b>Water Source</b>	<b>GPS Location</b>
Tlawng (Reiek road)	River	N23.71202, E092.66412
Chite (Armed Veng, Aizawl)	River	N23.72988, E092.73791
Khurpui (Hlimen, Aizawl)	Spring	N23.68069, E092.7155
Tuikhur (Hlimen, Aizawl)	Spring	N23.6747, E092.7151
Tuikhur (Bawngkawn, Aizawl)	Spring	N23.75152, E092.72735
Chawnpui Veng, Aizawl.	Runoff	N23.73081, E092.70778

## **2.2. CHEMICALS AND APPARATUS**

All chemicals and reagents obtained are preferably analytical or equivalent grade and are used without further purifications. Details of all the chemicals are listed in Table 2.2. Titanium wire (0.81 mm) utilized for fabrication of carbon paste electrodes was obtained from Sigma-Aldrich, USA. Glassy carbon plate (1 mm thick, type 1: CAS no. 7440-44-0) used for investigation of surface morphology and roughness of the casted film of nanocomposite materials was purchased from Alfa Aesar (by Thermo Fischer Scientific).

**Table 2.2.** Details of various chemicals used for complete experimental works.

Sl. No.	Chemicals used	IUPAC Name	Formula	Company	CAS No./I D
1.	Silver nitrate	Silver nitrate	AgNO <sub>3</sub>	Sigma Aldrich, USA	7761-88-8
2.	Gold chloride hydrate	Trichlorogold (1-); hydrate	HAuCl <sub>3</sub> .xH <sub>2</sub> O	Sigma Aldrich, USA	16961-25-4
3.	Trichloro(octadecyl) silane	Trichloro (octadecyl) silane	CH <sub>3</sub> (CH <sub>2</sub> ) <sub>17</sub> SiCl <sub>3</sub>	Sigma Aldrich, USA	112-04-9
4.	Sulfamethoxazole	4-amino-N-(5-methyl-1,2-oxazol-3-yl)benzene-1-sulfonamide	C <sub>10</sub> H <sub>11</sub> N <sub>3</sub> O <sub>3</sub> S	Sigma Aldrich, USA	723-46-6
5.	Sulfamethazine	4-amino-N-(4,6-dimethylpyrimidin-2-yl)benzene-1-sulfonamide	C <sub>12</sub> H <sub>14</sub> N <sub>4</sub> O <sub>2</sub> S	Sigma Aldrich, USA	57-68-1
6.	Glassy spherical powder (2-12 µm)	Carbon	C	Sigma Aldrich, USA	7440-44-0
7.	Glycine	2-Aminoethanoic acid	C <sub>2</sub> H <sub>5</sub> NO <sub>2</sub>	Himedia, India	56-40-6
8.	Sodium meta arsenite	Sodium meta arsenite	NaAsO <sub>2</sub>	Himedia, India	7784-46-5
9.	Paraffin oil		C <sub>n</sub> H <sub>2n+2</sub>	Himedia, India	8012-95-1
10.	Potassium ferricyanide	Potassium hexacyanoferrate (III)	K <sub>3</sub> [Fe(CN) <sub>6</sub> ]	Merck	13746-66-2

11.	Potassium ferrocyanide	Potassium hexacyanoferrate (II) trihydrate	$K_4[Fe(CN)_6] \cdot 3 H_2O$	Merck	14459-95-1
12.	Potassium chloride	Potassium chloride	KCl	Merck	7447-40-7
13.	Acetic acid	Acetic acid	$CH_3COOH$	Merck	64-19-7
14.	Sodium acetate	Sodium acetate	$CH_3COONa$	Merck	127-09-3
15.	Cadmium nitrate tetrahydrate	Cadmium nitrate tetrahydrate	$Cd(NO_3)_2 \cdot 4H_2O$	Merck	10022-68-1
16.	Disodium hydrogen phosphate anhydrous	Sodium hydrogen phosphate	$Na_2HPO_4$	Merck	7558-79-4
17.	Ethylenediaamine - tetraacetic acid	2,2',2'',2'''- (Ethane-1,2-diyl dinitrilo) tetraacetic acid	$C_{10}H_{16}N_2O_8$	Qualigens Fine Chemicals, India	60-00-4
18.	Manganese(II) chloride	Manganese dichloride	$MnCl_2$	Qualigens Fine Chemicals, India	7773-01-5
19.	Toluene	Methylbenzene	$C_7H_8$	Qualigens Fine Chemicals, India	108-88-3
20.	Ethanol	Ethanol	$CH_3CH_2OH$	Qualigens Fine Chemicals, India	64-17-5
21.	Ferric chloride	Iron trichloride hexahydrate	$FeCl_3 \cdot 6H_2O$	Himedia, India	10025-77-1

22.	Mercuric chloride	Mercury dichloride	HgCl <sub>2</sub>	Himedia, India	7487- 94-7
23.	Potassium iodide	Potassium iodide	KI	Himedia, India	7681- 11-0
24.	Chloroform	Trichloromethane	CHCl <sub>3</sub>	Himedia, India	67-66- 3
25.	Conc. Sulphuric acid	Sulphuric acid	H <sub>2</sub> SO <sub>4</sub>	Himedia, India	7664- 93-9
26.	Conc. nitric acid	Nitric acid	HNO <sub>3</sub>	Himedia, India	7697- 37-2
27.	Sodium hydroxide	Sodium hydroxide	NaOH	Himedia, India	1310- 73-2
28.	1-naphthol	Naphthalen-1-ol	C <sub>10</sub> H <sub>8</sub> O	Himedia, India	90-15- 3

All solutions were prepared with purified water as obtained from Satorius (Arium Mini Plus UV Lab) water purification system. Stock solution for lead (II) was prepared from 1000 ppm of AAS reference solutions using the acetate buffer as electrolyte. Acetate buffer solutions of varying pH were prepared by dissolving appropriate amounts (calculated according to the Handerson-Hasselbach equation;  $K_a$  of acetic acid =  $1.75 \times 10^{-5}$ ) of acetic acid (weak acid) and its salt (sodium acetate) in distilled water (Vogels, 1979; G.D Christian, 2009). All standard solutions were diluted from the stock solution using acetate buffer or KCl supporting electrolyte and pH was adjusted using the 0.1 mol/L HCl or NaOH solutions. Copper (II), iron (II), mercury (II), zinc (II), and manganese (II) solutions for interference studies were also prepared by using 1000 ppm AAS standard solutions (Merck).



### 2.3. INSTRUMENTS

Electronic balance (HPB220, Wensar, India) was employed for weighing of solids. pH measurements for all solutions were conducted using a pH meter (HI2002, Hanna Instruments, USA). Silver and gold nanoparticles (AgNP and AuNP) colloidal solution was analysed by the UV-Visible spectrophotometer (UV-1800; Shimadzu, Japan). Characterization of synthesized materials was conducted using the Fourier Transform Infra-Red Spectrometer (IR Affinity-1S, Shimadzu, Japan), SEM-EDX (Oxford xmax) and TEM (Oxford xtreme). SEM-EDX and TEM analysis of synthesized materials were performed at Central Salt and Marine Chemicals Research Institute (CSIR-CSMCRI), Bhavnagar, India. Atomic force microscope (AFM) (Multi Mode 8, Bruker, USA) was used for analysis of materials surface roughness and measurements were conducted under the tapping mode. Electrochemical measurements viz., electrochemical impedance spectroscopy (EIS), cyclic voltammetry (CV), linear sweep voltammetry (LSV), and differential pulse anodic stripping voltammetry (DPASV) were carried out using the electrochemical work station (Biologic Instruments, France; Model SP-200). All experiments were carried out at room temperature using Ag/AgCl (BaSi, USA, Model: RE-5B) as reference electrode, platinum electrode (outer diameter-6 mm, inner diameter 1.6 mm; Model: A-002013) as the counter electrode, and glassy carbon electrode (outer diameter - 6 mm, inner diameter - 3 mm; Model: A-002421) as working electrode. The electrochemical data were analysed using inbuilt computer software ECLab®. Real water samples were analysed for various water parameters using the Multiphotometer (Hanna Instruments, USA; Model: HI98194). Similarly, total organic and inorganic carbon of water samples was obtained using the TOC analyser, (Shimadzu, Japan; Model: TOC-VCPH/CPN) and the elemental analysis was conducted using an Atomic Absorption Spectrometer (Shimadzu, Japan; Model: AA-7000).

## **2.4. ELECTROCHEMICAL TECHNIQUES**

The charge transfer processes occurring at the electrode surface forms the basis of electrochemical reactions. Various processes like electrolyte solution resistance, charge transfer resistance, adsorption of electroactive species, and mass transfer from the bulk solution to the surface of the electrode take place in the electrochemical processes. Hence, the presence of heavy metal ions or any other electroactive species may lead to a change of potential/voltage, current, electrochemical impedance, capacitance, or electrochemiluminescence. The electrochemical method thus is classified according to these detection signals as potentiometry, voltammetry, amperometry, electrochemical impedance (or impedimetry), capacitance, and electrochemiluminescence methods. The most commonly used technique involves systematic control of either current or potential, hence, named as potentiostatic or galvanostatic methods. Voltammetry is a widely used potentiostatic method in electroanalytical techniques. The sub-categories of voltammetry such as cyclic voltammetry, linear sweep voltammetry, and differential pulse voltammetry are utilized for the trace level detection of analytes in the present study. In addition, to have a better insight into the electrochemical mass transfer kinetics at the employed electrodes, the electrochemical impedance spectroscopy was also included in the study for the preliminary electrochemical characterization of the electrodes before electrochemical detection of the target pollutants.

### **2.4.1. Electrochemical impedance spectroscopy**

Electrochemical impedance spectroscopy (EIS) is an electrochemical technique that measures the impedance of a system depending on the frequency of AC (alternating current) potentials. The impedance is an electrical parameter used in real-world circuit elements that exhibit complex behaviours, unlike the ideal resistor. Similar to resistance, impedance is also a measure of the circuit's potential to resist the current flow. However, it is not limited by the ideal resistor properties such as independence of frequency, fulfilment of Ohm's law at all levels of voltage and current, and lastly, the phase coherence of current and voltage signals through the

resistor. While resistance is the ratio of voltage/potential and current for a direct current (DC) system, the impedance is the ratio of voltage/potential and current for AC systems. Usually, it is measured by the application of an AC potential to an electrochemical cell and then measuring the current through the cell. Assuming that we apply a sinusoidal potential excitation, the response to this potential is an AC signal. This current signal is analysed as a sum of sinusoidal functions (a Fourier series). Electrochemical impedance is normally measured using a small excitation signal so that the response of the cell is pseudo-linear. In a linear (or pseudo-linear) system, the current response to a sinusoidal potential will be a sinusoid at the same frequency but shifted in phase. Therefore, it behaves like a wave, and because of this nature, it is necessary to define impedance with two parameters which are (i) total impedance ( $Z$ ) and (ii) phase shift ( $\Phi$ ). These are expressed in the impedance spectra in the form of Nyquist plots and Bode plots. The expression for  $Z(\omega)$  (where  $\omega$  is angular velocity of current;  $\omega = 2\pi\nu$ ; where  $\nu$  is the frequency) is made up of two components - real and imaginary components. In the Bode plot, the impedance is plotted against log frequency on the X-axis and absolute impedance values ( $|Z|=Z_0$ ) and phase-shift on the Y-axis. A "Nyquist Plot" is obtained by plotting the real component on the X-axis and the imaginary component on the Y-axis of the graph (Cf Figure 2.1). The Y-axis is negative in this plot, and each point on the Nyquist Plot represents the impedance at a given frequency. Fitting EIS data to an equivalent electrical circuit model is a common method of analysing EIS data. The majority of the circuit elements in the model are standard electrical components such as resistors, capacitors, and inductors. In EIS experiments of real samples, capacitors frequently do not behave ideally. Rather, they function as a constant phase element. These circuit components relate to certain electrochemical properties such as solution resistance, double layer capacitance, polarization resistance, charge transfer resistance, etc. which are important factors in the impedance of electrolytic cells. Thus, by fitting experimental EIS data collected from electrolytic cells to a suitable electrical circuit model, the values of these electrochemical parameters are optimized by the least square fitting method and accordingly the equivalent circuit is obtained.

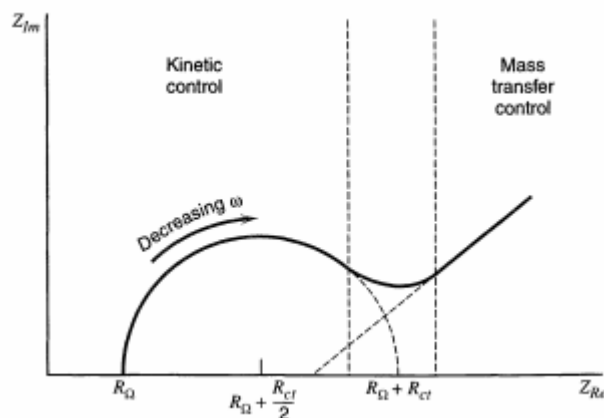


**Figure 2.1.** Nyquist impedance plot for an electrochemical system. Regions of mass-transfer and kinetic control are found at low and high frequencies, respectively (Bard and Faulkner, 1980).

#### 2.4.2. Cyclic voltammetry and linear sweep voltammetry

Cyclic voltammetry (CV) is a widely used electrochemical technique that is based on a linear potential waveform, which means that the potential changes as a linear function of time and the rate at which potential changes over time is called the scan rate. Linear sweep voltammetry (LSV) is the most basic technique that employs the waveform. The potential range is scanned from the initial potential to the final potential. The recorded linear sweep voltammograms are affected by several factors, including the rate of electron transfer reaction (s), the electroactive species and its chemical reactivity, and the voltage scan rate. CV is an extension of LSV in that the potential scan direction is reversed at the end of the first scan (the first Switching Potential) and the potential range is scanned again in the opposite direction. The experiment is terminated at the final potential, or the potential is scanned past it to the second switching potential, where the direction of the potential scan is reversed once again. For several cycles, the potential is cycled between the two switching potentials before the experiment is terminated at the final potential. In these techniques, the potential applied to the working electrode is higher or more positive than the potential of a redox couple in the electrolytic solution, the corresponding species are oxidized,

with electrons flowing from the solution to the electrode, resulting in an anodic current. On the return scan, as the working electrode potential approaches the redox couple's reduction potential, reduction i.e., electrons flowing away from the electrode, occurs, resulting the cathodic current. The magnitude of these faradaic currents gives information on the rate of the overall rate of the various processes occurring at the working electrode surface. The magnitude of these faradaic currents provides information on the overall rate of the various processes taking place at the working electrode surface. Further, the reversibility of the coupled reduction and oxidation events are also be assessed using the peak potential ( $E_{pa}$  and  $E_{pc}$ ) and peak current ( $i_{pa}$  and  $i_{pc}$ ) values for both oxidation and reduction processes. Using the relation from the Nernst equation, if  $\Delta E_p$  (i.e.,  $E_{pa} - E_{pc}$ ) is equal to  $59/n$  mV ('n' is the number of electrons involved) at various scan rates, the system is considered reversible, but if it is greater than  $59/n$  mV and increases with scan rate, the system is called quasi-reversible. The absence of a reverse peak in the cyclic voltammogram is considered as chemical irreversibility of the system, but may not necessarily electron transfer irreversibility. Moreover, larger values of  $\Delta E_p$  indicate slower electron transfer kinetics.

#### **2.4.3. Differential pulse voltammetry**

The differential pulse voltammetry (DPV) technique is based on measuring the differences in the rates of charging and faradaic current decay when a potential pulse is applied. It uses the faradic current as a function of time during the scanning. The potential is scanned with a series of pulses, and the current is measured at the start and end of each one. In other words, the signal in differential pulse voltammetry is the difference between two signals – the signal immediately before the pulse and the signal immediately after the pulse. Each pulse is fixed with a small amplitude, and the current produces a peak-shaped voltammogram. Comparing to CV and LSV, the DPV technique provides improved selectivity for observing various redox processes. This technique possesses high sensitivity and is often used to estimate the qualitative and quantitative values of redox species. It is often used with the stripping method

(cathodic or anodic stripping) in which the analyte of interest is accumulated at the electrode surface in a preconcentration process during which a negative potential is applied for a specified time and then stripped back to the solution when more positive scan potential is applied. This final step produces a peak current in the anodic region, called an anodic peak current. This process is often utilized in the detection of heavy metals and organic compounds as well.

## **2.5. PREPARATION OF MATERIALS**

### **2.5.1. Leaf extract of *Persea americana***

Fresh leaves of locally grown *Persea americana* (Avocado) were collected from Hlimen, Aizawl City, India. (N23.683222, E092.714749). Leaves were washed 2 to 3 times using purified water and dried in an oven at 60 °C. The dried leaves were crushed with mortar and pestle. 20 g of crushed leaves were taken in a beaker and added 200 mL of deionized water. The mixture was heated at 80 °C for about 30 mins. The resulting aqueous leaves extract (about 80 mL) was then allowed to cool down at room temperature, filtered with Whatman filter paper (20 µm pore size), and then stored in refrigerator for subsequent use.

### **2.5.2. Phytochemical screening**

Screening of phytochemical contents of the aqueous extract was performed qualitatively based on colouring and precipitation reactions. Various tests for the phytochemical contents of the extract were conducted using the standard protocols reported elsewhere (Chandraker *et al.*, 2020; Auwal *et al.*, 2014; Obouayeba *et al.*, 2015).

**1) Test for alkaloids:** In 1 mL of extract solution, slowly 6-8 drops of Mayer's reagent were added. This gives a cream precipitate which confirmed the presence of alkaloids. Mayer's reagent was prepared by dissolving 5 g of potassium iodide and 1.358 g of mercuric chloride in 100 mL distilled water (Sanghani, 2017).

**2) Test for flavonoids:** 1 mL of the extract was taken in a test tube and added few drops of neutral ferric chloride solution to it. The formation of black-red precipitate confirmed the presence of flavonoid.

**3) Test for tannins:** 2 mL of 5% ferric chloride and 1 mL of extract was vigorously mixed in a test tube. This gives a greenish-black/dark blue colour, which confirmed the presence of tannins in extract solution.

**4) Test for phlobatannins:** 10 mL of extract solution was boiled with 2-3 mL of 10% HCl for 5 mins. The formation of a red precipitate confirmed phlobatannin contents in the extract solution.

**5) Test for triterpenes:** The test was done with Salkowski test where equal volumes of chloroform and leaf extract were shaken with few drops of concentrated  $\text{H}_2\text{SO}_4$ . The lower layer turned yellow, which confirmed the presence of triterpenes.

**6) Test for saponins:** 1 mL extract was shaken vigorously with 2 mL distilled water and the persistence of foam indicated saponin contents.

**7) Test for glycosides:** 1 mL extract was added with 2-3 drops of Molisch's reagent followed by few drops of conc.  $\text{H}_2\text{SO}_4$ . A reddish-purple ring on the junction showed the presence of glycosides. Molisch's reagent was prepared by dissolving 20 g naphthol in 100 mL of ethanol (Sanghani, 2017).

**8) Test for anthocyanins:** 2 mL of plant extract was mixed with 2 mL of 2 mol/L HCl. The presence of anthocyanins was indicated by the development of a pink-red tint that becomes purple-blue when ammonia solution is added.

**9) Test for reducing sugars:** In a test tube, 2 mL of aqueous leaf extract solution was taken and 5 mL of a mixture solution containing equal volumes of Fehling's solutions A and B is added slowly (Fehling's solution A is an aqueous blue solution of copper (II) sulphate, while Fehling's solution B is a clear solution of aqueous potassium

sodium tartrate and a strong base, mostly sodium hydroxide). The solution mixture was heated for about 2 mins in a water bath. The presence of reducing sugars was confirmed by occurrence of brick-red precipitate.

**10) Test for polyphenols:** Two drops of alcoholic solution of 2 percent ferric chloride were added with 2 mL of plant extract. The presence of polyphenolic chemicals was indicated by a more or less dark blackish-blue or green colour.

### **2.5.3. Synthesis of nanoparticles**

Synthesis of Ag nanoparticles (Ag(NP)) and Au nanoparticles (Au(NP)) was conducted by chemical reduction method using aqueous leaf extract of *Persea americana* as a reducing agent. 20 mL each of AgNO<sub>3</sub> or AuCl<sub>3</sub> solution (2 mmol/L) was taken in a beaker and a 0.2 mL aliquot of the leaf extract is added slowly to it. The solutions mixture was stirred at 500 rpm and heated at 50 °C for 60 mins. The initial metal precursor and leaf extract solution are almost colourless (or slight/dull yellowish) but a distinct colour change was noticed with a lapse of time and finally a dark yellow and purple colour was observed for Ag and Au nanoparticles, respectively. These colour changes are attributed to the formation of colloidal nanoparticle solutions due to the reduction of Ag<sup>+</sup> to Ag<sup>0</sup> and Au<sup>3+</sup> to Au<sup>0</sup>. Various phytochemicals present in the leaf extract are assumed to be potentially active to reduce the metal precursor ion to zerovalent state as well as to stabilize in the prevention of aggregation of nanoparticles by capping it. The UV-Visible spectra of the resulting Ag(NP) and Au(NP) colloidal solutions were then subjected for obtaining the absorption spectra recorded within the wavelength range of 300-600 nm and 400-800 nm, respectively. Measurements were taken in a quartz cuvette having a path length of 1 cm using ultrapure water as a blank.

### **2.5.4. Synthesis of nanocomposite materials**

The commercially available bentonite (BN) was thoroughly washed with deionized water for the elimination of sand particles and other particulate impurities



and dried at 90 °C in a drying oven. The organic silane-modified bentonite clay was obtained by the grafting of silane with the clay network under a non-aqueous medium. Further, utilizing a simple wet impregnation procedure, the nanocomposite material was decorated with the Ag or Au nanoparticles. The dried bentonite was sieved (BSS No. 325) and 15 g of it was dispersed in 200 mL of toluene and the mixture was stirred for 15 mins and then 10 mL of trichloro(octadecyl) silane is slowly added in it. The solution is stirred and refluxed for 24 hrs at 80 °C in an N<sub>2</sub> atmosphere. The slurry was cooled at room temperature and toluene was decanted. The silane grafted bentonite (TCBN) was collected, washed with ethanol, and then dried in a drying oven at 60 °C for 24 hrs. TCBN was further decorated with the biosynthesized Ag(NP) or Au(NP) separately by a simple wet impregnation process. 10 g of TCBN was taken in a beaker and then 50 mL of ethanol was added. It was shaken mechanically for 10 mins. Further, 5 mL of freshly prepared Ag(NP) colloidal solution was added and stirred for 24 hrs at 50 °C. This enabled to decorate the nanocomposite with Ag(NP). The solid was washed with purified water and dried at 60 °C. The solid was finally collected and termed as Ag(NP)/TCBN. Similarly, the Au(NP) decorated nanocomposite was obtained and termed as Au(NP)/TCBN. The synthesized nanocomposite materials were then characterized by various analytical tools *viz.*, FT-IR, SEM-EDX, TEM and AFM analyses.

## **2.6. CHARACTERIZATION OF MATERIALS**

UV-Visible spectrophotometer (Model: UV-1800; Shimadzu, Japan) was used to obtain the absorbance spectra of synthesized Ag(NP)/or Au(NP) colloidal solutions. Fourier Transform- Infra-Red (FT-IR) spectra for the pristine bentonite and other synthesized nanocomposite materials were recorded using a FT-IR Spectrometer (IR Affinity-1S, Shimadzu, Japan). The surface morphology of nanocomposite casted on glassy carbon plates were obtained by Scanning Electron Microscope/Energy Dispersive X-ray Analysis (SEM-EDX) (Model: Oxford xmax) while powder forms of the nanocomposite are used for Transmission Electron Microscope (TEM) (Model:

Oxford xtreme) analysis. Further, the surface roughness of the nanocomposite casted on glassy carbon plates were obtained using atomic force microscopy (AFM) (Model: Multi Mode 8, Bruker, USA).

## **2.7. FABRICATION OF MODIFIED ELECTRODES**

### **2.7.1. Carbon paste electrode**

Carbon powder and bentonite (BN) or nanocomposite (TCBN) powder were used to make the working electrodes. The carbon powder was mixed with the pristine bentonite/or nanocomposite having the ratio of 6:1 (w/w). Furthermore, the powders of these two materials are thoroughly mixed, and a paste was made using 1 g of paraffin oil. The paste was manually introduced and packed into a Teflon tube having 5 cm and 0.21 cm of length and radius, respectively. The top of the tube was sealed with a Teflon tape, and then a titanium wire was carefully inserted within the tube until half of the tube length. The tube's bottom end was kept open, ready to use as a working electrode. The open surface of the tube was rinsed with purified water, polished with glassy paper, and used for the electrochemical experiments. The open end of the tube was also cut with a sharp knife at the end of each experiment to create an unexposed active surface.

### **2.7.2. Glassy carbon electrode**

The modified glassy carbon working electrodes were fabricated by a simple drop-casting process. Before casting, the glassy carbon electrode was thoroughly polished by alumina (0.05  $\mu\text{m}$ ) followed by a diamond polishing solution using a polishing cloth. The polished surface of the glassy carbon electrode was again sonicated with ethanol solution followed by distilled water for 5 mins each to obtain an ultra-clean and mirror-like smooth surface of electrode. The casting solution is prepared by mixing 5 mg of the pristine BN/or the nanocomposite materials *viz.*, TCBN, Ag(NP)/TCBN, Au(NP)/TCBN separately in 4 mL of 1:1 DMF and double-

distilled water. The suspension was stirred for 24 hrs. Further, the solution mixture was ultrasonicated for 5 mins before performing the casting process. Finally, 2.5  $\mu\text{L}$  of the homogeneous mixture was dropped onto the cleaned and dry surface of GCE and dried at 40 - 50  $^{\circ}\text{C}$  for 15 mins. Similarly, the glassy carbon plate piece was used to cast the surface with these nanocomposite materials and intended for SEM/EDAX and AFM analyses.

## **2.8. ELECTROCHEMICAL PROCEDURES**

### **2.8.1. Electrochemical characterization of electrodes**

All fabricated micro-electrodes modified with the nanocomposite materials as well as the bare or unmodified electrode i.e., carbon paste electrode (CPE) or glassy carbon electrode (GCE) were characterized by electrochemical techniques using the cyclic voltammetry and electrochemical impedance spectroscopic studies using 0.001 mol/L  $\text{Fe}(\text{CN})_6^{3-}/\text{Fe}(\text{CN})_6^{4-}$  redox system prepared in 0.1 mol/L KCl as supporting electrolyte solution. Cyclic voltammograms at different scan rates i.e., from 50-200 mV/s (for carbon paste electrodes) and 20 to 150 mV/s (for glassy carbon electrodes) at a potential window of -0.5 V to 1.0 V were recorded for each electrode. Similarly, impedance spectra for the fabricated electrodes were collected in the redox probe solution between 80 kHz to 100 MHz at 6 points per decade with an amplitude of 10 mV. The EIS Nyquist plots are fitted using the equivalent circuit:  $R_1+Q_2/(R_2+W_2)$  where  $R_1$ ,  $Q_2$ ,  $R_2$ , and  $W_2$  representing the  $R_s$  (solution resistance),  $C_{dl}$  (double layer capacitance at solution and electrode interface),  $R_{ct}$  (Charge transfer resistance) and  $W$  (Warburg impedance) elements in the Randle's circuit, respectively. The equivalent circuit fitting and evaluation of the electrical parameters for each impedance spectra are performed with the EClab software based on the least square fitting method.

### 2.8.2. Electrochemical detection of pollutants

Detection of As(III) was carried out using the modified carbon paste electrode (TCBN/CPE). A known concentration of As(III) solution was prepared using the 0.1 mol/L KCl solution as background electrolytes. The KCl solution pH was adjusted using the 0.1 mol/L HNO<sub>3</sub> or NaOH solutions. The cyclic voltammetric (CV) and linear sweep voltammetric data were recorded at an exciting potential of +1.0 V and -0.2 V against an Ag/AgCl reference electrode. The CV data was recorded for three consecutive cycles and the second cycle was utilized for further calculations. The detection of other contaminants viz., Pb(II), Cd(II), sulfamethoxazole and sulfamethazine are conducted using the modified glassy carbon electrodes. The detection method was developed using the differential pulse stripping voltammetry. The supporting electrolyte solutions having 0.1 mol/L KCl in acetate buffer are utilized for analysing these contaminants in aqueous media. Cyclic voltammetric scans for Pb(II) and Cd(II) were carried out at a potential range of -1.2 V to 0.2 V and -1.5 V to 0.2 V, respectively, whereas a potential window of -0.2 to 1.2 V was used for sulfamethoxazole and sulfamethazine. pH dependence studies were conducted varying the solution pH 3.6-7.0 (in case of Pb(II) and Cd(II) using acetate buffer) and 2.0-9.0 (in case of sulfamethoxazole and sulfamethazine using mixed electrolyte solution of acetate buffer and KCl). The differential pulse anodic stripping voltammetry (DPASV) detection method is optimized for the deposition potential between -0.8 V to -1.3 V and deposition time of 30-300 s in the detection of these pollutants. All other conditions including pulse amplitude of 50 mV, scan increment of 10 mV, and pulse width of 50 ms is used for obtaining the voltammograms. All potentials for the entire experiments were recorded against the reference electrode (Ag/AgCl) at an ambient temperature of 25±1 °C. The electrolytic solutions are always purged with N<sub>2</sub> gas for 10 mins before conducting electrochemical experiments. Further, the limit of detection (LOD) and limit of quantification (LOQ) were obtained using the equations:  $LOD = 3 \frac{\sigma}{m}$  and  $LOQ = 10 \frac{\sigma}{m}$  where  $\sigma$  is the standard deviation of five replicates of blank solutions and 'm' is the slope of the calibration line ((Yola *et al.*, 2015; Duddukuru *et al.*, 2017; Shrivastava and Gupta, 2011)).

# **CHAPTER 3**

## **RESULTS AND DISCUSSION**

### 3. RESULTS AND DISCUSSION

#### 3.1. CHARACTERIZATION OF MATERIALS

##### 3.1.1. Phytochemical studies of *Persea americana* leaf extract

The qualitative screening for various phytochemical contents of aqueous *Persea americana* leaf extract revealed the presence of various phytochemical compounds (Cf Table 1). These compounds are assumed to serve as reducing agents for the reduction of  $\text{Ag}^+$  and  $\text{Au}^{3+}$  to  $\text{Ag}^0$  and  $\text{Au}^0$ , respectively. Moreover, it also acts as stabilizing or capping agents in the green synthesis of nanoparticles. It was reported previously that different parts of the Avocado are used for medicinal purposes and the secondary metabolite contents are utilized for antimicrobial purposes (Dabas *et al.*, 2013; Duarte *et al.*, 2016; Gupta *et al.*, 2018). Similar phytochemicals were found in methanolic extracts of *Persea americana* leaf and it was studied for the possible bacterial strains *Escherichia coli* and *Pseudomonas aeruginosa* (Ajayi *et al.*, 2017). In addition, Kumar and Cumbal (2016) performed FT-IR studies on extracts of the leaf, peel, pulp, and oil of Avocado in water emulsion and the IR-studies confirmed the presence of triglycerides, esters, olefins, polyphenols, and flavonoids (Kumar and Cumbal, 2016). The screening tests for flavonoids, saponins and tannins using concentrated HCl, distilled water and ferric chloride as reactors, respectively show strong positive results which confirmed the presence of these metabolites at high concentrations. (Rahman *et al.*, 2018).

**Table 3.1.** Qualitative phytochemical analysis of leaf extract of *Persea americana* leaves.

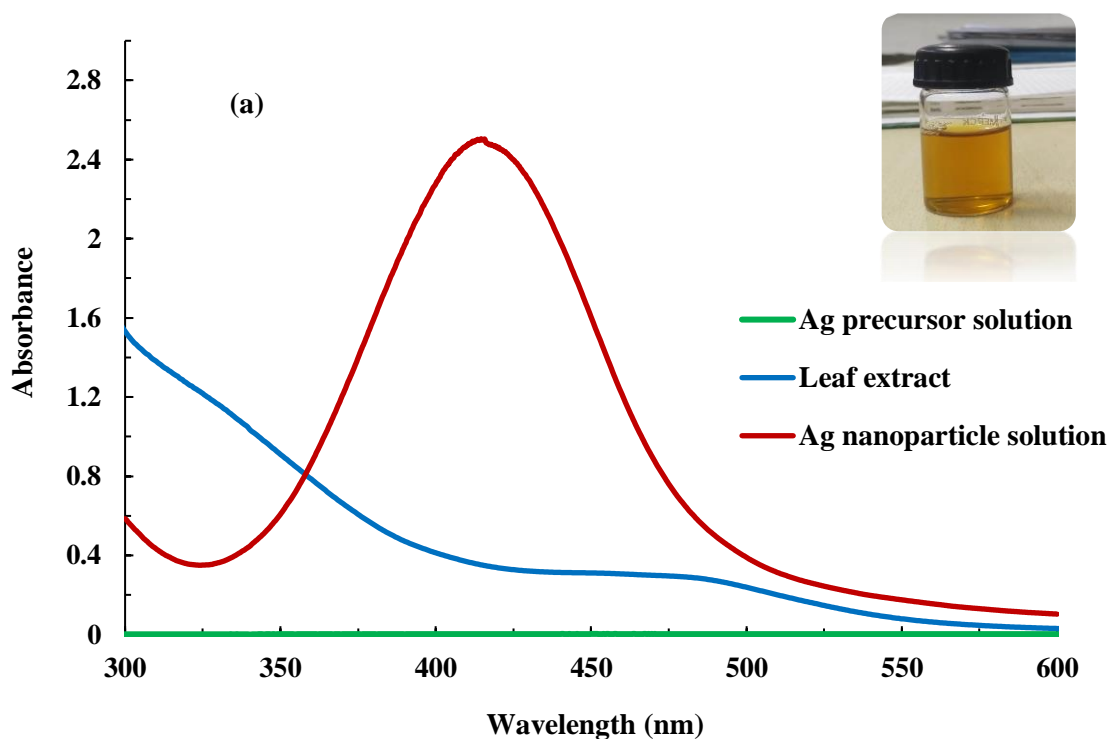
Phytochemicals	Test	Result
Alkaloids	Mayer's test	+
Tannins	Ferric chloride test	+
Phlobatannins	HCl test	-
Saponins	Foam test	+
Flavonoids	Ferric chloride test	+
Anthocyanins	HCl test	-
Glycosides	Molisch test	+
Reducing sugars	Fehling's test	+
Triterpenes	Salkowski test	+
Polyphenols	Ferric chloride test	+

(+) = present, (-) = absent

### 3.1.2. UV-Vis spectroscopic analysis of nanoparticles

The UV-Vis spectra for the colloidal solution of Ag and Au nanoparticles are presented in Figure 3.1(a & b). Figure clearly showed the surface plasmon resonance (SPR) peaks occurring at 414 nm and 550 nm, respectively for the Ag and Au nanoparticle colloidal solutions. This confirms the presence of silver nanoparticles (Ag(NP)) and gold nanoparticles (Au(NP)). Further, the positions of these surface plasmon resonance (SPR) peaks are rough estimates of the shape and size of the particles. It is known that the intensity, as well as the wavelength positions of SPR band, is dependent on several factors including the shape, size, and composition of particles and dielectric constant of medium environment that greatly affects the charge density of electrons on the surface of nanoparticle (Mie, 1908). Moreover, small-sized spherical silver nanoparticles give resonance band at *Ca* 350-500 nm region with peak position at 410 nm (Tsuji *et al.*, 2002; Murphy and Jana, 2002). Similarly, the small sized gold nanoparticles (*Ca* 9 nm) typically showed absorption maxima at around 520 nm and showed more redshift as the size of the particle

increases (Link and El-Sayed, 1999). Therefore, the observed absorption maxima of silver and gold nanoparticles colloidal solution suggested that the spherical and small-sized Ag and Au particles are formed in the biosynthesized process. The phytochemicals in the leaf extract are potentially active to reduce the metal precursor ions to zerovalent metals while acting as stabilizing and capping agents to prevent the aggregation of the synthesized nanoparticles. Hence, the leaf extract of *Persea americana* functions as a green chemical, suitable alternative to the toxic and reactive chemical often used in the conventional synthesis of nanoparticles.





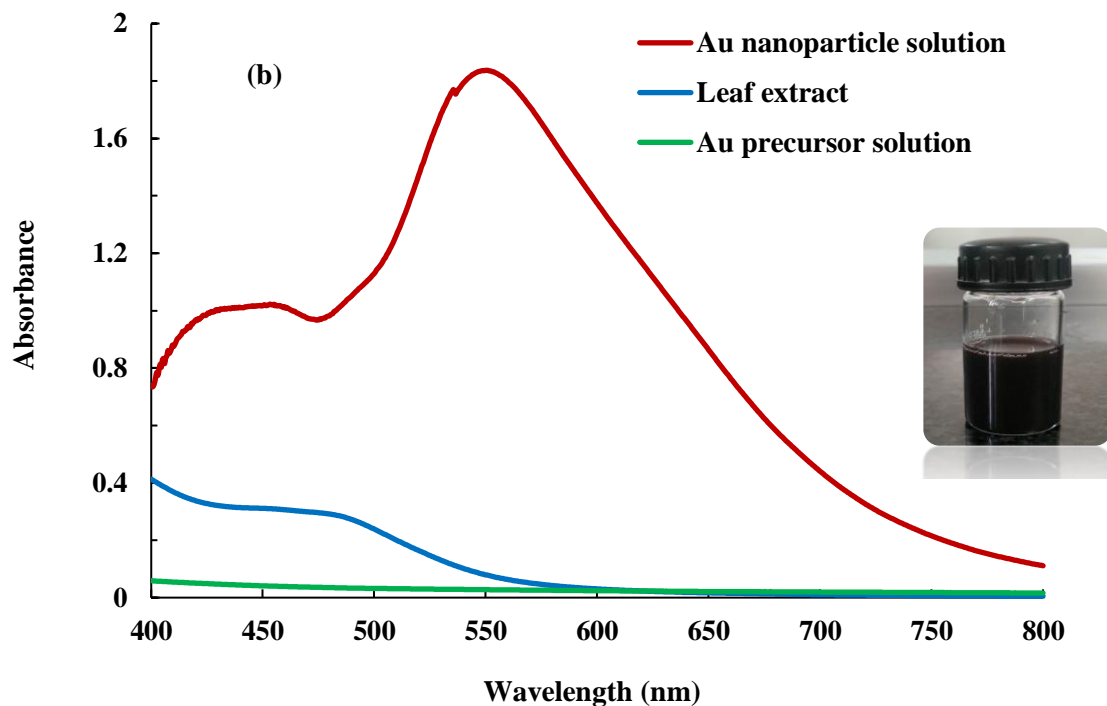


**Figure 3.1. (a-b)** UV-Vis spectra of (a) Ag precursor solution, *Persea americana* leaf extract and Ag nanoparticle solution (2.0 mmol/L); and (b) Au nanoparticle solution, *Persea Americana* leaf extract and Au<sup>3+</sup> precursor solutions (2.0 mmol/L) [Inset: Colloidal solution of gold nanoparticles].

### 3.1.3. Fourier transform infra-red (FT-IR) spectroscopy

FT-IR spectra of the pristine bentonite (BN) and nanocomposites *viz.*, TCBN, Ag(NP)/TCBN, and Au(NP)/TCBN are presented in Figure 3.2. IR results indicated that these solids showed common vibrational peaks at 1652 cm<sup>-1</sup> and 3423 cm<sup>-1</sup> which is assigned to the bentonitic water -OH stretching and bending vibrations. Similarly, the vibrational peaks occurred at 1124 cm<sup>-1</sup>, 3703 cm<sup>-1</sup>, and 3623 cm<sup>-1</sup> are primarily due to the Al-OH and Si-OH bending and stretching vibrations (Alkaram *et al.*, 2009). Further, Si-O-Si and Si-O-Al linkages in clay structure results in-plane and out-plane vibration bands of Si-O which is occurred at 927 cm<sup>-1</sup> and 1003 cm<sup>-1</sup>. Further, additional Si-O quartz vibrations are occurred at 810 cm<sup>-1</sup> and 702 cm<sup>-1</sup> (Jović-Jovićić *et al.*, 2013). However, additional peaks are observed at 2924 cm<sup>-1</sup> and 2862 cm<sup>-1</sup> in the IR spectra of TCBN, Ag(NP)/TCBN, and Au(NP)/TCBN which is

because of the asymmetric and symmetric stretching vibrations of the C–CH<sub>2</sub> group from the alkyl chain of the silane. Similarly, the scissoring oscillations of an aliphatic chain of the organic silane are observed at 1473-1481 cm<sup>-1</sup> (Alkaram *et al.*, 2009). Therefore, these results confirmed that the organic silane (TCODS) is successfully grafted with the bentonite structure.

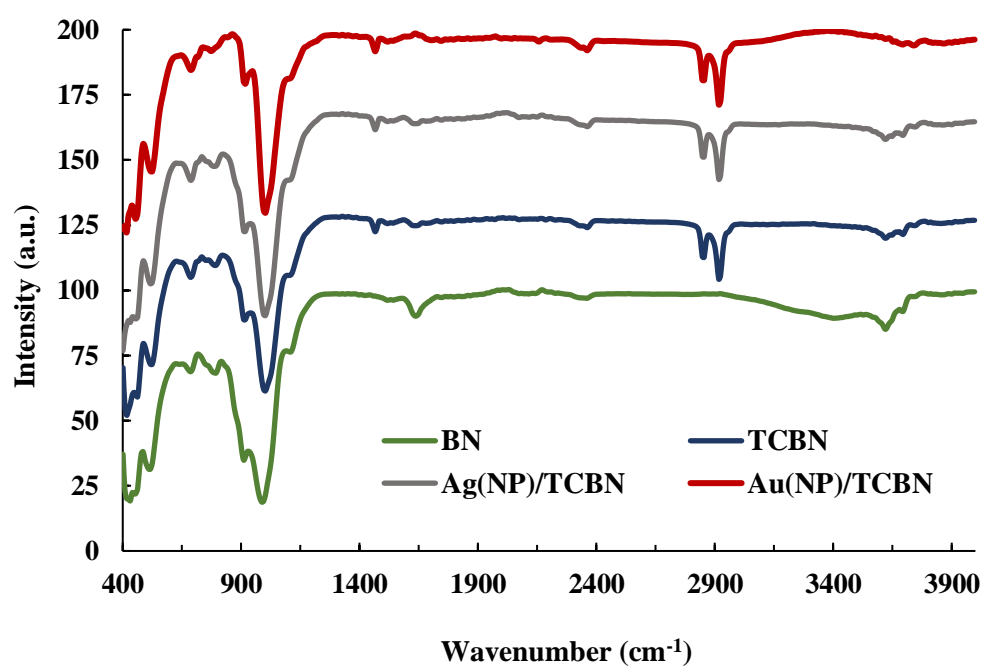


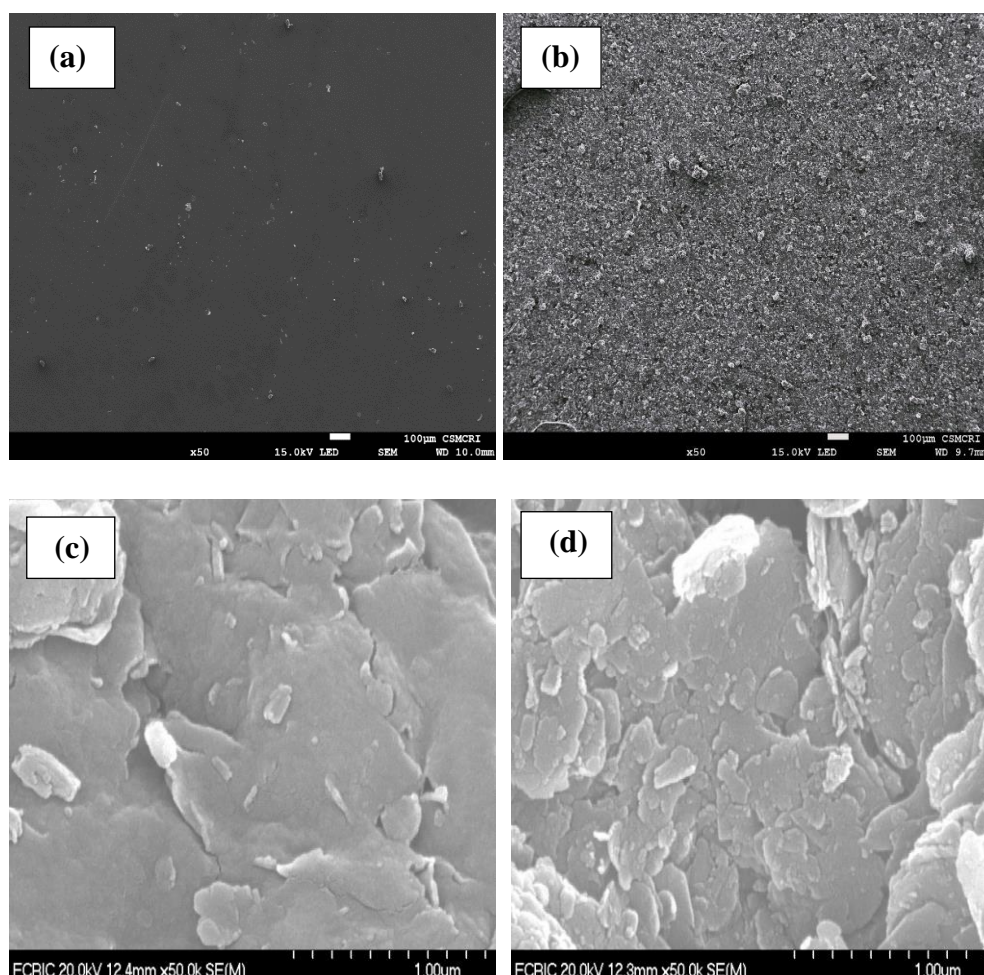
**Figure 3.2.** FT-IR spectra of pristine bentonite and nanocomposite materials (TCBN, Ag(NP)/TCBN and Au(NP)/TCBN).

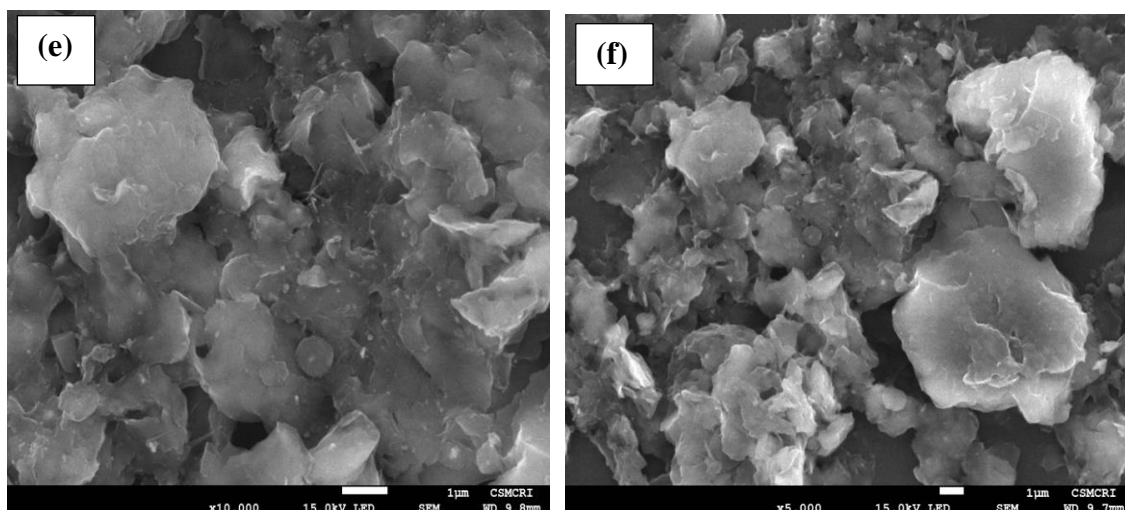
#### 3.1.4. Surface morphological studies of materials

Surface morphology of the pristine bentonite or nanocomposites coated glassy carbon plate is obtained by the scanning electron microscopic (SEM) analyses. SEM images of the bare glassy carbon plate and coated glassy carbon plates (i.e., coated with BN, TCBN, Ag(NP)/TCBN and Au(NP)/TCBN) are obtained and shown in Figure 3.3. Figure 3.3(a & b) shows the SEM images of bare glassy carbon plate. This clearly showed that the surface of glassy carbon is very smooth and no aggregation of impurity is observed on the surface. Further, the SEM micrographs of pristine bentonite (BN) and silane grafted bentonite (TCBN) coated glassy carbon sheets are shown in Figures 3.3(c & d). The image clearly shows that pristine bentonite possesses a uniform but heterogeneous structure, with silica contents visible on the surface. Furthermore, the layers of bentonite on the surface are well arranged and also reveals a porous structure with large smooth flakes. On the other hand, the nanocomposite (TCBN), exhibited a more disordered structure and increased heterogeneity on the solid surface. It is clear that the organic silane molecules have occupied spaces within the clay layers and grafted with the terminal -OH group of bentonite. Moreover, the material is more compact, and less porosity is observed. Similar observations were reported with 3-aminotriethoxysilane grafted bentonite (Abeywardena *et al.*, 2017). A decrease in BET (Brunauer, Emmett and Teller) specific surface area and increase in pore volume and pore size of HDTMA (hexadecyltrimethylammonium bromide) modified clay was reported elsewhere (Thanhmingliana *et al.*, 2016). Decrease in specific surface area of the modified clay in comparison to the bare clay was attributed to the presence of HDTMA cation at the clay interspace which on the other hand, allow the interlayers to prop up and led to increased pore volume and size of the clay solids (Thanhmingliana *et al.*, 2016).

Similarly, the SEM micrographs are obtained for the silver and gold nanoparticles decorated nanocomposite materials i.e., Ag(NP)/TCBN and Au(NP)/TCBN is coated on the surface of glassy carbon plate and shown in Figure 3.3(e & f). The porous nanocomposites are equally dispersed throughout the glassy carbon surface and the roughness of the surfaces is quite diverse. Small porous aggregates are visible on the Ag(NP)/TCBN and Au(NP)/TCBN coated glassy

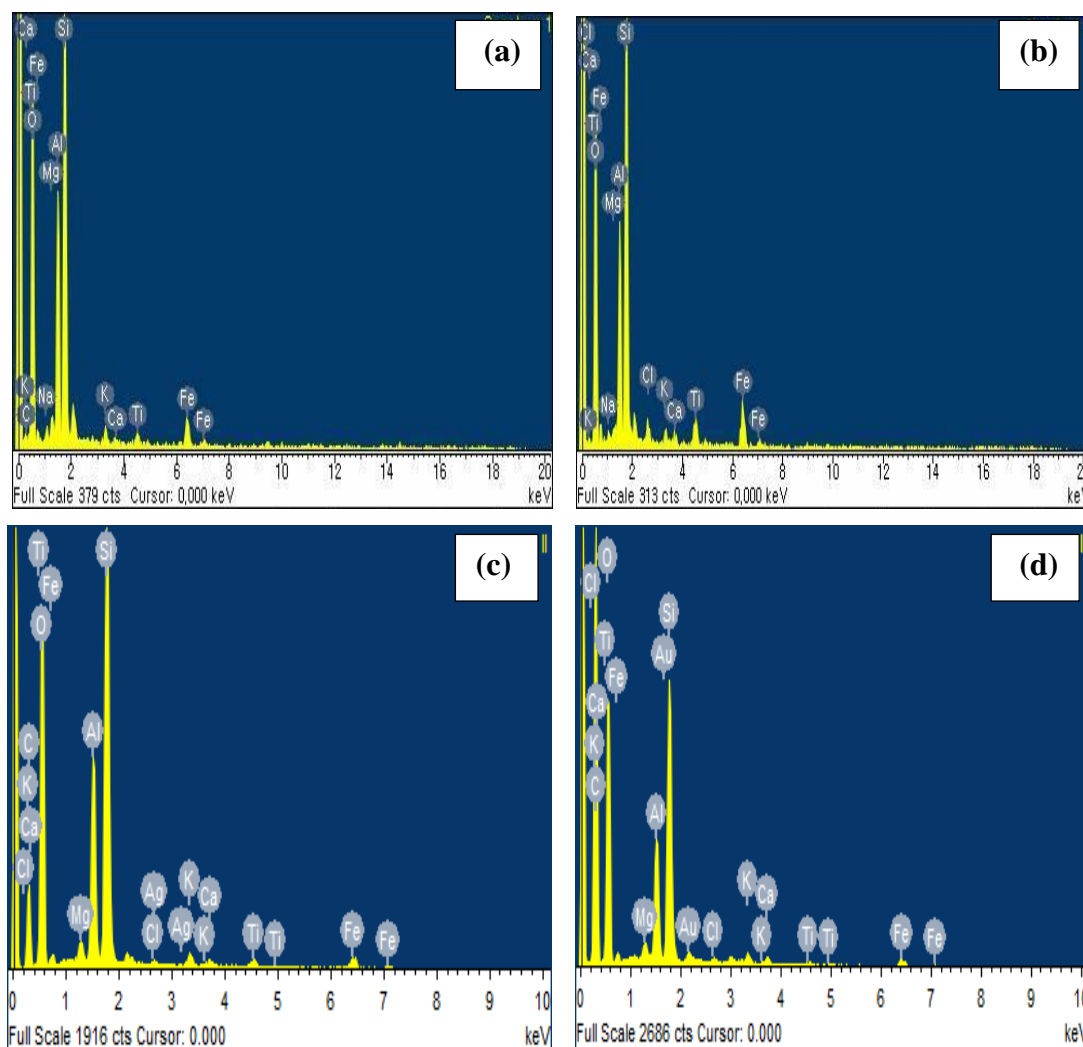
carbon surfaces. This is, perhaps, due to additional bonding pockets facilitating agglomeration. Further, the tiny dots are visible on the surfaces indicating the presence of Ag or Au nanoparticles (Figures 3.3(e & f)). The silver and gold nanoparticles are very evenly distributed on the respective surfaces. The *in situ* decoration of the silver and gold nanoparticles enabled even distribution of these nanoparticles also restricted the agglomeration of nanoparticles onto the composite surfaces. Similarly, the SEM images of silver and gold nanoparticle doped titania film on borosilicate disks showed smooth surface that displayed fine-grains of small-sized  $\text{TiO}_2$  and an apparent distribution of the doped silver or gold particles on the titania framework (Lalliansanga *et al.*, 2018; Tiwari *et al.*, 2019a).





**Figure 3.3.(a-f)** Scanning electron micrographs (SEM) of (a & b) bare glassy carbon sheet; (c) pristine bentonite coated glassy carbon sheet; (d) silane grafted bentonite (TCBN) coated glassy carbon sheet; (e) Ag(NP)/TCBN coated glassy carbon sheet; and (f) Au(NP)/TCBN coated glassy carbon sheet.

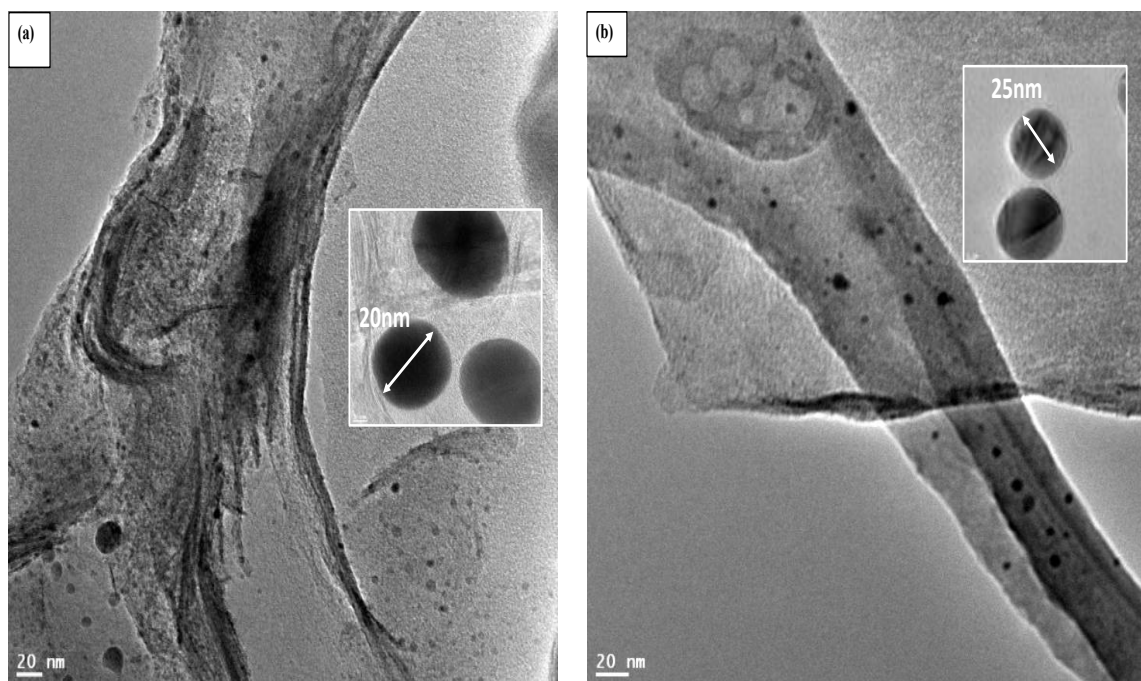
Further, Figure 3.4 (a-d) shows the results of the energy dispersive X-ray (EDX) analysis for the samples pristine bentonite (BN), TCBN, Ag(NP)/TCBN, and Au(NP)/TCBN coated glassy carbon sheets. The EDX elemental mapping revealed that very distinct peaks of Si, O, Fe, Mg, Na, C is observed in all these samples including the bentonite coated sheet (*Cf* Figure 3.4(a)). Further, the TCBN coated sheets showed additional EDX peak for Cl which confirms the presence of silane (trichloro-octadecyl silane) with the bentonite (*Cf* Figure 3.4(b)). This infers the grafting of silane with bentonite network. On the other hand, the EDX elemental mapping of the Ag(NP)/TCBN and Au(NP) coated sheets showed additional peaks of Ag and Au, respectively (*Cf* Figure 3.4(c & d)). Hence, the EDX elemental mapping reaffirms the presence of silver and gold nanoparticles with in the nanocomposite solid.



**Figure 3.4.(a-d)** EDX elemental mapping for the (a) pristine bentonite (BN); (b) TCBN Composite; (c) Ag(NP)/TCBN; and (d) Au(NP)/TCBN coated glassy carbon sheets.

The Ag(NP)/TCBN and Au(NP)/TCBN nanocomposite powder samples are then utilized for the TEM analysis and the TEM images are displayed in Figure 3.5 (a-d). The TEM images revealed that Ag(NP) and Au(NP) are distinctly but uniformly distributed throughout the nanocomposite (*Cf* Figure 3.5(a & b). Moreover, the nanoparticles *viz.*, Ag(NP) and Au(NP) are not aggregated or agglomerated within the nanocomposite solid. Further, it is interesting to observe that the silver and gold nanoparticles are spherical in shapes and the average size of the

particle is 20-25 nm (*Cf* Figure 3.5(a & b) insets). The shape and size of the nanoparticles are in consistent to the results with the UV-vis absorption spectra of the Ag(NP) and Au(NP) colloidal solutions, which showed SPR absorption maxima at 414 nm and 550 nm. Furthermore, the d-spacings of the Ag(NP) and Au(NP) are obtained using the TEM fringes and are found to be 0.12 and 0.25 nm, respectively (*Cf* Figure 3.5(c & d)).





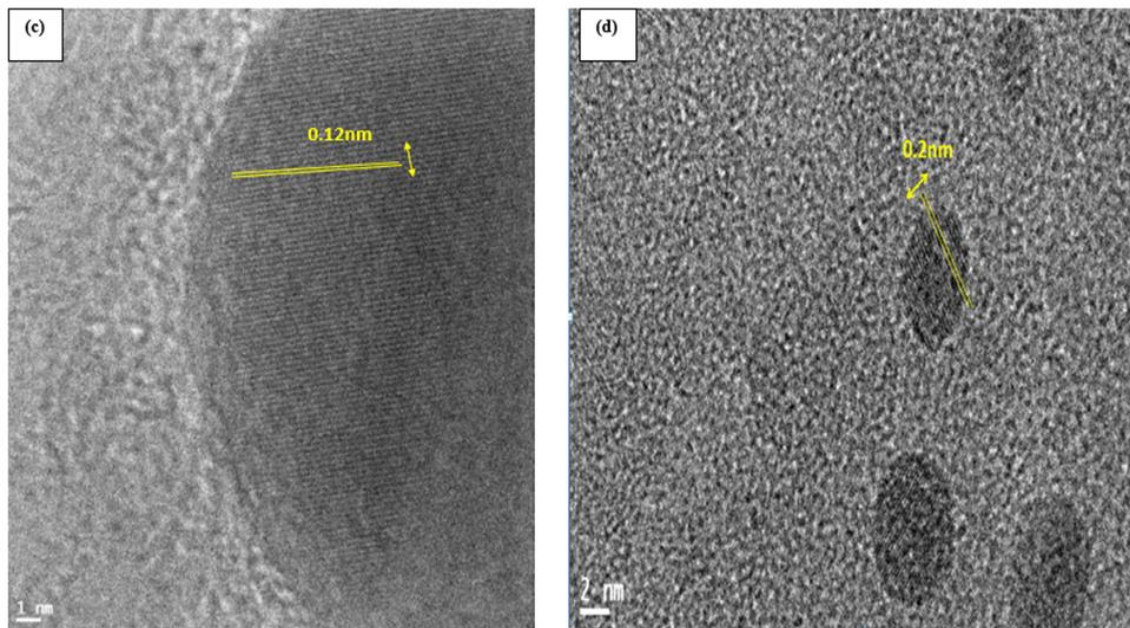


**Figure 3.5.(a-d)** TEM micrographs of (a) Ag(NP)/TCBN; and (b) Au(NP)/TCBN materials and the d-spacings of (c) Ag(NP)/TCBN; and (d) Au(NP)/TCBN materials.

In addition, the surface roughness of Ag(NP)/TCBN and Au(NP)/TCBN nanocomposites coated glassy carbon sheets are subjected for the atomic force microscopic (AFM) analysis and results are depicted in figure 3.6 (a & b). 3D images of these samples showed that the surface is quite uneven and disordered. Moreover, the nanocomposite solids are forming fine pillars on the surface of glassy carbon plate (Cf figure 3.6 (a & b)). Further, the arithmetic average roughness ( $R_a$ ) and root mean square average of the profile heights over the evaluation length ( $R_q$ ) is found to be 17.6 nm and 22.8 nm (for Ag(NP)/TCBN coated glassy carbon sheet) and 11.9 nm, 15.5 nm (for Au(NP)/TCBN coated glassy carbon sheet), respectively. Moreover, the image  $Z_{range}$  is taken as 181 nm and 251 nm, respectively for the Ag(NP)/TCBN and Au(NP)/TCBN nanocomposites coated sheets (Cf. Figure 3.6 (c & d)). It was reported previously that the heterogeneous surface structure of Ag(NP)/TiO<sub>2</sub> thin film as coated on borosilicate glass disk showed the  $R_q$  and  $R_a$  values of 16.95 nm and 12.25 nm, respectively (Lalliansanga *et al.*, 2020). Similarly, the 3D-AFM results of gold nanoparticle doped TiO<sub>2</sub> disk possessed fairly high heterogeneity and the  $R_q$  and  $R_a$  values of the nanostructure were found to be 124.33 nm and 94.65 nm, respectively (Tiwari *et al.*, 2019b).



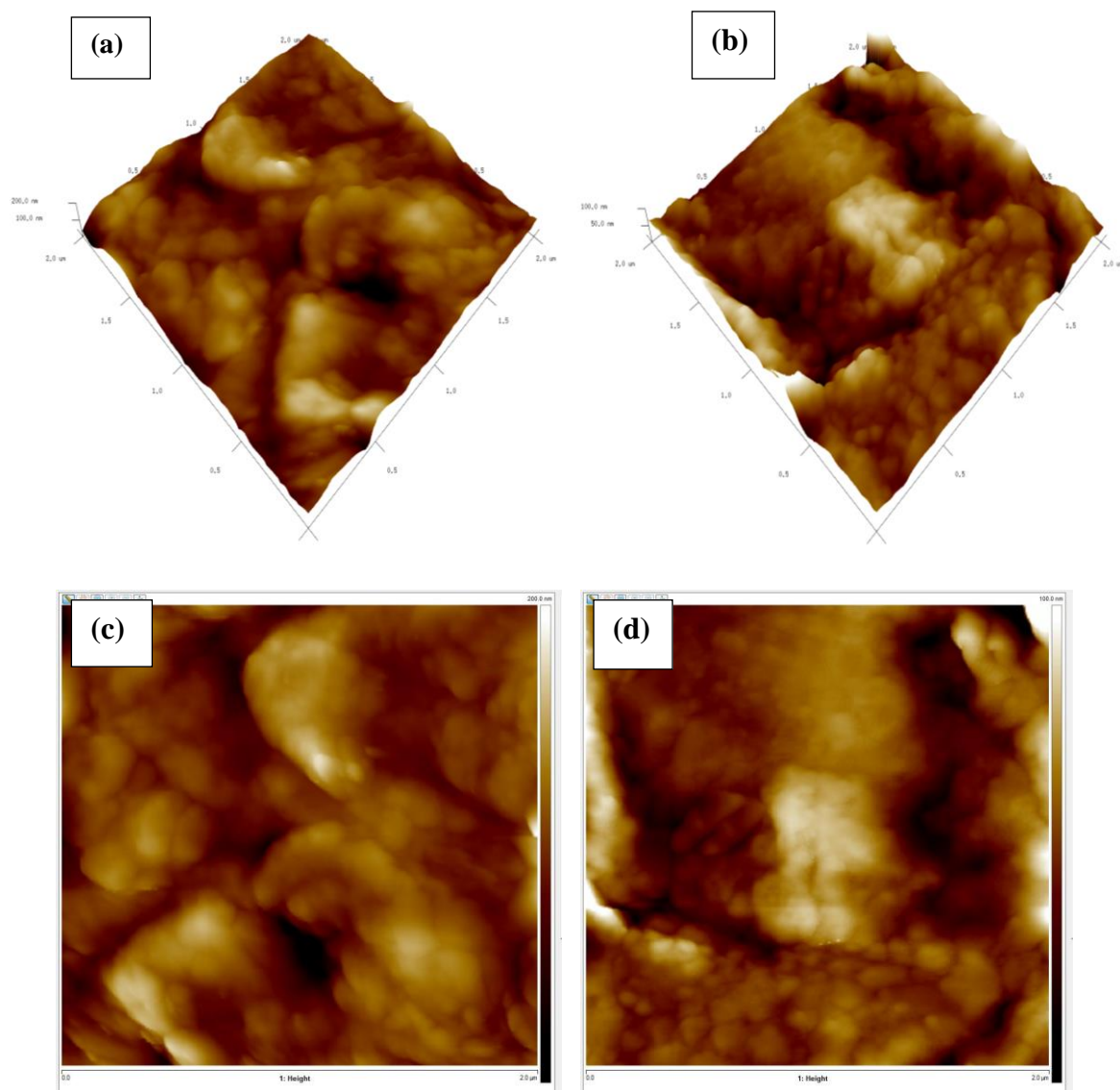


**Figure 3.6.(a-d)** 3D-AFM images of (a) Ag(NP)/TCBN; (b) Au(NP)/TCBN coated carbon sheets and surface roughness of (c) Ag(NP)/TCBN; and (d) Au(NP)/TCBN coated carbon sheets.

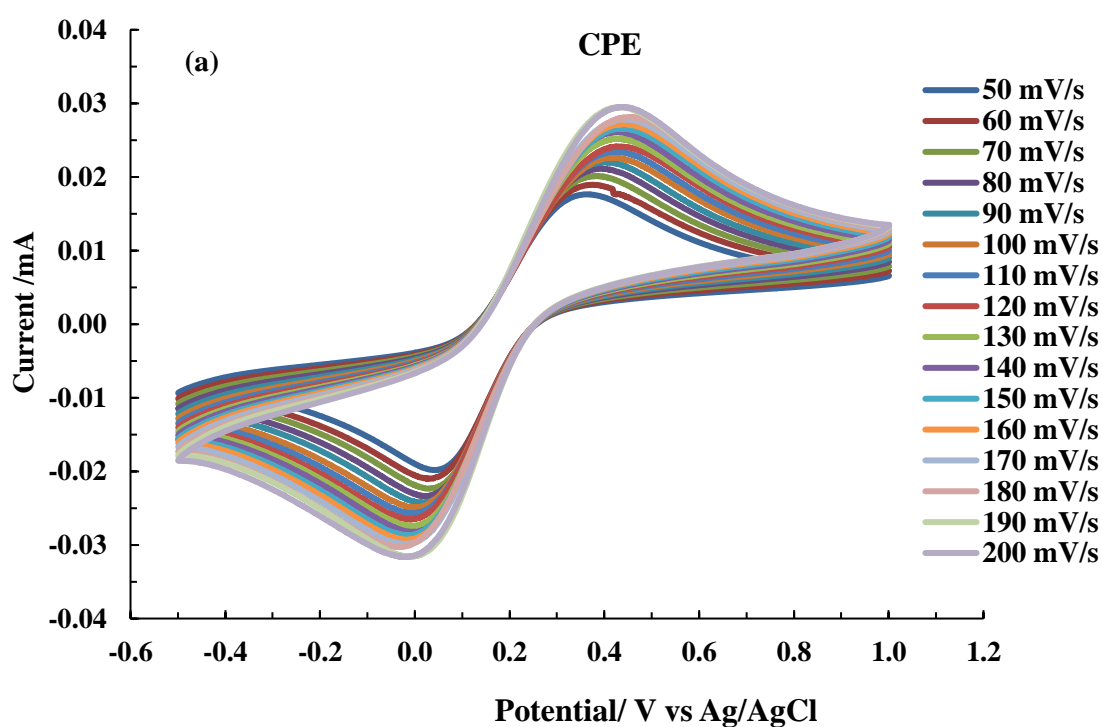
### 3.2. ELECTROCHEMICAL STUDIES USING CARBON PASTE ELECTRODES

The electrochemical measurements using bare carbon paste electrode (CPE), pristine bentonite modified carbon paste electrode (BN/CPE), and silane grafted bentonite modified paste electrodes (TCBN/CPE) were carried out for detection of arsenic using the cyclic voltammetric technique. Before detection experiments were performed, the fabricated carbon paste electrodes were electrochemically studied using the cyclic voltammetric and electrochemical impedance spectroscopic studies. In order to study the characteristics of electrodes in the mass transfer reactions, the scan rate studies were conducted varying the scan rates from the 50 mV/s to 200 mV/s at an excitation potential window of -0.5 to 1.0 V. Impedance spectroscopic data was collected in 0.001 mol/L  $\text{Fe}(\text{CN})_6^{3-}/\text{Fe}(\text{CN})_6^{4-}$  solution having the background electrolyte concentration of 0.1 mol/L KCl. The frequency range was employed as 80 kHz to 100 MHz with 6 points per decade at an employed 10 mV peak to peak sinusoidal potential.

#### 3.2.1. Scan rate studies using cyclic voltammetry

The electrochemical performance of the working electrodes *viz.*, carbon paste electrode (CPE), bentonite modified CPE, and nanocomposite modified CPE are studied using the standard redox probe (0.001 mol/L  $\text{Fe}(\text{CN})_6^{3-}/\text{Fe}(\text{CN})_6^{4-}$ ) employing the cyclic voltammetry. The cyclic voltammograms for various electrodes are illustrated in Figure 3.7(a-c). The figures clearly indicated that these working electrodes possessed well-defined electrochemical performance for the redox process to take place since the pronounced cathodic and anodic peaks were obtained with the voltammograms. Further, the electrochemical response with the TCBN/CPE was significantly increased (Figure 3.7(c)) since the cathodic and anodic peak currents are significantly increased compared to the BN/CPE or bare CPE electrodes. Moreover, the peak-to-peak separation i.e.,  $\Delta E_p$  is fairly low as compared to the bare CPE or TCBN/CPE. This signifies that using the nanocomposite modified CPE possessed an enhanced electron transfer rates at the electrode surface and eventually

favored the electrochemical process to occur at the electrode surface (Zhou *et al.*, 2016). Therefore, the enhanced electrochemical signal obtained by using the TCBN nanocomposite modified CPE, inferred that the material greatly facilitated the electron transfer reactions at the surface of electrode (Lee *et al.*, 2016; Tiwari *et al.*, 2016).



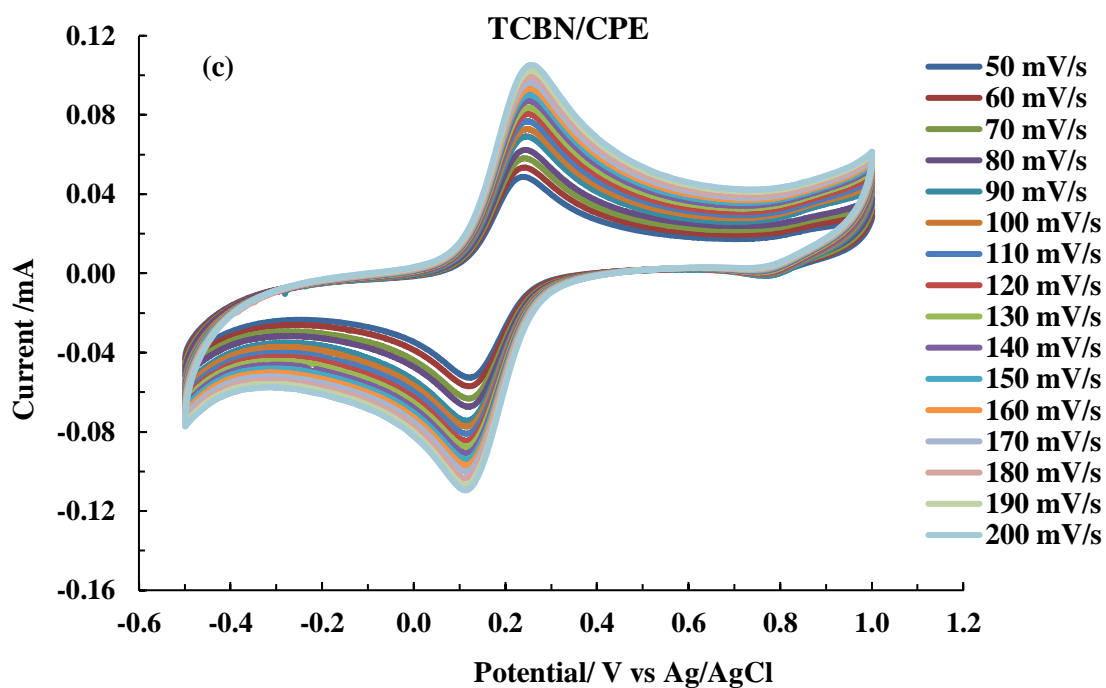
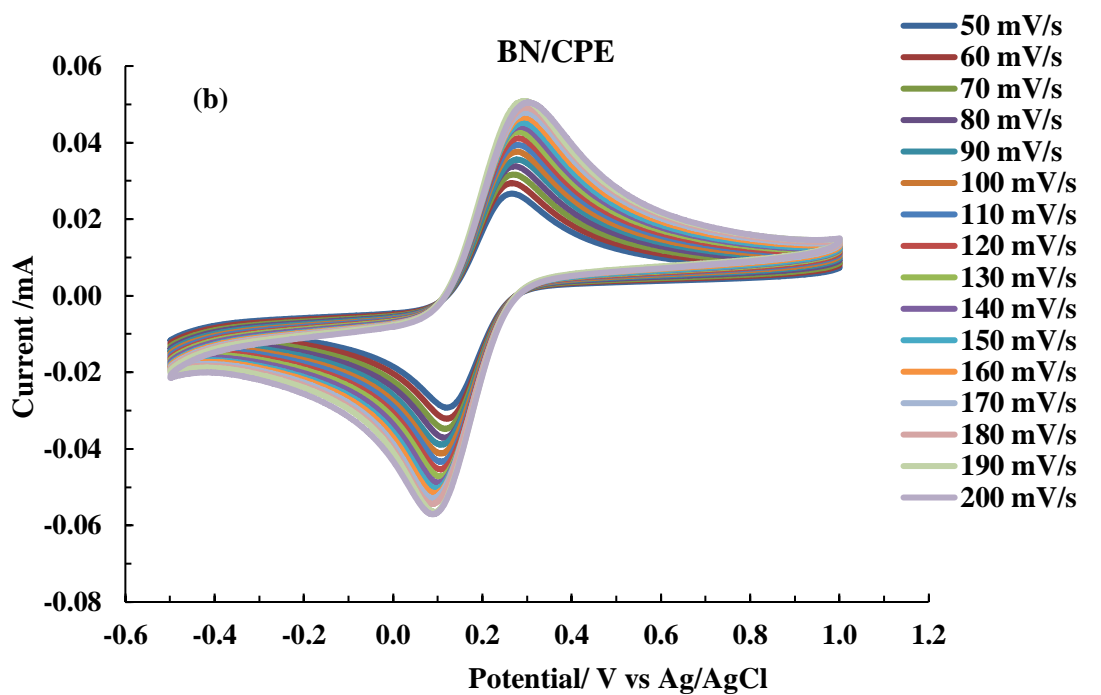


**Figure 3.7. (a-c)** Effect of potential and scan rates on the redox behavior of 0.001 mol/L  $\text{Fe}(\text{CN})_6^{3-}/\text{Fe}(\text{CN})_6^{4-}$  using (a) CPE; (b) BN/CPE; and (c) TCBN/CPE working electrodes.

Further, the mass transfer reactions at the electrode-electrolyte are studied using the Randle–Sevick equation (3.1) (Lee *et al.*, 2016):

$$I_m = 2.69 \times 10^5 \cdot n^{3/2} \cdot \nu^{1/2} \cdot D^{1/2} \cdot C \cdot A \quad (3.1)$$

where  $I_m$  is the peak current (A), ‘ $n$ ’ is the number of electrons in the redox process,  $D$  is the diffusion coefficient of  $\text{Fe}(\text{CN})_6^{3-}/\text{Fe}(\text{CN})_6^{4-}$  system ( $\text{cm}^2/\text{s}$ ) in an aqueous medium and equal to  $7.6 \times 10^{-6} \text{ cm}^2/\text{s}$ , ‘ $\nu$ ’ is the scan rate ( $\text{V/s}$ ), ‘ $C$ ’ is the bulk concentration of the electroactive species ( $\text{mol}/\text{cm}^3$ ) and ‘ $A$ ’ is the electroactive surface area of the working electrode ( $\text{cm}^2$ ). The equation provides the content of electroactive sites available on the surface of the working electrode (Bathinapatla *et al.*, 2015). It was observed that fairly a good linear relationship is obtained between the anodic peak current ( $I_m$ ) and  $\nu^{1/2}$  values (where  $\nu$  is the scan rate) since the regression coefficient ( $R^2$ ) values are always  $> 0.995$  (Cf figure 3.8). A linear relationship between the peak current and the square root of scan rate suggested that the interfacial kinetics was primarily diffusion-controlled (Ndlovu *et al.*, 2014). Further, using the slopes of these lines and the diffusion coefficient of  $\text{Fe}(\text{CN})_6^{3-}/\text{Fe}(\text{CN})_6^{4-}$  in aqueous media  $7.6 \times 10^{-6} \text{ cm}^2/\text{s}$ , the electroactive surface area of these working electrodes was calculated and returned in Table 3.2. It is interesting to note that the surface area of the nanocomposite was 4.88 times higher than the carbon paste electrode and also 2.37 times higher than the pristine bentonite modified carbon paste electrode. This significant increase in the electroactive surface area using nanocomposite modified carbon paste electrode could enable to detect the As(III) even at the ultra-trace levels. Similar diffusion-controlled kinetics was suggested for the As(III) using the bismuth modified exfoliated graphite (EG-Bi) working electrode and reported that electroactive surface area was found to be  $1.31 \text{ mm}^2$  and  $16.3 \text{ mm}^2$  respectively for EG (exfoliated graphite) and EG-Bi electrode (Guo *et al.*, 2016).

**Table 3.2.** Calculated electroactive surface area of fabricated carbon paste electrodes.

Electrode	Electroactive surface area (cm <sup>2</sup> )
CPE	0.244 x 10 <sup>-3</sup>
BN/CPE	0.503 x 10 <sup>-3</sup>
TCBN/CPE	1.19 x 10 <sup>-3</sup>

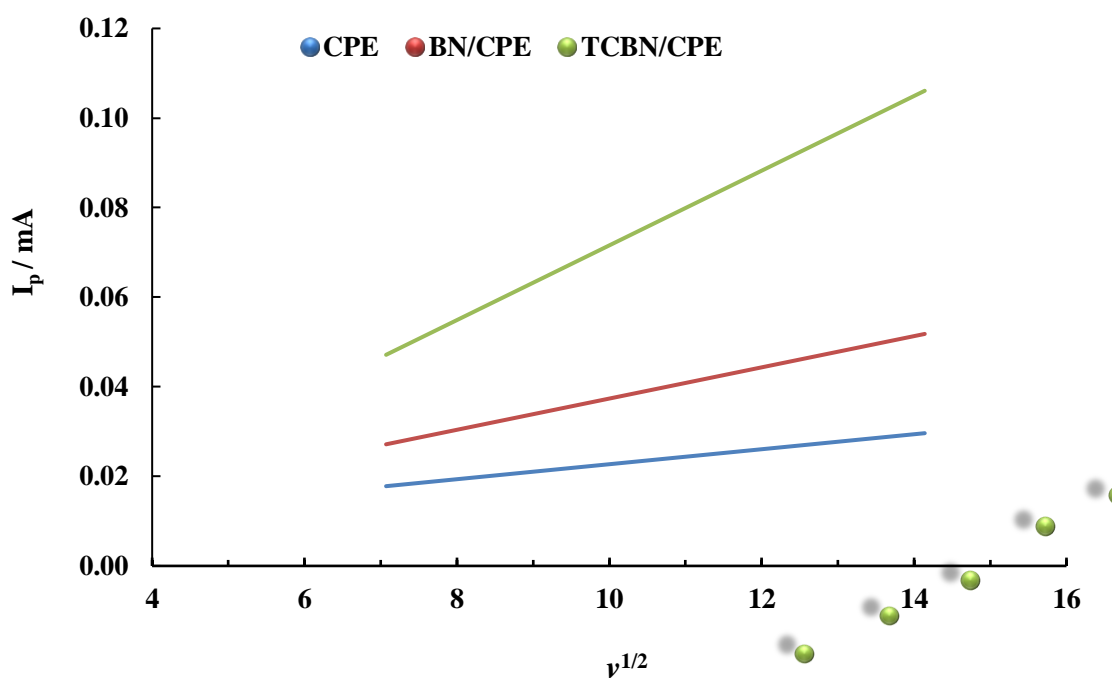


**Figure 3.8.** Linear plots of  $v^{1/2}$  against oxidative peak current ( $I_p$ ) of 0.001 mol/L  $\text{Fe}(\text{CN})_6^{3-}/\text{Fe}(\text{CN})_6^{4-}$  obtained using various carbon paste electrodes.

### 3.2.2. Electrochemical impedance spectroscopy (EIS) studies

The electrochemical impedance spectroscopic studies were conducted using the 0.001 mol/L  $\text{Fe}(\text{CN})_6^{3-}/\text{Fe}(\text{CN})_6^{4-}$  standard solutions at pH 6.0 having background electrolyte 0.1 mol/L KCl and employing the unmodified and TCBN modified carbon paste electrodes. This study eventually demonstrates the solid (working electrode)–electrolytic solution interfacial behavior. The applied frequency range of 80 kHz to 100 MHz was used with 6 points per decade at peak-to-peak sinusoidal potential of 10 mV. The measured imaginary impedance ( $-Z_{\text{im}}$ ) was plotted against the real impedance ( $Z_{\text{real}}$ ). The results are shown in the Nyquist plot (Figure 3.9). Further, the equivalent circuit was drawn for different electrodes. The measured data were best fitted with the Randles circuit as shown in Figure 3.9 (Inset). The Randles circuit assumes the diffusional element (Warburg or Warburg short (W)) which is connected in series with the charge transfer resistance ( $R_{\text{ct}}$ ) (Sacco, 2017). Therefore, the equivalent circuit contained with the  $R_s$  i.e., a series resistance that comes due to the solution, wires, or even contact resistances,  $C_d$  which is double-layer capacitance at the surface of electrode and electrolyte interface. The  $R_{\text{ct}}$  is practically a charge transfer resistance that takes place at the electrode surface and bulk ionic species and W is the Warburg coefficient or Warburg diffusion impedance obtained because of diffusion of ionic species into the bulk solution (Lakhe *et al.*, 2018). The data was fairly fitted well to the Randles plot and the fitted values for bare carbon paste electrode and nanocomposite modified electrode as shown in Figure 3.9 (continuous line). Further, the optimized parameters are obtained and returned in Table 3.3. It is evident from the table that the value of  $R_s$  almost constant for both the electrodes. The semi-circle diameter of the Nyquist plot determines the interfacial charge transfer resistance (Miao *et al.*, 2014). It is noted that the semicircle diameter was significantly decreased using the TCBN nanocomposite electrode and therefore a lower  $R_{\text{ct}}$  value was obtained which indicated that an efficient and faster redox reaction occurred at the interface region of the electrolytic cell (Gu *et al.*, 2018).

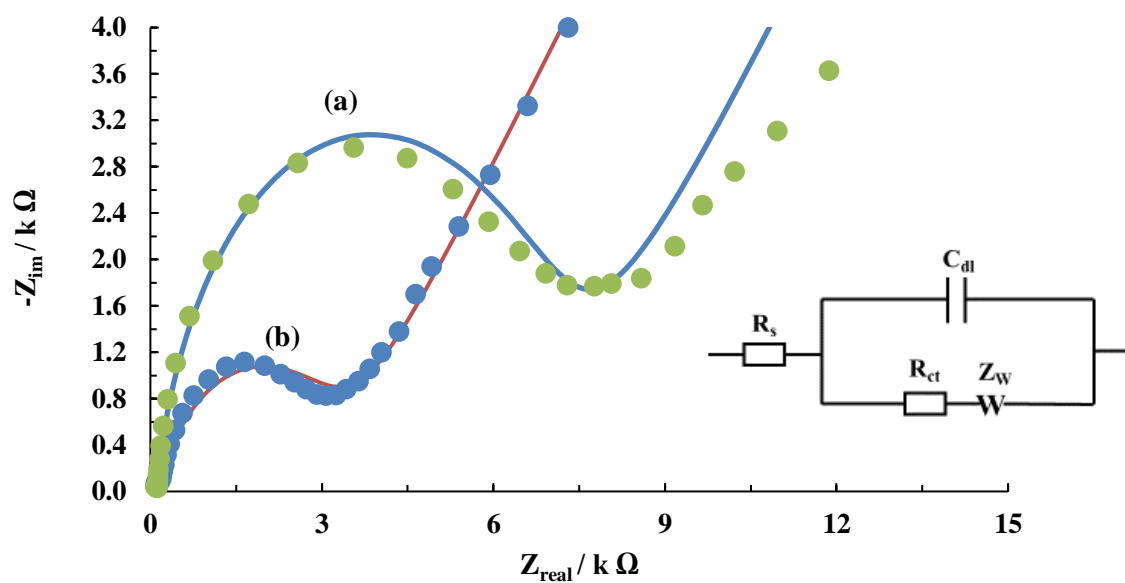


**Figure 3.9.** EIS Nyquist plots (circles) obtained for the  $\text{Fe}(\text{CN})_6^{3-}/\text{Fe}(\text{CN})_6^{4-}$  (0.1 mol/L KCl solution) and the fitted line for equivalent circuit (continuous line) obtained with (a) bare CPE; and (b) TCBN/CPE [Inset: Fitted equivalent circuit].

**Table 3.3.** EIS parameters estimated from the fitted electrical circuit model of the Nyquist plots of carbon paste working electrodes.

Parameters	Working Electrodes	
	CPE	TCBN/CPE
$R_s$ (k $\Omega$ )	0.108	0.102
$C_{dl}$ ( $\mu\text{F}$ )	1.380	3.650
$R_{ct}$ (k $\Omega$ )	6.342	3.002

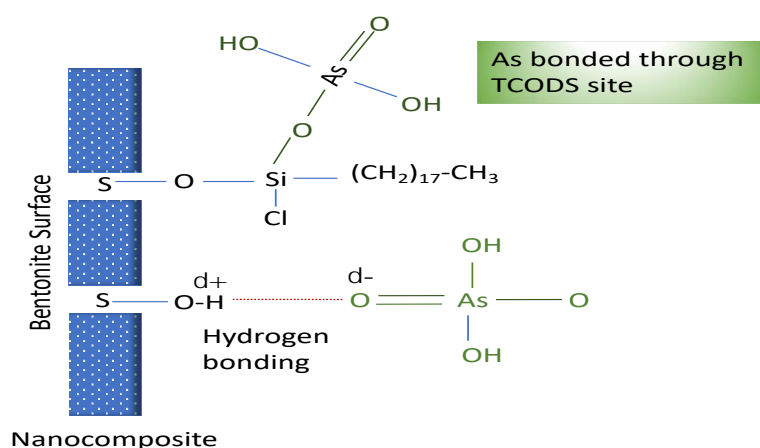


### 3.3. ELECTROCHEMICAL DETECTION OF As(III)

#### 3.3.1. Cyclic voltammetric studies of As(III)

A known concentration of As(III) solution was prepared using the 0.1 mol/L KCl solution and the pH of KCl solution was adjusted using the 0.1 mol/L HNO<sub>3</sub> or NaOH solution. The cyclic voltammograms were recorded at an exciting potential of +1.0 V and -0.2 V against an Ag/AgCl reference electrode. The CV data was recorded for three consecutive cycles and the second cycle was always utilized for further studies. Moreover, three replicates are studied, and hence the error is calculated and shown as  $\pm 3\sigma$  values. Further, linear sweep voltammetry (LSV) is employed for the different electrochemical studies like concentration studies, the effect of interference, and application in real water samples. Initially, the cyclic voltammogram of 30.0  $\mu\text{g/L}$  As(III) solution was recorded with CPE, BN/CPE, and TCBN/CPE electrodes and compared based on the peak current responses. Both oxidation and reduction current for As(III) was barely visible on the voltammogram of the CPE, while small and broad peaks appeared with the BN/CPE. Thus, both electrodes showed a weak electrochemical response for the arsenic analyte, and their voltammograms were characterized by a large peak on the anodic branch which is probably due to the evolution of oxygen. The comparative voltammograms are represented in Figure 3.10. It is evident from the figure that the voltammogram obtained using the TCBN/CPE; As(III) showed a characteristic anodic and cathodic peak around the applied potential of 0.61 and 0.25 V (*vs* Ag/AgCl), respectively. Moreover, the cathodic and anodic peaks are sharp and smooth. These peaks are asserted as the corresponding signal responses when As(III) undergoes a single step, three electron oxidation and reduction processes i.e., As(III) reduced to As(0) and As(0) oxidized to As(III). It was reported previously that the As(III) was reduced in a single step process around the applied potential of 400 mV and oxidized around -300 mV using the bismuth modified exfoliated graphite (EG-Bi) working in a 0.1 M KNO<sub>3</sub> (pH~ 6) (Guo *et al.*, 2016). The information obtained from the CV was used to determine the preconcentration potential. The observed  $\Delta E$  value is found to be 0.36 V. Hence, the observed low value of  $\Delta E$  indicated that the redox process of arsenic was greatly favorable at the nanocomposite electrode (Loučka, 1973). The other

studies showed that As(III) showed no redox reactions on to the CNTs (carbon nanotube) electrode; however, gold-CNTs electrode showed a dominant cathodic peak at the potential of -0.25 V (vs SCE). It was further regarded that As(III) undergo three electron reduction i.e., As(III) to As(0) (Xiao *et al.*, 2008; Lalhmunsiamma *et al.*, 2012). Therefore, given the surface properties, a possible mechanism of As(III) was proposed assuming that arsenic is preferentially adsorbed on the surface of nanocomposite with relatively strong chemical bonds at the electrode surface and undergoes with redox reactions and giving rise to an enhanced signal of the cathodic or anodic peak current. As(III) forms a chemical bond with the available surface active group of the silane grafted with the bentonite i.e, Si-O-As(III) which then undergoes with redox reactions at the surface of the solid (Saha *et al.*, 2016). The other possibility is due to the presence of an unoccupied bentonite surface site. The surface is likely to form a hydrogen bond with the arsenite molecule (Ramesha and Sampath, 2011). Possible interaction between the TCBN electrode surface and arsenite is presented in Scheme 1. Therefore, the presence of arsenite on the electrode surface either by the chemical bonding or by the hydrogen bonding enabled efficiently the redox process to take place at the surface. Hence, an enhanced electrochemical signal was obtained. Concluding from the comparison of the electrochemical response of As(III) at the three electrodes, the response at the TCBN modified electrode is better compared to the CPE or BN/CPE, hence, further studies for detection of As(III) is carried out using the TCBN/CPE.



**Scheme 1:** Proposed scheme of As(III) sorption onto the electrode surface.

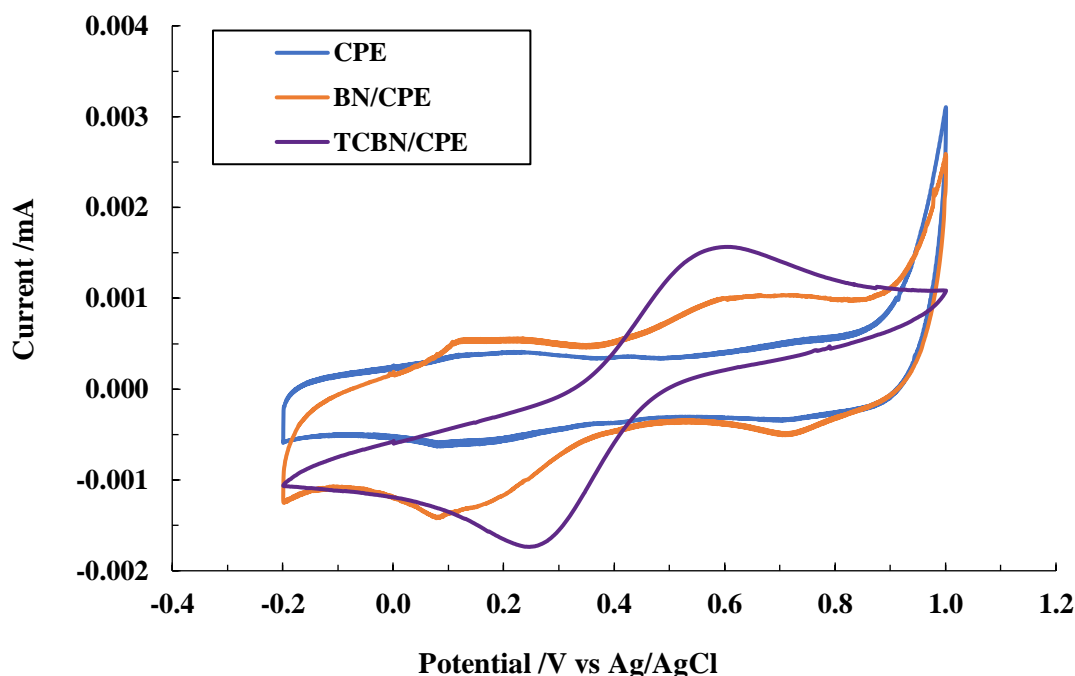


**Figure 3.10.** Cyclic voltammograms of As(III) (30.0 µg/L) in 0.1 mol/L KCl (pH 2.0) background electrolytes employing the CPE, BN/CPE, and TCBN/CPE.

### 3.3.2. pH dependence studies on detection of As(III)

The solution pH is an important parameter to be studied since the speciation of arsenite varies with pH (Lee *et al.*, 2015). As(III) exists predominantly within the pH region 2.0-8.0 to its non-ionic form i.e.,  $\text{H}_3\text{AsO}_3$  which gradually turns to anionic species of  $\text{H}_2\text{AsO}_3^-$  beyond pH 8.0. The response of the pH dependence studies is shown in Figure 3.11 which clearly shows that the electrochemical behavior of As(III) is almost similar at different pH values, however, the peak intensity and peak positions are greatly affected by varying the solution pH. Increasing the pH, the cathodic and anodic peak positions were shifted with an enhanced  $\Delta E$  values. The increased  $\Delta E$  value makes the redox process more non-favorable. However, at pH 2.0 the  $\Delta E$  was found as low as *Ca* 0.34 V with significantly high current density. A

similar observation was obtained for As(III) where high current density was obtained at lower pH values using the EG-Bi electrode (Guo *et al.*, 2016). The low electrochemical signal received at higher pH conditions is possibly due to the hydroxide formation that hinders the arsenic detection. Therefore, a solution pH of 2.0 is chosen as a suitable pH for the detection of As(III) using the TCBN/CPE, and all further studies were performed at this pH.

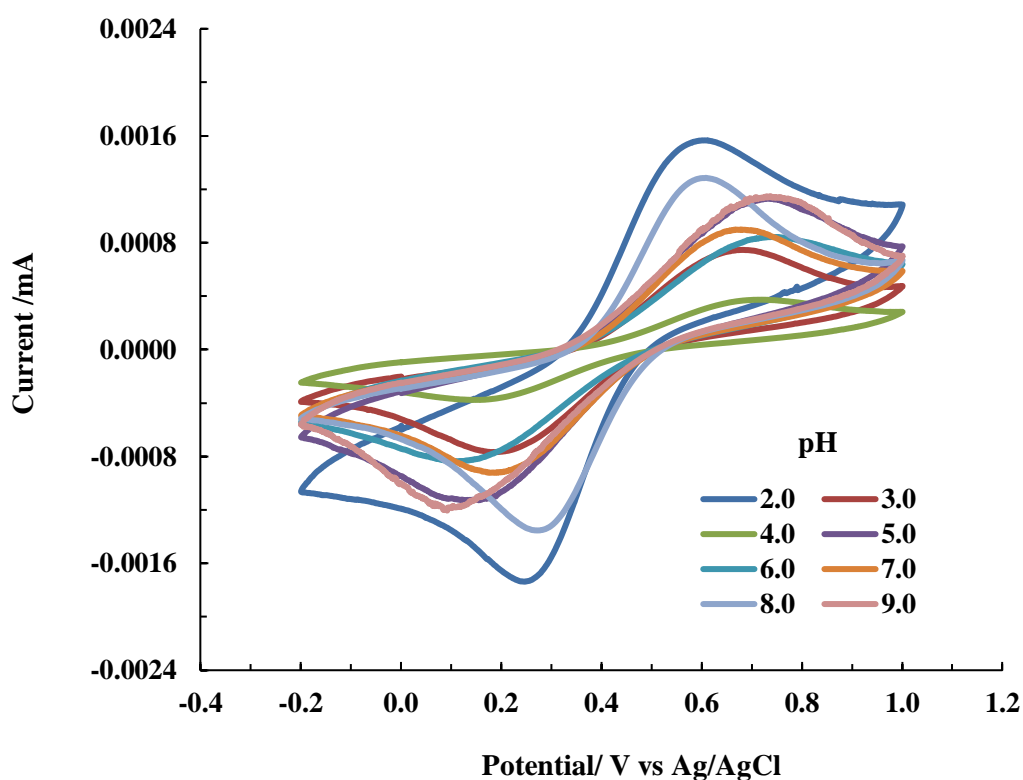


**Figure 3.11.** Cyclic voltammograms of 30.0  $\mu\text{g/L}$  As(III) (0.1 mol/L KCl) as a function of solution pH (2.0 to 9.0) employing the TCBN/CPE.

### 3.3.3. Concentration studies and calibration of As(III) detection

The detection of As(III) was carried out using the linear sweep voltammetry (LSV) at the applied potential of 0.4 to 1.0 V. The LSV is a useful electrochemical tool since it provides a low detection limit compared to the cyclic voltammetry. The LSV curve was obtained varying the concentration of As(III) from 0.5 µg/L to 20.0 µg/L at pH 2.0 in 0.1 mol/L KCl employing the nanocomposite modified carbon paste electrode. The results are depicted in Figure 3.12(a). It is evident from the figure that an increase in the concentration of As(III) caused to increase the anodic peak current. Further, the calibration line was drawn between the anodic peak current against the As(III) concentration. The results are shown in Figure 3.12(b). The figure indicates that fairly a good linearity is achieved between the anodic peak current and As(III) concentration. Further, the linear regression of straight line is attained having the linear equation of:  $I_p (\mu A) = 0.027x C (\mu g/L) + 0.168$  ( $R^2 = 0.979$ ). The results indicated that the detection of As(III) is efficient even at a very low concentration of arsenic in aqueous media.

Further, the limit of detection calculated using slope of the calibration line and standard deviation of six replicates of blank solution measurement was found to be 0.0036 µg/L. Similarly, the limit of quantification was calculated as 0.012 µg/L. The LOD is found to be much below to the permissible limit of arsenic in the drinking water (10.0 µg/L) as prescribed by the World Health Organization or Environmental Protection Agency. This enables the greater applicability of the analytical method at least for the low-level detection of As(III) in aqueous solutions. Moreover, the replicates of data showed good reproducibility of results as the observed relative standard deviations (RSD (%)) are always less than 4%. The LOD obtained in the present study is found to be reasonably lower than many previous reports (Cf Table 3.4) and hence could have potential implications in the detection of As(III) in water bodies.

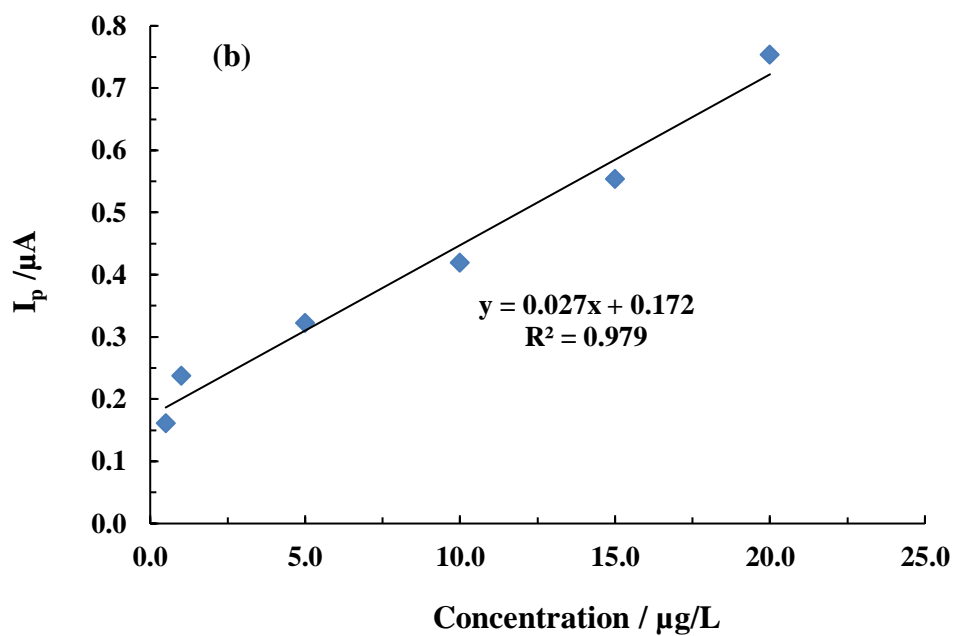
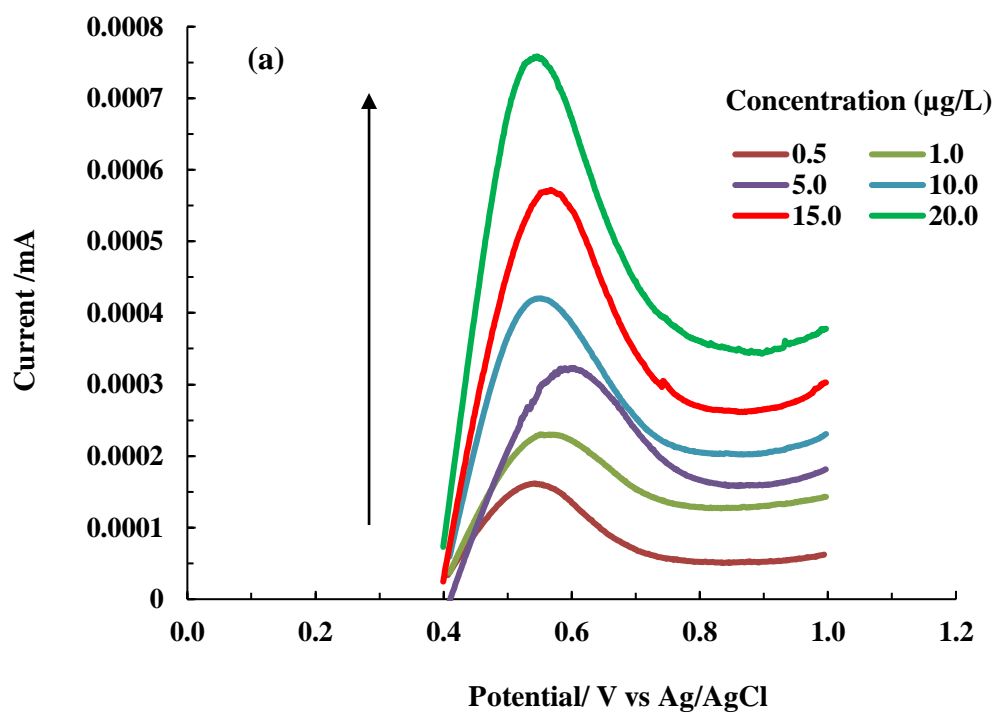


**Figure 3.12.** (a) LSV voltammograms of arsenic (III) at different concentrations of As(III) (0.5 to 20.0 µg/L) using the 0.1 mol/L KCl (pH 2.0) and employing the TCBN/CPE; and (b) Calibration plot of peak current ( $I_p$ ) vs concentration of As(III).

**Table 3.4.** Comparison of LOD for As(III) detection obtained with previous reported materials

Method Employed	Materials Used	LOD	Reference
SWASV	Au-Cu bimetallic nanoparticle	2.09 $\mu\text{g/L}$	Yang <i>et al.</i> , 2016
ASV	Au modified	0.022 $\mu\text{g/L}$	Simm <i>et al.</i> , 2005
SWASV	Au Nanoparticles modified	0.38 $\mu\text{g/L}$	Mafa <i>et al.</i> , 2016
SWASV	F-doped CdO electrode	0.0045 $\mu\text{g/L}$	Zhou <i>et al.</i> , 2017
CV	Ultra-thin graphene oxide film	0.5 mg/L	Kumar <i>et al.</i> , 2016
SWASV	AuNPs-EGE (Exfoliated graphite electrode)	0.58 $\mu\text{g/L}$	Feeney and Kounaves., 2000
LSASV	Au-Pt bimetallic nanoparticles	0.28 $\mu\text{g/L}$	Bu <i>et al.</i> , 2015
LSASV	MnO <sub>x</sub> with Au nanoparticles	0.057 $\mu\text{g/L}$	Wu <i>et al.</i> , 2014
LSV	TCBN nanocomposite	<b>0.0036 <math>\mu\text{g/L}</math></b>	<b>Present study</b>

SWASV-Square wave anodic stripping voltammetry, ASV-Anodic stripping voltammetry, LSASV-Linear sweep anodic stripping voltammetry

#### 3.3.4. Effect of coexisting ions

The influences of several co-ions are studied in presence of 150.0  $\mu\text{g/L}$  of each ion. The As(III) concentration was taken at 28.2  $\mu\text{g/L}$  in 0.1 mol/L KCl (pH 2.0). The co-ions are chosen as cadmium (II), chromium (VI), copper (II), manganese (II), phosphate, and EDTA. The comparison of peak current intensity of As(III) in absence and presence of each ion is presented in Figure 3.13. It is observed that no significant interference occurred in presence of cadmium (II), chromium (VI), phosphate, and EDTA. However, the presence of copper (II) and manganese (II) caused an enhancement of the anodic peak current. Hence, these ions interfere with the As(III) detection. Copper and manganese are oxidized at the same potential and hence, the anodic peak current was increased. The Au/GO/Leucine/Nafion electrode showed no interference in presence of Zn(II), Pb(II), Hg(II) and Cd(II) both having the same concentration of 10 mg/L (Kumar *et al.*, 2015). Similarly, the detection of As(III) in presence of Pb(II), Co(II), Ni(II), Cd(II), Cu(II), Zn(II) and K(I) was not affected significantly using the F-doped CdO electrode (Bhargavi *et al.*, 2016). However, the presence of Pb(II), Hg(II) and Cu(II) caused a reduction of stripping current by 10, 30, and 65% for As(III) using the gold ultra-micro electrode (Feeney and Kounaves, 2000).



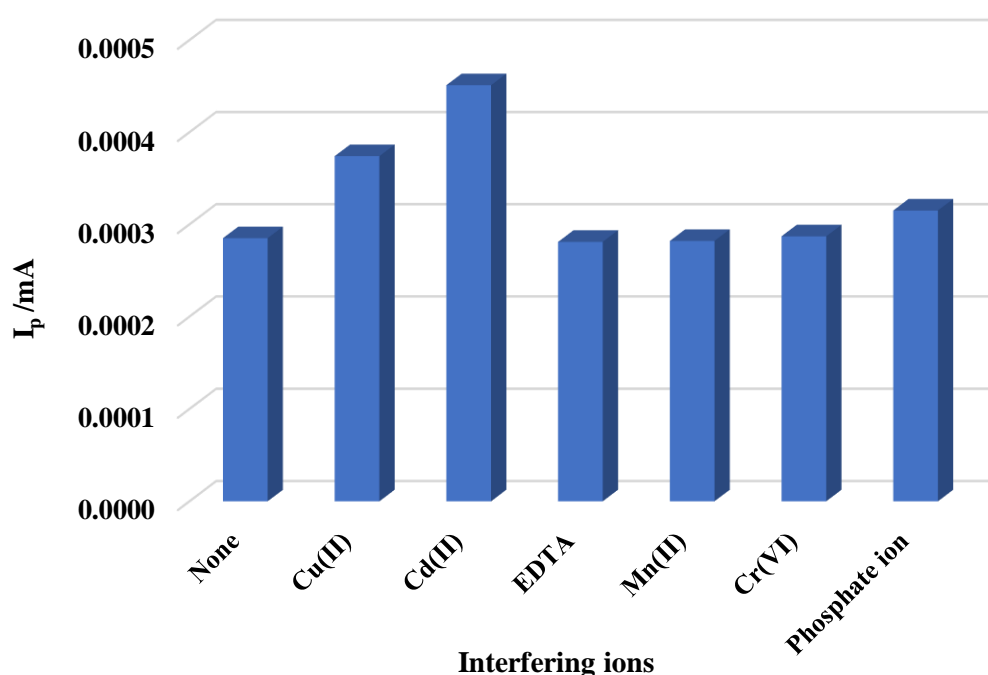


**Figure 3.13.** Effect of various co-existing ions (150.0  $\mu\text{g/L}$ ) in the detection of 28.2  $\mu\text{g/L}$  As(III) in 0.1 mol/L KCl (pH 2.0) background electrolyte.

### 3.3.5. Studies in real water sample

The intention of the study is the implication of an analytical method for the detection of As(III) in real water samples. The physical/chemical nature of river or groundwater is complex and it changes with time and space. The water quality is greatly affected by the temperature, human intrusion, microorganism activities, or even the nature of soil and rocks (Forzani *et al.*, 2007). Therefore, a real matrix analysis enables us to find the suitability, selectivity, and feasibility of the analytical method. Hence, the water was collected from the Tlawng River, Mizoram, India, and employed without further treatment. However, the river water sample was subjected to various physico-chemical analyses. The results are appended in Table 3.5. The results indicated that the water is free from several heavy metals; however, it contained with Ca, Zn, and Fe. On the other hand, the high value of inorganic carbon and some non-purgeable organic carbon (NPOC) is present. Further, the river water

was spiked with varying concentrations of As(III) at pH 2.0 in 0.1 mol/L KCl background electrolyte. The LSV analysis was conducted and results are shown in Figure 3.14(a) where smooth curves are obtained. Moreover, on increasing the concentration of As(III), the anodic peak current was increased gradually. Further, a regression line between the As(III) concentration against the corresponding anodic peak current was obtained as shown in Figure 3.14(b). The regression line is obtained as:  $I(\mu\text{A}) = 0.046 \mu\text{g/L} + 0.152$  ( $R^2 = 0.971$ ). Reasonably a good linearity was obtained between the concentration of As(III) and the anodic peak current. It is interesting to note that the relative standard deviations (RSD (%)) are always found  $< 3\%$ . Further, a solution of As(III) having a known concentration of  $5.0 \mu\text{g/L}$  at pH 2.0 in 0.1 mol/L KCl was prepared with the same river water and subjected to LSV analysis. Using the regression line, the As(III) concentration is estimated and found to be  $4.9 \pm 0.02 \mu\text{g/L}$ . This indicated that the recovery of arsenic is more than 98%. These results indicated that the devised method is useful in the precise and efficient detection of arsenic at an ultra-trace level. It provides fairly good selectivity and sensitivity. Previously, it was reported that the  $\text{SnO}_2/\text{Nafion}/\text{C}$  pencil electrode provided fairly a good applicability in qualitative and quantitative detection of As(III) from industrial wastewater samples (Bhanjana *et al.*, 2018).

**Table 3.5.** Various physico-chemical parametric analyses of Tlawng river water.

<b>Parameters Studied</b>	<b>Analytical Results</b>
<b>pH</b>	7.95
<b>Conductivity</b>	118 mS/cm
<b>Resistivity</b>	0.0085 mOhm.cm
<b>Salinity</b>	0.06 PSU
<b>Ox. Red. Potential</b>	+221 mV
<b>Elements studied (AAS)</b>	<b>(mg/L)</b>
<b>Ni(II)</b>	ND
<b>Zn(II)</b>	0.43
<b>Pb(II)</b>	ND
<b>Mn(II)</b>	ND
<b>Fe(II)</b>	0.49
<b>Ca(II)</b>	6.68
<b>Cu(II)</b>	ND
<b>TOC Analysis</b>	<b>(mg/L)</b>
<b>Inorganic Carbon</b>	8.34
<b>NPOC</b>	0.01

**ND: Not Detected**

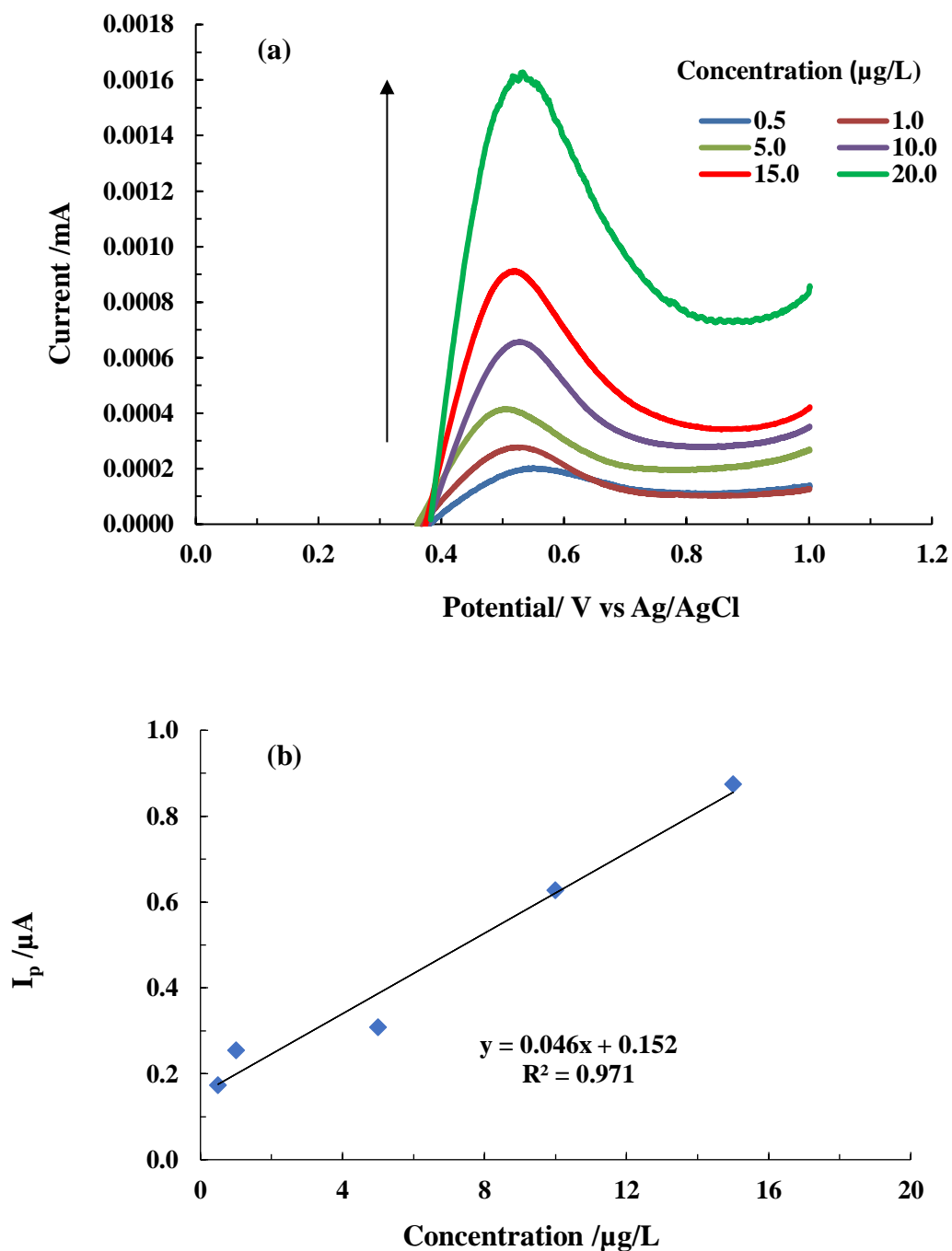


**Figure 3.14.** (a) LSV voltammograms of river water samples as spiked with various concentrations of As(III) (0.5 to 15.0 µg/L) at pH 2.0 in 0.1 mol/L KCl background electrolyte; and (b) Calibration plot of obtained between the peak current ( $I_p$ ) vs concentration of As(III).

### 3.3.6 Conclusion

Novel trichloro(octadecyl)silane grafted bentonite nanocomposite (TCBN) was synthesized using a simple non-aqueous grafting method. The nanocomposite material was employed in the electrochemical detection of As(III). The impedance spectroscopic data revealed a significant decrease of semicircle loop of Nyquist plot using the TCBN/CPE as compared to the bare carbon paste electrode or bentonite modified CPE. Moreover, the  $R_{ct}$  (charge transfer resistance) value is significantly low using the TCBN/CPE as compared to the bare CPE which implies that the fabricated electrode showed faster or better electron transfer rate at the electrode/solution interface. The electroactive surface area was found to be  $0.244 \times 10^{-3}$ ,  $0.503 \times 10^{-3}$ , and  $1.19 \times 10^{-3} \text{ cm}^2$ , respectively for the carbon paste, bentonite, and nanocomposite modified carbon paste electrodes. pH dependence studies indicated an enhanced electrochemical signal was obtained at pH 2.0 with a minimum  $\Delta E$  values. The sensor studies enabled low-level detection of As(III) with a limit of detection  $0.0036 \text{ }\mu\text{g/L}$ . The observed relative standard deviations (RSD) always were found to be less than 4%. The presence of several cations and anions could not affect the detection of As(III). However, a marked deviation was observed in presence of Cu(II) and Mn(II). The nanocomposite showed fairly good selectivity and sensitivity using the river water samples as spiked with As(III). The proposed method is a useful analytical method to be employed for the ultra-trace and, perhaps, on-site detection of arsenic.

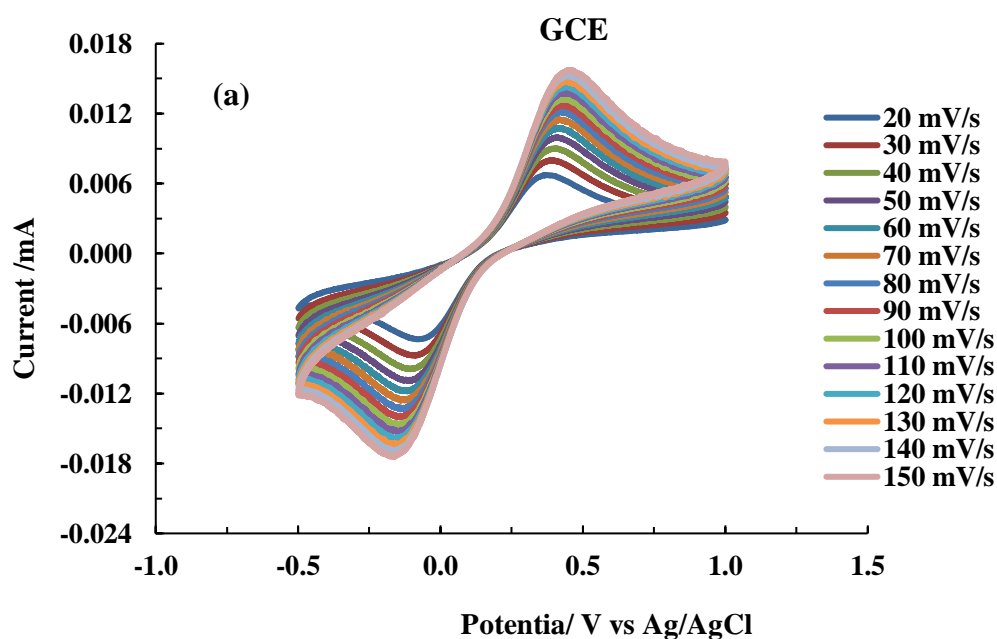
### 3.4. ELECTROCHEMICAL STUDIES USING GLASSY CARBON ELECTRODES

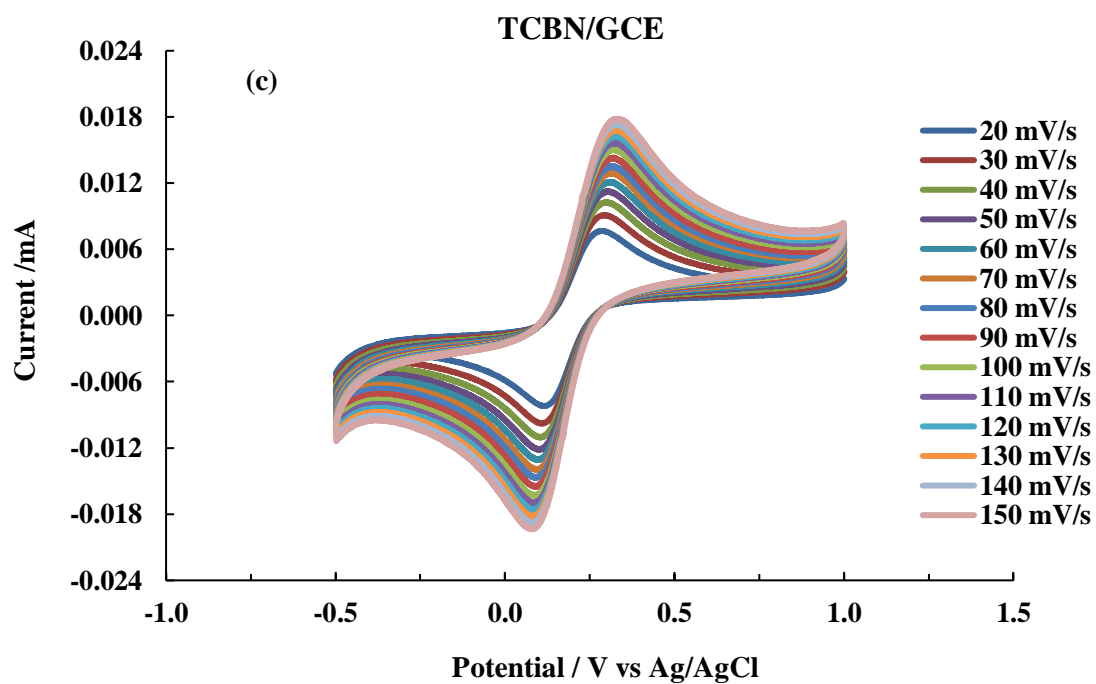
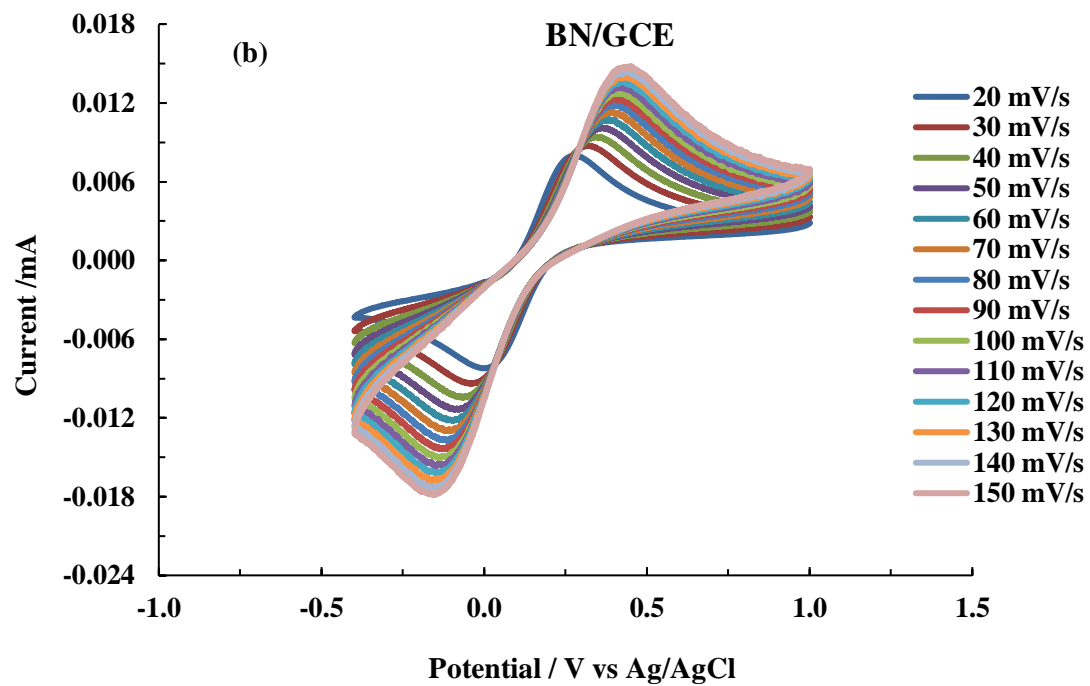
The bare glassy carbon electrode (GCE) and fabricated electrodes (pristine bentonite modified (BN/GCE), silane-grafted bentonite (TCBN/GCE), nanocomposite decorated with silver nanoparticles ((Ag(NP)/TCBN/GCE)), and nanocomposite decorated with gold nanoparticles ((Au(NP)/TCBN/GCE)) coated glassy carbon electrodes) are characterized by the electrochemical techniques viz., cyclic voltammetry (CV) and electrochemical impedance spectroscopy (EIS) using the standard redox probe  $\text{Fe}(\text{CN})_6^{3-}/\text{Fe}(\text{CN})_6^{4-}$  (0.001 mol/L prepared in 0.1 mol/L KCl as supporting electrolyte solution). Cyclic voltammograms at different scan rates from 20 to 150 mV/s at a potential window of -0.5 V to 1.0 V are recorded for each electrode. The EIS experiments are performed with the application of 10 mV amplitude in the frequency range of 80 kHz to 100 MHz.

#### 3.4.1. Scan rate studies using cyclic voltammetry

The electrochemical characterization of the bare GCE and fabricated GCEs using scan rates studies were carried out using cyclic voltammetry technique. The cyclic voltammograms of 1.0 mmol/L  $\text{Fe}(\text{CN})_6^{3-}/\text{Fe}(\text{CN})_6^{4-}$  (0.1 mol/L KCl solution; pH 6.1) are obtained at varied scan rates 20-150 mV/s within the excitation window of 0.4 V to 1.0 V employing the fabricated electrodes along with the bare GCE. These results are shown in Figure 3.16(a-e). Figure 3.15(a-e) clearly showed the well-defined oxidation-reduction peaks of  $\text{Fe}(\text{CN})_6^{3-}/\text{Fe}(\text{CN})_6^{4-}$  redox probe for these electrodes. Further, increase in scan rates enabled to enhance the intensity of peak current both for oxidation and reduction. This shows that mass transfer resulting from the oxidation and reduction process occurred favorably at the electrode surfaces. However, the ease with which redox processes occur at the electrode surface greatly differs with the different electrodes employed. The cyclic voltammograms obtained by using the Ag(NP)/TCBN/GCE and Au(NP)/TCBN/GCE showed significantly enhanced oxidation-reduction peak currents for  $\text{Fe}(\text{CN})_6^{3-}/\text{Fe}(\text{CN})_6^{4-}$  as compared to the bare GCE, BN/GCE, or

TCBN/GCE. For example, at scan rate 100 mV/s, the oxidation peak current was increased from  $\sim 0.012$  mA to 0.0165 for GCE and BN/GCE, respectively. Similarly, it was increased to *Ca* 0.0169 mA for the Ag(NP)/TCBN and Au(NP)/TCBN modified glassy carbon electrodes. The higher current response obtained for the Ag(NP) or Au(NP) nanocomposite modified electrodes affirmed that the electroactive species have relatively possessed enhanced affinity towards the modified surface hence, the number of analyte species are increased at the electrode surface to undergo the electrode reactions. Further, the peak-to-peak separation i.e., between the oxidative and reductive peak current position (or  $\Delta E_p$ ) is significantly low compared to the bare GCE and BN/GCE which inferred that the nanocomposite modified GCEs possessed an enhanced electron transfer rates at the electrode surface and eventually favors the electrochemical process at the electrode surface (Zhou *et al.*, 2016). Hence, these results suggested that the modification of the glassy carbon electrode surface with the nanocomposites enabled to increase the sensitivity of the electrodes for redox reactions of electroactive species (Ndlovu *et al.*, 2014).







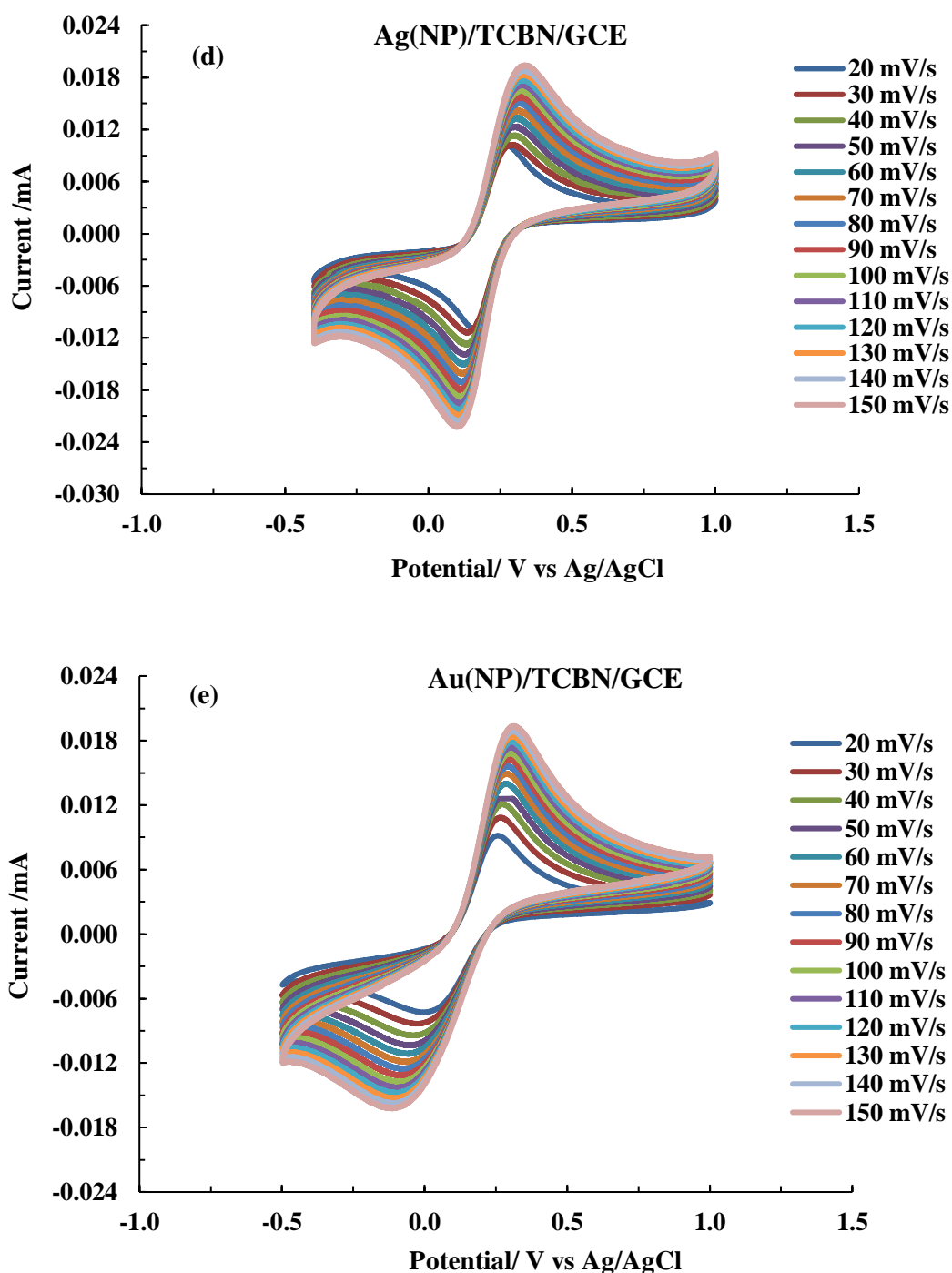


**Figure 3.15(a-e).** Effect of potential scan rate on the redox behavior of 0.001 mol/L  $\text{Fe}(\text{CN})_6^{3-}/\text{Fe}(\text{CN})_6^{4-}$  (0.1 mol/L KCl solution; pH 6.1) at (a) GCE; (b) BN/GCE; (c) TCBN/GCE; (d) Ag(NP)/TCBN/GCE; and (e) Au(NP)/TCBN/GCE working electrodes.

Further, the linear plots are drawn between the oxidation peak current ( $I_p$ ) vs square root of the scan rate ( $v^{1/2}$ ) for all these electrodes and shown in Figure 3.16.

Figure showed that fairly a good linearity was obtained between the peak current ( $I_p$ ) against  $v^{1/2}$ . This inferred that the redox process on the electrode surface proceeds predominantly through the analyte diffusion (Liu *et al.*, 2019). Moreover, the slope of the linear lines was utilized to obtain the electroactive surface area of the electrodes employed *viz.*, GCE, BN/GCE, TCBN/GCE, and Ag(NP)/TCBN/GCE and Au(NP)/TCBN/GCE using the Randles-Sevcik equation and employing the diffusion coefficient value for  $\text{Fe}(\text{CN})_6^{3-}/\text{Fe}(\text{CN})_6^{4-}$  system as  $7.6 \times 10^{-6} \text{ cm}^2/\text{s}$  (Lee *et al.*, 2016b). The electroactive surface areas were calculated and returned in Table 3.6. These results showed that there is an apparent increase in electroactive surface area of the fabricated GCE compared to the bare GCE. It is further noted that the Ag or Au nanoparticles decorated nanocomposite materials possessed *Ca.* 3 times higher the electroactive surface area compared to the bare GCE. Therefore, the nanostructured materials enabled to enhance significantly the sensitivity of the electrode and provides rather better electrochemical platform for the mass transfer reactions at the electrode surface. It was reported previously that the decoration or immobilization of Ag or Au nanoparticles on other sensor materials enabled to enhance the electroactive surface area of electrodes which allow improved electrochemical activity (Amidi *et al.*, 2017; Li *et al.*, 2021; Shams *et al.*, 2016). Similarly, silver nanoparticle doped polyaniline nanotube (AgNP@PANINTs) modified pencil graphite electrode showed an increased surface area as well as better sensitivity towards the low-level detection of fluorouracil as compared to the bare pencil graphite electrode (PGE) or polyaniline nanotube modified electrode (PANINTs PGE) (Zahed *et al.*, 2018). The estimated surface area of the PGE, PANINTs PGE and AgNP@PANINTs PGE electrodes based on the scan rate studies using 0.001 mol/L  $\text{Fe}(\text{CN})_6^{3-}/\text{Fe}(\text{CN})_6^{4-}$  (in 0.1 mol/L KCl) as a probe were 0.195  $\text{cm}^2$ , 0.221  $\text{cm}^2$  and 0.293  $\text{cm}^2$ , respectively. The effective surface areas for bare GCE, p-melamine modified GCE (PMel/GCE) and gold nanoparticles electrodeposited p-melamine modified GCE (PMel-Au nano/GCE) were calculated as 0.058, 0.103 and 0.141  $\text{cm}^2$ , respectively (Amidi *et al.*, 2017). Hence, the enhanced peak currents, increased surface area and smaller peak potentials separation (increased reversibility) at the Ag(NP)/TCBN/GCE or Au(NP)/TCBN/GCE reveals

that the electron transfer reaction at the electrode surface is favored both kinetically and thermodynamically (Salinas-Torres *et al.*, 2011).

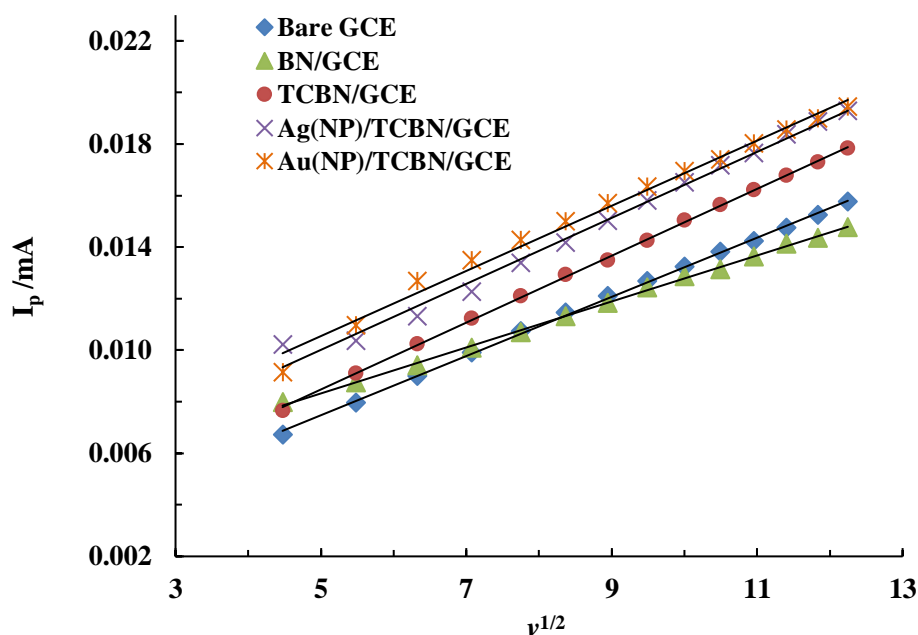


**Figure 3.16.** Linear plots of  $v^{1/2}$  against oxidative peak current ( $I_p$ ) obtained for the 0.001 mol/L  $\text{Fe}(\text{CN})_6^{3-}/\text{Fe}(\text{CN})_6^{4-}$  (in 0.1 mol/L KCl solution; pH 6.1) using bare glassy carbon electrode and various fabricated glassy carbon electrodes.

**Table 3.6.** Calculated electroactive surface area of various fabricated glassy carbon electrodes

Working electrode	Electroactive surface area ( $\text{cm}^2$ )
Bare GCE	$0.269 \times 10^{-3}$
BN/GCE	$0.4048 \times 10^{-3}$
TCBN/GCE	$0.418 \times 10^{-3}$
Ag(NP)/TCBN/GCE	$0.539 \times 10^{-3}$
Au(NP)/TCBN/GCE	$0.6747 \times 10^{-3}$

### 3.4.2. Electrochemical impedance spectroscopic (EIS) studies

The interfacial behavior between the employed glassy carbon electrodes and electrolytic solutions were analyzed using the EIS measurements. The impedance spectra were recorded as in the form of Nyquist plots for the bare and fabricated GCEs using 0.001 mol/L  $\text{Fe}(\text{CN})_6^{3-}/\text{Fe}(\text{CN})_6^{4-}$  redox probe in 0.1 mol/L KCl background electrolyte and at pH 6.1. The EIS results are shown in Figure 3.17.

The best-fitted circuit used for these plots is given as:  $R_1+Q_2/(R_2+W_2)$  where the circuit elements  $R_1$ ,  $R_2$ ,  $W_2$  and  $Q_2$  represent solution resistance ( $R_s$ ), charge transfer resistance ( $R_{ct}$ ), Warburg impedance ( $Z_w$ ) and double-layer capacitance ( $C_{dl}$ ), respectively as using the Randles circuit (Figure 3.17 inset). The constant phase element (Q) is commonly used in the replacement of  $C_{dl}$  in real electrochemical systems which are more complicated than the ideal systems represented by the simple Randles circuit. The best fitted electrochemical parameters are computed and given in Table 3.7. The impedance spectra are characterized by a semicircle domain whose diameter equals to the  $R_{ct}$  of electrode/bulk ionic interfacial layer and controls electron transfer kinetics of  $\text{Fe}(\text{CN})_6^{3-}/\text{Fe}(\text{CN})_6^{4-}$  redox probe occurred at electrode surface (Afkhami *et al.*, 2016). It is observed that the semicircle loop decreased significantly for TCBN/GCE and Ag(NP)/TCBN/GCE and Au(NP)/TCBN/GCE as compared to the bare GCE implying better current conductivity with the bentonite precursor materials. The high  $R_{ct}$  value of GCE (16.5 k $\Omega$ ) falls sharply to 6.21 k $\Omega$  and 5.28 k $\Omega$  for the BN and TCODS/BN modified GCE, respectively. Interestingly, the Ag(NP)/TCBN/GCE and Au(NP)/TCBN/GCE showed much-decreased semicircle with  $R_{ct}$  values of 3.22 and 3.13 k $\Omega$ , respectively. The clearly indicated that the decoration with Ag(NP) or Au(NP) within the nanocomposite TCBN provides significantly increased surface area and further facilitated the electron transfer and conductivity at the GC electrode surface (Mourya *et al.*, 2019). Hence, the EIS results confirm that the electrochemical activity of the bentonite clay increases with modification by organic silane and further with the decoration of Ag(NP) or Au(NP). These results are consistent with the cyclic voltammetric results as obtained previously.

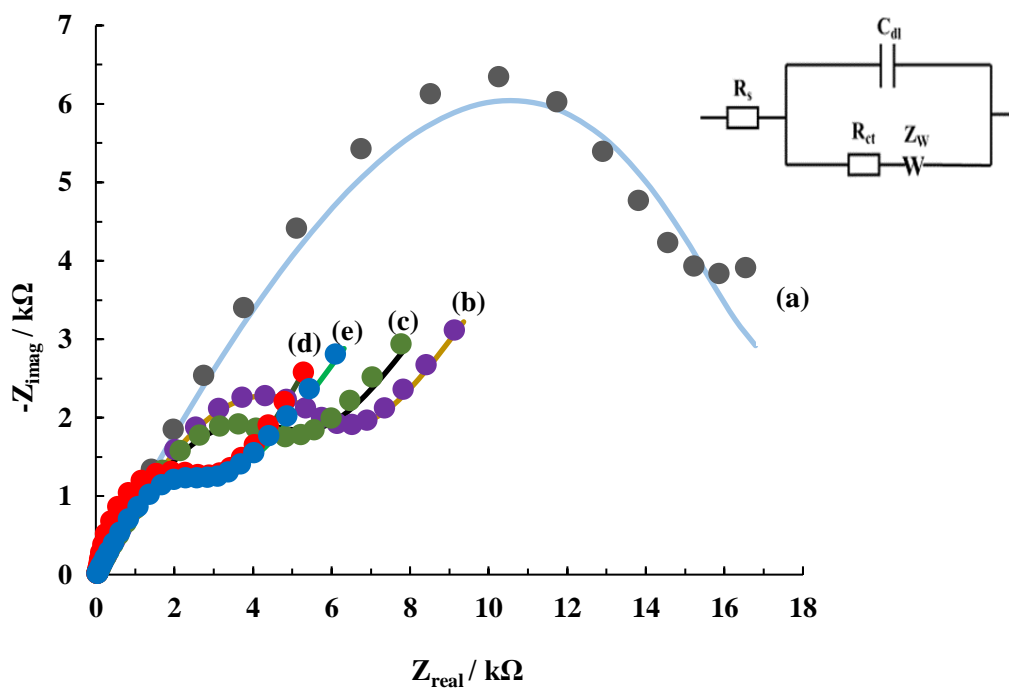


**Figure 3.17.** EIS Nyquist plots (circles) obtained for the  $\text{Fe}(\text{CN})_6^{3-}/\text{Fe}(\text{CN})_6^{4-}$  (0.1 mol/L KCl solution) and the fitted line for equivalent circuit (continuous line) obtained with (a) bare GCE and (b) BN/GCE (c) TCBN/GCE (d) Ag(NP)TCBN/GCE and (e) Au(NP)TCBN/GCE [Inset: Fitted equivalent circuit].

**Table 3.7.** EIS parameters estimated from the fitted electrical circuit model of the Nyquist plots of various glassy carbon working electrodes.

Working electrode	Parameters		
	$R_s$ ( $\Omega$ )	$R_{ct}$ ( $k\Omega$ )	$C_{dl}$ ( $\mu F$ )
Bare GCE	47.8	10.4	16.5
BN/GCE	32.1	7.81	6.2
TCBN/GCE	30.0	13.7	5.2
Ag(NP)TCBN/GCE	32.6	14.3	3.2
Au(NP)TCBN/GCE	28.5	12.6	3.1

### 3.5. ELECTROCHEMICAL DETECTION OF Pb(II)

The electrochemical detection of Pb(II) was performed using the nanocomposite modified electrode, Au(NP)/TCBN/GCE. The electrochemical measurements were carried out using differential pulse voltammetry and applying the anodic stripping technique for more sensitive detection of the analyte. Initially, the electrochemical behavior of Pb(II) was investigated with cyclic voltammetry and the cyclic voltammogram of Pb(II) was recorded for bare GCE, BN/GCE, TCBN/GCE, and Au(NP)/TCBN/GCE which were compared and studied. Further investigations for effective sensing and detection of the Pb(II) ion were carried on with the Au(NP)/TCBN/GCE. A supporting electrolyte solution of 0.1 mol/L acetate buffer (AcBF) was used throughout the measurements.

#### 3.5.1. Electrochemical studies of Pb(II) using cyclic voltammetry

Cyclic voltammograms are obtained for blank electrolyte solution (0.1 mol/L acetate buffer; pH 4.0) and 5.0 mg/L Pb(II) employing GCE and fabricated GCEs viz., BN/GCE, TCBN/GCE, and Au(NP)/TCBN/GCE. The voltammograms are collected within the excitation potential window of -1.2 V to 0.1 V and scan rate 100 mV/s. The voltammograms obtained for each electrode is shown in Figure 3.18. The figure indicated that apparently, no peak occurred with the blank electrolyte solution whereas, in presence of the electroactive species i.e., Pb(II), and all these electrodes show a similar pattern of voltammograms. A sharp and intense anodic peak at an applied potential of *Ca.* -0.40 V was observed for all the electrodes. This oxidative peak current is due to the oxidation of  $\text{Pb}^0$  to  $\text{Pb}^{2+}$ . The electrosynthesis of  $\text{Pb}^{2+}$  ended shortly above potential of -0.42 V while only oxygen evolution continues up to 0.1 V. However, the reverse scan ensembles a much smaller and broader cathodic peak in the region of -0.5 V to -0.8 V resulting from the reduction of  $\text{Pb}^{2+} \rightarrow \text{Pb}^0$ . The current densities of the oxidation and reduction are not possessed with equal magnitudes; hence, this implied that redox processes are not completely reversible. An increase in current densities with the fabricated glassy carbon electrodes using the BN indicate that the bentonite layered structure allows better conductivity of the

current signal. The current response was further improved with the TCBN on the GCE due to the attractive interaction with the electroactive metal ions. Finally, the material Au(NP)/TCBN showed much sharper and enhanced oxidation-reduction peak. The oxidative peak is increased significantly compared to the GCE and BN/GCE. It was further noted that the peak current was increased by 5-8 times using the modified electrodes compared to the bare GCE. This indicated that the materials provided better conductivity and attractive forces between the modified electrodes and  $\text{Pb}^{2+}$ . This enabled to an enhanced peak current (Mourya *et al.*, 2019). In a previous report of Pb(II) detection with graphene-gold nanocomposite modified glassy carbon electrode, G-Au/GCE showed improved electrochemical response for Pb(II) as compared to the bare GCE. This was explained as the Pb(II) showed low interaction and adsorption on the GCE surface as compared to the modified electrode surface where more Pb(II) ions were adsorbed and electro-catalyzed by the decorated Au nanoparticles ( Lee *et al.*, 2015). Therefore, the AuNP decorated TCBN provided a useful material in the detection Pb(II) and further investigations are carried out using the nanocomposite modified electrodes.

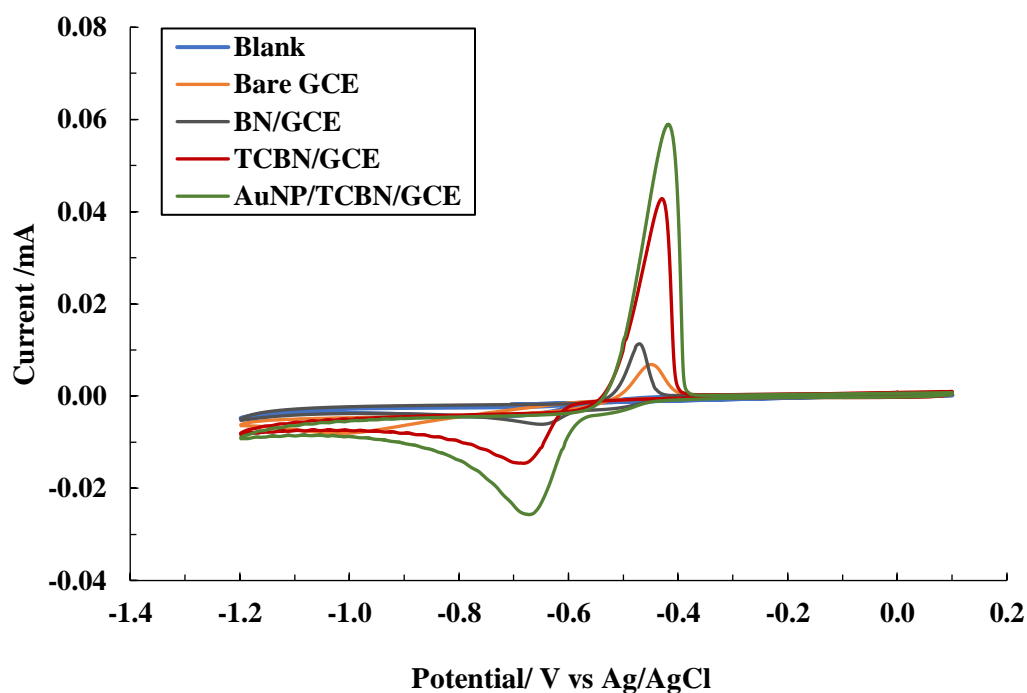


**Figure 3.18.** Cyclic voltammograms of 5.0 mg/L Pb(II) in acetate buffer (pH 4.0) using the bare GCE, BN/GCE, TCBN/GCE and Au(NP)/TCBN/ GCE at scan rate 100 mV/s.

### 3.5.2. pH dependence studies on detection of Pb(II)

The influence of pH on the electrochemical response of Pb(II) was studied using cyclic voltammetry at varied pH (3.6-7.0) of supporting electrolyte solutions. The Pb(II) concentration was maintained at 1.0 mg/L and it was scanned within a potential range of -1.2 to 0.1 V at a scan rate of 100 mV/s. The cyclic voltammograms obtained at different pH conditions are presented in Figure 3.19. It is evident from the Figure 3.19 and 3.20 that the oxidative/reductive peak potentials are slightly shifted with the change in pH. It shifted towards the negative potential side as the pH values were increased. The results clearly indicated that the presence of protons play an important role in the electrode reaction processes (Danyıldız *et al.*, 2017). More intense anodic peaks were observed in the acidic condition from 3.6 to 4.5, being maximum at pH 4.0 and gradually decreases from pH 5.0 to 7.0. Moreover, two sharp peaks in the cathodic branch between -0.52 V to -0.70 V attributed to the two reduction processes ( $\text{Pb}^{2+} \rightarrow \text{Pb}$ ) and are observed at pH 3.6,



4.0, and 4.5 which is most defined at pH 4.0 (He *et al.*, 2016). On the other hand, a single oxidative peak corresponding to one-step oxidation of  $\text{Pb} \rightarrow \text{Pb}^{2+}$  was observed at all solutions. Further, relatively high peak current was recorded at pH 4.0, this indicated that the  $\text{Pb}^{2+}$  showed high affinity towards the nanocomposite material at the electrode surface. However, low current was observed at lower pH i.e., pH 3.6 using the Au(NP)/TCBN/GCE material is because of the competition of  $\text{H}^+$  ions and  $\text{Pb(II)}$  ions towards the electrode surface. Similarly, increasing the pH from 4.0 to 5.0 a sharp decrease in peak current is observed which is perhaps due to the hydrolysis of  $\text{Pb(II)}$  ions (Dahaghin *et al.*, 2018). Similarly, almost a constant peak current was observed within the pH regions 5.0 to 7.0. Therefore, in view of the pH dependence studies, the further studies were conducted at pH 4.0 using the DPASV for low detection of  $\text{Pb(II)}$ .

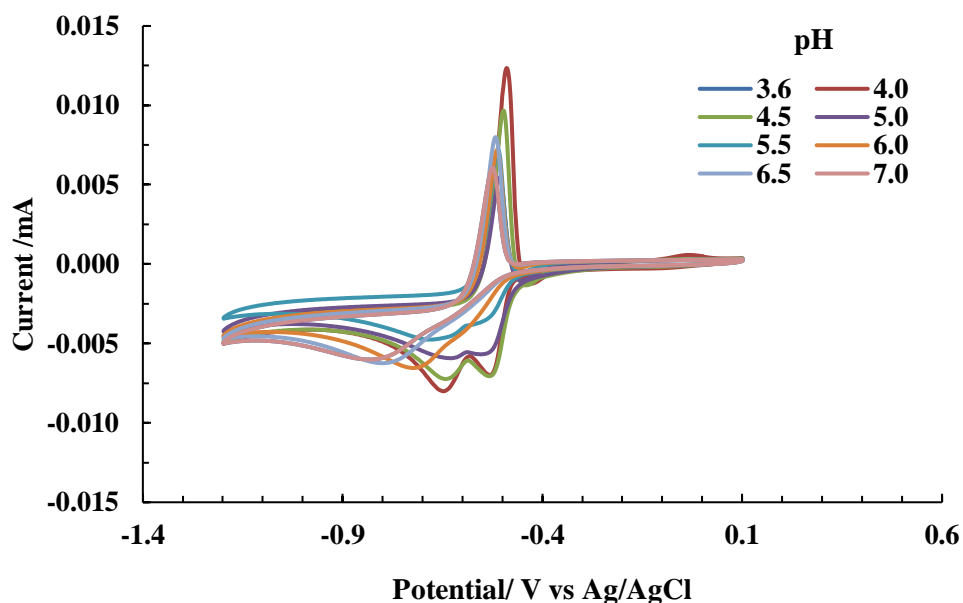


**Figure 3.19.** Cyclic voltammograms of 1.0 mg/L  $\text{Pb(II)}$  (in 0.1 mol/L Acetate buffer) at varying pH of 3.6 to 7.0 using scan rate 100 mV/s.

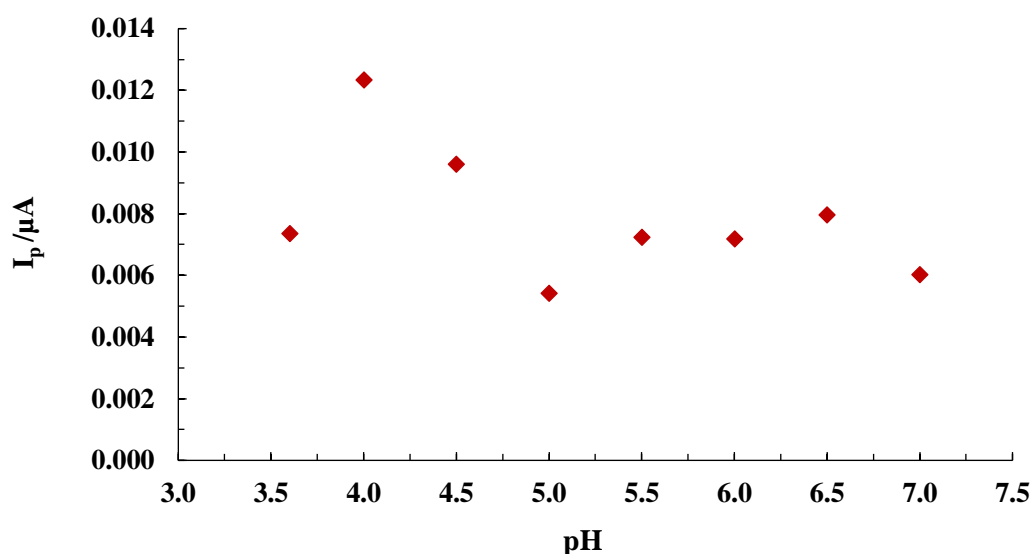
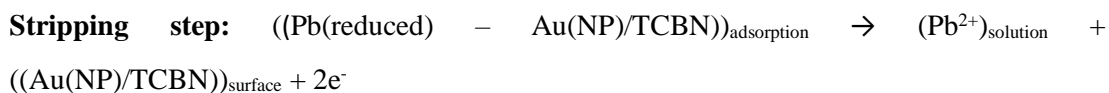
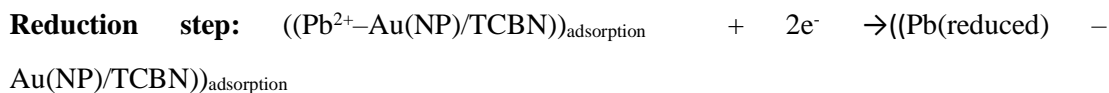
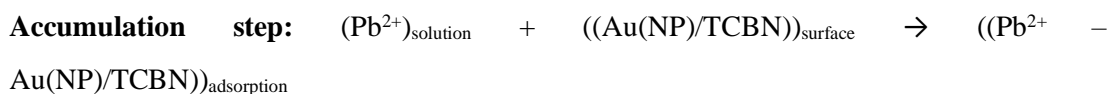


**Figure 3.20.** pH dependence of oxidative peak current ( $I_p$ ) of 1.0 mg/L Pb(II) at Au(NP)/TCBN/GCE.

### 3.5.3. Electroanalytical performance of modified electrode for Pb(II)

The low-level detection of Pb(II) using Au(NP)/TCBN/GCE was conducted using the differential pulse voltammetry and employing the anodic stripping technique. The differential pulse anodic stripping voltammetry (DPASV) is a commonly adopted method in trace electrochemical detection of variety of analytes including metal ions and many other organic and inorganic electroactive species. The method offers high sensitivity with lower background current contributions. The detection method includes primarily three steps: 1) accumulation; 2) reduction; and 3) stripping. Initially, the electroactive species are accumulated at the electrode surface and then electrochemically reduced by applying the potential that is much lower or negative than the oxidation-reduction potential. All electro-reduced species are then oxidized back to the solution by applying a potential scan towards the positive region. The resulting electrochemical signal is recorded as oxidation current or the anodic peak current. Hence, in the detection of Pb(II) at low levels, the

following processes were assumed to take place at the electrode surface-solution interface region:



The oxidation current occurring through these reactions is utilized for sensitive detection of Pb(II).

### 3.5.4. Optimization of electrochemical parameters

The DPASV technique is associated with preconcentration and measurement steps, the efficiency of the detection process is highly dependent upon the parameters controlling these steps. The potential applied during the preconcentration step called deposition/accumulation potential and the duration of accumulation of the electroactive species at the deposition potential is termed as accumulation time. These two parameters greatly demonstrate the peak intensity or even the sensitivity of the working electrode (Wang *et al.*, 2018). Hence, in order to achieve the best electrochemical response, different deposition potentials from -0.8 V to -1.4 V are studied using 50.0 µg/L Pb(II) solution (pH 4.0, time = 120 s, amplitude = 50 mV) and the corresponding DPASV signals are recorded. A plot of oxidative peak current vs applied depositional potential is represented as in Figure 3.21(a & b). The peak current increased from the applied potential -0.8 V and reaches to its maximum value at -1.0 V. However, further increase towards more negative potentials > -1.0 V results in decrease in anodic current intensities. This pattern of the current signal is in good agreement with the deposition potential studied previously using reduced graphene oxide (RGO) incorporated with Au(NP) modified GC electrode for lead (Lee *et al.*, 2015). Similarly, varied deposition potentials using graphitic carbon

nitride modified GCE for 400  $\mu\text{g/L}$  Pb(II) solutions showed an enhanced peak current intensity at moderate deposition potential of -1.0 V (Hatamie *et al.*, 2019). Higher negative potential enabled an enhanced hydrogen gas evolution and the bubbles produced at the electrode surface eventually hinder the deposition of the metal ions, and hence decreased the peak currents (Lee *et al.*, 2015; Segura *et al.*, 2015). Similarly, the effect of time duration for accumulation i.e., from 30 s to 300 s is studied for 50.0  $\mu\text{g/L}$  Pb(II) solution at deposition potential of -1.0 V. Figure 3.22(b) infers that the current signal increases proportionally with accumulation time until it reaches a maximum of 180 s and almost shown a constant value up to 210 s. However, the deposition time > 210 s, the peak current intensity was decreased as studied for the prolonged deposition time of 300 s. The electrochemical response signal is almost similar to the previously reported process using graphene quantum dots and Nafion coated GCE (GC/GQD-NF) and magnetite graphene oxide-benzothiazole-2-carboxaldehyde nanocomposite modified GCE (GO@Fe<sub>3</sub>O<sub>4</sub>@2-CBT/GCE) where the maximum current was observed at 180 s (Pizarro *et al.*, 2020; Dahaghin *et al.*, 2018). Hence, the concentration of Pb(II) accumulated at the electrode surface was intensified with time but become saturated at the deposition time of 180 s. Therefore, the results indicated that the prolonged deposition time could not favor the current response. The potential of -1.0 V and time duration of 180 s are hence, chosen as the optimized conditions for effective preconcentration and more sensitive measurements of Pb(II).

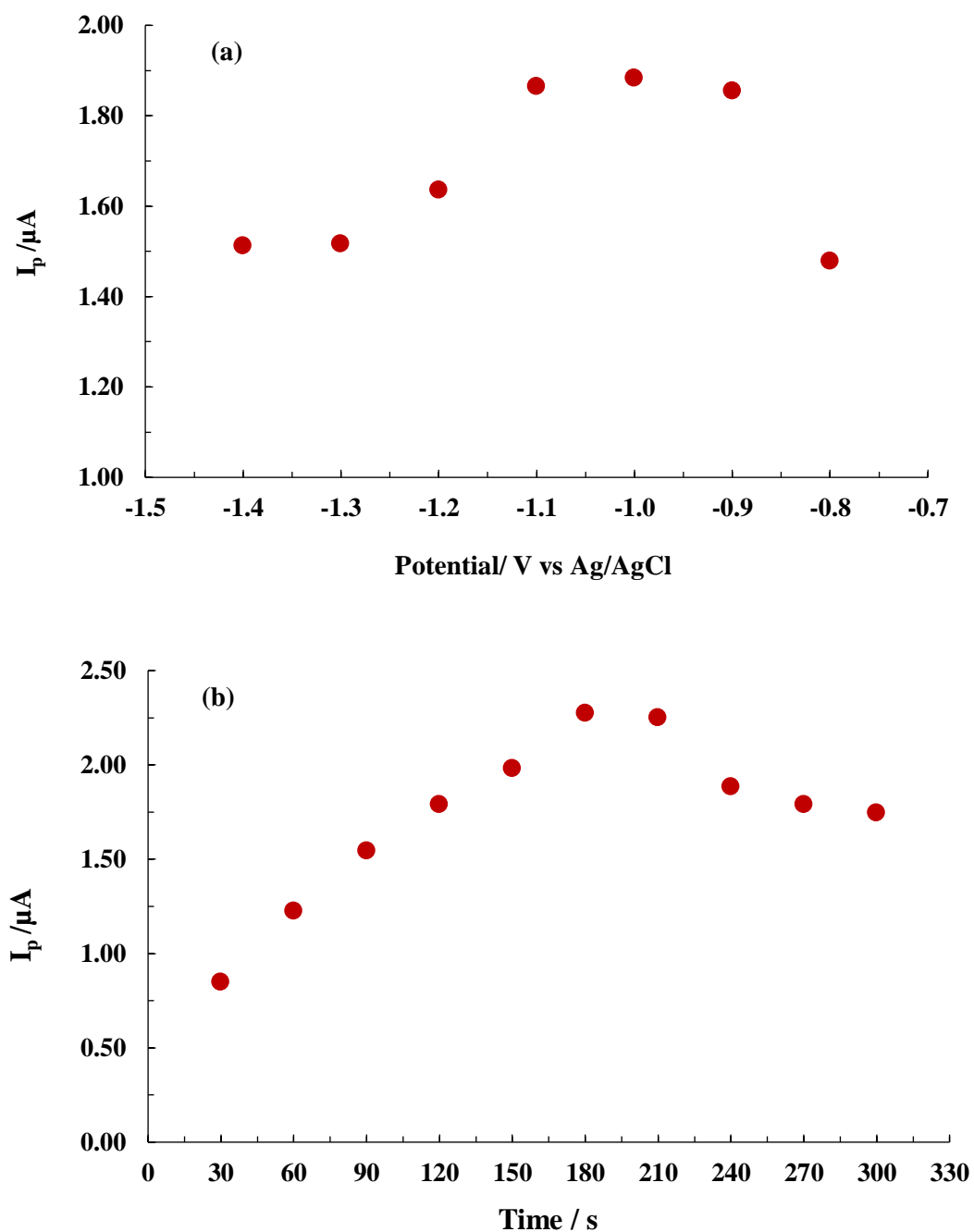


**Figure 3.21 (a-b).** Effects of (a) deposition potential; and (b) deposition time for the anodic peak current for the Au(NP)/TCBN/GCE in 0.1 mol/L acetate buffer, 50.0  $\mu g/L$  Pb(II) solution (Other conditions: pH = 4.0, pulse amplitude = 50 mV, frequency = 10 Hz, pulse increment = 10 mV).

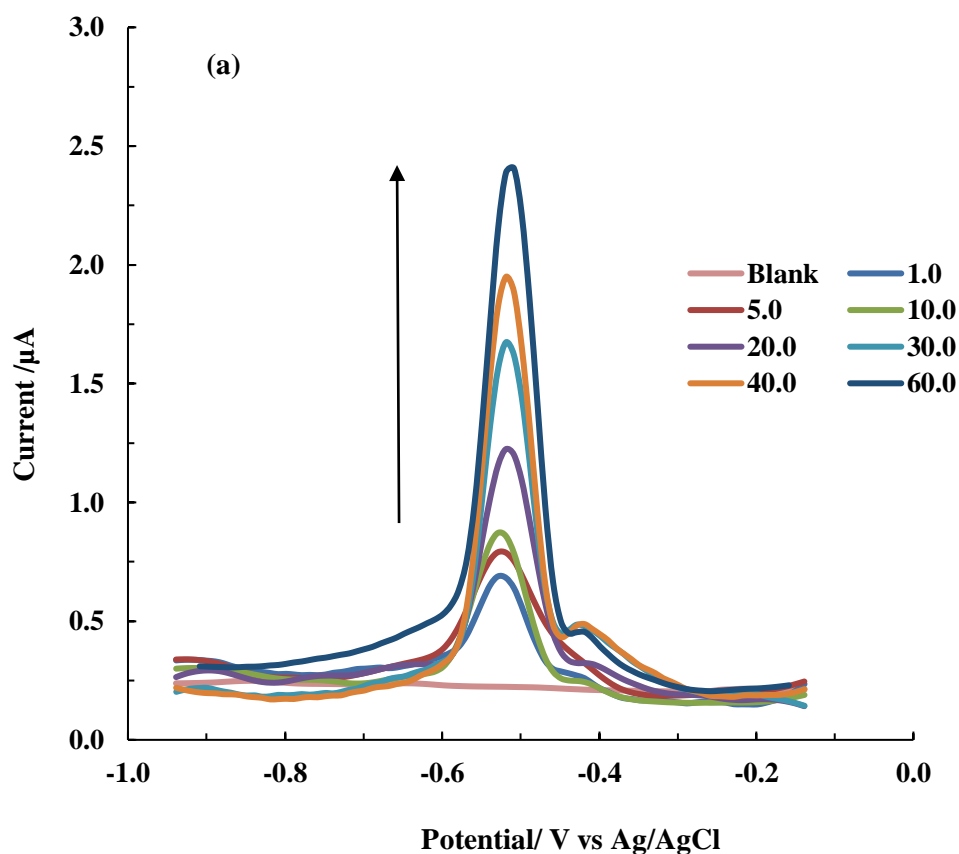
### 3.2.4. Concentration dependence studies and calibration

The Au(NP)/TCBN/GCE was utilized for trace level sensing of Pb(II) employing previously optimized preset conditions in the DPASV measurements. The practical implication of the electrode for the detection of Pb(II) is based on the calibration line and the detection limit of measurements. Therefore, the DPASV measurements were carried out with a wide range of Pb(II) concentrations (1.0 – 60.0 µg/L). Results are illustrated as in Figure 3.22(a). The oxidation peak current for Pb(II) occurred at *Ca* -0.45 to -0.52 V and it was observed that by increasing the concentration of Pb(II) from 1.0 to 60.0 µg/L, the anodic current was increased steadily using the Au(NP)/TCBN/GCE modified electrode.

Further, the regression line was drawn between the oxidative peak current and concentration of Pb(II) (*Cf* Figure 3.22(b)). The calibration line is reasonably fitted well to the straight-line equation  $I(\mu A) = 0.031(\mu g/L) + 0.611$  ( $R^2 = 0.984$ ). Similarly, LOD and LOQ were obtained by the slope of this equation. The LOD and LOQ are calculated as 0.817 µg/L and 2.72 µg/L, respectively. This value falls much below to the maximum permissible level (15.0 µg/L) of Pb(II) as suggested by the US-EPA in drinking water. Therefore, the detection level achieved with the proposed simple electrochemical method is quite useful for trace level sensing of Pb(II) in water bodies. Further, a possible comparison of the present work with some recently reported electrochemical detection of Pb(II) is shown in Table 3.8. It is evident from the table that the detection limit achieved with the Au(NP)/TCBN/GCE sensing platform is significantly lower than several other studies. Hence, this showed the potential of Au(NP)/TCBN/GCE material towards the development of efficient and miniaturized device.

The stability of fabricated electrode is important for repeated use in detection of lead (II). This implies the practical implacability of electrode for prolonged use. Therefore, the stability test of Au(NP)/BNTCODS/GCE electrode was carried out using the 50.0 g/L Pb(II) solution and the repeated measurements were taken under the optimum measurement conditions i.e., 0.1 mol/L acetate buffer, 50.0 µg/L Pb(II) solution [Other conditions: pH = 4.0, pulse amplitude = 50 mV,

frequency = 10 Hz, pulse increment = 10 mV. Each time the measurements were carried out for three times and hence the relative standard deviation (RSD (%)) was obtained. The electrode was washed with distilled water and dried at 40 °C and again employed for next day operations. Similarly, the electrode was employed for third day operations and results are shown in Table 3.9. It is evident from the table that even after third day of operations, the detection of Pb(II) is within the acceptable level since the RSD (%) vales are less than 5%. (*Cf* Table 3.9). These results clearly indicated that the fabricated electrode Au(NP)/TCBN/GCE possessed reasonably fair stability and could be utilized for greater practical implications.



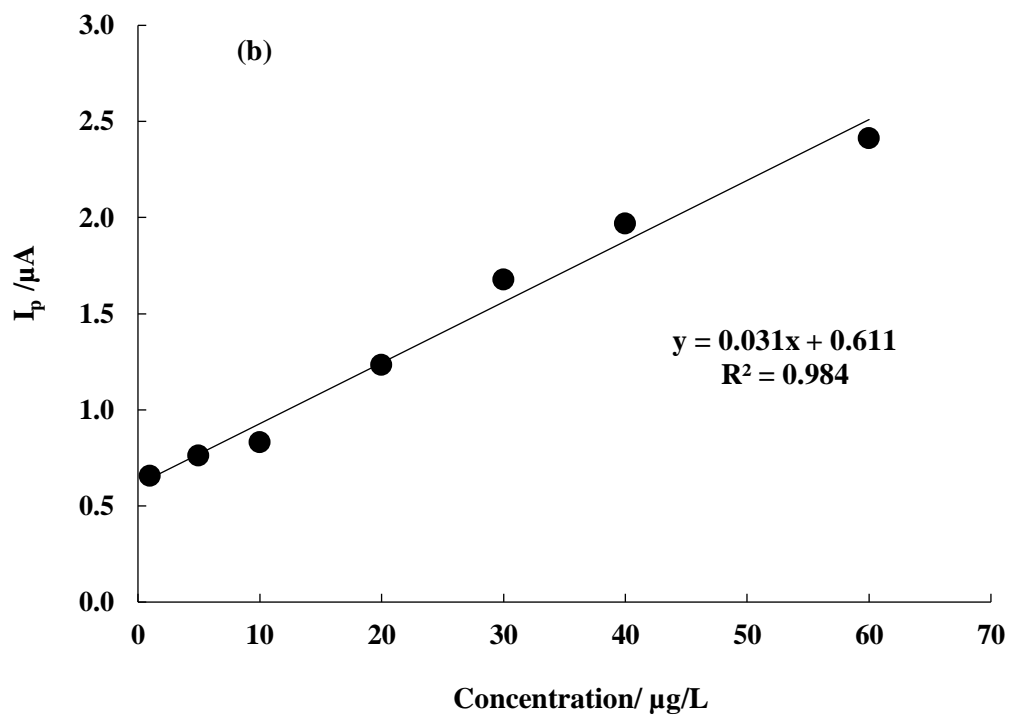


**Figure 3.22.** (a) DPASV voltammograms recorded with Au(NP)/TCBN/GCE (*vs.* Ag/AgCl) at increasing Pb(II) concentrations at a range of 1.0-60.0  $\mu\text{g/L}$ . (pH = 4.0 acetate buffer, deposition potential = -1.0 V, accumulation time = 180 s, pulse amplitude = 50 mV, frequency = 10 Hz, pulse increment = 10 mV) (b) Calibration line for anodic peak current ( $i_{pa}$ ) *vs* Pb(II) concentration



**Table 3.8.** Electrochemical detection of Pb(II) using different electrode materials.

Modifier material	Electrode	Electrochemical method	LOD ( $\mu\text{g/L}$ )	Linear range ( $\mu\text{g/L}$ )	Reference
<b>g-C<sub>3</sub>N<sub>4</sub></b>	GCE	DPASV	1.00	2.5-1000	(Hatamie <i>et al.</i> , 2019)
<b>T3T</b>	GCE	DPASV	1.54	9.93-2845	(Danyıldız <i>et al.</i> , 2017)
<b>G/PANI/PS</b>	SPCE	SWASV	3.30	10-500	(Promphet <i>et al.</i> , 2015)
<b>AgNF</b>	GCE	SWASV	0.74	10-700	(Swetha <i>et al.</i> , 2020)
<b>MWCNT</b>	CPE	SWASV	6.20	20.0-62.0	(Abdel-Galeil <i>et al.</i> , 2014)
<b>BiOCl/MWCNT</b>	GCE	SWASV	1.90	5.0-50.0	(Cerovac <i>et al.</i> , 2015)
<b>MWCNT-<math>\beta</math>CD</b>	SPE	DPASV	0.90	3.1-103.3	(Alam <i>et al.</i> , 2019)
<b>poly(crystal violet)/ graphene</b>	GCE	DPV	1.30	4.1–4040	(Chen <i>et al.</i> , 2014)
<b>Au(NP)/TCBN</b>	<b>GCE</b>	<b>DPASV</b>	<b>0.81</b>	<b>1.0-60.0</b>	<b>This work</b>

T3T - 1H-1,2,4-triazole-3-thiol,  $\gamma$ -C<sub>3</sub>N<sub>4</sub> – graphene coated carbon nitride, AgNF – silver nanoflower, MWCNT-Multiwalled carbon nanotube, RGO-AuNP - Reduced graphene oxide (RGO) decorated gold nanoparticles, SPE – Screen printed electrodes, MWCNT-

Multiwalled carbon nanotube, MWCNT- $\beta$ CD – Multiwalled carbon nanotube- beta cyclodextrin, CPE-carbon paste electrode, SPE-Screen printed electrode.

**Table 3.9.** Stability and repeatability test for Au(NP)/TCBN/GCE electrode in the detection of 50.0  $\mu\text{g/L}$  Pb(II) solution. (pH = 4.0 acetate buffer, deposition potential = -1.0 V, accumulation time = 180 s, pulse amplitude = 50 mV, frequency = 10 Hz, pulse increment = 10 mV).

Time	Repetition	RSD (%)
First Day	3	3.05
Second Day	3	3.80
Third Day	3	4.40

### 3.2.5. Effect of co-existing ions

Selectivity of fabricated electrode Au(NP)/TCBN/GCE towards Pb(II) in presence of several cations is an important aspect for the practical implication of the studies or even to scaling up the proposed method for miniaturized device development. Therefore, ten-fold concentration of each metal ions *viz.*, Hg(II), Zn(II), Ca(II), Cu(II), Fe(II) and Mn(II) was added to 0.1 mol/L acetate buffer solution having known concentration of Pb(II) (i.e., 30.0  $\mu\text{g/L}$ ). Further, the voltammograms for each solution is obtained using the DPASV technique employing the optimal conditions (i.e., pH = 4.0 acetate buffer, deposition potential = -1.0 V, accumulation time = 180 s, pulse amplitude = 50 mV, frequency = 10 Hz, pulse increment = 10 mV). The results depicted in Figure 3.23. The presence of ten-fold of Hg(II), Zn(II), Ca(II), Cu(II), Fe(II) and Mn(II) apparently has not altered the detection of Pb(II) since the concentration of Pb(II) calculated from the stripping peak current is not altered to a considerable degree as compared to the actual concentration of Pb(II). However, the co-existence of Cd(II) enhances the peak current of Pb(II) hence, hampers the detection of Pb(II). DPASV response for Cd(II)

also appeared at the working potential range of Pb (i.e., between -1.0 V and -0.2 V) which indicated that the proximity of the stripping current peak is very close to that of lead ions hence, it interferes the detection of Pb(II).

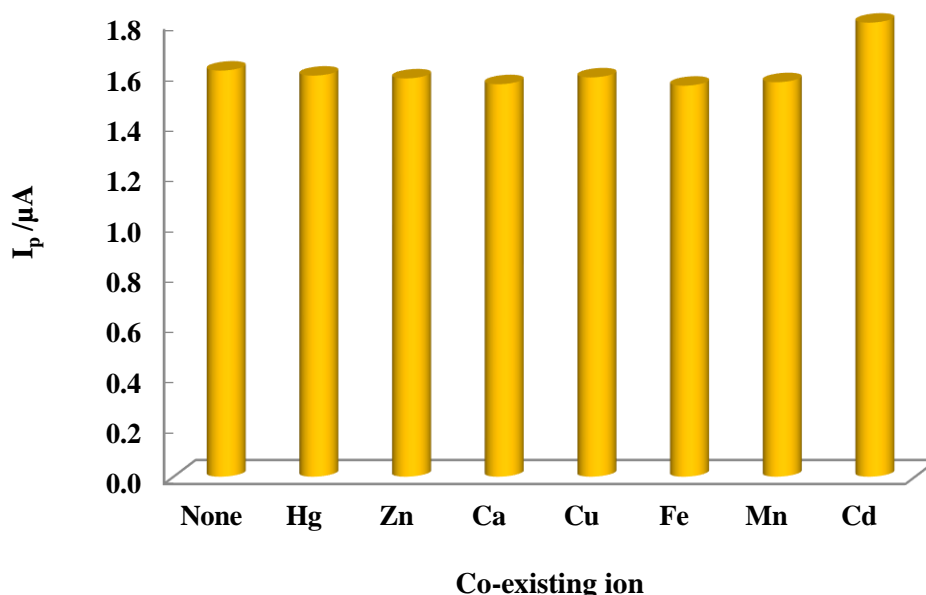


**Figure 3.23.** Bar graph for the DPASV current signal of 30.0  $\mu\text{g/L}$  Pb(II) at Au(NP)/TCBN/GCE in the presence of 300.0  $\mu\text{g/L}$  other co-existing cations (pH = 4.0 acetate buffer, deposition potential = -1.0 V, accumulation time = 180 s, pulse amplitude = 50 mV, frequency = 10 Hz, pulse increment = 10 mV).

### 3.2.6. Studies in real water samples

The practical implication of fabricated electrode for sensitive and efficient measurement of Pb(II) was further validated by investigating the electrochemical experiments with real water samples. The water samples are collected from two natural sources *viz.*, river and spring water in Aizawl City, Mizoram, India. The water samples are extensively analyzed and results are shown in Table 3.7. Varied

values of inorganic carbon (IC) and non-purgeable organic carbon (NPOC) were obtained in these two water samples. Similarly, elemental concentrations and other parameters are also varied in the two water samples. Having marked variation in the physicochemical parameters of these two water samples eventually provides a good choice for selectivity measurements of the fabricated electrode in trace detection of Pb(II). DPASV measurements are conducted using the three different concentrations of Pb(II) i.e., 5.0, 10.0 and 15.0  $\mu\text{g/L}$  using the 0.1 mol/L acetate buffer prepared in these water samples. The other optimal conditions are maintained as described previously (i.e., (pH = 4.0 acetate buffer, deposition potential = -1.0 V, accumulation time = 180 s, pulse amplitude = 50 mV, frequency = 10 Hz, pulse increment = 10 mV). The results are summarized in Table 3.10. DPASV response signal of the electrochemical sensor for detection of Pb(II) in natural water samples is recorded (*cf* Figure 3.24) and compared with the current values from the previous calibration plot ( $I(\mu\text{A})=0.031(\mu\text{g/L}) + 0.611$ ). The results obtained are hence, shown in Table 3.11. These results were in good agreement with the known spiked standard concentrations along with the lead concentration present in water samples as measured by AAS. Further, the recovery percentage is calculated and it is evident that reasonably good recovery was achieved. Results further indicated that the detection of Pb(II) is not noticeably affected in the real water samples; hence, this proved the practical applicability of the device in the detection of Pb(II) in real-world samples.

**Table 3.10.** Analysis of river and spring water quality for different parameters.

Analysis	Parameter	Spring water	River water
<b>TOC</b>	IC	8.25 mg/L	22.5 mg/L
	NPOC	0.69 mg/L	4.42 mg/L
AAS	Element	Conc. (mg/L)	Conc. (mg/L)
	Mn(II)	ND	0.009
	Zn(II)	0.430	0.807
	Ni(II)	ND	ND
	Ca(II)	0.341	11.9
	Pb(II)	ND	0.008
	Fe(II)	0.164	0.231
	Cu(II)	ND	0.0029
<b>Other parameters</b>	pH	6.09	7.33
	ORP	+279 mV	+182 mV
	Resistivity	0.0286 mΩcm	0.0023 mΩcm
	TDS	18.0 mg/L	221 mg/L
	Salinity	0.02 PSU	0.23 PSU
	Conductivity	0.0035 S/m	0.044 S/m
	Nitrate	0.30 mg/L	24.0 mg/L
	Sulphate	1.00 mg/L	14.0 mg/L
	Phosphate	0.04 mg/L	0.20 mg/L

**ND - Not Detected**

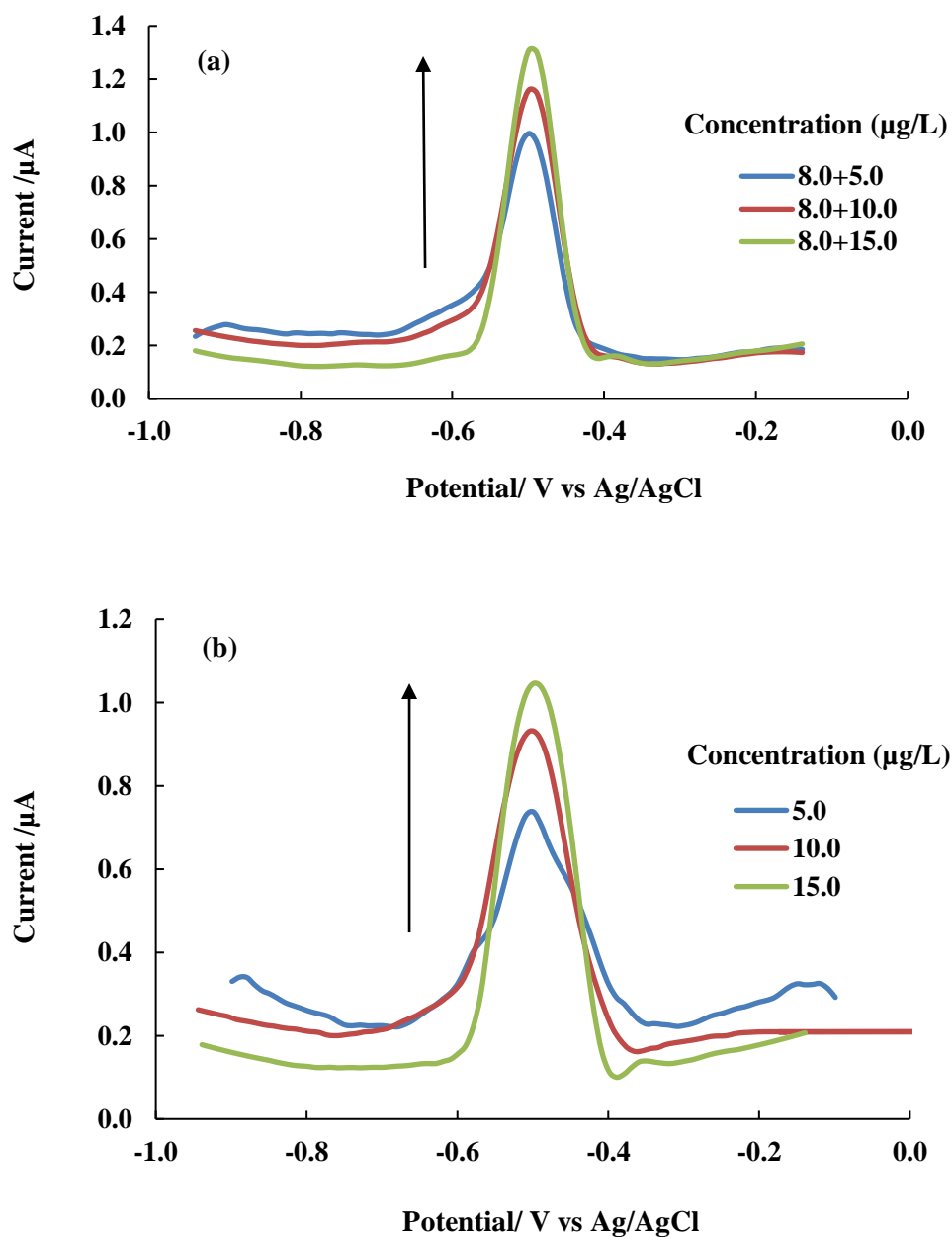


**Figure 3.24.** DPASV for (a) river and (b) spring water samples spiked with 5.0, 10.0 and 15.0  $\mu\text{g/L}$  Pb(II) (pH = 4.0 acetate buffer, deposition potential = -1.0 V, accumulation time = 180 s, pulse amplitude = 50 mV, frequency = 10 Hz, pulse increment = 10 mV).

**Table 3.11.** Determination of Pb(II) in real water samples using Au(NP)/TCBN/GCE.

<b>Water Samples</b>	<b>Amount found in water using AAS (µg/L)</b>	<b>Spiked amount (µg/L)</b>	<b>Total concentration found (µg/L)</b>	<b>% Recovery</b>
<b>Spring</b>	ND	5.0	3.48±0.30	91.6
		10.0	9.61±0.60	96.1
		15.0	14.0±0.29	93.3
<b>River</b>	8.0	5.0	12.3±0.15	94.6
		10.0	17.7±0.45	98.2
		15.0	22.5±0.44	97.7

**ND - Not Detected**

### 3.2.7. Conclusion

The electrochemical determination of Pb(II) employing Au(NP)/TCBN/GCE was studied using 0.1 mol/L acetate buffer as background electrolyte solution at optimum pH of 4.0. The increased electroactive surface area of Au(NP)/TCBN/GCE compared to the bare glassy carbon electrode enabled higher rates of mass transfer for highly sensitive detection of the target analyte. The enhanced electrochemical efficiency towards the detection of lead is correlated with surface structure fabricated electrode having the gold nanoparticles decorated composite materials (TCBN/BN). Ultrasensitive detection of Pb(II) in aqueous media showed that the Au(NP)/TCBN/GCE exhibited a low detection limit of Pb(II) i.e., 0.817  $\mu\text{g/L}$  at a wide linear calibration range 1-60  $\mu\text{g/L}$  having calibration line  $I(\mu\text{A})=0.031(\mu\text{g/L}) + 0.611$  ( $R^2 = 0.984$ ). The nanocomposite sensing platform enabled to detect efficiently the Pb(II) in presence of other common existing metal cations *viz.*, Cu(II), Fe(II), Ca(II), Mn(II), Hg(II), Zn(II) and Cd(II). Moreover, the real matrix analysis of Pb(II) employing the river and spring water showed that the recovery of Pb(II) is ranged from 91.6 to 98.2%. Therefore, the indigenously synthesized Au(NP) and decorated with silane grafted nanocomposite is an efficient material in ultra-trace level detection of Pb(II) and, perhaps, possessed highly sensitive and fairly selective sensing platform.



### 3.6. SINGLE AND SIMULTANEOUS ELECTROCHEMICAL DETECTION OF Cd(II) AND Pb(II)

#### 3.6.1. Electrochemical studies of Pb(II) and Cd(II) using cyclic voltammetry

Studies on electrochemical behavior of Cd(II) and Pb(II) were conducted using cyclic voltammetry technique. The concentrations of these two ions are taken as 5.0 mg/L in 0.1 mol/L acetate buffer (pH 4.0) as supporting electrolyte. The cyclic voltammograms of Cd(II) and Pb(II) are shown in Figure 3.25(a-b). The cyclic voltammograms of Cd(II) and Pb(II) are measured at an optimum potential window of -1.5 to 0.2 V and -1.2 to 0.2 V, respectively at the scan rate of 100 mV/s. A sharp oxidation peak for  $\text{Cd}^{2+}$  occurred at an applied potential of -0.68 V whereas a single reduction peak was obtained at -0.919 V. This implies that the redox process of cadmium involves two-electron transfers i.e.,  $\text{Cd}^{2+} \leftrightarrow \text{Cd}^0$ . Similarly, oxidative and reductive peaks for lead were observed at -0.43 V and -0.64 V attributed to the equilibrium  $\text{Pb}^{2+} \leftrightarrow \text{Pb}^0$  (He *et al.*, 2016). It is to be noted that there is a marked difference in the current intensity of the oxidation and reduction reactions for both these metal ions which suggests that the process is not completely reversible. Further, the current intensity increases using the different modified working electrodes. The peak current values followed the order for the electrodes employed bare GCE, BN/GCE, TCBN/GCE and Ag(NP)/TCBN/GCE. A remarkable increase in peak current was recorded using the nanocomposite materials suggested that these metal ions possessed relatively higher affinity towards the nanocomposite materials viz., BNTCODS and Ag(NP)/TCBN which allowed further enhancement of the electrochemical response for both these metal ions. Relatively, the Ag(NP)/TCBN/GCE electrode showed remarkably higher peak current than the TCBN/GCE electrode, revealed that the presence of Ag(NP) improves significantly the catalytic and conductive property of the material which is useful for its utilization in sensor development. Hence, this enabled us to conduct further studies using the Ag(NP)/TCBN/GCE electrode for low-level detection of Cd(II) and Pb(II).

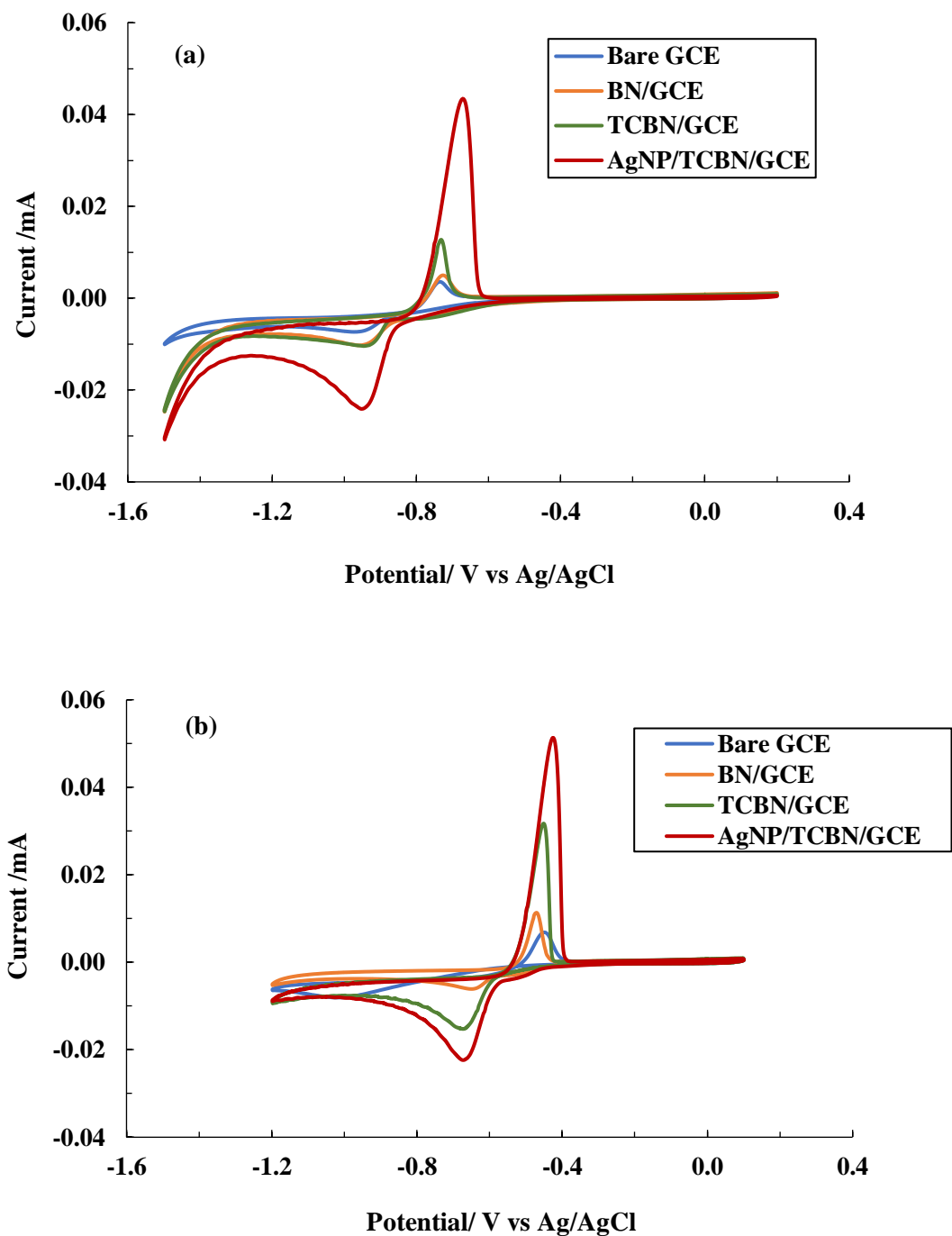
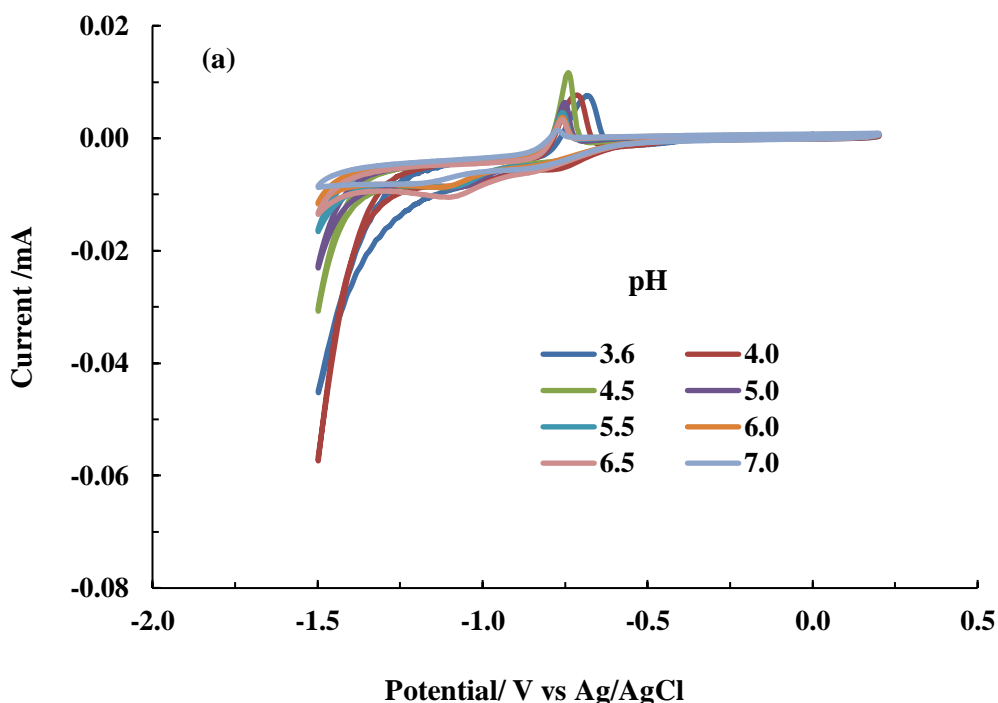


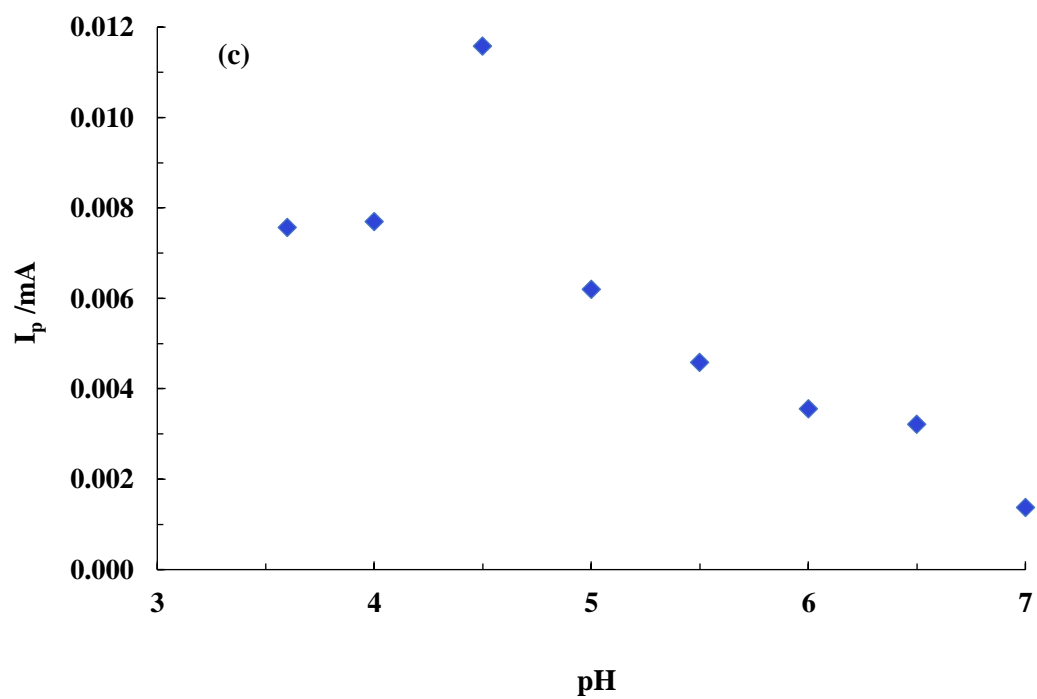
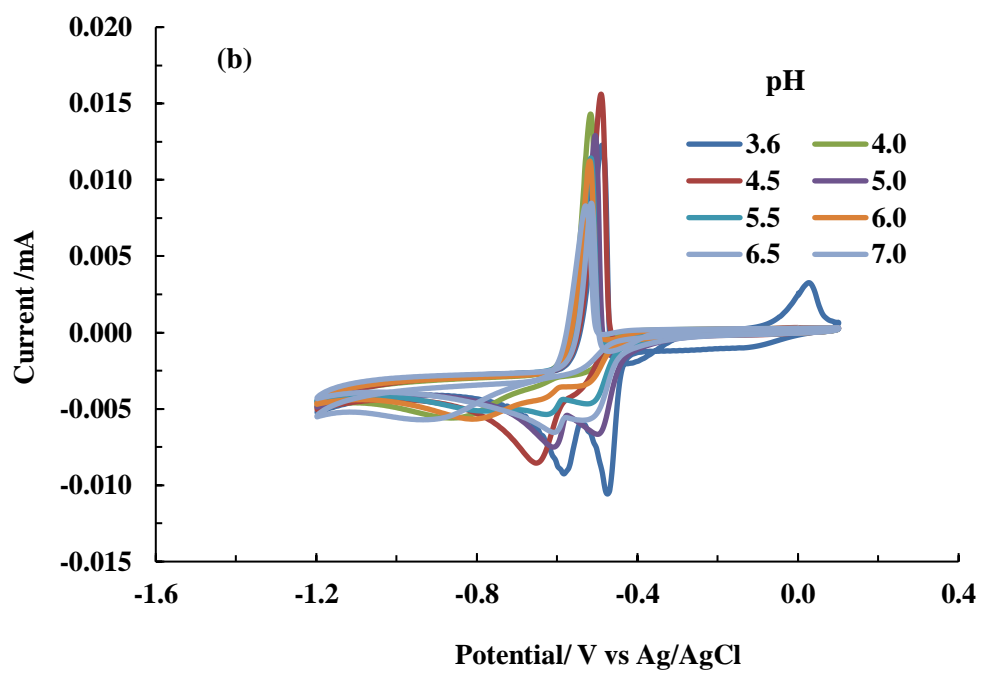
**Figure 3.25 (a-b).** Cyclic voltammograms of 5.0 mg/L (a) Cd(II) and (b) Pb(II) in 0.1 mol/L acetate buffer (pH 4.0) at bare GCE, BN/GCE, TCBN/GCE and Ag(NP)/TCBN/GCE electrodes at the scan rate 100 mV/s.

### 3.6.2. pH dependence studies on detection of Cd(II) and Pb(II)

The electrochemical behavior of Cd(II) and Pb(II) as a function of solution pH (pH 3.6 to 7.0) was investigated using the Ag(NP)/TCBN/GCE electrode. The study was conducted using the 0.1 mol/L acetate buffer and at the scan rate of 100 mV/s. The cyclic voltammograms and change in anodic peak current values with pH is illustrated in Figure 3.26(a-d). Figure 3.26(c & d) demonstrated that the oxidative peak current values were greatly affected by the number of protons in electrolyte solutions since the ionic forms or species of the heavy metals changed with solution pH. At pH below 6.0, Cd and Pb mostly exist in the ionic forms as Cd(II) and Pb(II) whereas at higher pH values, the hydroxo species predominantly exists (e.g.,  $\text{Pb(OH)}_2$ ,  $\text{Pb(OH)}^+$ ,  $\text{Pb}_2(\text{OH})_3^+$ ,  $\text{Cd(OH)}^+$ ,  $\text{Cd(OH)}_2$ ,  $\text{Cd(OH)}_4^{2-}$ ) and the ionic concentrations decrease (Hwang *et al.*, 2019a). The hydroxo species are invariably not attracted by the electrode surface hence, a reduced current response was recorded at higher pH values. Therefore, an enhanced peak current was obtained at slightly acidic or lower pH values (pH *Ca.* 4.5) and decreased peak current at higher pH conditions. This implied that the detection of  $\text{Cd}^{2+}$  and  $\text{Pb}^{2+}$  is preferable at lower pH values using the Ag(NP)/BNTCODS/GCE. It is noted that a maximum peak current for both the ions i.e., Cd(II) and Pb(II) are observed at pH 4.5. At pH < 4.5, slightly a reduced peak current was recorded. This is, perhaps, due to the fact that protonation process and competition between analyte species (Cd(II) and Pb(II)) and protons for the active sites at the electrode/solution interface which hinders significantly the electrochemical process to occur. However, increasing the pH > 4.5 greatly suppressed the current which is ascribed due to the enhanced hydrolysis of Cd(II) and Pb(II) ions to their insoluble hydroxide forms (Dali *et al.*, 2018). Apart from the behavior and species distribution of the target metal ions at different pH values, changes and availability of various structural components based on the conditions of the medium also played crucial role since the bond formations or electrostatic interactions between active sites and analytes are greatly affected by it. An increase in Pb(II), Hg(II) and Cd(II) peak current with pH changed from 3 to 4.5 and declined at pH > 5.5 using the Ch-MMON/GCE (a chitosan mediated bimetallic iron-aluminate mixed metal oxide nanocomposite modified GCE) (Sengupta *et al.*,

2021). Occurrence of higher peak current at lower pH values (i.e., till pH 5.0) was ascertained to possible electrostatic interactions between amine and hydroxyl groups in chitosan and the heavy metals ions. Since the active sites of chitosan are more active in mild acidic conditions, the adsorption as well as binding of the metal ions on its surface are more pronounced between pH 3-5 (Baghayeri *et al.*, 2018). Likewise, interactions through the hydroxyl groups of bentonite and Ag(NP) present on the clay structures are more favored at lower pH values resulting an enhanced current for Cd(II) and Pb(II) ions. Therefore, the pH dependence studies enabled to conduct further experiments at pH 4.5 for the trace determination of Cd(II) and Pb(II).





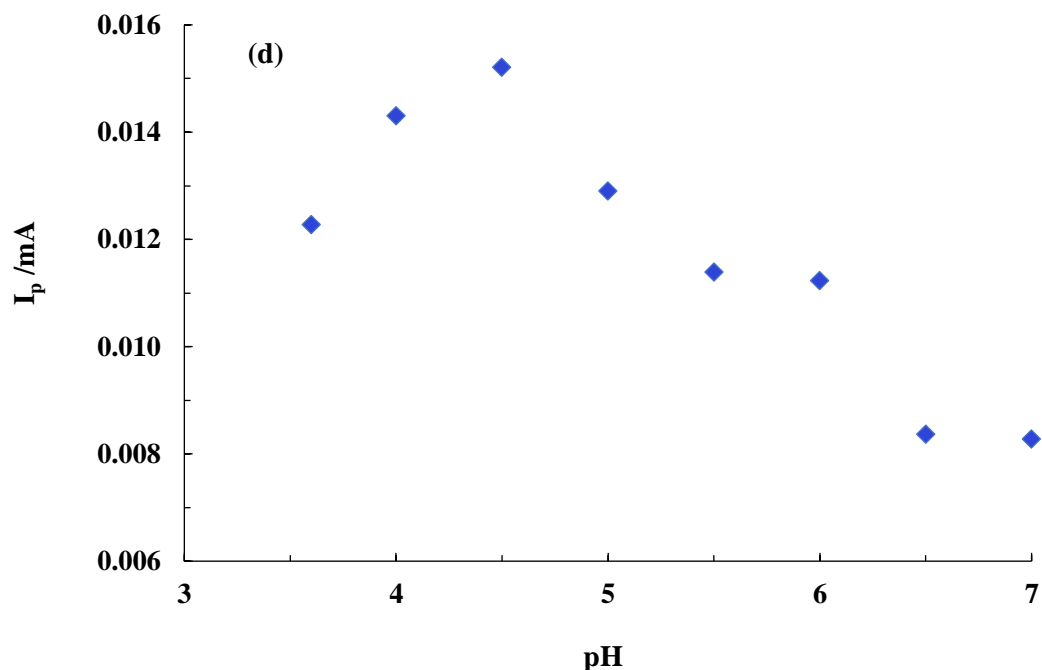


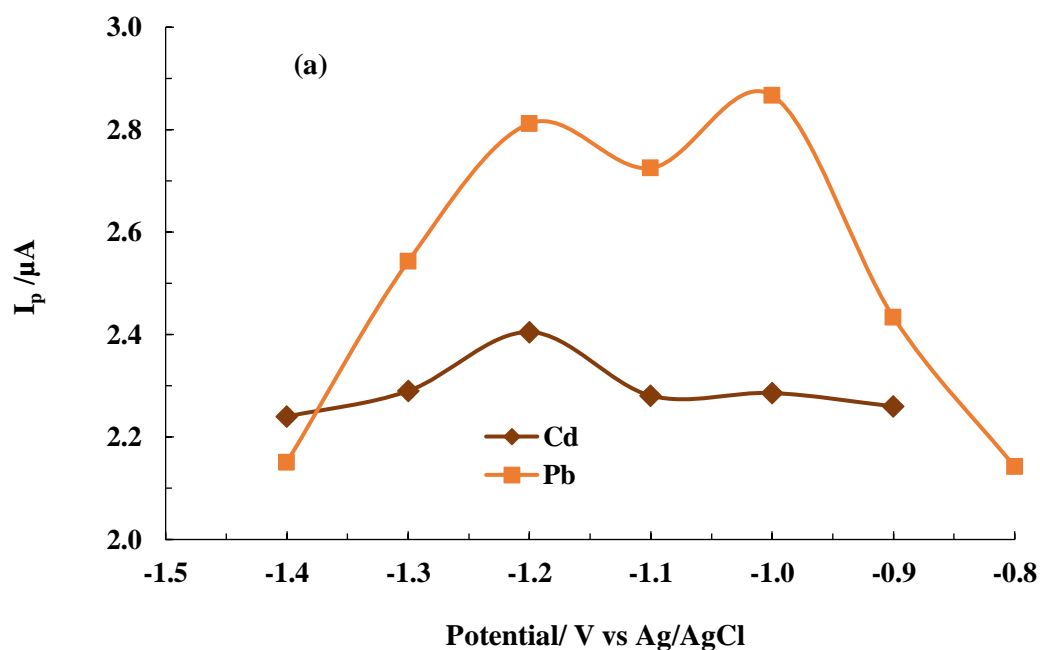
**Figure 3.26 (a-d).** Effect of pH on cyclic voltammograms of 1.0 mg/L (0.1 mol/L acetate buffer) (a) Cd(II); and (b) Pb(II) and change in intensity of oxidative peak currents of (c) Cd(II); and (d) Pb(II) as a function of pH .

### 3.6.3. Electroanalytical performance of modified electrode for Cd(II) and Pb(II)

Anodic stripping voltametric technique was employed for the individual and simultaneous detection of Cd(II) and Pb(II) ions. The method was optimized for the preconcentration step which involves three steps as: i) electrochemical preconcentration step where a negative potential is applied for a specified time to allow accumulation of Cd(II) and Pb(II) at the electrode surface; ii) reduction step where the accumulated ions are reduced; and iii) stripping step where the reduced metal ions are stripped back electrochemically into the solution when scanned towards more positive potentials (Dali *et al.*, 2018; del Pozo *et al.*, 2019). Further, the proposed detection scheme is represented in Scheme 2. Differential voltammograms are collected based on the optimized preconcentration step studied at different potentials and time.



optimal time for deposition/accumulation was obtained using similar experimental conditions at varied time intervals from 30 s to 300 s. The anodic peak currents were obtained as a function of deposition/accumulation time and illustrated in Figure 3.27(b). Figure 3.27(b) indicated that the peak current was increased gradually with the accumulation time and reached to its maximum value at *Ca* 180 s for Cd(II) and at 210 s for Pb(II). It is further observed that the current is almost identical within the deposition/accumulation time of 180-240 s for Pb(II). The strategy was adopted as sensitive detection with least time requirement; hence, the preferred deposition/accumulation time was chosen as 180 s for the detection of these two cations.





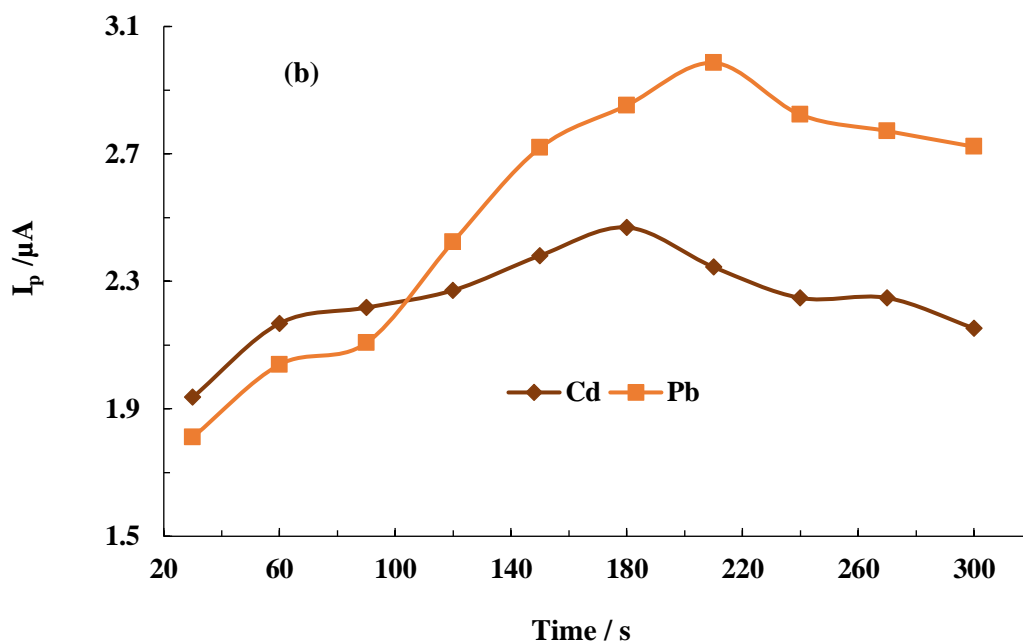
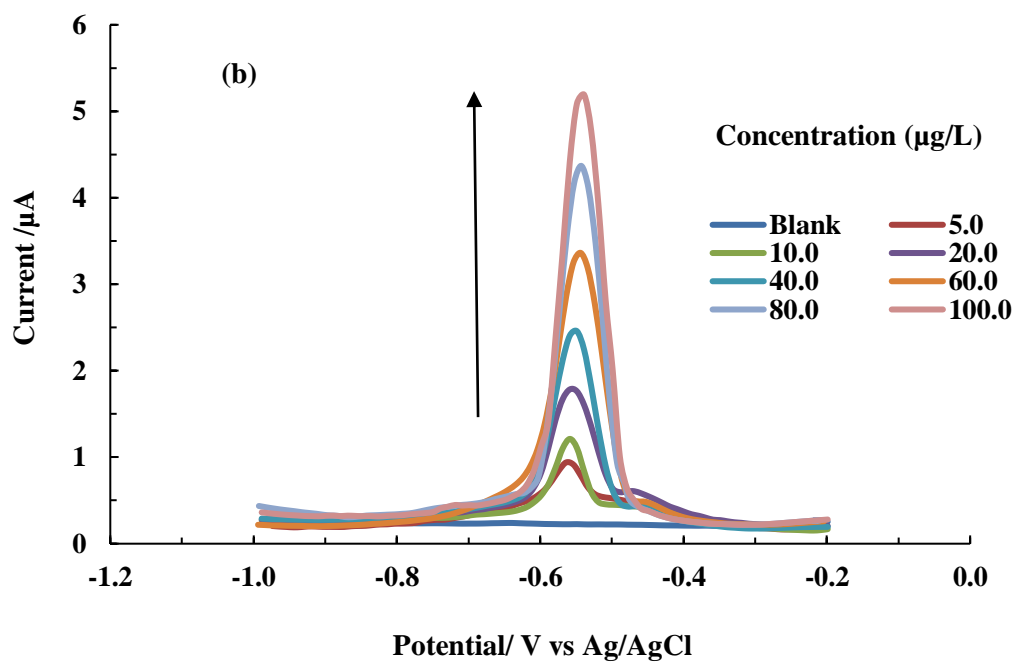
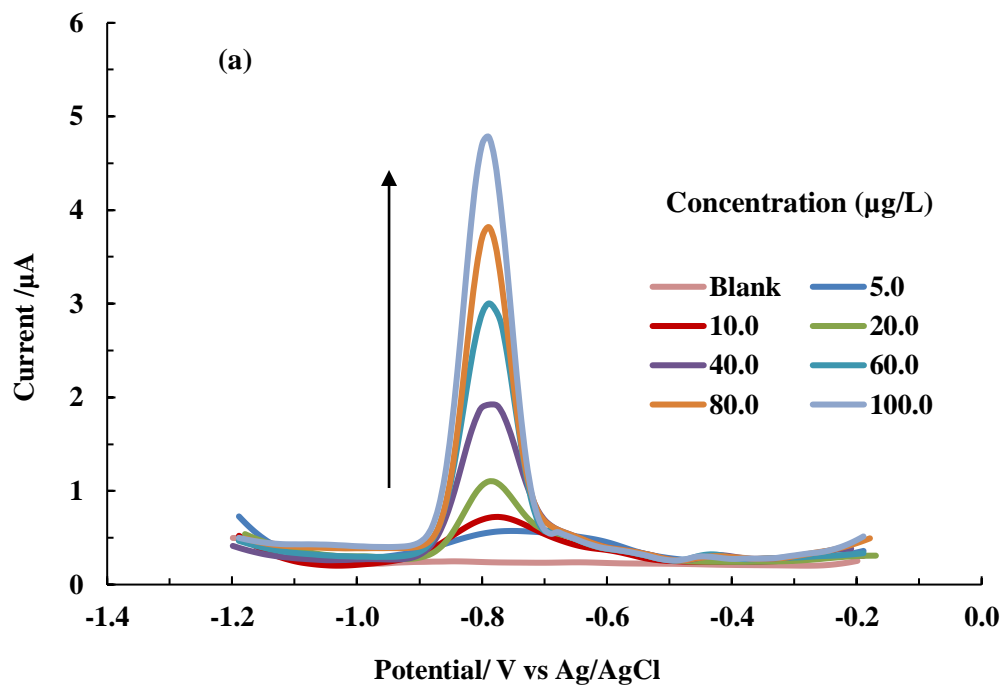


**Figure 3.27 (a-b).** Effect of (a) accumulation potential; and (b) deposition/accumulation time on anodic peak current for 50.0  $\mu\text{g/L}$  Cd(II) and Pb(II) in 0.1 mol/L acetate buffer (pH 4.5) (Other conditions: pulse amplitude = 50 mV, pulse increment = 10 mV and pulse width = 50 ms).

### 3.6.5. Concentration dependence studies and calibration for single species

The single species measurements of Cd(II) and Pb(II) using the Ag(NP)/TCBN/GCE electrode was conducted at different concentrations of analyte in 0.1 mol/L acetate buffer (pH 4.5). Using the optimized preconcentration conditions for each ion, DPASV voltammograms for Cd(II) and Pb(II) are collected at varied concentration range 5.0-100.0  $\mu\text{g/L}$  and shown as in Figure 3.28(a & b). It is observed that well-defined anodic peaks of Cd(II) and Pb(II) occurred at the applied potentials of -0.78 V and -0.55 V, respectively. Although the oxidative peak potentials for these two metal ions are found close to each other however, it is possible to detect these two ions simultaneously by employing the nanocomposite modified GCE. Further, the anodic peak current was increased as the analyte concentration was increased and the calibration line was drawn between the peak

current and analyte concentrations (Figure 3.28(c & d)). Further, reasonably, a good linearity was obtained between the anodic peak current and analyte concentrations having the calibration lines  $I_p(\mu A) = 0.045 \mu g/L + 0.288$  ( $R^2 = 0.994$ ) and  $I_p(\mu A) = 0.044 \mu g/L + 0.792$  ( $R^2 = 0.995$ ), respectively for Cd(II) and Pb(II). These results are very similar to the straight line equations of Cd(II) calibration line i.e.,  $I_p(\mu A) = 0.048 (\mu M) + 0.288$  ( $R^2 = 0.999$ ) obtained with a sensing platform based on chitosan, gold nanoparticles and graphene nanocomposite (Wu *et al.*, 2020). The LOD and LOQ were obtained using the known equations as given previously (Shrivastava and Gupta, 2011). The LOD and LOQ were found to be 0.710  $\mu g/L$  and 2.348 for Pb(II), and 0.726  $\mu g/L$  and 2.42  $\mu g/L$  for Cd(II), respectively. Hence, these results revealed that the proposed electrochemical sensing platform using the nanostructured material possessed a fair affinity for these analytes. This is attributed due to the porous nature of the bentonite clay and the large number of active sites available for interaction with these cations. Further, the presence of Ag(NP) provides large surface area and aided the conductivity as well which enhances the electrocatalytic performance of the material and hence enabled an efficient and selective low-level detection of Cd(II) and Pb(II). Similarly, in previous studies, enhanced electrochemical activities towards target metal ions were achieved due to the surface features exhibited by silver nanoflowers and Ag(NP) for detection of Pb(II) and Cd(II) ions respectively in cigarette and cosmetics (Swetha *et al.*, 2020; Wu *et al.*, 2020).



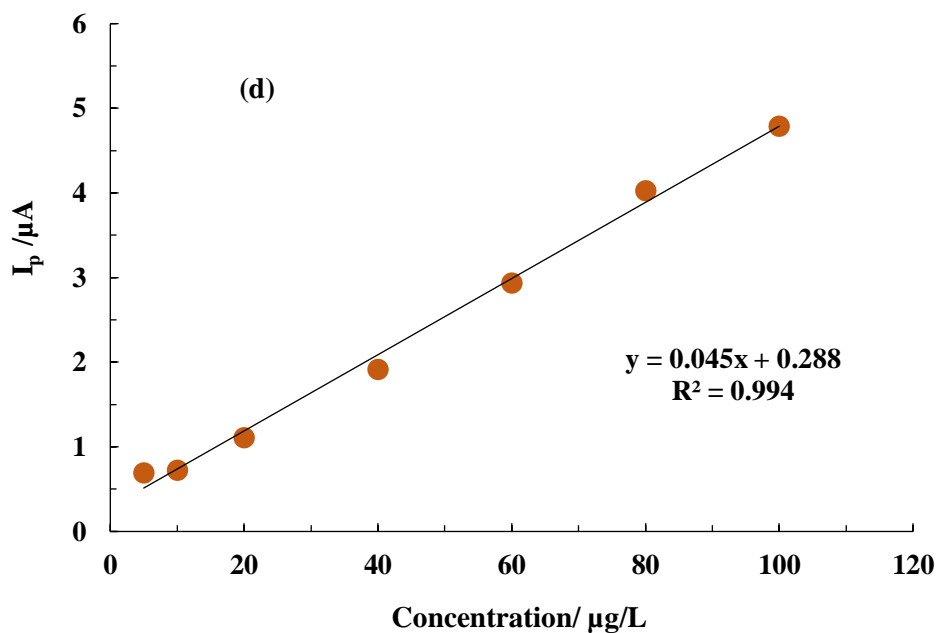
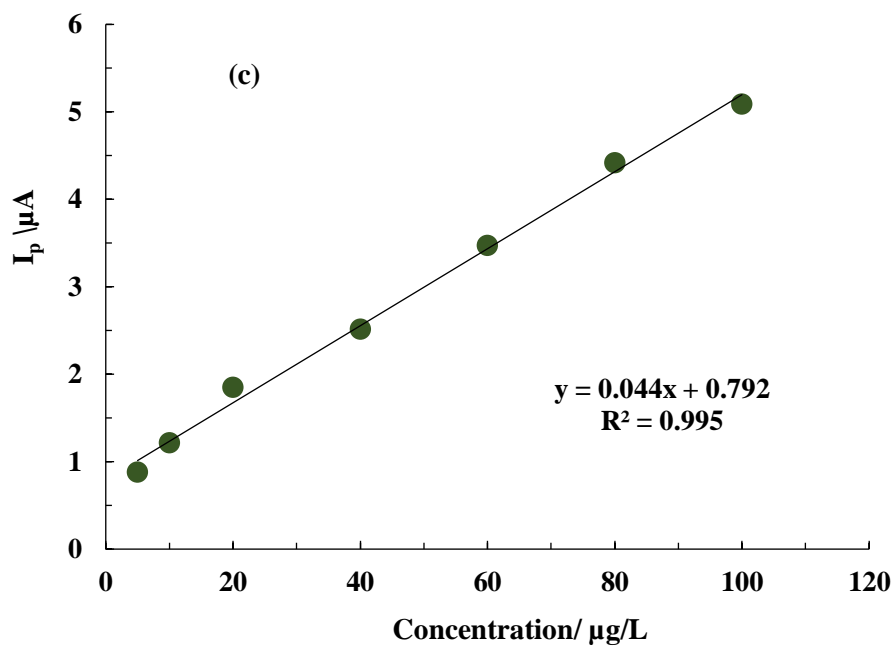


**Figure 3.28.(a-d)** DPASV curves obtained for (a) Cd(II) ; and (b) Pb(II) using the Ag(NP)/TCBN/GCE electrode (Acetate buffer: 0.1 mol/L; pH: 4.5); Calibration curves obtained for (c) Cd(II); and (d) Pb(II) detection [Other conditions: pulse amplitude = 50 mV, pulse increment = 10 mV and pulse width = 50 ms].

### 3.6.6. Concentration studies and calibration for simultaneous detection

Based on the preconcentration conditions and DPASV results obtained for the Cd(II) and Pb(II) detection individually, the concurrent detection of the two metal ions were performed using the Ag(NP)/TCBN/GCE electrode. The deposition potential of -1.2 V and deposition/accumulation time of 180 s were chosen as the pre-optimized condition for the detection of these two ions simultaneously. It was observed that very well-defined two separate peaks for Cd(II) and Pb(II) are obtained and these two peaks were not overlapped with each other even though the oxidation potentials of these two ions were in close proximity. The oxidation peak current for both ions was increased linearly with increase in concentrations of Cd(II) and Pb(II). Further, the calibration curves for both the ions were obtained at a linear concentration range of 5.0-60.0 µg/L. The equations were obtained as:  $I_p(\mu A) = 0.045(\mu g/L) + 0.288$  and  $I_p(\mu A) = 0.044(\mu g/L) + 0.792$  having the regression constants ( $R^2$ ) of 0.994 and 0.995 for Cd(II) and Pb(II), respectively (*cf* Figure 3.29(a-b)). These values are not having marked difference from the calibration line obtained for single ion detection i.e., the Cd(II) and Pb(II). Further, the LOD and LOQ values were calculated as 0.79 µg/L and 2.66 µg/L ((for Cd(II))) and 0.88 µg/L and 2.96 µg/L ((for Pb(II))), respectively which are quite close to those obtained from the single system detection. Thus, the fabricated working electrode using the nanocomposite material showed greater affinity towards the Cd(II) and Pb(II), allowing low level and efficient detection of Cd(II) and Pb(II) simultaneously. Indeed the detection limit obtained in the present method is found to be comparable or even better than many other reports. A different method of accumulating metal ions to electrode surface was introduced by Deshmukh and co-workers using EDTA (Deshmukh *et al.*, 2018). EDTA was incorporated to the polyaniline/multiwalled carbon nanotubes nanocomposite (PANI/SWCNTs) through covalent bonding and the EDTA\_PANI/SWCNTs nanocomposite modified stainless steel electrode (EDTA\_PANI/SWCNTs/SS) was used for single species detection of Pb(II), Cu(II) and Hg(II). However, the LOD obtained for Pb(II) detection was 1.65 µM (or 2.607 µg/L) which is higher than LOD reported in the present work. Similarly, the bidentate ligand, 1,10-phenanthroline was employed for modifying GCE and was

used for detection of Cd(II) via complexation with the 1,10-phenanthroline modified GCE film (Oztekin *et al.*, 2011). Comparison of the present work with other chemically modified electrodes employed for simultaneous detection of Cd(II) and Pb(II) are summarised in Table 3.12.

Further, the stability and reproducibility of the fabricated electrode was assessed for repeated operations as performed for three consecutive days. The stability of the Ag(NP)/BNTCODS/GCE electrode was determined using 50.0 µg/L solution of Cd(II) and Pb(II) and repetitive measurements were made using the optimized measurement conditions. The relative standard deviation (RSD (%)) from triplicate measurements were obtained for three consecutive days. The results are shown in Table 3.13. It is evident from the Table that the RSD (%) obtained for the detection of both these ions was always less than 5%. Nearly identical values of oxidative peak current were obtained for all the measurements. Therefore, the Ag(NP)/BNTCODS coated electrode possessed a good reproducibility and is stable enough to detect Cd(II) and Pb(II) repeatedly.

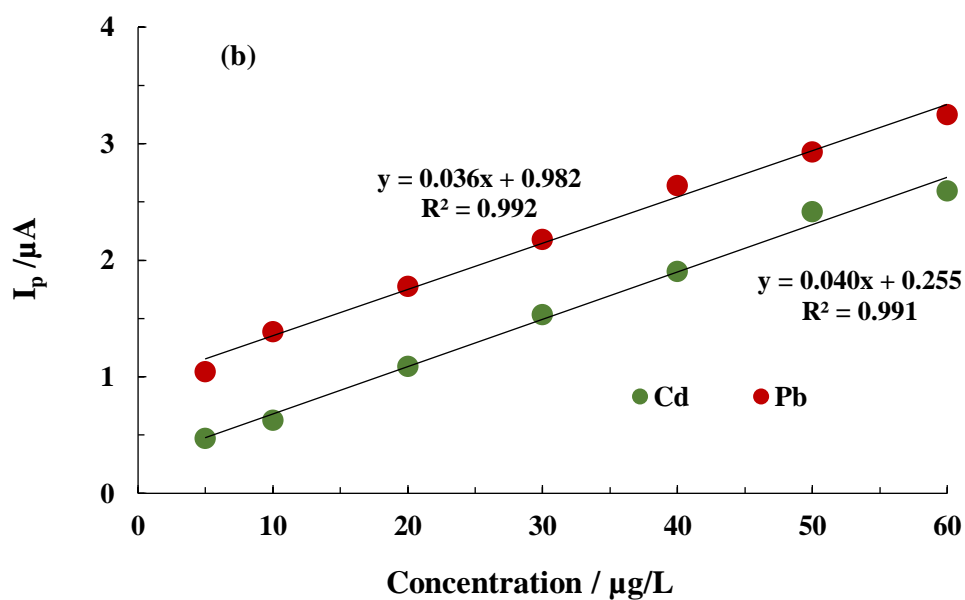
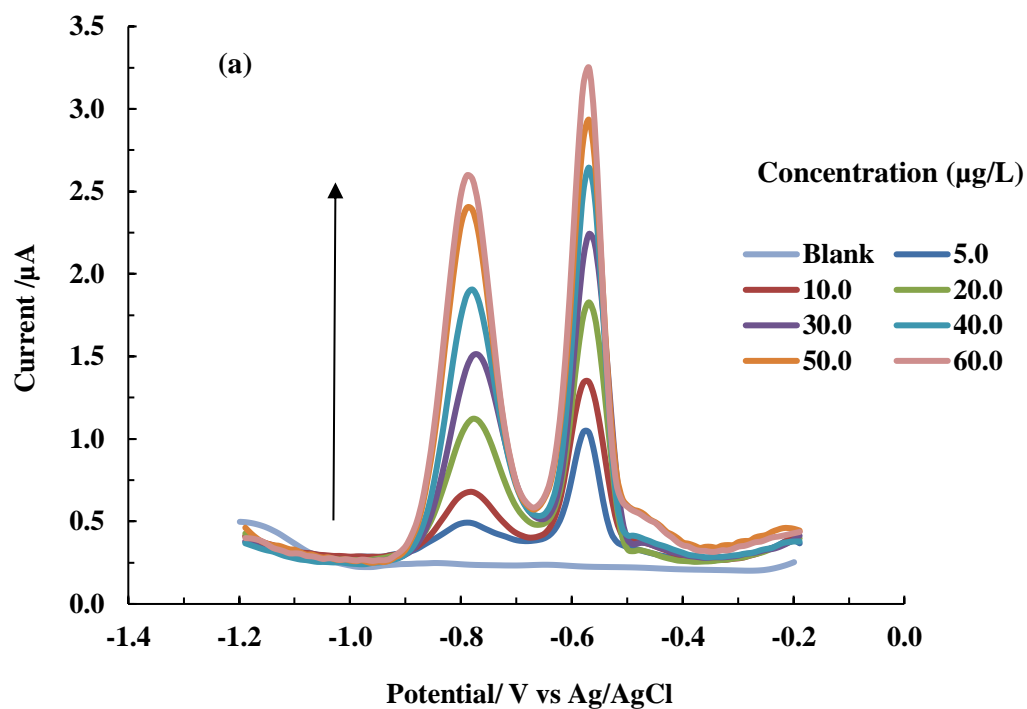


**Figure 3.29** (a) DPASV for simultaneous detection of Cd(II) and Pb(II) at 5.0-60.0  $\mu\text{g/L}$  concentration range (b) Calibration plot of Cd(II) and Pb(II) (Other conditions: pulse amplitude = 50 mV, pulse increment = 10 mV and pulse width = 50 ms).

**Table 3.12.** Comparison of the present work with other recent reports for simultaneous detection of Cd(II) and Pb(II) on the basis of LOD values.

Sensing platform	Method	LOD ( $\mu\text{g/L}$ )		Linear range ( $\mu\text{g/L}$ )	Reference
		Cd(II)	Pb(II)		
BBKS-CPE	CV, SWV	9.56	8.98	1000-100, 80.0-8.5	(Hermouche <i>et al.</i> , 2021)
Sb <sub>2</sub> O <sub>3</sub> /MWCNT/CPE	LSASV	1.932	2.964	80.0-150.0	(Hai <i>et al.</i> , 2020)
GSH@Fe <sub>3</sub> O <sub>4</sub> /MGCE	SWASV	0.171	0.182	0.5-100.0	(Baghayeri <i>et al.</i> , 2018)
Hg-Bi/PDAAQ/GCE	SWASV	0.107	0.105	0-50.0 (Cd) 0.012-0.12 (Pb)	(Hassan <i>et al.</i> , 2020)
GO@Fe <sub>3</sub> O <sub>4</sub> @2-CBT /GCE	SWASV	0.03	0.02	0.07- 13, 13-80(Cd) 0.03-7.2,7.2-43 (Pb)	(Dahaghin <i>et al.</i> , 2018)
2D bismuthene-graphene/GCE	SWASV	0.3	0.3	1-30	(Lazanas <i>et al.</i> , 2020)
ZnFe <sub>2</sub> O <sub>4</sub> /GCE	DPASV	1.26	0.56	10.0-130.0	(Ns <i>et al.</i> , 2018)
modified-NPBiE	SWASV	1.3	1.5	5.0-40.0	(Hwang <i>et al.</i> , 2019b)
Fe <sub>3</sub> O <sub>4</sub> /MWCNT/LSG/CS/GCE	SWASV	0.1	0.07	1.0-200.0	(Xu <i>et al.</i> , 2019)
BOC/GCE	DPASV	4.24	3.97	10.0-50.0	(Zhang <i>et al.</i> , 2020)
BiONPs-CS-GCE	DPASV	7.98	31.08	0.8 – 5.6 $\mu\text{M}$ (Cd) 0.4-2.8 $\mu\text{M}$ (Pb)	(Hao <i>et al.</i> , 2016)
Ag(NP)/TCBN/GCE	DPASV	0.79	0.88	<b>5.0-60.0</b>	<b>This work</b>



CPE- Carbon paste electrode, NPBiE- modified nanoporous bismuth electrode , Fe<sub>3</sub>O<sub>4</sub>/MWCNT/LSG/CS -Fe<sub>3</sub>O<sub>4</sub>/multiwalled carbon nanotube/laser scribed graphene/chitosan, BOC – bismuth oxycarbide, GO@Fe<sub>3</sub>O<sub>4</sub>@2-CBT –magnetized graphene oxide modified with benzothiazole-2-carboxaldehyde, Hg-Bi/PDAAQ –bismuth (Hg-Bi) /poly(1,2-diaminoanthraquinone), GSH@Fe<sub>3</sub>O<sub>4</sub>/M – glutathione functionalized magnetic nanocomposite, BBKS-*Bigarreau Burlat* kernel shell, BiONPs-CS - Bismuth oxide nanoparticles and chitosan

**Table 3.13.** Stability and repeatability tests using the Ag(NP)/TCBN/GCE in the detection of 50.0 µg/L Cd(II) and Pb(II) (Acetate buffer: 0.1 mol/L; pH: 4.5).

Time	Repetition	RSD (%)	
		Cd(II)	Pb(II)
First day	3	3.7	4.1
Second day	3	4.2	3.9
Third day	3	4.4	4.7

### 3.6.7. Effect of co-existing ions

The selectivity of the nanocomposite modified electrode for the detection of Cd(II) and Pb(II) was conducted in presence of several co-existing ions. The experiment was conducted by 10-fold addition of Hg(II), Zn(II), Ca(II), Cu(II), Fe(II) and Mn(II) (i.e., 500.0 µg/L) and having the 50.0 µg/L of analytes solutions. The DPASV graphs were obtained and shown as in Figure 3.30. It clearly shows that sharp and well-separated oxidation peaks for Cd(II) and Pb(II) were obtained even in presence and absence of interfering ions. It was also noted that one additional and prominent peak was occurred at the potential *Ca* -1.10 V which was attributed due to the Zn oxidation (Hassan *et al.*, 2020). Further, a small shift in peak position was recorded for Cd(II) and Pb(II). This is possibly explained with the fact that the

observed current is primarily dependent on the rate at which analytes move from the bulk of solution to the fabricated electrode surface i.e., the mass transport phenomenon. The diffusion of analyte is a random movement through the bulk solutions and favored with low concentrations however, at high bulk concentrations it is disrupted and requires more potential to compensate the mass transport of analytes. Therefore, in presence of high concentrations of other ions, resulted a slight shift of peak potential towards the positive side for the Cd(II) and Pb(II).

Moreover, a slight decrease in peak current of Cd(II) was observed. This is, possibly, because some of Zn(II) ions, which are present at high concentrations occupied some of the active sites of electrodes. This indicates that the simultaneous detection of Zn(II) ions is also feasible within a certain range of concentration using the nanocomposite electrode. However, the oxidation peak intensity of Pb(II) was almost unaffected or a small increase of  $< 1\%$  was observed. In general, however, the nanocomposite modified electrode showed relatively very high affinity towards the Cd(II) and Pb(II) and the studies reaffirmed the greater selectivity for these two ions. This eventually enabled it to detect the analyte ions at trace levels efficiently with high selectivity.

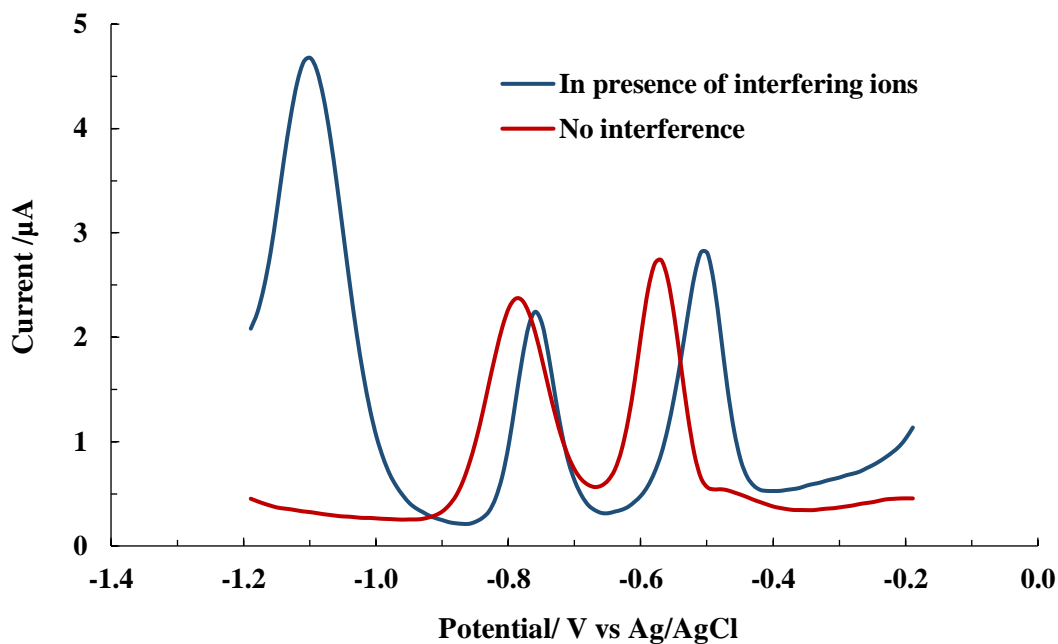


**Figure 3.30.** Effect of various interfering ions on the detection of 50.0  $\mu\text{g/L}$  of Cd(II) and Pb(II) using the DPASV measurements at pH 4.5 (0.1 mol/L acetate buffer) in the absence and presence of 500.0  $\mu\text{g/L}$  of each co-existing ion ((Hg(II), Zn(II), Ca(II), Cu(II), Fe(II) and Mn(II)).

### 3.6.8. Studies on real water sample

Real water sample was collected from Khurpui, a spring water from a small locality in Aizawl City, Mizoram, India during the post monsoon dry season. The sample was filtered with Whatman filter paper (20-25  $\mu\text{m}$ ) and subjected for the elemental contents, carbon contents and other water parameters using the AAS (atomic absorption spectrometer), TOC (total organic carbon) and Multiparameter photometer, respectively. Various parametric analyses of spring water are given as in Table 3.14. The elemental analyses showed that various ions *viz.*, Zn, Ca, Fe, Mn and Mg are present at low levels. However, the TOC results showed that organic and inorganic carbon contents are present in water samples at significantly high levels. The high value of TOC (2.431 mg/L) is possible because of humic substances present in water. Similarly, the inorganic carbon (7.219 mg/L) is due to the carbonate and bicarbonate contents. Further, the real water samples were spiked with various

concentrations of Pb(II) and Cd(II). The differential pulse voltammograms were collected using the spiked water samples and results were shown in Figure 3.31. The figure clearly showed that the anodic peak current was almost similar to that obtained for the calibration studies for these two ions. The concentrations of the metal ions obtained compared to the spiked amount are given in Table 3.15 along with the recovery percentage of these two ions. Reasonably a good recovery was obtained for these two ions. These results confirmed that the electrochemical performance of the nanocomposite modified glassy carbon electrode was found to be a useful sensing platform for simultaneous trace level detection of Cd(II) and Pb(II) in real water samples. The technique could eventually be implied for the analytical tool development for efficient and simultaneous detection of Cd(II) and Pb(II) in aqueous solutions.

**Table 3.14.** Analysis of Spring water (Khurpui) quality for different parameters.

Analysis	Parameter	Spring water (Khurpui)
TOC	IC	7.21 mg/L
	NPOC	2.43 mg/L
AAS	Element:	Conc. (mg/L)
	Mn(II)	0.0029
	Zn(II)	0.387
	Ni(II)	ND
	Ca(II)	0.542
	Pb(II)	ND
	Fe(II)	0.143
	Cu(II)	ND
	Mg(II)	1.00

<b>Other parameters</b>	pH	6.61
	ORP	+204 mV
	Resistivity	0.036 mΩcm
	TDS	16.0 mg/L
	Salinity	0.050 PSU
	Conductivity	0.008 S/m
	Nitrate	0.600 mg/L
	Sulphate	0.800 mg/L
	Phosphate	0.030 mg/L

ND-Not Detected

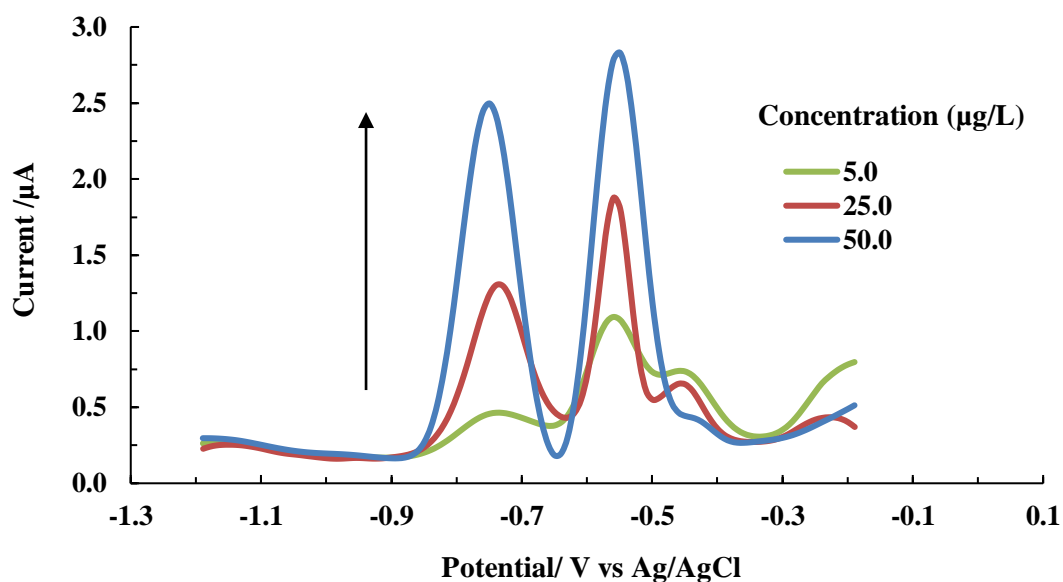


**Figure 3.31.** DPASV graphs obtained for various concentrations of Cd(II) and Pb(II) in real water sample (spring) using Ag(NP)/TCBN/GCE electrode.

**Table 3.15.** Determination of Cd(II) and Pb(II) in spring water using DPASV technique.

Spiked amount of analyte ( $\mu\text{g/L}$ )	Found ( $\mu\text{g/L}$ ) $\pm 3\sigma$		Recovery %	
	Cd(II)	Pb(II)	Cd(II)	Pb(II)
<b>5.0</b>	4.67 $\pm$ 0.32	5.68 $\pm$ 0.61	93.5	113.6
<b>25.0</b>	24.8 $\pm$ 0.28	24.8 $\pm$ 0.30	99.6	99.5
<b>50.0</b>	54.0 $\pm$ 0.73	49.9 $\pm$ 0.44	108	99.9

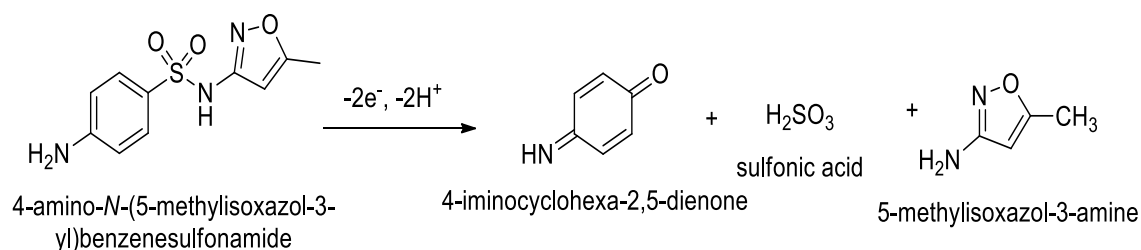
### 3.6.9. Conclusion

The determination of Cd(II) and Pb(II) utilizing the nanocomposite modified electrode, Ag(NP)/TCBN/GCE was studied and demonstrated using cyclic voltametric and DPASV techniques. Comparison of electrochemical behavior of both the species show highly improved signal with the Ag(NP)/TCBN/GCE as compared to the unmodified GCE and even the pristine BN and TCBN. The studies were optimized for solution pH, preconcentration time and deposition potential for enhanced and efficient detection of Cd(II) and Pb(II). Further, calibration lines were obtained separately with individual and simultaneous detection of Cd(II) and Pb(II). The calibration lines were obtained for Cd(II) and Pb(II) as  $I_p(\mu A) = 0.045 \mu g/L + 0.288$  ( $R^2 = 0.991$ ) and  $I_p(\mu A) = 0.044 \mu g/L + 0.792$  ( $R^2 = 0.992$ ), respectively in the individual detection of these two ions. Further, the simultaneous detection showed limit of detection limit (LOD)  $0.79 \mu g/L$  for Cd(II) and  $0.88 \mu g/L$  for Pb(II). It was found that linear plots and detection limits obtained at single species detection is not differed significantly with the simultaneous detection of these two ions in aqueous medium. The detection method was intended to be utilized in the simultaneous detection of the metal ions in real matrix samples which gave the recovery of 93 to 108 % for cadmium and 99 to 113 % for lead detection. Presence of several interfering ions viz., Hg(II), Zn(II), Ca(II), Cu(II), Fe(II) and Mn(II) are not apparently affected the detection of these two ions. However, the presence of Zn(II) has shown additional and well separated oxidative peak. The real matrix analysis using the spiked Cd(II) and Pb(II) river water showed reasonably a good recovery of analytes. Therefore, the Ag(NP)/TCBN/GCE is an efficient and selective sensing platform for trace detection of Cd(II) and Pb(II) in aqueous media and the studies provide useful input data for development of miniaturized sensing device.

### 3.7. ELECTROCHEMICAL DETECTION OF SULFAMETHOXAZOLE

#### 3.7.1. Electrochemical studies of sulfamethoxazole using cyclic voltammetry

The electrochemical behavior of sulfamethoxazole (SMX) was investigated by CV and the voltammograms were recorded using the bare GCE, BN/GCE, TCBN/GCE, Ag(NP)/TCBN/GCE and Au(NP)/TCBN/GCE fabricated electrodes. The CV scans of SMX (50.0 mg/L prepared in 0.1 mol/L KCl; acetate buffer (pH 4.0)) was recorded at a potential window of -0.2 V to 1.2 V at a scan rate of 100 mV/s and presented in Figure 3.32. It is evident from the figure that a sharp anodic peak current is observed with all the electrodes employed. This indicated that the oxidation of SMX occurred on the electrode surface and resulted with the sharp anodic peak current. However, no reductive peak current was observed in the reverse scan of the voltammograms for all these electrodes. Thus, oxidation of SMX on the electrode surface is an irreversible process. Further, the SMX oxidation peak potentials at bare GCE, BN/GCE, and TCBN/GCE is appeared *Ca.* +1.15 V, while it is *Ca.* 1.02-1.06 V using Ag(NP)/TCBN/GCE and Au(NP)/TCBN/GCE. A small shift in overpotential was observed using the Ag or Au nanoparticles decorated nanocomposite. The oxidation reaction on the surface of the electrode is demonstrated with the two electrons loss and the oxidation of SMX resulted with 4-iminocyclohexa-2,5-dienone and 5-methylisoxazol-3 amine through the -NH<sub>2</sub> group. The possible reaction is demonstrated as in equation (3.2):



It was mentioned previously that the oxidation of sulphonamides is accompanied by a corresponding iminobenzoquinone intermediate formation (Czupryniak *et al.*, 2012). A similar result was obtained for the oxidation of SMX using the carbon paste electrode. The shift of overpotential position was also



obtained for piroxicam i.e., 0.63 V to 0.56 V with a multiwalled carbon nanotube (MWCNT) modified carbon paste electrode in comparison to the bare carbon paste electrode (Abbaspour and Mirzajani, 2007). This was explained due to the enhanced electrocatalysis of the piroxicam oxidation process on of the surface of MWCNT. Moreover, the peak current values for the Ag(NP)/TCBN/GCE and Au(NP)/TCBN/GCE were significantly increased as compared to the bare GCE, BN/GCE, and TCBN/GCE. This revealed that the electro-catalyzed oxidation process was greatly favored at the nanoparticles decorated nanocomposite surfaces. These results prompted us to utilize the Ag(NP)/TCBN/GCE and Au(NP)/TCBN/GCE for further studies in the trace and efficient detection of SMX.

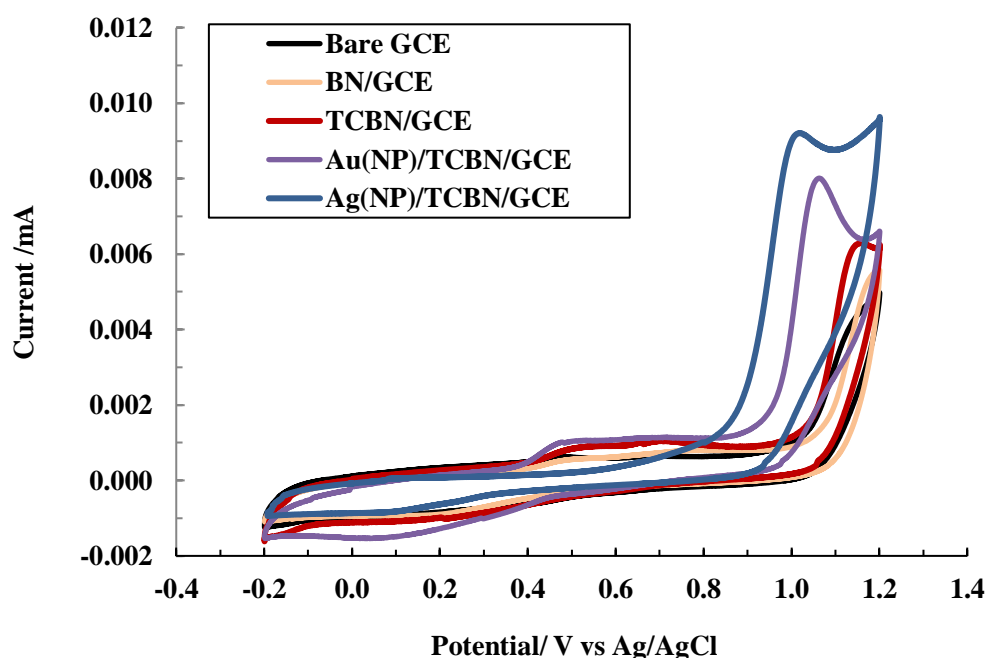


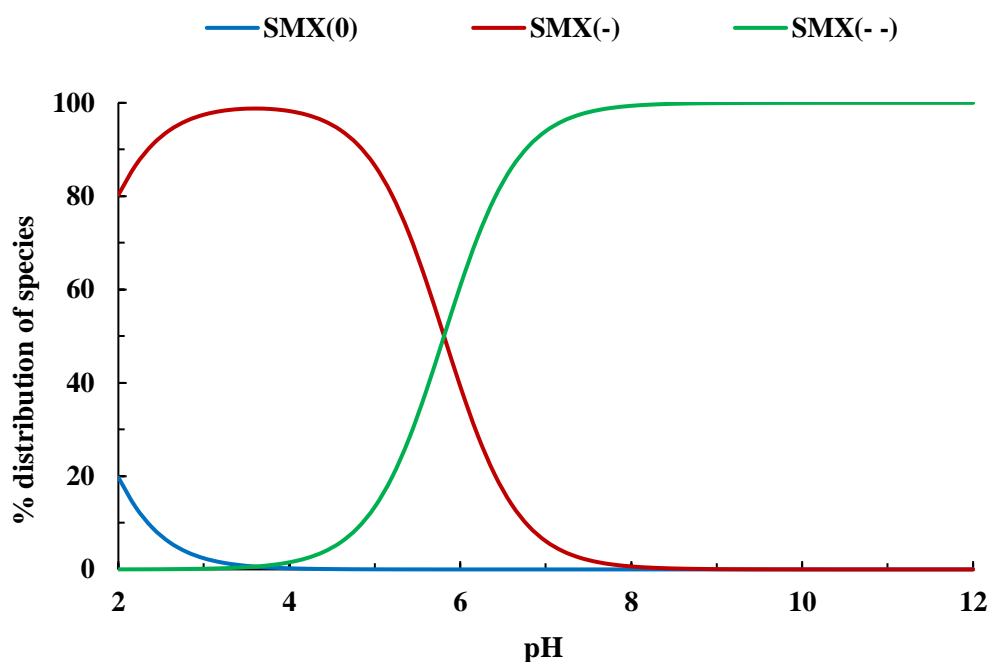
**Figure 3.32.** Cyclic voltammograms of 50.0 mg/L SMX using the bare glassy carbon electrode and various fabricated glassy carbon electrodes [Background electrolytes: 0.1 mol/L KCl, Acetate buffer: pH 4.0].

### 3.7.2. Electroanalytical performance of modified electrodes for sulfamethoxazole

Differential pulse anodic stripping voltammetry showed better solution as compared to the cyclic voltammetry. This is due to better charging current as compared to the overall background current which is insignificant in DPASV. Therefore, the DPASV technique is chosen for other electroanalytical studies in the determination of SMX. The parameter optimizations and subsequent investigations with real samples are conducted using the nanocomposite (Ag(NP)/TCBN and Au(NP)/TCBN) supported glassy carbon electrodes. The detection strategy of SMX at modified electrodes is conducted by the anodic stripping method. The anodic peak current obtained as a result of electrochemical processes is utilized for determining SMX in aqueous samples.

### 3.7.3. pH dependence studies on detection of sulfamethoxazole

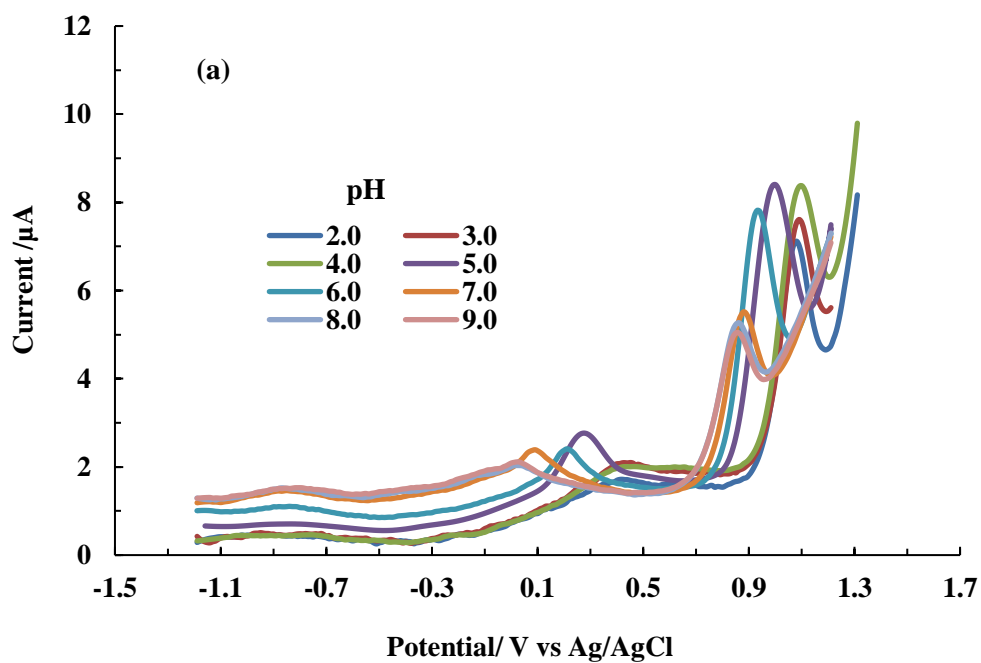
The effect of pH on oxidative peak current of SMX were investigated at wide range of pH 2.0 to 9.0. The species distribution of SMX at various pH is controlled by the acid dissociation constant values ( $pK_a$  values). The SMX molecule have  $pK_{a1} = 1.39$  and  $pK_{a2} = 5.81$  (Simon *et al.*, 2011). Therefore, using the  $pK_a$  values of SMX, the speciation studies are conducted separately and results are shown in Figure 3.33. The figure showed that SMX predominantly consists of the anionic species ( $SMX^-$  or  $SMX^{2-}$ ) within the pH 2.6-10.0. At  $pH \leq 2.6$ , the SMX is contained with neutral SMX species. Moreover,  $pH \geq 6.0$ , is predominantly contained with  $SMX^{2-}$  anionic species. Therefore, at neutral pH conditions SMX is having the di-anionic species. Similar speciation studies are demonstrated previously (Simon *et al.*, 2011).



**Figure 3.33.** Distribution of various species of SMX as a function of pH.

The species of SMX plays an important role in the adsorption or interaction on the surface of the electrode having a nanostructured sensing platform accordingly influences the current signals in the voltammetric measurements. The differential pulse voltammograms of SMX at different pH values are presented in Figures 3.34(a & b). Figure reveals that peak current as well as peak potentials are significantly affected by the solution pH. The dependance of peak potential on the pH condition reveals that the electrochemical process at the electrode surfaces is controlled by proton transfer reactions (Abbaspour and Mirzajani, 2007). At mild acidic medium (pH 4.0-5.0), a maximum peak current was observed at both the fabricated electrodes. This gradually falls at pH >7.0. Moreover, the peak potential also shifted towards more negative potential as the solution pH approaches pH 7.0. This is because of the deprotonation of SMX hence, enabled the oxidation process is more favored at higher pH values (Arvand *et al.*, 2011). The fluctuation patterns of peak current values with pH at both electrodes are displayed in Figure 3.34(c). The figure reveals that the best response of peak current is obtained at pH 4.0 to 5.0 using these

electrodes. Therefore, pH 4.0 to 5.0 is the optimum pH for enhanced electrocatalytic oxidation of SMX. Hence, pH 4.0 is chosen as suitable pH and the subsequent measurements were continued at this pH using both the nanostructured electrodes.



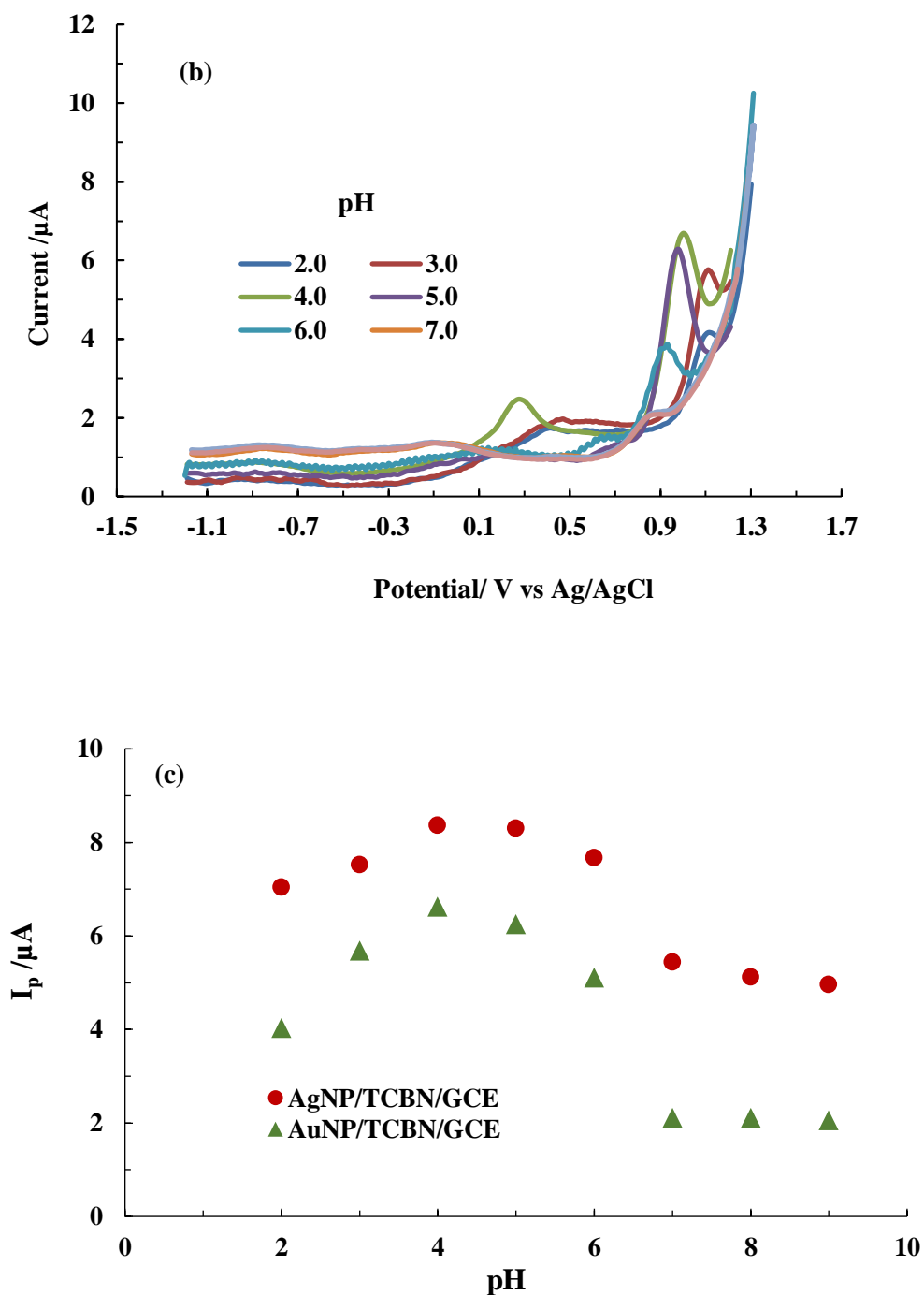


**Figure 3.34. (a-c).** DPASV graphs of 20.0 mg/L SMZ at different pH values obtained with (a) Ag(NP)/TCBN/GCE; (b) Au(NP)/TCBN/GCE; and (c) Plots of peak current ( $I_p$ ) values as a function of pH. (Other conditions; pulse amplitude = 50 mV, pulse increment = 10 mV and pulse width = 50 ms).

#### 3.7.4. Optimization of electrochemical parameters

The impact of deposition potential and time duration on the anodic peak current of sulfamethoxazole were investigated taking 20.0 mg/L of SMX as prepared in 0.1 mol/L KCl in acetate buffer (pH 4.0) within excitation potentials of -1.3 V to -0.7 V. The DPASV measurement conditions are chosen as: pulse amplitude: 50 mV, pulse increment: 10 mV, and pulse width: 50 ms. The peak current values with respect to different depositional potentials follow almost a linear increase as the potential is increased with more negative values. The electrochemical response is maximum at an applied potential of -1.2 V, thereafter, the anodic peak current was decreased for both the nanostructured electrodes (*Cf* Figure 3.35(a)). Hence, a depositional potential of -1.2 V was chosen as the optimum potential for preconcentration of SMX. Furthermore, studies on deposition times between 30-300 s at an increment of 30 s are performed at deposition potential of -1.2 V and keeping other electrochemical conditions as: pulse amplitude: 50 mV, pulse increment: 10 mV, and pulse width: 50 ms. The peak current values for both electrodes (*Cf* Figure 3.35(b)) are showed almost a linear increase as the deposition time is increased up to 210 s. However, further increase in deposition time > 210 s, a slight decrease or almost a constant peak current is observed. Therefore, the results suggested that a relatively longer deposition time (i.e., 210 s) is required for complete saturation of SMX to the fabricated electrode surface. Hence, a period of 210 s was chosen as an optimal time for accumulating SMX at the Ag(NP)/TCBN/GCE and Au(NP)/TCBN/GCE electrode surface.

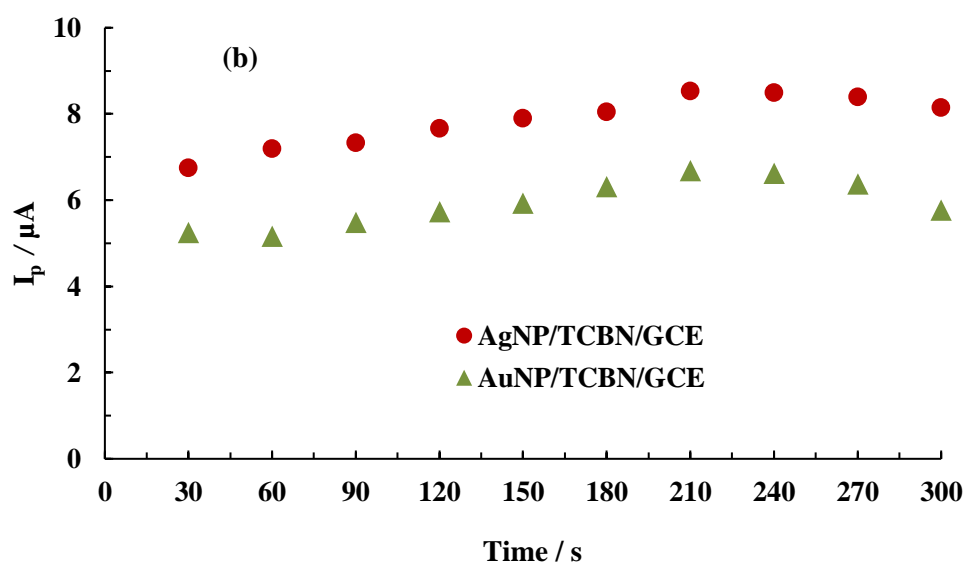
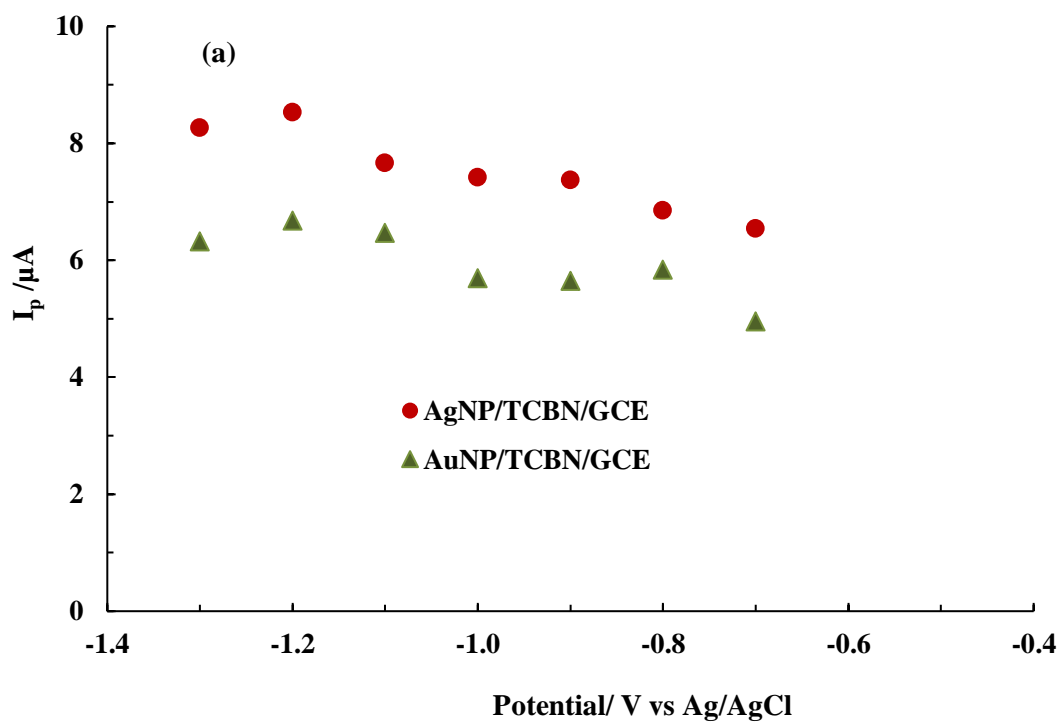
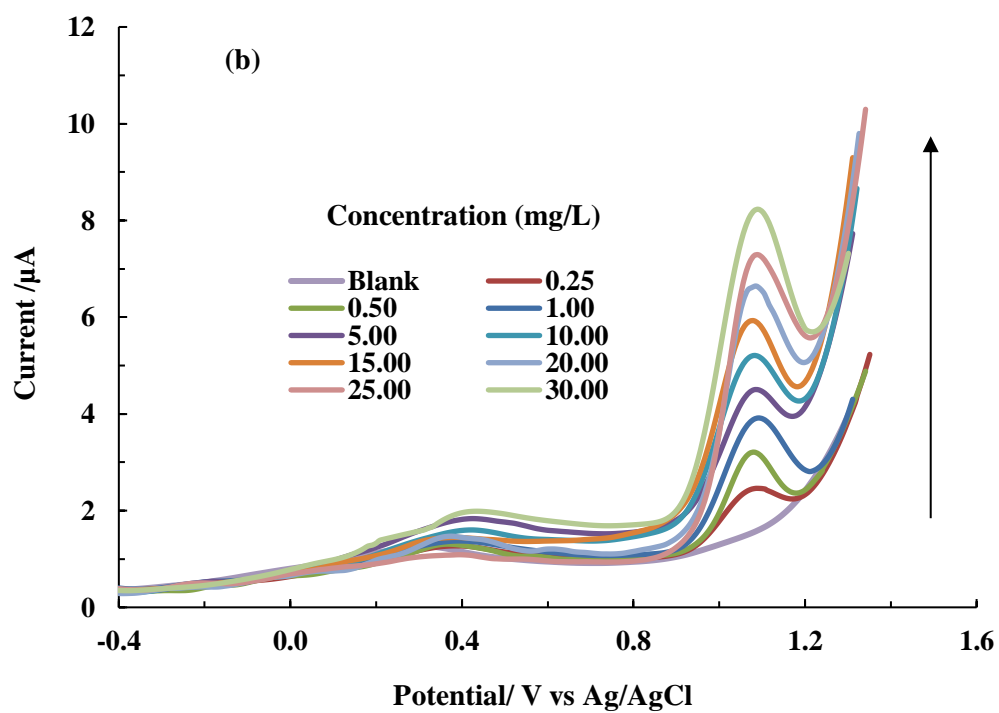
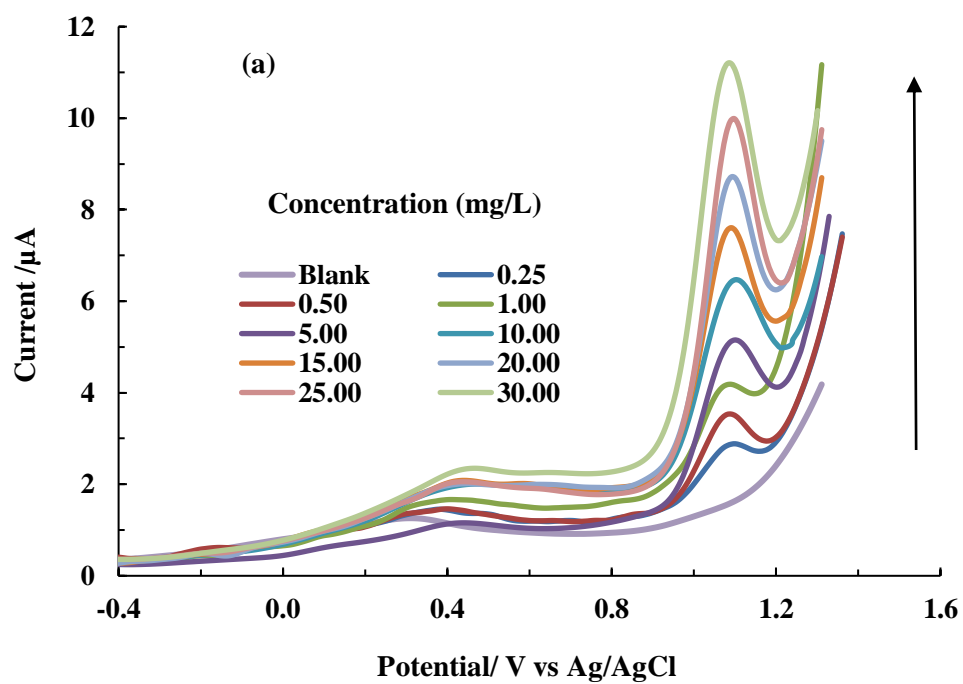


**Figure 3.35(a-b).** Plots of peak currents of 20.0 mg/L SMX (0.1 mol/L KCl in acetate buffer pH: 4.0) as a function of (a) deposition potentials (V); and (b) deposition times (s). (Other conditions: pulse amplitude = 50 mV, pulse increment = 10 mV and pulse width = 50 ms).

### 3.7.5. Concentration dependence studies and calibration

For the investigation of concentration effect on the oxidative current signal of SMX, DPASV voltammograms were recorded in the SMX concentration range of 0.25 to 30.00 mg/L employing Ag(NP)/TCBN/GCE and Au(NP)/TCBN/GCE under optimized DPASV parametric conditions. A systematic increment of peak current values were obtained at varied concentrations of SMX and results are depicted in Figure 3.36(a-b). Peak current increased linearly as SMX concentration increased. Therefore, a linear calibration line was drawn between the  $I_p$  vs concentration of SMX and illustrated in Figure 3.36(c & d). The calibration lines were obtained as:  $I_p (\mu A) = 0.266 C (\text{mg/L}) + 3.422$  ( $R^2 : 0.987$ ) at the Ag(NP)/TCBN/GCE electrode and  $I_p (\mu A) = 0.166 C (\text{mg/L}) + 3.213$  ( $R^2 : 0.973$ ) at Au(NP)/TCBN/GCE electrode. The LOD and LOQ values were obtained using the slope of these lines. The LODs were calculated as 0.022 mg/L and 0.036 mg/L, respectively for Ag(NP)/TCBN/GCE and Au(NP)/TCBN/GCE electrodes, whereas the respective LOQ values were 0.075 mg/L and 0.120 mg/L. This indicated that the novel Ag(NP)/TCBN and Au(NP)/TCBN materials as supported on the GCE surface allowed a significantly low-level detection of SMX. The studies enabled to the utilization of the materials for device development to detect the potential micro-pollutant SMX in aqueous wastes.





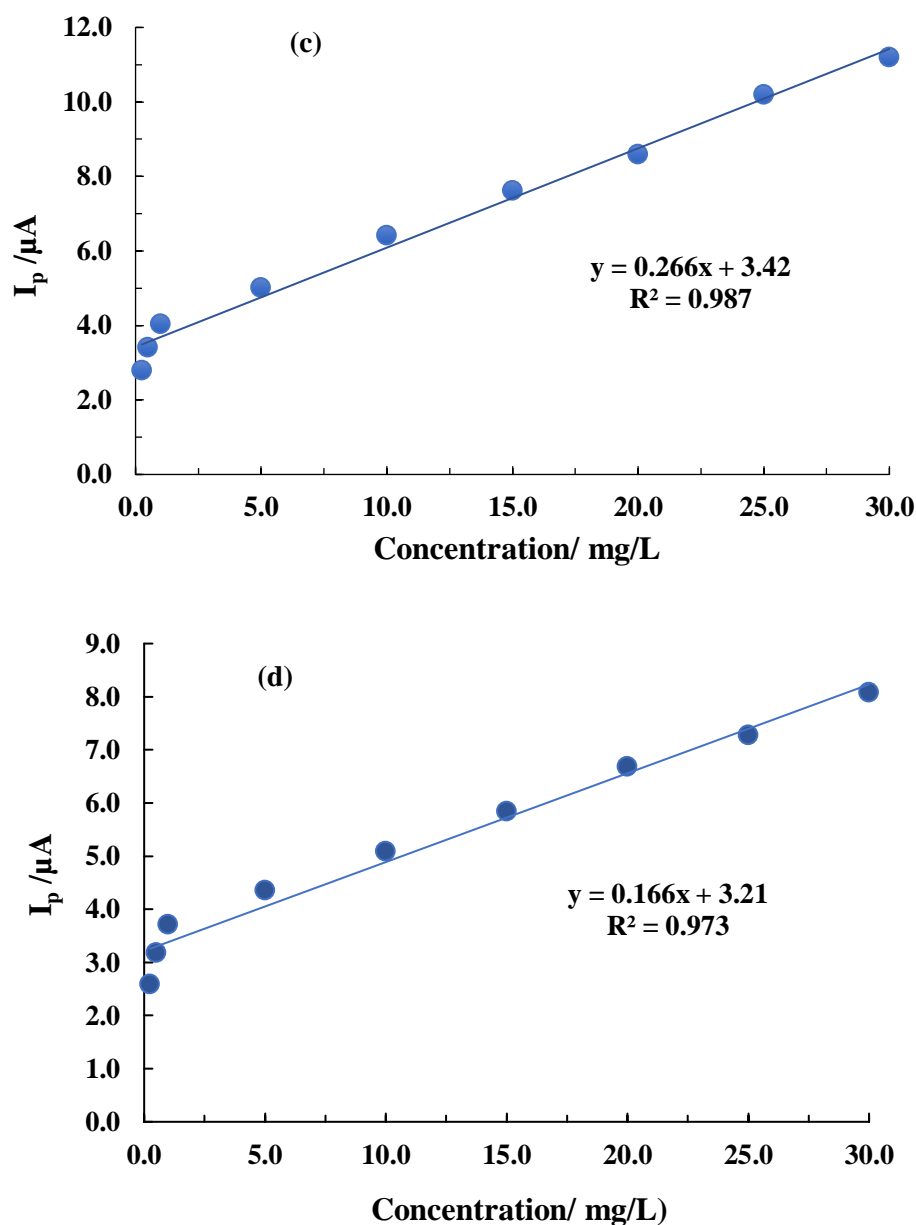


**Figure 3.36. (a-d)** DPASV of SMX solutions (0.25 to 30.00 mg/L) (Background electrolytes: 0.1 mol/L KCl (Acetate buffer; pH 4)) obtained at (a) Ag(NP)/TCBN/GCE; and (b) Au(NP)/TCBN/GCE. Calibration lines obtained between  $I_p$  vs Concentration of SMX at (c) Ag(NP)/TCBN/GCE; and (d) Au(NP)/TCBN/GCE (Other conditions: deposition potential = -1.2 V, deposition time = 210 s, pulse amplitude = 50 mV, pulse increment = 10 mV and pulse width = 50 ms).

Further, Table 3.16 includes the LOD values obtained for SMX detection utilizing various materials and different electrochemical platforms. The present studies showed that the results are quite comparable or even significantly better than many other studies since reasonably low detection limit is achieved utilizing the nanocomposite materials.

The repeatability of the current analytical approach was further tested by analyzing a 20.0 mg/L SMX solution with both nanostructured electrodes, the results of which are presented in Table 3.17. The procedure was carried out three times per day for three days in consecutive days. It is observed that employing the same electrode for second measurement of SMX on the second day measurement, the RSD (%) was found to be 3.7% and 3.3% for Ag(NP)/TCBN/GCE and Au(NP)/TCBN/GCE, respectively. Similarly, the third measurement conducted provides the RSD (%) of 3.6% and 4.1% for these two electrodes.

**Table 3.16.** Comparative table of various modified electrodes employed for SMX determination.

Electrodes used	Electrochemical Techniques employed	Linear range( $\mu\text{M}$ )	LOD ( $\mu\text{M}$ )	Real sample	Reference
BDDE	SWV	6.10-60.1	1.15	Pharmaceutical	(Souza <i>et al.</i> , 2008)
MIP(Oppy)	DPV	25-750	$3.5 \times 10^2$	Pharmaceutical	(Özkorucuklu <i>et al.</i> , 2008)
MWCNT/GCE	DPV	50-1000	10	Pharmaceutical, urine	(Issac and Girish Kumar 2009)

MWCNT/CPE	DPV	1.38-118.45	0.395	Pharmaceutical	(Arvand <i>et al.</i> , 2011)
GCE	SWV	5.5-395	8.5	Pharmaceutical	(Calaça <i>et al.</i> , 2014)
GR-ZnO/GCE	DPV	1-120	0.4	Real water, urine, serum	(del Torno-de Román <i>et al.</i> , 2016)
(TYR)/SPCE	Amperometry	20-200	22.6	Real water	(Yue <i>et al.</i> , 2020)
Nano-MIP	CV	1.99-10.88	0.4	Milk	(Turco <i>et al.</i> , 2021)
Ag(NP)/TCBN/GCE	DPASV	0.9-118	<b>0.08</b>	Real water	<b>This work</b>
Au(NP)/TCBN/GCE	DPASV	0.9-118	<b>0.12</b>	Real water	<b>This work</b>

BDDE – Boron doped diamond electrode, MIP -molecularly imprinted electrode, OPPy – overoxidized polypyrrole, MWCNT – multiwall carbon nanotube, CPE- carbon paste electrode, nano-nanocomposite, PDA- polydopamine, TYR – tyrosinase, SPCE-screen printed carbon electrodes, GR – graphene oxide

**Table 3.17.** Stability and repeatability test for Ag(NP)/TCBN/GCE and Au(NP)/TCBN/GCE in 20.0 mg/L SMX solution (pH 4.0).

Time	Repetition	RSD (%)	
		Ag(NP)/TCBN/GCE	Au(NP)/TCBN/GCE
First Day	3	3.1	2.7
Second Day	3	3.7	3.3
Third Day	3	3.6	4.1

### 3.7.6. Effect of co-existing ions

The influence of several co-existing ions on the detection of SMX was studied. The studies were aimed to analyze the detection of SMX in presence of Ca(II), Fe(II), Zn(II), Cu(II), Ni(II) and Mn(II) which are often present in the effluent of treated wastewater and in natural water bodies. The concentration of co-ions and SMX was taken as 1.0 mg/L and 0.5 mg/L for each. The oxidative peak potential of these ions falls within the operating scan window as employed for SMX. Hence, the respective effect on the peak current of SMX was studied and represented in Figure 3.37. Comparison of peak current in the absence and presence of co-ions show only slight or no significant change in the detection of SMX. However, a decrease in peak current was pronounced in presence of Cu(II) and Zn(II) since these ions also oxidize at the employed electrodes within the same potential window as applied for SMX. The decrease in peak current response is attributed to the competition between the analytes and the interfering ions for the active sites of Ag(NP)/TCBN and Au(NP)/TCBN. Similar interference was reported for the detection of Cd(II) using graphene quantum dots and nafion modified GCE (GC/QDS-NF) in presence of Fe(III) and Zn(II) cations, which caused a decrease in peak current values by 35.1% and < 10% respectively. The main factor involved in the interference was attributed due to the competition analytes towards the active sites in QDS-NF (Pizarro *et al.*, 2020). Previous investigations showed that the potential interferents such as ascorbic acid, uric acid, xanthine, etc. present in urine and other medication such as trimethoprim, which is mostly mixed with SMX tablets and suspensions. These

studies further showed that no notable change is observed in the peak current intensity as well as peak potentials of SMX in presence of these interfering species (Chasta and Goyal, 2015; Chen *et al.*, 2018).

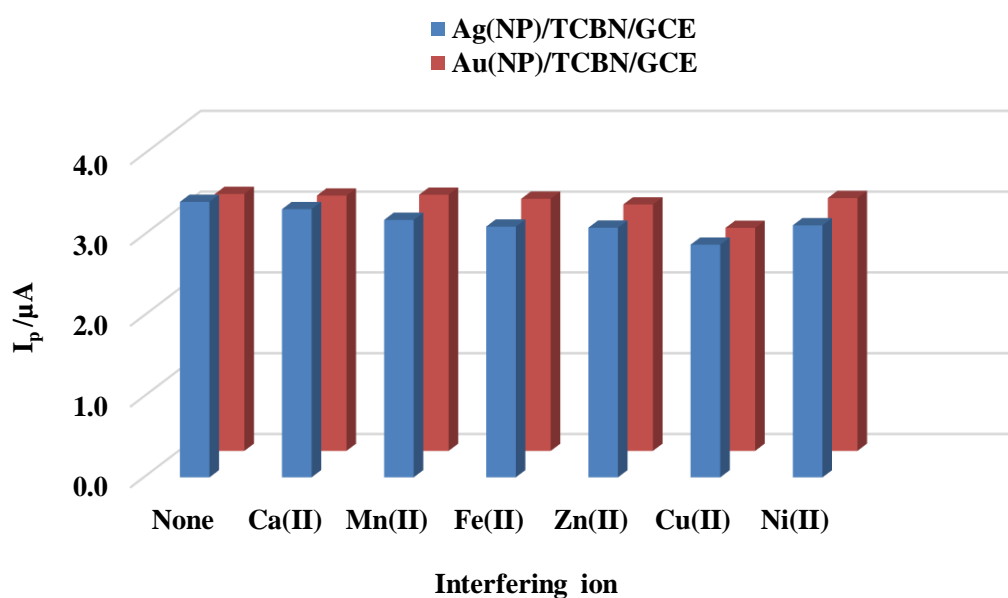


**Figure 3.37.** Effect of co-existing ions (1.0 mg/L) on peak current of 0.5 mg/L SMX (Background electrolytes: 0.1 mol/L KCl (Acetate buffer; pH 4)) using Ag(NP)/TCBN/GCE and Au(NP)/TCBN/GCE (Other conditions: deposition potential = -1.2 V, deposition time = 210 s, pulse amplitude = 50 mV, pulse increment = 10 mV and pulse width = 50 ms).

### 3.7.7. Studies in real water samples

To assess the practical applicability of the proposed electrochemical sensor in the real aquatic systems, determination of SMX was performed in surface runoff water collected near hospital sites (Near Ebenezer Hospital, Aizawl, Mizoram (India)). The quality of the water sample was analyzed using various parametric studies and the results are shown in Table 3.18. It was observed that the water sample have a high load of inorganic and organic carbon. Similarly, water also have high content of Ca, Mg, and Zn elements. The TDS, sulfate, and nitrates also occurred at high levels.

**Table 3.18.** Analysis of water quality for different parameters.

Analysis	Parameter	Surface runoff water
TOC	IC	12.3 mg/L
	NPOC	4.67 mg/L
AAS	Element:	Conc.(mg/L)
	Mn(II)	0.004
	Zn(II)	0.680
	Ni(II)	0.0014
	Ca(II)	3.42
	Pb(II)	0.0043
	Fe(II)	0.209
	Cu(II)	0.0056
	Mg(II)	2.00
Other parameters	pH	7.53
	ORP	+213 mV
	Resistivity	0.0294 mΩcm
	TDS	211 mg/L
	Salinity	0.340 PSU

	Conductivity	0.0450 S/m
	Nitrate	20.4 mg/L
	Sulphate	10.8 mg/L
	Phosphate	0.300 mg/L

Further, the real water sample was spiked with the known concentrations of SMX and DPASV scans are recorded using the Ag(NP)/TCBN/GCE and Au(NP)/TCBN/GCE and utilizing the previously optimized parameters. It was found that no noticeable change in peak potential position is observed. Hence, it made feasible for the detection of SMX in the real water samples efficiently. Further, the detection of SMX is obtained using three standard concentrations of SMX (0.5 mg/L to 10.0 mg/L). The results obtained with DPASV scans of the spiked samples are summarized in Table 3.19. The recovery percentage falls in the range of 93.08-103.7%. Further, reasonably a good linear relationship was achieved between the oxidative peak current values against the spiked SMX concentrations (*Cf* Figure 3.38). Hence, these analytical results indicated that the developed electroanalytical method is useful in the devise development for the low level and on-site detection of SMX in real water samples.



**Table 3.19.** Determination of SMX in real water samples using the Ag(NP)/TCBN/GCE and Au(NP)/TCBN/GCE [Background electrolytes: 0.1 mol/L KCl (Acetate buffer; pH 4.0)].

Electrode	Spiked amount of SMX (mg/L)	SMX Found (mg/L)	Recovery (%)	RSD (%) (n=3)
Ag(NP)/TCBN/GCE	0.5	0.518	103	3.17
	5.0	4.65	93.0	1.89
	10.0	10.2	102	1.36
Au(NP)/TCBN/GCE	0.5	0.47	95.1	0.91
	5.0	4.92	98.4	3.29
	10.0	10.04	100	3.7

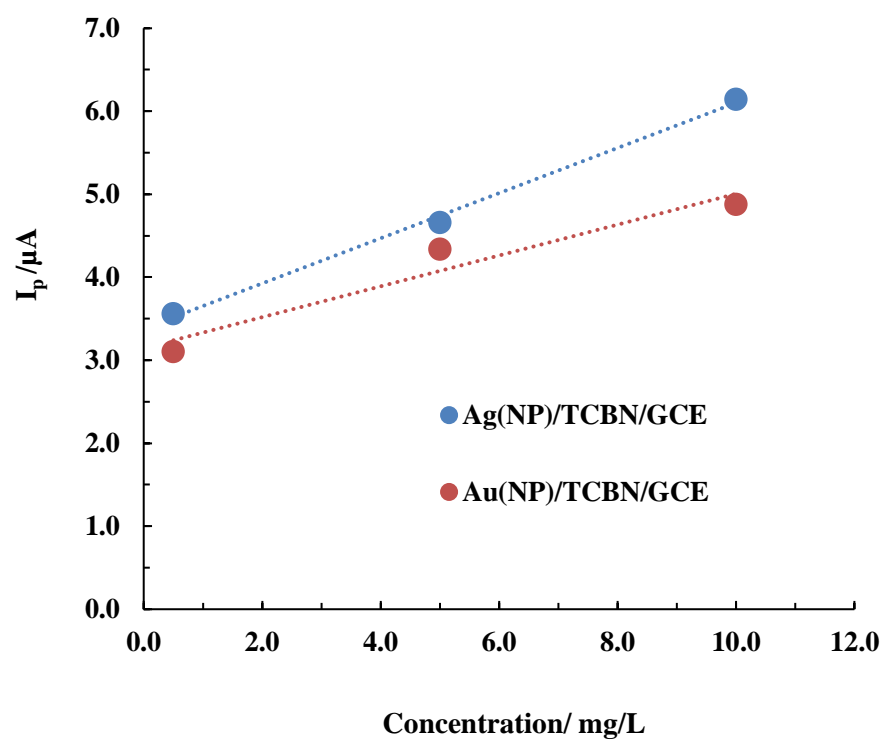


**Figure 3.38.** Linear calibration curves obtained between peak current ( $I_p$ ) and spiked SMX concentrations at Ag(NP)/TCBN/GCE and Au(NP)/TCBN/GCE in a real water sample.

### 3.7.8. Conclusion

The Ag(NP)/TCBN and Au(NP)/TCBN nanocomposite modified glassy carbon electrodes were employed for the low-level detection of SMX by electrochemical methods. The cyclic voltammogram showed a single oxidative peak at around excitation potential of *Ca* 1.04 V is obtained using the fabricated electrodes which suggested a single step oxidation of SMX having loss of two electrons. The oxidation process is irreversible in nature. The electrochemical responses using the nanocomposites Ag(NP)/TCBN and Au(NP)/TCBN materials were enabled to enhance the electrochemical signal significantly as compared to the bare GCE, BN/GCE, or TCBN/GCE. Consequently, the detection of SMX is optimized for the pH, deposition potential, and time as 4.0, 1.2 V and 210 s, respectively using the Ag(NP)/TCBN/GCE and Au(NP)/TCBN/GCE. The detection limit of SMX obtained under the optimized condition was 0.022 mg/L and 0.036 mg/L for Ag(NP)/TCBN/GCE and Au(NP)/TCBN/GCE, respectively. The presence of two times of several co-ions did not affect significantly the detection of SMX except in presence of Cu(II) and Zn(II). Moreover, the real water (collected from Ebenezer hospital sites, Aizawl, India) analyses showed that the detection recovery of SMX is within 93.08-103.7%. These results inferred that the materials are possessed with high affinity towards SMZ and useful materials for the trace detection of SMX in aqueous solutions.

### 3.8. ELECTROCHEMICAL DETECTION OF SULFAMETHAZINE

#### 3.8.1. Electrochemical studies of sulfamethazine using cyclic voltammetry

Sulfamethazine (SMZ) consists of sulfonamide group which is oxidizable. Therefore, if an appropriate potential is applied, the electrochemical detection of these drugs at low levels is feasible. Therefore, the electrochemical behavior of SMZ was investigated using bare GCE, BN/GCE, TCBN/GCE, Ag(NP)/TCBN/GCE, and Au(NP)/TCBN/GCE. The concentration of SMZ was taken 50.0 mg/L as prepared in 0.1 mol/L KCl + Acetate buffer (pH 4.0). The cyclic voltammograms were recorded at scan rate 0.01 V/s and potential window of -0.2 V to 1.2 V. The results are shown in Figure 3.39. A distinct oxidative peak is occurred at *Ca* 1.12-1.05 V for each electrode. The oxidative peak current followed the order: bare GCE < BN/GCE < TCBN/GCE < Au(NP)/TCBN/GCE < and Ag(NP)/TCBN/GCE. In fact, the peak current of bare GCE was not distinctive. However, Au(NP)/TCBN/GCE and Ag(NP)/TCBN/GCE showed a significant increase in electrical signals for SMZ as shown in Figure 3.39, implying that these materials showed enhanced applicability for the trace detection of SMZ in water. Further, the CV showed no reductive peak in the reverse scan of SMZ, indicating the oxidation of SMZ is irreversible in nature. Similar results were reported previously in which SMZ was oxidized using a graphene and Au(NP) electrode (Cesarino *et al.*, 2016). In figure 3.39, the shape of the oxidative peaks of the Ag(NP)/TCBN and Au(NP)/TCBN coated electrodes look sharper than that of bare GCE. Moreover, a shift in oxidation potential of SMZ was observed; the oxidation potentials of Ag(NP)/TCBN/GCE and Au(NP)/TCBN/GCE were lower than that of the bare GCE or even TCBN/GCE. This was attributed to the enhanced electroactive areas of Ag(NP)/TCBN/GCE and Au(NP)/TCBN/GCE that favored the rate of electron transfers (He *et al.*, 2016). Hence, the well-defined and enhanced oxidation peak was observed with the nanocomposite-impregnated electrodes. This suggested that the oxidation process would be electro-catalyzed by the nanoparticle-decorated surfaces. Therefore, the determination of SMZ could be conducted with the nanocomposite - Ag(NP)/TCBN or Au(NP)/TCBN impregnated electrode.

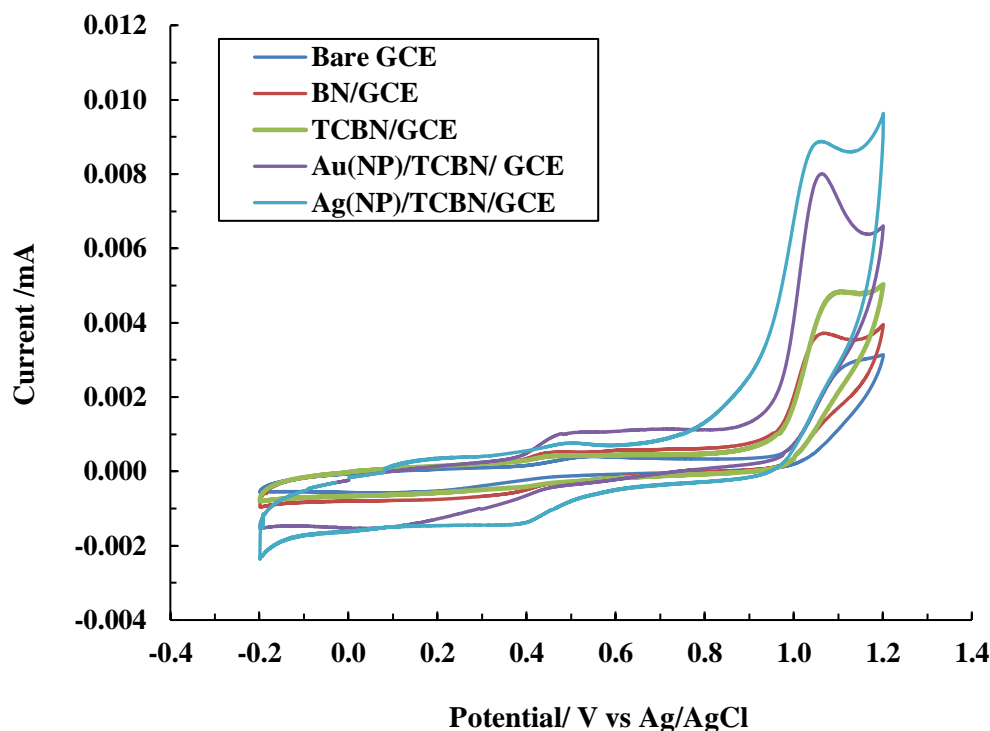


**Figure 3.39.** Cyclic voltammograms of 50.0 mg/L SMZ (in 0.1 mol/L KCl + Acetate buffer, pH 4.0) at 100 mV/s obtained with GCE and modified GCEs.

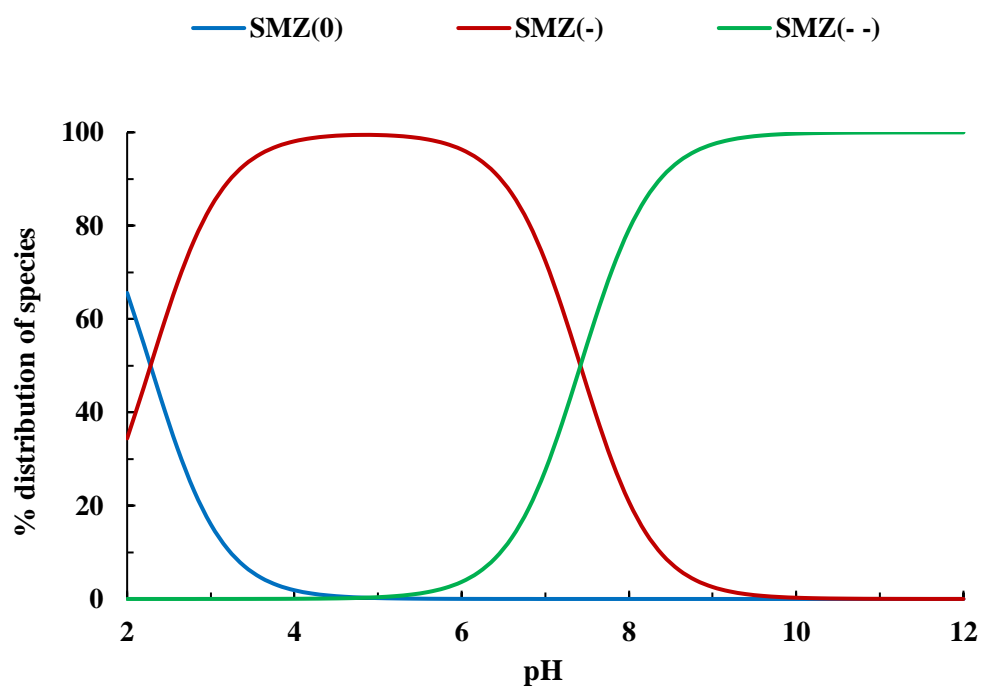
### 3.8.2. Electroanalytical performance of modified electrodes for sulfamethazine

The oxidation peak currents of Ag(NP)/TCBN/GCE and Au(NP)/TCBN/GCE were used as the analytical signal for the quantitative measurements of SMZ. The analytical method was developed using the differential pulse voltammetry in which determination of organic compounds could be made by the pulse amplitude (50 mV in this study), pulse increment (10 mV in this study), and pulse width (50 ms in this study). Other important parameters that greatly affect the current signal would be deposition potential (V) and deposition time (s). Hence, they were studied by varying ranges to acquire optimized experimental conditions for SMZ determination. The optimization process was carried out with water samples having 20.0 mg/L SMZ.

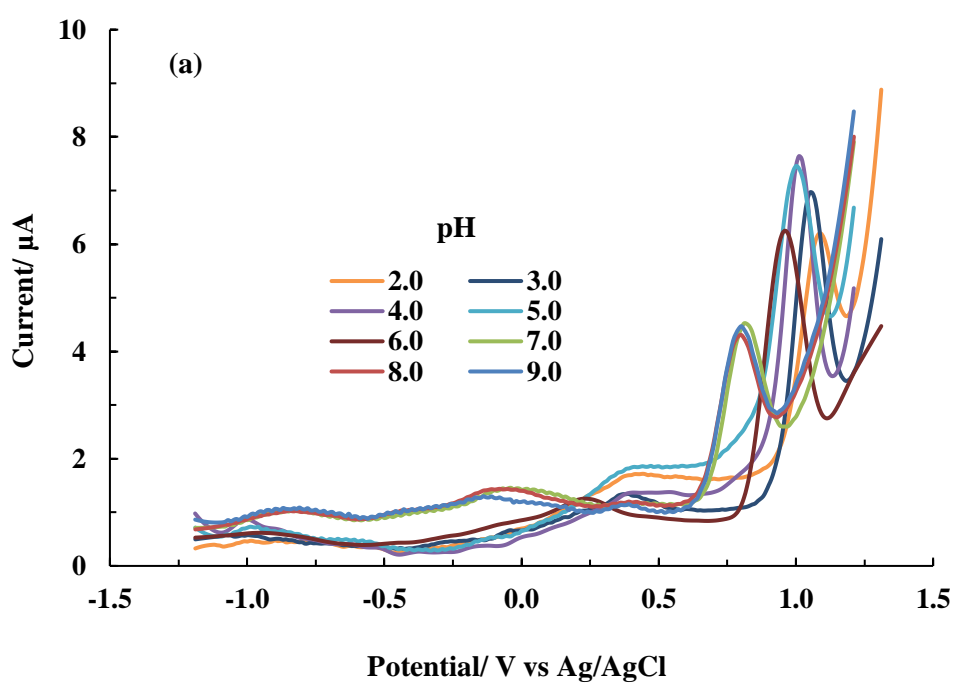
### 3.8.3. pH dependence studies on detection of sulfamethazine

The dependence of SMZ oxidation on solution pH was studied between pH 2.0 – 9.0 in 0.1 mol/L KCl + Acetate buffer containing 20.0 mg/L SMZ using the DPASV technique. The results obtained with Ag(NP)/TCBN/GCE and Au(NP)/TCBN/GCE are presented in Figures 3.41(a-d). The DPASV graphs showed that an apparent shift in peak potentials occurred at different pH values. It is observed that decreasing  $H^+$  causes oxidation potential to shift towards a more negative side for SMZ oxidation. The relationship between oxidation peak potential ( $E_{pa}$ ) and pH can reveal the SMZ oxidation process. Lower  $H^+$  concentration caused a shift of peak potential towards a more negative side which favors oxidation of SMZ (Cf Figures 3.40 a & b). The most significant anodic peak currents for SMZ were achieved at pH 4.0-5.0 at both electrodes. The observed trend in the current intensity as a function of pH was demonstrated with the species distribution of SMZ as well. Species distribution of SMZ are presented in Figure 3.40. SMZ has  $pK_a$  values of 2.65 and 7.65 (Mohamed-Ameen *et al.*, 2020); using these  $pK_a$  values, the speciation studies are conducted separately. Species distribution studies show that it exists as cationic species below pH 1.62, neutral species between pH 1.62 to 7.91, and as anionic species above pH 7.91 (Wegst-Uhrich *et al.*, 2014).

In this study, a higher peak current was recorded for both the fabricated electrodes at mild acidic pH (4.0~5.0). the peak gradually decreased from pH 6.0 and reached to a minimum value at pH 9.0. Within the pH 2~5, the negatively charged species of SMZ was greatly attracted by the surface of nanocomposite fabricated electrodes and resulted in an enhanced oxidative current. However, at extremely high pH, both the surface of nanocomposite and SMZ would carry the net negative charges which strongly repel each other and hence significantly suppress the oxidation of SMZ. In this case, a reduced peak current can be observed. A similar behavior of current was reported previously for the oxidation of sulfadiazine (a sulfonamide drug with almost similar structure as SMZ ) at different pH values (Rao *et al.*, 2000). Thus, based on the pH dependence study, the pH 4.0-5.0 was considered as the optimum for oxidation of SMZ using the Ag(NP)/TCBN/GCE and Au(NP)/TCBN/GCE.



**Figure 3.40.** Distribution graph of different species of SMZ as a function of pH.



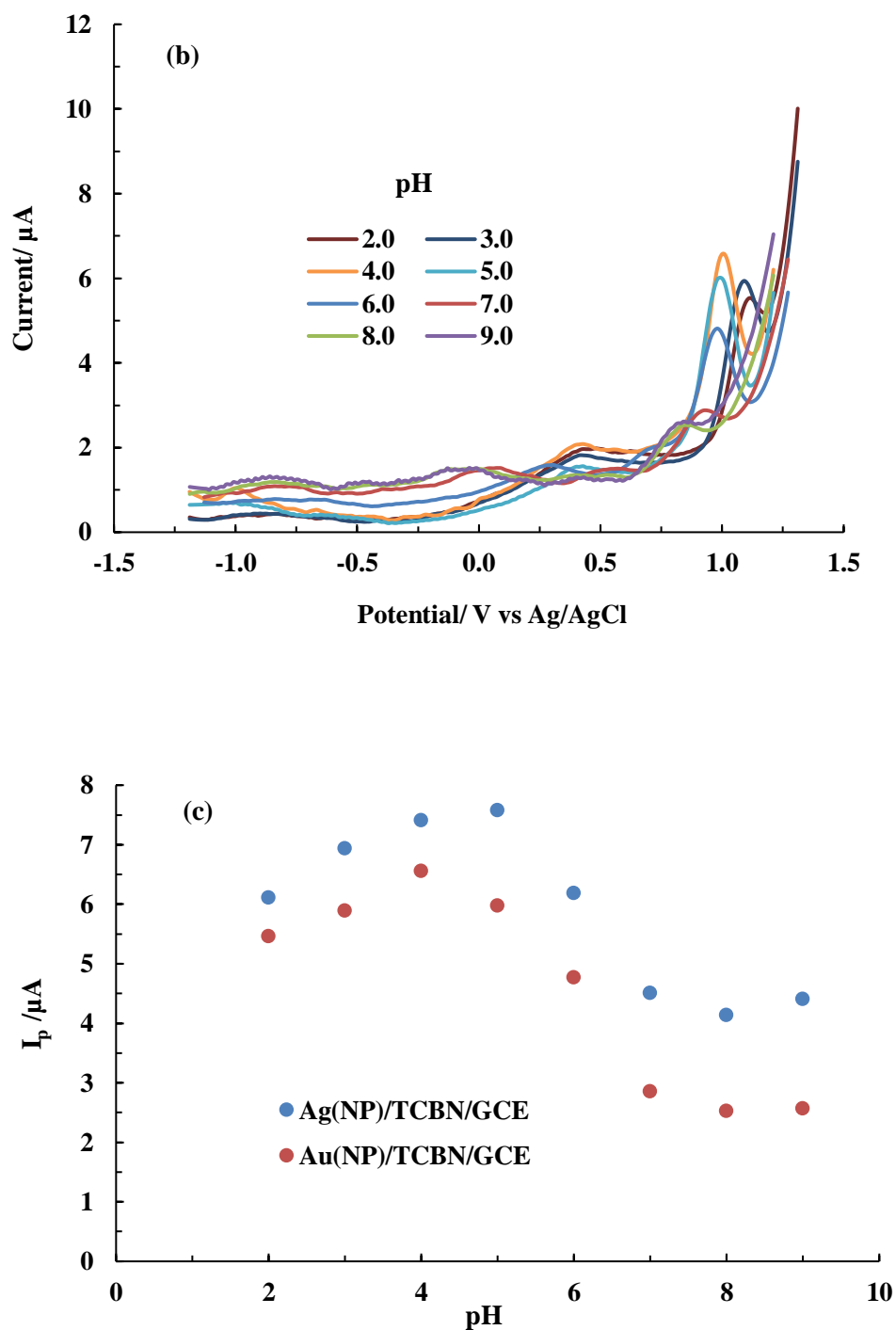


**Figure 3.41.**(a-c) DPASV graphs of 20.0 mg/L SMZ (0.1 mol/L KCl + acetate buffer pH 4.0) at different pH values obtained with (a) Ag(NP)/TCBN/GCE; (b) Au(NP)/TCBN/GCE; and (c) Plots of peak current ( $I_p$ ) values as a function of pH (Other conditions: pulse amplitude = 50 mV, pulse increment = 10 mV and pulse width = 50 ms).



#### 3.8.4. Optimization of electrochemical parameters

The effect of deposition potential and deposition time on the anodic peak of SMZ was investigated at 20.0 mg/L SMZ prepared in 0.1 mol/L KCl + acetate buffer (pH 4.0). The applied excitation potential was varied from -1.3 to -0.7 V and accumulation time was varied from 30 to 300 s. In general, the accumulation potential is the electrostatic potential maintained at the electrode surface mostly controlled by the interfacial charge at the electrode surface (Salihu *et al.*, 2019). The plot of accumulation potentials on the oxidation of SMZ shows that changing the potential from -0.7 V to -1.3 V, (Figure 3.42(a)), caused a gradual increase in the current for SMZ oxidation. In the case of both nanocomposite micro-electrodes, however, further increase of potential over -1.2 resulted in a sharp decrease in oxidative peak current for SMZ. These results indicated that more and more sulfamethazine molecules were reduced at the surface of nanocomposite electrodes at a relatively lower potential. Further, the current increased from 6.05 to 7.46  $\mu\text{A}$  for Ag(NP)/TCBN/GCE and from 4.53 - 6.27  $\mu\text{A}$  for Au(NP)/TCBN/GCE when the potential was decreased from -0.7 V to -1.2 V. However, at negative potentials less than -1.2 V, a slight drop in the peak current was observed. This is possibly due to the thickening layer of the analyte on the surface of an electrode, which resulted in the excess formation of hydrogen bubbles. Hence, this reduced the electrode sensitivity. These results inferred that the optimal accumulation potential for the voltammetric oxidation of SMZ at the surfaces of Ag(NP)/TCBN/GCE and Au(NP)/TCBN/GCE is -1.2 V (Fig. 3.42(a)). On the other hand, the accumulation time for the oxidation of SMZ was explored by utilizing DPASV measurements. Accumulation time is the time required for the analyte to be adsorbed onto the surface of Ag(NP)/TCBN/GCE or Au(NP)/TCBN/GCE. It is observed that the SMZ was rapidly adsorbed onto the surface of the nanostructured electrode. The oxidative peak current increased with an increase in accumulation time from 30 to 180 s (Fig. 3.42(b)). It is further noted that the peak current value of 6.56  $\mu\text{A}$  practically leveled off after 180 s. The leveling off is related to the saturation of SMZ onto the electrode surface i.e., Ag(NP)/TCBN/GCE and Au(NP)/TCBN/GCE electrodes. Therefore, an

optimum accumulation time of 180 s was chosen for further studies in the detection of SMZ using the nanostructured micro-electrodes.

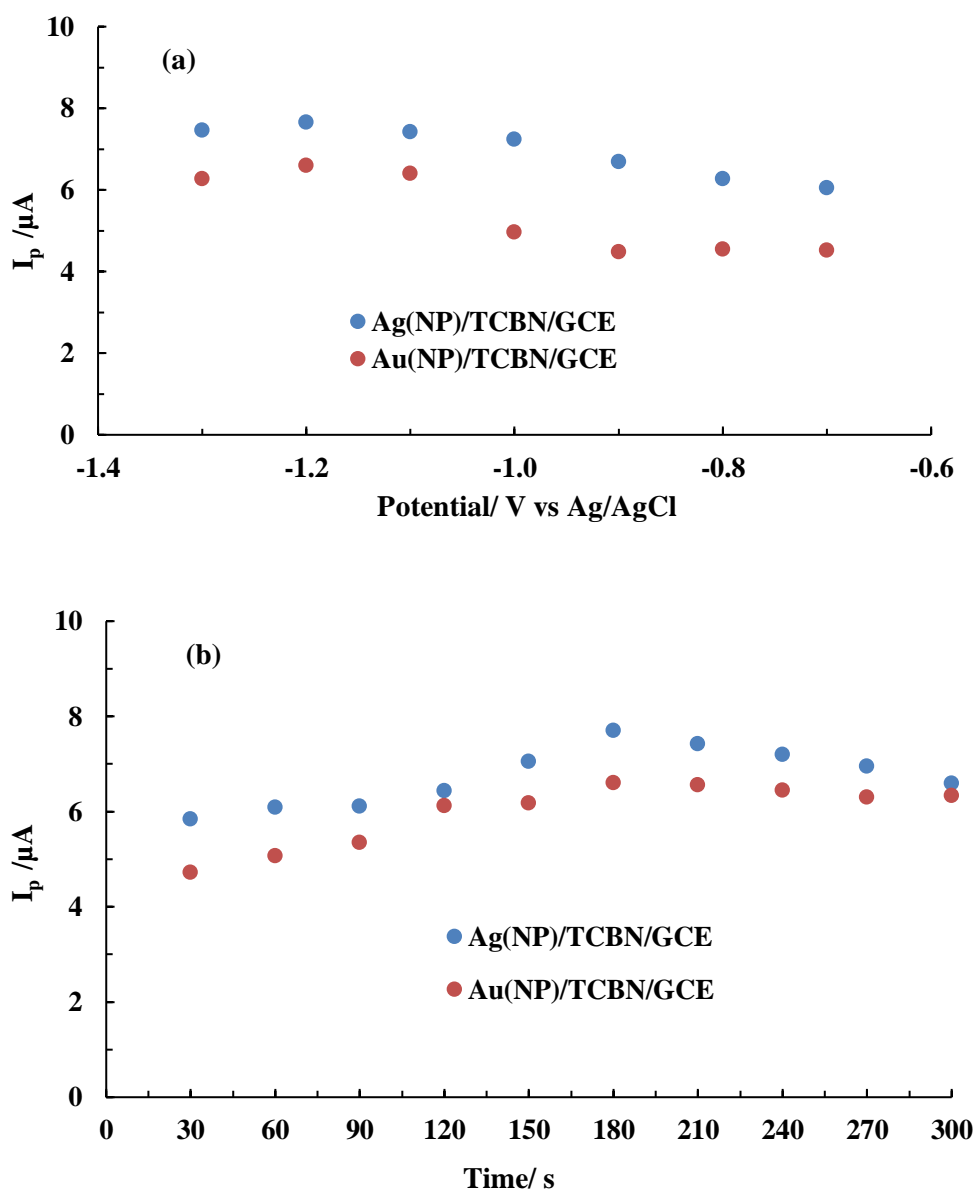
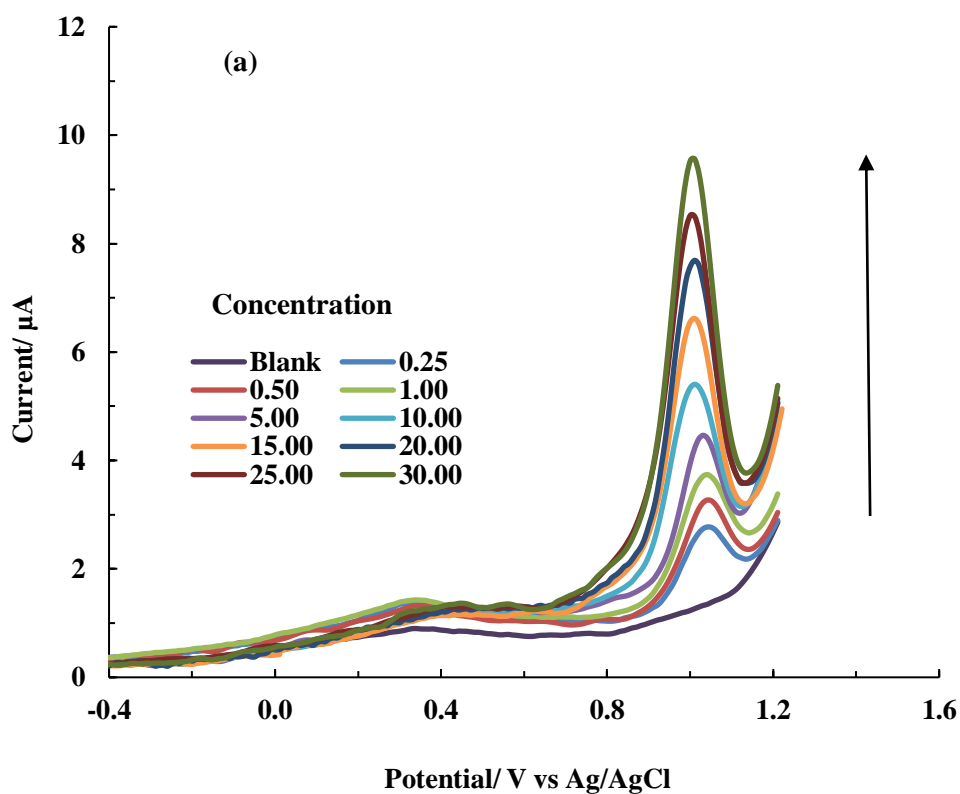


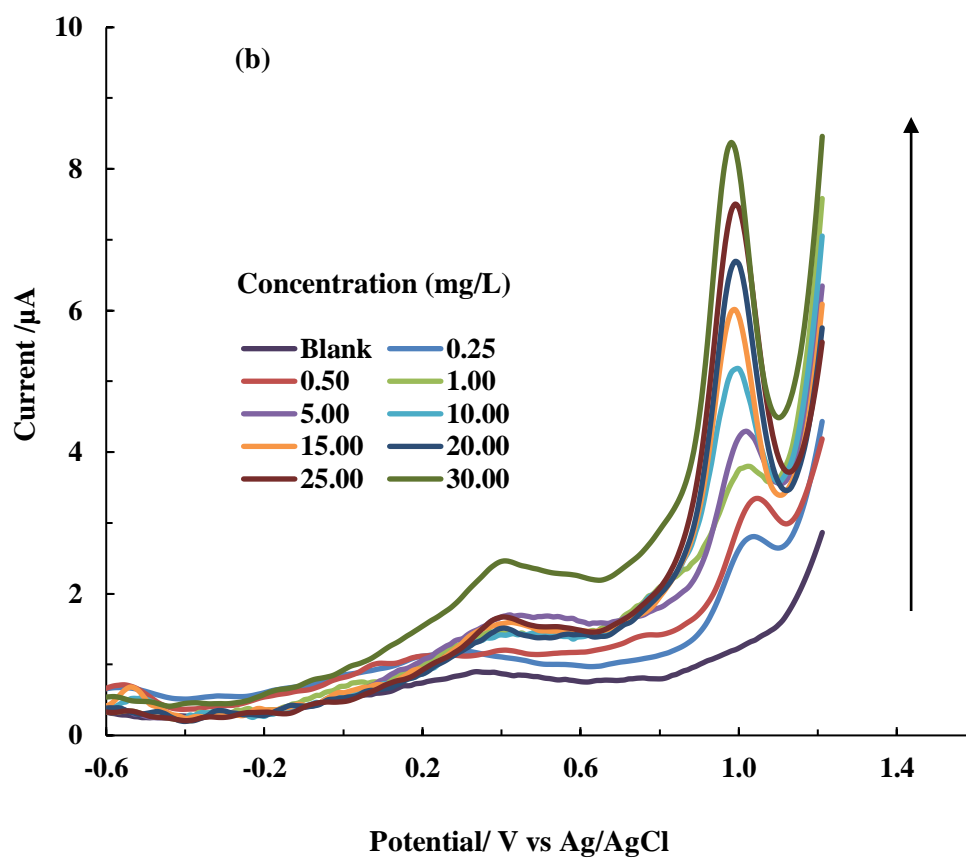
**Figure 3.42.(a-b).** Optimization of accumulation step with change in (a) deposition potential and (b) deposition time at Ag(NP)/TCBN/GCE and (b) Au(NP)/TCBN/GCE in 20.0 mg/L SMZ (0.1 mol/L KCl + acetate buffer pH 4.0). (Other conditions: pulse amplitude = 50 mV, pulse increment = 10 mV and pulse width = 50 ms).

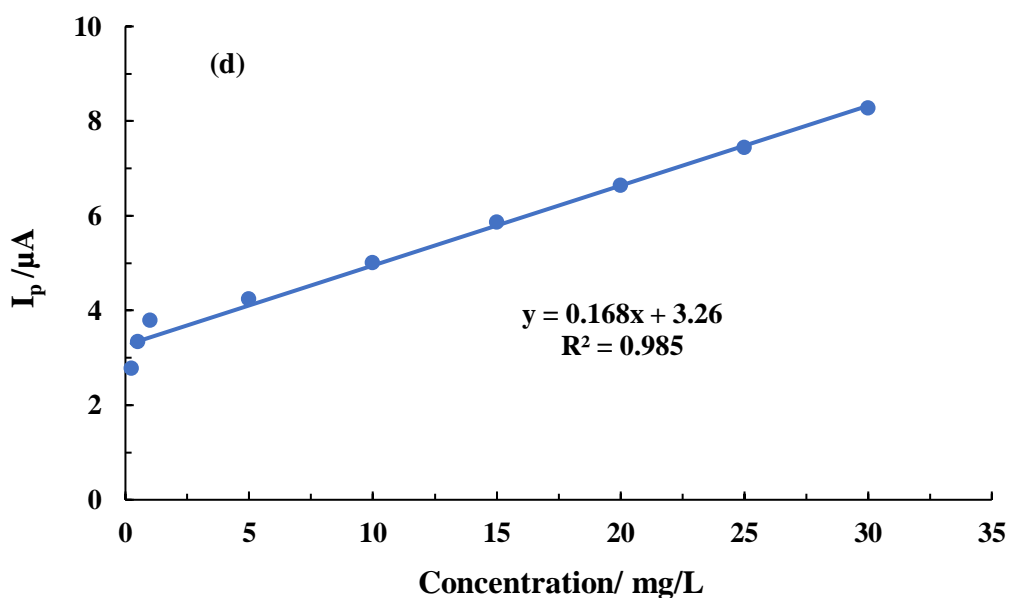
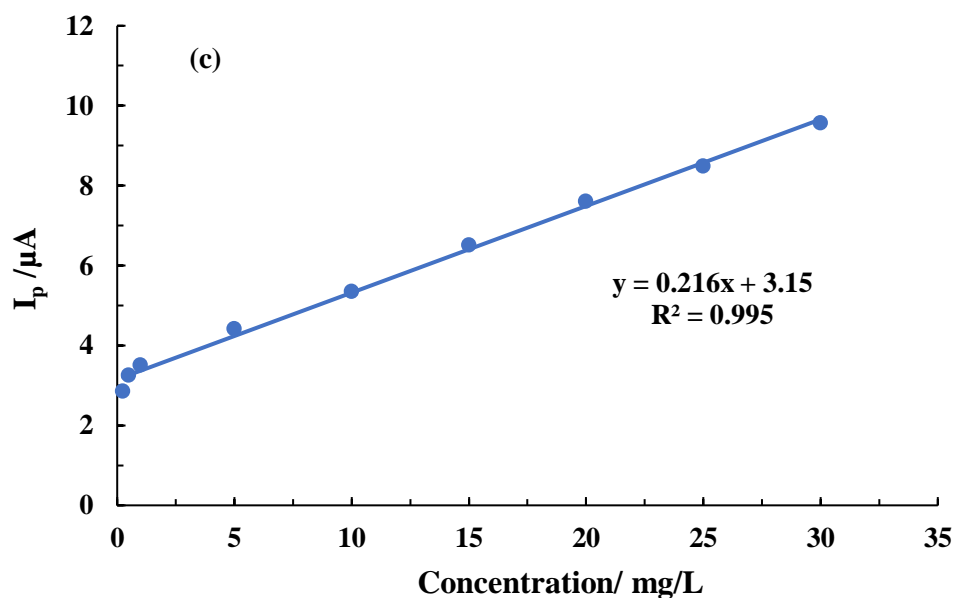
### 3.8.5. Concentration dependence studies and calibration

DPASV measurements are carried out under the optimized experimental conditions to obtain a suitable calibration curve for the determination of SMZ using the nanostructured Ag(NP)/TCBN/GCE and Au(NP)/TCBN/GCE modified electrodes. The electrochemical response at Ag(NP)/TCBN/GCE and Au(NP)/TCBN/GCE are represented in Figures 3.43(a-d). The increase in SMZ concentrations from 0.25 to 30.0 mg/L caused a gradual but linear increase in the peak oxidative current. Further, a good linearity between the sulfamethazine concentrations (0.25 to 30.0 mg/L) and the peak oxidative current was obtained (Figures. 3.43(a & b)) for the linear equations given as:  $I_p(\mu A) = 0.216(\mu A) + 3.15C(\text{mg/L})$  ( $R^2 = 0.995$ ) and  $I_p(\mu A) = 0.168(\mu A) + 3.26C(\text{mg/L})$  ( $R^2 = 0.985$ ). The LOD were found to be 0.027 mg/L and 0.035 mg/L Ag(NP)/TCBN/GCE and Au(NP)/TCBN/GCE, respectively. Similarly, the LOQ values were found to be 0.092 mg/L and 0.119 mg/L for Ag(NP)/TCBN/GCE and Au(NP)/TCBN/GCE, respectively. Thus, it is evident from the results that the electrooxidation of SMZ at the nanostructured materials enabled us to achieve reasonably low detection limit of measurements at least for the detection of SMZ. The detection limits of Ag(NP)/TCBN/GCE and Au(NP)/TCBN/GCE were compared with those of other chemically modified electrodes for SMZ or other sulfonamide drugs (Cf Table 3.20). Recently, Feizollahi *et al* (Feizollahi *et al.*, 2021) found a comparable LOD of 0.12 mg/L for SMZ using graphene oxide and Cu-Ag core-shell nanoparticles modified GCE. The proposed method proved to be a promising tool since its detection limits were comparable or even significantly lower than other reported methods. Further, the repeatability of the current analytical method was evaluated by analyzing 20.0 mg/L SMZ solution using both nanostructured electrodes and results are given in Table 3.21. The method was repeated for three times each day and continued for 3 consecutive days. The RSD (%) on the first measurement (first day of electrode fabrication) were 2.0% and 2.4% for Ag(NP)/TCBN/GCE and Au(NP)/TCBN/GCE, respectively. Further, it is observed that employing the same electrode for measurement of SMZ on the second day of electrode fabrication, the RSD (%) was found to be 2.2% and 2.8% for Ag(NP)/TCBN/GCE and Au(NP)/TCBN/GCE,

respectively. Similarly, the third measurement as conducted on third day, provides the RSD (%) of 2.8% and 2.6% for these two electrodes. It is interesting to observe that the RSD (%) is always below 5% even after the third day of consecutive measurements.







**3.43. (a-d).** Differential pulse voltammograms of SMZ solutions (0.25 to 30.0 mg/L) (Background electrolytes: 0.1 mol/L KCl (Acetate buffer; pH 4.0) obtained at (a) Ag(NP)/TCBN/GCE; and (b) Au(NP)/TCBN/GCE. Calibration line obtained between  $I_p$  vs Concentration of sulfamethazine at (c) Ag(NP)/TCBN/GCE (d) Au(NP)/TCBN/GCE (Other conditions: deposition potential = -1.2 V, deposition time = 180 s, pulse amplitude = 50 mV, pulse increment = 10 mV and pulse width = 50 ms).

**Table 3.20.** Comparison of present work with other modified electrodes employed for SMZ and other sulfonamide detection.

Electrodes employed	Electrochemical Techniques	Linear range ( $\mu\text{M}$ )	LOD ( $\mu\text{M}$ )	References
BDDE	SWV	6.10-60.1	1.15	Souza <i>et al.</i> , 2008
MIP(Oppy)	DPV	25-750	$3.5 \times 10^2$	Özkorucuklu <i>et al.</i> , 2008
MWCNT/GCE	DPV	50-1000	10	Issac and Girish Kumar, 2009
MWCNT/CPE	DPV	1.38-118.45	0.395	Arvand <i>et al.</i> , 2011
SPCE/PEDOT/MnO <sub>2</sub>	SWV	1-500	0.16	Su and Cheng, 2018
GR-ZnO/GCE	DPV	1-120	0.4	del Torno-de Román <i>et al.</i> , 2016
(TYR)/SPCE	Amperometry	20-200	22.6	Yue <i>et al.</i> , 2020
Nano-MIP	CV	1.99-10.88	0.4	Turco <i>et al.</i> , 2021
<b>Ag(NP)/TCBN/GCE</b>	<b>DPASV</b>	<b>0.9-118</b>	<b>0.08</b>	<b>This work</b>
<b>Au(NP)/TCBN/GCE</b>	<b>DPASV</b>	<b>0.9-118</b>	<b>0.12</b>	<b>This work</b>

SPCE- Screen printed carbon electrode, Nano-MIP - nanocomposite molecularly imprinted polymer, Poly/MWCNTs-Nafion -poly(cobalt tetraaminophthalocyanine)/multi-walled carbon nanotubes-Nafion, GO/Cu-Ag core-shell - graphene oxide decorated with Cu-Ag core-shell nanoparticles, MWCNTCOOH/BA - functionalized multiwalled carbon nanotubes (MWCNTCOOH) and benzyl acetate (BA), SMX- Sulfamethoxazole, SSZ- Sulfasalazine, SDZ – Sulfadiazine

**Table 3.21.** Stability and repeatability test for Ag(NP)/TCBN/GCE and Au(NP)/TCBN/GCE in 20.0 mg/L SMZ solution (pH 4.0).

Time	Repetition	RSD (%)	
		Ag(NP)/TCBN/GCE	Au(NP)/TCBN/GCE
First Day	3	2.0	2.4
Second Day	3	2.2	2.8
Third Day	3	2.8	2.6

### 3.8.6. Effect of co-existing ions

The interference studies were conducted to determine the impact of other species on the detection of SMZ using the suggested approach. The analysis was conducted by preparing 1.0 mg/L of various metal ions *viz.*, Mn(II), Ni(II), Ca(II), Fe(II), Zn(II) and Cu(II) in 0.5 mg/L SMZ under optimized conditions. Figure 3.44 shows that interference species had few changes in peak currents for each analysis except for Cu and Zn at both electrodes. The higher percentage of peak current changes with these ions is, perhaps, due to alterations caused by the accumulation at active sites and occurrence of oxidation potential within the scan window of SMZ. These results suggest that SMZ has no strong interactions with these ions to cause a significant change in SMZ oxidation onto the proposed electrode materials, thus showing its selectivity for SMZ over high concentrations of metal ions.



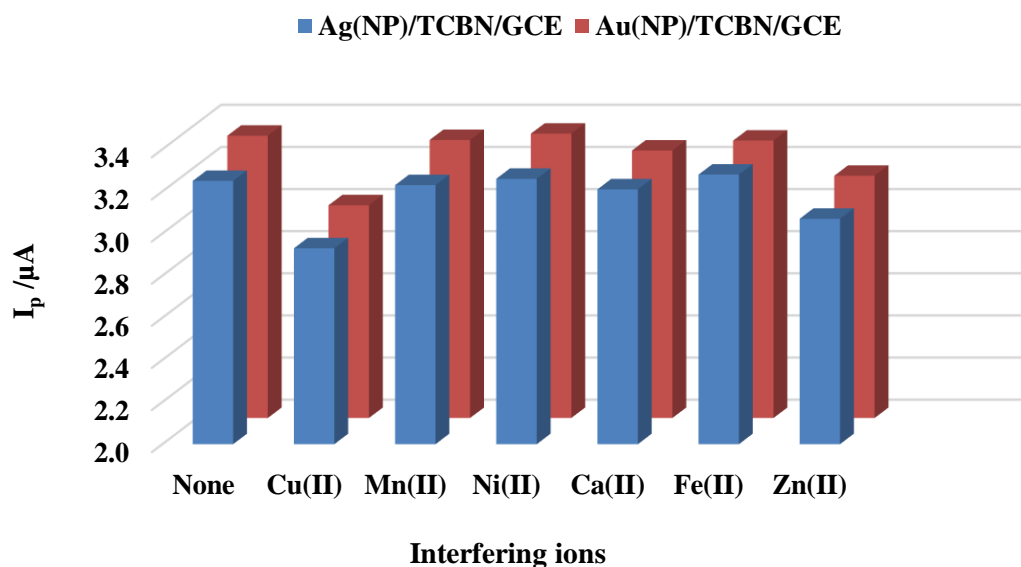


**Figure 3.44.** Effect of co-existing ions (1.0 mg/L) on peak current of 0.5 mg/L sulfamethazine using Ag(NP)/TCBN/GCE and Au(NP)/TCBN/GCE in 0.1 mol/L KCl + Acetate buffer; pH 4.0). (Other conditions: deposition potential = -1.2 V, deposition time = 180 s, pulse amplitude = 50 mV, pulse increment = 10 mV and pulse width = 50 ms).

### 3.8.7. Studies in real water samples

The usability of the synthesized nanostructured materials was tested for the detection of trace SMZ in real water samples. The stripping voltammetry experiments were performed using the spring water. The spring water sample was collected from Aizawl City, India and various physico-chemical parametric studies are conducted. The results are given in Table 3.22. The analytical results of the spring water show that the spring water is contained with high content of inorganic carbons along with Ca and Mg. This inferred that the calcium and magnesium carbonates or bicarbonates are present in the sample. Additionally, the water contained organic carbon at a moderate level. Moreover, the spring water has several metal ions *viz.*, Zn, and Fe and insignificant concentrations of Pb and Mn. On the other hand, the anionic species *viz.*, nitrate, sulfate and phosphates are present at

moderate to high levels. Water samples were prepared by spiking SMZ of concentrations 0.5, 5.0 and 10.0 mg/L in the spring water. The DPASV data are collected using the nanocomposite fabricated electrodes i.e., Ag(NP)/TCBN/GCE and Au(NP)/TCBN/GCE. The peak currents obtained from the voltammograms are very close to those obtained with purified deionized water. Further, using the calibration line previously obtained with different concentrations of SMZ, the actual concentration of SMZ is obtained and its recovery is calculated using the spiked concentration taken. The results obtained for both electrodes are presented in Table 3.23. SMZ recoveries between 92.47% and 106% were found from spring water samples spiked with 0.5 mg/L, 5.0 mg/L, and 10.0 mg/L of SMZ, and the corresponding RSD (%) values were satisfactorily low. Further, reasonably a good linear relationship is achieved between the peak current values against the spiked concentrations (*Cf* Figure 3.45). Since no significant variations in SMZ concentrations is obtained between the observed and that of supplemented hence, indicated that under the optimized conditions the Ag(NP)/TCBN/GCE and Au(NP)/TCBN/GCE electrodes are useful and efficient platform for the selective detection of SMZ in natural water bodies.

**Table 3.22.** Analysis of spring water quality for different parameters.

Analysis	Parameter	Spring water
TOC	IC	9.52 mg/L
	NPOC	3.44 mg/L
AAS	Element	Concentration (mg/L)
	Mn(II)	0.004
	Zn(II)	0.241
	Ni(II)	ND
	Ca(II)	0.463
	Pb(II)	0.072
	Fe(II)	0.192
	Cu(II)	ND
	Mg(II)	1.200
Other parameters	pH	6.22
	ORP	+246.5.mV
	Resistivity	0.023 mΩcm
	TDS	12.00 mg/L
	Salinity	0.06 PSU
	Conductivity	0.0043 S/m
	Nitrate	0.54 mg/L
	Sulphate	2.00 mg/L
	Phosphate	0.09 mg/L

**ND-Not Detected**

**Table 3.23.** Determination of SMZ in real water sample.

Electrode	Spiked amount (mg/L)	Found (mg/L)	Recovery (%)	RSD (%)
Ag(NP)/TCBN/GCE	0.5	0.488	97.8	6.12
	5.0	5.33	106	2.77
	10.0	9.90	99.1	1.78
Au(NP)/TCBN/GCE	0.5	0.46	92.4	5.41
	5.0	5.49	105	4.25
	10.0	10.4	104	1.69

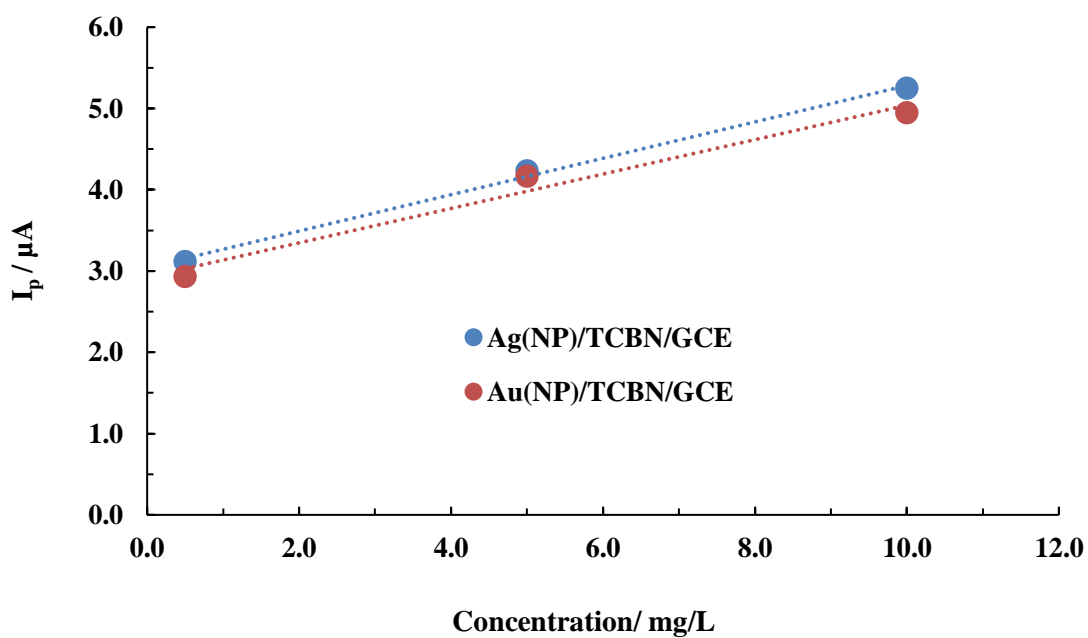


**Figure 3.45.** Linear calibration curves obtained between peak current ( $I_p$ ) and spiked SMZ concentration at Ag(NP)/TCBN/GCE and Au(NP)/TCBN/GCE in a real water sample.

### 3.8.8. Conclusion

The prepared nanocomposites Ag(NP)/TCBN and Au(NP)/TCBN were successfully utilized for the determination of SMZ with the DPASV method. The cyclic voltammogram collected at various electrodes show irreversible oxidation peak where weak and undefined peak occurred at bare GCE and BN/GCE. The peak response become more defined and intense with modified bentonite composites TCBN, Ag(NP)/TCBN and Au(NP)/TCBN/GCE, thus the proposed electrodes not only accelerate electron transfer but also provide large binding sites for SMZ which greatly enhance the sensitivity of the sensor. The pH dependence analysis results show that the species distribution of SMZ with varying pH conditions greatly affect the detection method and the electrochemical detection using DPASV method was most suitable at pH 4.0. Hence, using pH 4.0 as the optimum pH, the electroanalytical performance of the Ag(NP)/TCBN/GCE and Au(NP)/TCBN/GCE electrodes were investigated at a wide range of SMZ concentration i.e., 0.25 to 30.0 mg/L. The anodic peak current show linear increase with concentration giving regression values of 0.995 and 0.985 for the linear calibration plots; the detection limits of 0.027 mg/L and 0.035 mg/L for Ag(NP)/TCBN/GCE and Au(NP)/TCBN/GCE electrodes, respectively under optimized experimental parameters. The effects of high concentrations of electroactive metal ions on the determination of SMZ was also studied and it was found that presence of Cu(II) and Zn(II) show noticeable changes in the peak current, with highest effect caused by Cu(II). The interference caused by these ions is attributed to the competition for active sites and oxidation in similar potential range employed for SMZ detection. Further, the Ag(NP)/TCBN/GCE and Au(NP)/TCBN/GCE electrodes were successfully applied to measure SMZ in spring water with high percentage recovery, indicating its feasibility in future applications in this field.

# **CHAPTER 4**

## **CONCLUSIONS**

#### 4. CONCLUSIONS

An electrochemical detection method based on chemically modified carbon paste and glassy carbon electrodes are successfully introduced in this research. The electrodes were fabricated using the low-cost, nanocomposite materials. The facile and simple synthetic route was adopted for the synthesis of nanocomposite materials. The materials were obtained precursors to the bentonite clay and silanes along with the biosynthesized silver and gold nanoparticles. The synthesis method, characterization of synthesized materials and the detection methods for selected target pollutants viz., As(III), Pb(II), Cd(II), sulfamethoxazole (SMX) and sulfamethazine (SMZ) using the fabricated electrodes were extensively investigated and presented.

Initially, the bentonite clay was carefully washed and then exploited for hybrid material synthesis. The washed and dried bentonite was grafted with trichloro(octadecyl)silane (TCODS), which is a commonly used alkyltrichlorosilane for the formation of self-assembled monolayers (SAM's) which in turn suitable for chemical sensing application. The TCODS modified bentonite (TCBN) was then used for fabricating carbon paste electrode (TCBN/CPE) and employed in As(III) detection. Further, the TCBN composite material was decorated with the Ag and Au nanoparticles utilized for immobilization of nanoparticles (Ag(NP) and Au(NP)) to obtain the nanostructure materials viz., Ag(NP)/TCBN and Au(NP)/TCBN. These materials were utilized for surface modification of glassy carbon electrode and used for efficient detection of pollutants (lead, cadmium, SMX and SMZ). The nanoparticles used in the studies were obtained by the greener synthetic route i.e., using the *Persea americana* (avocado) leaf extracts. It efficiently reduces the silver and gold ions to zero valent Ag<sup>0</sup> and Au<sup>0</sup> colloidal particles. Therefore, the use of low-cost and abundantly available substrate material (bentonite) and a green synthesis of nanoparticles, make it useful materials utilizing for the efficient and low-level electrochemical detections of several analytes including micro-pollutants.

Characterization of the bare bentonite (BN) and the nanocomposite materials viz., TCBN, Ag(NP)/TCBN and Au(NP)/TCBN was carried out utilizing the FT-IR and SEM/EDX analyses. The FT-IR spectra of all these solids showed the -OH stretching and bending vibrations of bentonite water peaks occurring at 1652 cm<sup>-1</sup> and

3423  $\text{cm}^{-1}$ , respectively. Further, the -OH bending and stretching vibration peaks from Al-OH and Si-OH, in-plane and out-plane vibration bands of Si-O from Si-O-Si as well as the Si-O-Al quartz Si-O vibrations were observed at 1124  $\text{cm}^{-1}$ , 3703  $\text{cm}^{-1}$ , 927  $\text{cm}^{-1}$ , 1003  $\text{cm}^{-1}$ , 810  $\text{cm}^{-1}$  and 702  $\text{cm}^{-1}$ , respectively. Further, the IR spectra of TCBN, Ag(NP)/TCBN and Au(NP)/TCBN show vibrational peaks around wave numbers 3039 and 2880  $\text{cm}^{-1}$  which is due to asymmetric and symmetric stretching of the C-CH<sub>2</sub> group of the TCODS alkyl chain and a scissoring oscillation of aliphatic organic chain which occurred around the wavenumber 1489  $\text{cm}^{-1}$ . No additional peaks were observed due to the presence of nanoparticles on TCBN which implied that NPs have only a weak chemical interaction with the TCBN clay, or these were physically occupying the place within the layered structure of the clay. SEM image of BN exhibits a heterogeneous structure with visible silica contents and the layered structure of bentonite which is well-organized, revealing a porous structure with huge smooth flakes. On the other hand, TCBN had a more disordered structure having good heterogeneity on the solid surface. Organic silane molecules were clearly occupied places on clay layers and surfaces, and are likely to be grafted with the bentonite. Furthermore, the material is more compact, with less visible porosity. The SEM morphological studies of Ag(NP)/TCBN and Au(NP)/TCBN casted on the glassy carbon (GC) surface showed porous structure spread across the glassy carbon surface, with a good roughness and the decorated nanoparticles are confirmed by the small spots on the flakes or surface of the heterogeneous silane grafted bentonite shown in higher magnifications of the Ag(NP)/TCBN and Au(NP)/TCBN GC plates. The EDX spectra showed prominent peaks of Si, O, Fe, Mg, Na, C, Ca, Al, etc. with these solids viz., BN, TCBN, Ag(NP)/TCBN and Au(NP)/TCBN solids. Further, in addition to these elements the TCBN, Ag(NP)/TCBN and Au(NP)/TCBN showed the additional peaks of Cl, Ag and Au, respectively indicated the grafting of silane with bentonite and decoration of Ag and Au nanoparticles with the respective solids. Further, the microstructure of Ag(NP)/TCBN and Au(NP)/TCBN nanocomposites was obtained by the TEM analysis which showed that the small and spherical sized Ag(NP) and Au(NP) were very evenly dispersed and immobilized onto the solid surface. The average diameter of the Ag(NP) and Au(NP) was obtained as 10-30 nm. Additionally, the AFM analyses of Ag(NP)/TCBN and Au(NP)/TCBN coated glassy carbon sheet



showed that the surfaces were highly uneven, disordered and the nanocomposites materials were pillared on the surface. The arithmetic average roughness ( $R_a$ ) and root mean square average of the profile heights over the evaluation length ( $R_q$ ) was found to be 17.6 nm and 22.8 nm (for Ag(NP)/TCBN coated sheet) and 11.9 nm, 15.5 nm (for Au(NP)/TCBN coated sheet), respectively. These results indicated that the silane grafted bentonite was successfully synthesized and the Ag(NP) and Au(NP) were efficiently decorated within the composite materials. Moreover, the *in situ* decoration of Ag(NP) and Au(NP) were restricted the aggregation or clustering of nanoparticles within the composite material.

The synthesized materials TCBN and BN were introduced to modify the carbon paste electrode. Moreover, in addition to the BN, TCBN; the Ag(NP)/TCBN and Au(NP)/TCBN were utilized to fabricate the glassy carbon electrode. These electrodes were employed as working electrode in the three-electrode electrochemical cell assembly comprising the Ag/AgCl electrode and platinum electrode as reference and counter/auxiliary electrodes. The carbon paste electrodes (with the carbon powder paste, CPE, BN/CPE and TCBN) were fabricated by preparing the paste of carbon powder/ or carbon powder and synthesized materials with paraffin oil. The paste was introduced inside a teflon tube along with a titanium wire for electrical connectivity. On the other hand, glassy carbon electrodes were fabricated using these materials and are referred as BN/GCE, TCBN/GCE, Ag(NP)/TCBN/GCE and Au(NP)/TCBN/GCE). All these electrodes were characterized electrochemically under the cyclic voltammetric and electrochemical impedance spectroscopic measurements with a known 0.001 mol/L  $\text{Fe}(\text{CN})_6^{3-}/\text{Fe}(\text{CN})_6^{4-}$  (prepared in 0.1 mol/L KCl in neutral pH) standard redox couple. The redox process of the probe was clearly displayed in each of the cyclic voltammograms collected using these electrodes. The increase in scan rate enabled to increase gradually the well demonstrated oxidation and reduction peak currents of  $\text{Fe}(\text{CN})_6^{3-}/\text{Fe}(\text{CN})_6^{4-}$  couple. The plot of oxidative peak current against the square root of scan rate showed diffusion-controlled system behavior and the line obtained was utilized for calculating the electroactive surface area using the Randles-Sevcik equation. The estimated areas were  $0.244 \times 10^{-3} \text{ cm}^2$ ,  $0.503 \times 10^{-3} \text{ cm}^2$ ,  $1.19 \times 10^{-3} \text{ cm}^2$ ,  $0.269 \times 10^{-3} \text{ cm}^2$ ,  $0.404 \times 10^{-3} \text{ cm}^2$ ,  $0.418 \times 10^{-3} \text{ cm}^2$ ,  $0.539 \times 10^{-3} \text{ cm}^2$  and  $0.674 \times 10^{-3} \text{ cm}^2$  for CPE, BN/CPE, TCBN/CPE, GCE,

TCBN/GCE, Ag(NP)/TCBN/GCE and Au(NP)/TCBN/GCE, respectively. The impedance spectroscopic data were collected as Nyquist plots and the equivalent circuit was fitted to the Randles circuit. Semicircle diameter of Nyquist plot which determines the interfacial charge transfer resistance ( $R_{ct}$ ) was significantly decreased using the TCBN nanocomposite compared to the bare CPE i.e., 3.00 k $\Omega$  to 6.34 k $\Omega$ . Similarly, the bare GCE's high  $R_{ct}$  value (16.5 k $\Omega$ ) was dropped significantly to 6.21 k $\Omega$  and 5.28 k $\Omega$  for the BN and TCODS/BN modified GCEs, respectively. Further, the  $R_{ct}$  value obtained for Ag(NP)/TCBN/GCE and Au(NP)/TCBN/GCE showed further and remarkable decrease i.e., 3.20 k $\Omega$  and 3.13 k $\Omega$ , respectively.

The electrochemical response of As(III) was investigated using the carbon paste electrodes (CPE), BN/CPE and TCBN/CPE. The resulting voltammograms showed that increased response was achieved with the TCBN/CPE and therefore subsequent measurements for As(III) was conducted using the TCBN/CPE. At pH 2.0, As(III) at an applied potential of 0.36 V showed a single step oxidation/reduction process. pH dependence studies further indicated that an enhanced electrochemical signal was obtained at pH 2.0 with a minimum  $\Delta E$  value. The concentration dependent studies of As(III) (0.5 to 20.0  $\mu\text{g/L}$ ) using the linear sweep voltammetry showed reasonably good linearity between the concentration of As(III) and anodic peak current values. Therefore, the detection limit for As(III) was determined to be 0.0036  $\mu\text{g/L}$ , with observed relative standard deviations (RSD) smaller than 4%. The presence of numerous cations and anions could not affect the detection of As(III). However, the presence of Cu(II) and Mn(II) impacted the detection of As(III). The selectivity of As(III) was accomplished using a water sample from the Tlawng river spiked with As(III).

The electrochemical detection of Pb(II) was conducted using the Ag(NP)/TCBN/GCE (simultaneous detection with Cd(II)) and Au(NP)/TCBN/GCE (single species detection) fabricated electrodes. The electrochemical behavior of Pb(II) and Cd(II) using CV at various modified GCEs showed that an enhanced oxidation with smaller reduction peak occurred around the applied potential of -0.42 to -0.50 V and 0.64 to -0.66 V, respectively. The intensity and sharpness of these peaks was increased progressively from bare GCE, BN and TCBN to Ag(NP)/TCBN and Au(NP)/TCBN modified GCE's. pH condition of 4.0 and preconcentration parameters

i.e., deposition potential and time of -1.0 V and 180 s was set the best condition for detection with Au(NP)/TCBN/GCE using DPASV technique. Study of Pb(II) at various concentrations in aqueous media revealed that the Au(NP)/TCBN/GCE showed very low detection limit of 0.817  $\mu\text{g/L}$  throughout a large linear calibration range of 1.0-60.0  $\mu\text{g/L}$  having the defined calibration line  $I(A)=0.031(\mu\text{g/L}) + 0.611$  ( $R^2 = 0.984$ ). In presence of several metal cations viz., Cu(II), Fe(II), Ca(II), Mn(II), Hg(II), Zn(II) and Cd(II), the nanocomposite sensing platform could efficiently detect Pb(II). Furthermore, the actual matrix analysis of Pb(II) using river and spring water revealed that Pb(II) recovery varied from 91.6 to 98.2%. As a result, the indigenously synthesized Au(NP) adorned with silane grafted nanocomposite is an effective material for ultra-trace detection of Pb(II) and, perhaps, would be very sensitive and selective sensing platform. Similarly, the individual and simultaneous detection of Pb(II) and Cd(II) was studied with Ag(NP)/TCBN/GCE. Calibration lines for individual and simultaneous detection of Cd(II) and Pb(II) were achieved at the optimum conditions (pH 4.5, deposition potential -1.2 V and deposition time of 180 s) using DPASV. In the individual detection of Cd(II) and Pb(II), the calibration lines were obtained as  $I_p(A)=0.045 \text{ g/L} + 0.288$  ( $R^2 = 0.994$ ) and  $I_p(A)=0.044 \text{ g/L} + 0.792$  ( $R^2 = 0.995$ ), respectively. Interestingly, the material was able to detect the Pb(II) and Cd(II) simultaneously with the LOD of 0.79  $\mu\text{g/L}$  for Cd(II) and 0.88  $\mu\text{g/L}$  for Pb(II). The detection technique was designed to be used in the simultaneous detection of metal ions in actual matrix samples, with a cadmium detection recovery of 93 to 108% and a lead detection recovery of 99 to 113%. Several interfering ions viz., Fe(II), Ni(II), Zn(II), Hg(II), Cu(II) and Mn(II) appears to have no effect on the detection of these two ions simultaneously. The presence of Zn(II), on the other hand, revealed an extra and well-separated oxidative peak. The actual matrix analysis of spiked Cd(II) and Pb(II) river water revealed that analytes were recovered appropriately utilizing the fabricated electrode.

Apart from the heavy metal toxic ions, the micro-pollutants, sulfamethoxazole (SMX) and sulfamethazine (SMZ) were detected using Ag(NP)/TCBN/GCE and Au(NP)/TCBN/GCE sensing platforms. The cyclic voltammograms of 50.0 mg/L SMX and SMZ at bare GCE, TCBN/GCE, Ag(NP)/TCBN/GCE and Au(NP)/TCBN/GCE showed that the electrochemical response signal in terms of

oxidation current was weak or negligible with GCE, which later increased with TCBN/GCE and become more prominent utilizing the Ag(NP)/TCBN/GCE and Au(NP)/TCBN/GCE. Both SMX and SMZ displayed a single oxidative peak at roughly *Ca* 1.04 V excitation potential, which is assumed to involve two electrons process. Due to absence of reverse reductive peak, the process is inherently irreversible in nature. Further, the DPASV technique was employed for the detection of these two micro-pollutants utilizing the Ag(NP)/TCBN/GCE and Au(NP)/TCBN/GCE. The optimized pH, deposition potential, and time was found to be 4.0, -1.2 V, and 210 s (for SMX) and 180 s (for SMZ), respectively. Detection limit for SMX was obtained as 0.022 mg/L and 0.036 mg/L for Ag(NP)/TCBN/GCE and Au(NP)/TCBN/GCE, respectively. Similarly, for SMZ, the LOD were found to be 0.027 mg/L and 0.035 mg/L using Ag(NP)/TCBN/GCE and Au(NP)/TCBN/GCE, respectively. The presence of two times of several co-cations had no discernible effect on SMX detection. Furthermore, surface run-off water spiked SMX studies revealed that SMX detection recovery was within 93.08 - 103.7%. Similarly, the SMZ detection was investigated in spring water spiked with 0.5 mg/L, 5.0 mg/L and 10.0 mg/L which gave apparent recovery between 92.47 and 106.65%. However, the studies on effects of high concentrations of electroactive metal ions on SMZ determination, showed that the presence of Cu(II) and Zn(II) affected the detection of sulfamethazine. The interference occurred in presence of Cu(II) was primarily due to the competition of analytes and Cu(II) towards the surface-active sites on the electrode surface. Moreover, the oxidation potential of sulfamethazine was found almost at same potential region.

Finally, the limit of detection (LOD) obtained for As(III), Pb(II), Cd(II), sulfamethoxazole and sulfamethazine using various modified electrodes are compiled and presented in Table 4.1. The LOD values are compared with the permissible maximum contamination level (MCL) suggested by the World Health Organization (WHO) and United States Environmental Protection Agency (US EPA) in drinking water. Observations from the given table clearly revealed that the estimated LODs with this investigation are significantly lower than the MCL of each pollutant. Hence, the current analytical approach is found to be greater practical implacability of future device development employing these novel materials. In addition, the newly

fabricated electrodes offer cost-effectiveness, green impact, and simplicity, as well as outstanding selectivity and sensitivity.

**Table 4.1.** Comparison of LOD values of various pollutants obtained with modified electrodes and MCL values given by WHO and US-EPA guidelines.

Sl.no	Pollutant	Working Electrode	LOD (µg/L)	MCL (µg/L)
1.	Arsenic (III)	TCBN/CPE	0.0036	10
2.	Lead (II)	Ag(NP)/TCBN/GCE	0.68	10 (WHO) 15 (US-EPA)
		Au(NP)/TCBN/GCE	0.78	
3.	Cadmium (II)	Ag(NP)/TCBN/GCE	0.80	5 (WHO) 3 (US-EPA)
4.	Sulfamethoxazole	Ag(NP)/TCBN/GCE	22.50	No fixed MCL
		Au(NP)/TCBN/GCE	36.10	
5.	Sulfamethazine	Ag(NP)/TCBN/GCE	27.00	No fixed MCL
		Au(NP)/TCBN/GCE	35.50	

## References:

- Abbaspour, A., Mirzajani, R., (2007). Electrochemical monitoring of piroxicam in different pharmaceutical forms with multi-walled carbon nanotubes paste electrode. *Journal of Pharm. Biomed. Anal.*, **44**(1): 41–48.
- Abdel-Galeil, M., Ghoneim, M., El-Dosky, H., Hattori, T., Matsuda, A., (2014). Anodic Stripping Voltammetry Determination of Lead ions using Highly Sensitive Modified Electrodes Based on Multi-walled Carbon Nanotube. *J. Chem. Biochem.*, **2** (2):25-43.
- Abdulla, A., Issa, A., Al-Degs, Y., Al-Rabady, N., (2009). Selective Electrochemical Detection of Toxic Heavy Metals at Ultra Trace Levels using Natural Clay-Modified-Electrode. *Eurasian J. Anal. Chem.*, **4**(3): 245-256.
- Abeywardena, S., Perera, S., de Silva, P., Tissera, N., (2017). A facile method to modify bentonite nanoclay with silane. *Int. Nano Lett.*, **7**:237-241.
- Afkhami, A., Bahiraei, A., Madrakian, T., (2016). Gold nanoparticle/multi-walled carbon nanotube modified glassy carbon electrode as a sensitive voltammetric sensor for the determination of diclofenac sodium. *Mater. Sci. Eng., C*, **59**:168–176.
- Agarwal, V. K., (1992). High-performance liquid chromatographic methods for the determination of sulfonamides in tissue, milk and eggs. *J. Chromatogr.*, **624**(1–2): 411–423.
- Ajayi, O., Awala, S. I., Olalekan, O., Alabi, O., (2017). Evaluation of Antimicrobial Potency and Phytochemical Screening of *Persea americana* Leaf Extracts against Selected Bacterial and Fungal Isolates of Clinical Importance. *Microbiol. Res. J. Int.*, **20**:1–11.
- Alam, A. U., Howlader, M. M. R., Hu, N.-X., Deen, M. J., (2019). Electrochemical sensing of lead in drinking water using  $\beta$ -cyclodextrin-modified MWCNTs. *Sens. Actuators B: Chem.*, **296**: 126632.

- Ali, H., Khan, E., Ilahi, I., (2019). Environmental Chemistry and Ecotoxicology of Hazardous Heavy Metals: Environmental Persistence, Toxicity, and Bioaccumulation. *J. Chem.*, 1–14.
- Alkaram, U. F., Mukhlis, A. A., Al-Dujaili, A. H., (2009). The removal of phenol from aqueous solutions by adsorption using surfactant-modified bentonite and kaolinite. *J. Hazard. Mater.*, **169**(1): 324–332.
- Almeida, S. A. A., Montenegro, M. C. B. S. M., Sales, M. G. F., (2013). New and low-cost plastic membrane electrode with low detection limits for sulfadimethoxine determination in aquaculture waters. *J. Electroanal. Chem.*, **709**: 39–45.
- Almeida, S. A. A., Moreira, F. T. C., Heitor, A. M., Montenegro, M. C. B. S. M., Aguilar, G. G., Sales, M. G. F., (2011). Sulphonamide-imprinted sol–gel materials as ionophores in potentiometric transduction. *Mater. Sci. Eng., C*, **31**(8):1784–1790.
- Amidi, S., Ardakani, Y. H., Amiri-Aref, M., Ranjbari, E., Sepehri, Z., Bagheri, H., (2017). Sensitive electrochemical determination of rifampicin using gold nanoparticles/poly-melamine nanocomposite. *RSC Advances*, **7**(64):40111–40118.
- An, H., Park, B., Kim, D., (2001). Crab Shell for the Removal of Heavy Metals from Aqueous Solution. *Water Res.*, **35**:3551–3556.
- Anekwe, J., Abou-Elwafa Abdallah, M., Harrad, S., (2017). Pharmaceuticals and personal care products (PPCPs) in the freshwater aquatic environment. *Emerging Contaminants*, **3**.
- Arvand, M., Ansari, R., Heydari, L., (2011). Electrocatalytic oxidation and differential pulse voltammetric determination of sulfamethoxazole using carbon nanotube paste electrode. *Mater. Sci. Eng., C*, **31**(8): 1819–1825.
- Arvand, M., Ansari, R., Heydari, L., (2011). Electrocatalytic oxidation and differential pulse voltammetric determination of sulfamethoxazole using carbon nanotube paste electrode. *Mater. Sci. Eng., C*, **31**(8): 1819–1825.

- Auwal, M. S., Saka, S., Mairiga, I. A., Sanda, K. A., Shuaibu, A., Ibrahim, A., (2014). Preliminary phytochemical and elemental analysis of aqueous and fractionated pod extracts of *Acacia nilotica* (Thorn mimosa). *Veterinary Res. Forum*, **5(2)**:95–100.
- Azad, U.P., Prajapati, N., Ganesan, V., (2014). Selective determination of isoniazid using bentonite clay modified electrodes. *Bioelectrochem.*, **101**:120-125
- Baghayeri, M., Amiri, A., Maleki, B., Alizadeh, Z., Reiser, O., (2018). A simple approach for simultaneous detection of cadmium(II) and lead(II) based on glutathione coated magnetic nanoparticles as a highly selective electrochemical probe. *Sens. Actuators B: Chem.*, **273**:1442–1450.
- Bathinapatla, A., Kanchi, S., Singh, P., Sabela, M. I., Bisetty, K., (2015). Fabrication of copper nanoparticles decorated multiwalled carbon nanotubes as a high performance electrochemical sensor for the detection of neotame. *Biosens. Bioelectron.*, **67**: 200–207. <https://doi.org/10.1016/j.bios.2014.08.017>
- Batt, A. L., Snow, D. D., Aga, D. S. (2006). Occurrence of sulfonamide antimicrobials in private water wells in Washington County, Idaho, USA. *Chemosphere.*, **64(11)**: 1963–1971.
- Bernard, A., (2008). Cadmium and its adverse effects on human health. *Indian J Med Res.* **128(4)**:557-64.
- Bhanjana, G., Mehta, N., Chaudhary, G., Dilbaghi, N., Kim, K.-H., Kumar, S., (2018). Novel electrochemical sensing of arsenic ions using a simple graphite pencil electrode modified with tin oxide nanoneedles. *J. Mol. Liq.*, **264**.
- Bhargavi, M., Mani, Dr. G. K., Nesakumar, N., Jayalatha, A., Karanam, J., Rayappan, J. B. B., (2016). Electrocatalytic Nanocauliflower Structured Fluorine Doped CdO Thin Film as a Potential Arsenic Sensor. *Sens. Actuators B: Chem.*, **234**.
- Bhatnagar, A., Sillanpää, M., (2010). Utilization of agro-industrial and municipal waste materials as potential adsorbents for water treatment—A review. *Chem. Eng. J.*, **157(2–3)**: 277–296.



- Bhattacharyya, K. G., Gupta, S. S., (2008). Adsorption of a few heavy metals on natural and modified kaolinite and montmorillonite: A review. *Adv. Colloid Interface Sci.*, **140**(2): 114–131.
- Biswas, T., Parveen, O., Pandey, V. P., Mathur, A., Dwivedi, U. N., (2020). Heavy metal accumulation efficiency, growth and centelloside production in the medicinal herb *Centella asiatica* (L.) urban under different soil concentrations of cadmium and lead. *Ind. Crops Prod.*, **157**: 112948.
- Bouwer, H., (2000). Integrated water management: Emerging issues and challenges. *Agric. Water Management*, **45**(3): 217–228.
- Braga, O. C., Campestrini, I., Vieira, I. C., Spinelli, A., (2010). Sulfadiazine determination in pharmaceuticals by electrochemical reduction on a glassy carbon electrode. *J. Braz. Chem. Soc.*, **21**(5): 813–820.
- Calaça, G., Pessoa, C., Wohnrath, K., Nagata, N., (2014). Simultaneous determination of sulfamethoxazole and trimethoprim in pharmaceutical formulations by square wave voltammetry. *Int. J. Pharmacy Pharm. Sci.*, **6**: 438.
- Carrera, P., Espinoza-Montero, P. J., Fernández, L., Romero, H., Alvarado, J. (2017). Electrochemical determination of arsenic in natural waters using carbon fiber ultra-microelectrodes modified with gold nanoparticles. *Talanta* **166**: 198–206.
- Carvalho, I. T., Santos, L., (2016). Antibiotics in the aquatic environments: a review of the European scenario. *Environ. Int.*, **94**: 736–757.
- Casado, M., Anawar, H. m., Garcia-Sanchez, A., Regina, I. S., (2008). Cadmium and zinc in polluted mining soils and uptake by plants (El Losar mine, Spain). *Int. J. Environ. Pollut.*, **33**(2–3): 146–159.
- CDCP, (1991). *Centre for Disease Control and Prevention*.  
<https://wonder.cdc.gov/wonder/prevguid/p0000029/p0000029.asp>
- Centi, S., Stoica, A. I., Laschi, S., Mascini, M., (2010). Development of an Electrochemical Immunoassay Based on the Use of an Eight-Electrodes

- Screen-Printed Array Coupled with Magnetic Beads for the Detection of Antimicrobial Sulfonamides in Honey. *Electroanalysis*, **22(16)**: 1881–1888.
- Cerovac, S., Guzsvany, V., Kónya, Z., Ashrafi, A., Švancara, I., Rončević, S., Kukovecz, A., Dalmacija, B., & Vytrás, K., (2015). Trace level voltammetric determination of lead and cadmium in sediment pore water by a bismuth-oxychloride particle-multiwalled carbon nanotube composite modified glassy carbon electrode. *Talanta*, **134**:640–649.
- Cesarino, I., Simões, R. P., Lavarda, F. C., Batagin-Neto, A., (2016). Electrochemical oxidation of sulfamethazine on a glassy carbon electrode modified with graphene and gold nanoparticles. *Electrochim. Acta*, **192**: 8–14.
- Chandraker, S., Lal, M., Ghosh, M., Tiwari, V., Ghorai, T., Shukla, R., (2020). Green synthesis of copper nanoparticles using leaf extract of *Ageratum houstonianum* Mill. And study of their photocatalytic and antibacterial activities. *Nano Express*, 1.
- Chasta, H., Goyal, R. N., (2015). A Simple and Sensitive Poly-1,5-Diaminonaphthalene Modified Sensor for the Determination of Sulfamethoxazole in Biological Samples. *Electroanal.*, **27(5)**:1229–1237.
- Chen, C., Chen, Y.-C., Hong, Y.-T., Lee, T.-W., Huang, J.-F., (2018). Facile fabrication of ascorbic acid reduced graphene oxide-modified electrodes toward electroanalytical determination of sulfamethoxazole in aqueous environments. *Chem. Eng. J.*, **352**:188–197.
- Chen, M., Chao, M., Ma, X., (2014). Poly(crystal violet)/graphene-modified electrode for the simultaneous determination of trace lead and cadmium ions in water samples. *J. Appl. Electrochem.*, **44**.
- Chu, H., Wang, Z., Liu, Y., (2016). Application of modified bentonite granulated electrodes for advanced treatment of pulp and paper mill wastewater in three-dimensional electrode system. *J. Environ. Chem. Eng.*, **4**.
- Collinson, M. M., (2002). Recent trends in analytical applications of organically modified silicate materials. *TrAC Trends Anal. Chem.*, **21(1)**: 31–39.

- Conde-Cid, M., Fernández-Calviño, D., Fernández-Sanjurjo, M. J., Núñez-Delgado, A., Álvarez-Rodríguez, E., Arias-Estévez, M., (2019). Adsorption/desorption and transport of sulfadiazine, sulfachloropyridazine, and sulfamethazine, in acid agricultural soils. *Chemosphere*, **234**: 978–986.
- Conzuelo, F., Campuzano, S., Gamella, M., Pinacho, D. G., Reviejo, A. J., Marco, M. P., Pingarrón, J. M., (2013). Integrated disposable electrochemical immunosensors for the simultaneous determination of sulfonamide and tetracycline antibiotics residues in milk. *Biosens. Bioelectron.*, **50**:100–105.
- Cornejo, L., Lienqueo, H., Arenas, M., Acarapi, J., Contreras, D., Yañez, J., Mansilla, H., (2008). In Field Arsenic Removal from Natural Water by Zero-Valent Iron Assisted by Solar Radiation. *Environ. Pollut.*, **156**:827–831.
- Cui, L., Wu, J., Ju, H., (2015). Electrochemical sensing of heavy metal ions with inorganic, organic and bio-materials. *Biosens. Bioelectron.*, **63**:276–286.
- Czupryniak, J., Fabiańska, A., Stepnowski, P., Ossowski, T., Bogdanowicz, R., Gnyba, M., Siedlecka, E., (2012). Application of BDD thin film electrode for electrochemical decomposition of heterogeneous aromatic compounds. *Open Phys.*, **10**(5).
- D'Alessio, M., Durso, L. M., Miller, D. N., Woodbury, B., Ray, C., Snow, D. D., (2019). Environmental fate and microbial effects of monensin, lincomycin, and sulfamethazine residues in soil. *Environ. Pollut.*, **246**: 60–68.
- Dabas, D., Shegog, R. M., Ziegler, G. R., Lambert, J. D., (2013). Avocado (*Persea americana*) seed as a source of bioactive phytochemicals. *Curr. Pharm. Design*, **19**(34): 6133–6140.
- Dahaghin, Z., Kilmartin, P. A., Mousavi, H. Z., (2018). Simultaneous determination of lead(II) and cadmium(II) at a glassy carbon electrode modified with GO@Fe<sub>3</sub>O<sub>4</sub>@benzothiazole-2-carboxaldehyde using square wave anodic stripping voltammetry. *J. Mol. Liq.*, **249**, 1125–1132.
- Dahaghin, Z., Mousavi, H. Z., Boutorabi, L., (2017). Application of magnetic ion-imprinted polymer as a new environmentally-friendly nonocomposite for a

- selective adsorption of the trace level of Cu(II) from aqueous solution and different samples. *J. Mol. Liq.*, **243**:380–386.
- Dai, B., Cao, M., Fang, G., Liu, B., Dong, X., Pan, M., Wang, S., (2012). Schiff base-chitosan grafted multiwalled carbon nanotubes as a novel solid-phase extraction adsorbent for determination of heavy metal by ICP–MS. *Hazard. Mater.*, **219–220**:103–110.
- Dali, M., Zinoubi, K., Chrouda, A., Abderrahmane, S., Cherrad, S., Jaffrezic-Renault, N., (2018). A biosensor based on fungal soil biomass for electrochemical detection of lead (II) and cadmium (II) by differential pulse anodic stripping voltammetry. *J. Electroanal. Chem.*, **813**: 9–19.
- Danyıldız, Z., Uzun, D., Calam, T. T., Hasdemir, E., (2017). A voltammetric sensor based on glassy carbon electrode modified with 1H-1,2,4-triazole-3-thiol coating for rapid determination of trace lead ions in acetate buffer solution. *J. Electroanal. Chem.*, **805**:177–183.
- Davis, J. G., Truman, C. C., Kim, S. C., Ascough, J. C., Carlson, K., (2006). Antibiotic Transport via Runoff and Soil Loss. *J. Environ. Qual.*, **35(6)**:2250–2260.
- de Almeida, J. C., de Barros, A., Odone Mazali, I., Ferreira, M. (2020). Influence of gold nanostructures incorporated into sodium montmorillonite clay based on LbL films for detection of metal traces ions. *Appl. Surface Sci.*, **507**: 144972.
- de Zayas-Blanco, F., García-Falcón, M. S., Simal-Gándara, J., (2004). Determination of sulfamethazine in milk by solid phase extraction and liquid chromatographic separation with ultraviolet detection. *Food Control*, **15(5)**: 375–378.
- del Pozo, M., Sánchez-Sánchez, C., Vázquez, L., Blanco, E., Petit-Domínguez, M. D., Martín-Gago, J. Á., Casero, E., & Quintana, C. (2019). Differential pulse voltammetric determination of the carcinogenic diamine 4,4'-oxydianiline by electrochemical preconcentration on a MoS<sub>2</sub> based sensor. *Microchimica Acta*, **186(12)**, 793.
- del Torno-de Román, L., Asunción Alonso-Lomillo, M., Domínguez-Renedo, O., Julia Arcos-Martínez, M., (2016). Tyrosinase based biosensor for the

- electrochemical determination of sulfamethoxazole. *Sens. Actuators B: Chem.*, **227**: 48–53.
- Deshmukh, M.A., Celiesiute, R., Ramanaviciene, A., Shirsat, M.D., Ramanavicius, A., (2018). EDTA\_PANI/SWCNTs nanocomposite modified electrode for electrochemical determination of copper (II), lead (II) and mercury (II) ions. *Electrochim. Acta*, **259**: 930–938.
- Dominquez-Gonzalez, R., Varela, L.G., Bermejo-Barerra, P., (2013). Functionalized gold nanoparticles for the detection of arsenic in water. *Talanta*, **118**: 262–269.
- Duarte, P. F., Chaves, M. A., Borges, C. D., Mendonça, C. R. B., (2016). Avocado: Characteristics, health benefits and uses. *Ciência Rural*, **46**(4): 747–754.
- Duddukuru, S., Sundupalle, K., Chougani, M., Venu, M., Guramma, R. K., Gajulapalli, M., (2017). A Sensitive determination of Rutin at Fe<sub>3</sub>O<sub>4</sub>@SiO<sub>2</sub> [FS-MCPE] – A Voltammetric Study. *Anal. Bioanal. Electrochem.*, **9**(4): 506–520.
- Duzgoren-Aydin, N. S. (2007). Sources and characteristics of lead pollution in the urban environment of Guangzhou. *Sci. Total Environ.*, **385**(1): 182–195.
- Edokpayi, J., Odiyo, J., Msagati, T., Popoola, E., (2015). A Novel Approach for the Removal of Lead(II) Ion from Wastewater Using Mucilaginous Leaves of *Diceriocaryum eriocarpum* Plant. *Sustainability*, **7**(10): 14026–14041.
- Environmental Protection Agency (1980). *Ambient Water Quality Criteria for Cadmium*.
- Feeney, R., Kounaves, S., (2000). On-Site Analysis of Arsenic in Groundwater Using a Microfabricated Gold Ultramicroelectrode Array. *Anal. Chem.* **72**: 2222–2228.
- Feizollahi, A., Rafati, A. A., Assari, P., Joghani, R. A., (2021). Development of an electrochemical sensor for the determination of antibiotic sulfamethazine in

- cow milk using graphene oxide decorated with Cu–Ag core–shell nanoparticles. *Anal. Methods*, **13**(7): 910–917.
- Ferrari, B., Mons, R., Vollat, B., Fraysse, B., Paxéus, N., Giudice, R., Pollio, A., Garric, J., (2004). Environmental risk assessment of six human pharmaceuticals: Are the current environmental risk assessment procedures sufficient for the protection of the aquatic environment? *Environ. Toxicol. Chem. / SETAC*, **23**:1344–1354.
- Forzani, E., Foley, K., Westerhoff, P., Tao, N., (2007). Detection of arsenic in groundwater using a surface plasmon resonance sensor. *Sens. Actuators B: Chem.*, **123**: 82–88.
- Friberg, L. T., Elinder, G.-G., Kjellstrom, T., Nordberg, G. F., (2019). Cadmium and Health: A Toxicological and Epidemiological Appraisal: Volume 2: Effects and Response. *United States, CRC Press*.
- Gaw, S., Thomas, K. V., Hutchinson, T. H., (2014). Sources, impacts and trends of pharmaceuticals in the marine and coastal environment. *Philos. Trans. R. Soc. B: Biol. Sci.*, **369**(1656): 20130572.
- Genchi, G., Carocci, A., Lauria, G., Sinicropi, M. S., Catalano, A., (2020). Nickel: Human Health and Environmental Toxicology. *Int. J. Environ. Res. Public Health*, **17**(3): 679.
- Ghoreishi, S.M., Behpour, M., Khoobi, A., (2012). Central composite rotatable design in the development of a new method for optimization, voltammetric determination and electrochemical behavior of betaxolol in the presence of acetaminophen based on a gold nanoparticle modified electrode. *Anal. Methods*, **4**: 2475–2485.
- Ghosh, P. K., Bard, A. J., (1984). Photochemistry of tris(2,2'-bipyridyl)(ruthenium(II) in colloidal clay suspensions. *J. Phys. Chem.*, **88**(23): 5519–5526.
- Gibbon-Walsh, K., Salaün, P., van den Berg, C. M. G., (2010). Arsenic speciation in natural waters by cathodic stripping voltammetry. *Anal. Chim. Acta*, **662**: 1–8.

- Gilbert, S. G., Weiss, B., (2006). A rationale for lowering the blood lead action level from 10 to 2 microg/dL. *Neurotoxicol.*, **27**(5): 693–701.
- Goel, J., Kadirvelu, K., Rajagopal, C., Garg, V. K., (2006). Cadmium(II) Uptake from Aqueous Solution by Adsorption onto Carbon Aerogel Using a Response Surface Methodological Approach. *Ind. Eng. Chem. Res.*, **45**(19):6531–6537.
- Gómez, Y., Fernández, L., Borrás, C., Mostany, J., Scharifker, B., (2011). Characterization of a carbon paste electrode modified with tripolyphosphate-modified kaolinite clay for the detection of lead. *Talanta*, **85**(3): 1357–1363.
- Gong, H., Chu, W., (2016). Determination and toxicity evaluation of the generated products in sulfamethoxazole degradation by UV/CoFe<sub>2</sub>O<sub>4</sub> /TiO<sub>2</sub>. *J. Hazard. Mater.*, **314**:197–203.
- Gu, H., Yang, Y., Chen, F., Liu, T., Jin, J., Pan, Y., Miao, P., (2018). Electrochemical detection of arsenic contamination based on hybridization chain reaction and RecJf exonuclease-mediated amplification. *Chem. Eng. J.*, **353**:305–310.
- Guirado, M., Garrido-Sanz, D., Pindado, O., Rodríguez-Rastrero, M., Merino-Martín, L., Sierra, M. J., Escolano, O., Rivilla, R., Millán, R., (2021). Effectiveness of biochar application and bioaugmentation techniques for the remediation of freshly and aged diesel-polluted soils. *Int. Biodeterior. Biodegrad.*, **163**:105259.
- Gumpu, M. B., Veerapandi, M., Krishnan, U. M., Rayappan, J. B. B., (2018). Electrochemical sensing platform for the determination of arsenite and arsenate using electroactive nanocomposite electrode. *Chem. Eng. J.*, **351**: 319-327.
- Guo, Z., Li, L., Huang, Y.-Y., Liu, J.-H., Zhou, Q., Huang, X.-J., (2016). Electrochemical determination of arsenic(III) with ultra-high anti-interference performance using Au-Cu bimetallic nanoparticles. *Sens. Actuators B: Chem.*, **231**.
- Guo, Z., Yang, M., Huang, X.-J., (2017). Recent developments in electrochemical determination of arsenic. *Curr. Opin. Electrochem.*, **3**(1): 130–136.

- Gupta, S.K., Singhal, P., Singh, A., Chauhan, R., Kumar, B., (2018). Nutritional and pharmaceutical benefits of Avocado Plants. *J Adv Sci Res.*, **9** (2): 04-11
- Ha, J., Zirliannurga, Tiwari, D., Lee, S., (2017). Efficient Use of Porous Hybrid Materials in a Selective Detection of Lead(II) from Aqueous Solutions: An Electrochemical Study. *Metals*, **7**: 124.
- Hai, T. L., Hung, L. C., Phuong, T. T. B., Ha, B. T. T., Nguyen, B.-S., Hai, T. D., Nguyen, V.-H., (2020). Multiwall carbon nanotube modified by antimony oxide (Sb<sub>2</sub>O<sub>3</sub>/MWCNTs) paste electrode for the simultaneous electrochemical detection of cadmium and lead ions. *Microchem. J.*, **153**: 104456.
- Haider, A., Ullah, M., Khan, Z., Kabir, F., Abedin, K. M., (2014). Detection of trace amount of arsenic in groundwater by laser-induced breakdown spectroscopy and adsorption. *Optics Laser Technol.*, **56**:299–303.
- Hakonen, A., Strömberg, N., (2018). Fluorescence and Naked-Eye Detection of Pb<sup>2+</sup> in Drinking Water Using a Low-Cost Ionophore Based Sensing Scheme. *Chemosensors*, **6**(4):51.
- Haller, M., Müller, S., Mc Ardell, C., Alder, A., Suter, M., (2002). Quantification of Veterinary Antibiotics (Sulfonamides and Trimethoprim) in Animal Manure by Liquid Chromatography–Mass Spectrometry. *J. Chromatogr. A*, **952**: 111–120.
- Han, R., Zheng, N., Wang, J., Zhen, Y., Li, S., Yu, Q., (2013). Survey of Tetracyclines, Sulfonamides, Sulfamethazine, and Quinolones in UHT Milk in China Market. *J. Integr. Agric.*, **12**(7): 1300–1305.
- Hao, C., Shen, Y., Shen, J., Xu, K., Wang, X., Zhao, Y., Ge, C., (2016). A glassy carbon electrode modified with bismuth oxide nanoparticles and chitosan as a sensor for Pb(II) and Cd(II). *Microchim. Acta*, **183**(6):1823–1830.
- Hart, B., (2017). Compilation of Australian water quality criteria. *Aust. Water Resour. Counc. Tech. Pap.*



- Hassan, K. M., Gaber, S. E., Altahan, M. F., Azzem, M. A., (2020). Single and simultaneous voltammetric sensing of lead(II), cadmium(II) and zinc(II) using a bimetallic Hg-Bi supported on poly(1,2-diaminoanthraquinone)/glassy carbon modified electrode. *Sens. Bio-Sens. Res.*, **29**: 100369.
- Hatamie, A., Jalilian, P., Rezvani, E., Kakavand, A., Simchi, A., (2019). Fast and ultra-sensitive voltammetric detection of lead ions by two-dimensional graphitic carbon nitride (g-C<sub>3</sub>N<sub>4</sub>) nanolayers as glassy carbon electrode modifier. *Measurement*, **134**:679–687.
- He, B., Chen, W., (2016). Voltammetric Determination of Sulfonamides with a Modified Glassy Carbon Electrode Using Carboxyl Multiwalled Carbon Nanotubes. *J. Braz. Chem. Soc.*, **27**: 2216–2225.
- He, S., Xu, R., Wang, J., Han, S., Chen, B., (2016). Temperature effects on the kinetics of a PbO<sub>2</sub> electrosynthesis process in an alkaline bath. *RSC Advances*, **6(91)**:88350–88357.
- He, Y., Zheng, Y., Locke, D. C., (2007). Cathodic stripping voltammetric analysis of arsenic species in environmental water samples. *Microchem. J.*, **85(2)**: 265–269.
- Hermouche, L., Aqil, Y., Abbi, K., El Hamdouni, Y., Ouanji, F., El Hajjaji, S., El Mahi, M., Lotfi, E. mostapha, Labjar, N., (2021). Eco-friendly modified carbon paste electrode by Bigarreau Burlat kernel shells for simultaneous trace detection of cadmium, lead, and copper. *Chem. Data Collections*, **32**: 100642.
- Holland Deborah, D. E., Katz, S. E., (1991). Competitive Direct Enzyme-Linked Immunosorbent Screening Assay for the Detection of Sulfamethazine Contamination of Animal Feeds. *J. AOAC Int.*, **74(5)**:784–789.
- Huang, J.-F., Chen, H.-H., (2013). Gold-nanoparticle-embedded nafion composite modified on glassy carbon electrode for highly selective detection of arsenic(III). *Talanta*, **116**:852–859.
- Hung, D. Q., Nekrassova, O., & Compton, R. G. (2004). Analytical methods for inorganic arsenic in water: a review. *Talanta*, **64(2)**: 269–277.

- Hwang, J.-H., Wang, X., Pathak, P., Rex, M.M., Cho, H.J., Lee, W.H., (2019a). Enhanced Electrochemical Detection of Multiheavy Metal Ions Using a Biopolymer-Coated Planar Carbon Electrode. *IEEE Trans. Instrum. Meas.*, **68**: 2387–2393.
- Hwang, J.-H., Wang, X., Zhao, D., Rex, M. M., Cho, H. J., Lee, W. H., (2019b). A novel nanoporous bismuth electrode sensor for in situ heavy metal detection. *Electrochim. Acta*, **298**: 440–448.
- IARC, (2018). Arsenic and arsenic compounds. *IARC Monographs-100C*.
- Indian Bureau of Mines, 2016. Indian Minerals Yearbook, 2015 (Part-II: metals and Alloys).
- International Agency for Research on Cancer (IARC). Monographs – Cadmium. Lyon, France: 1993.
- Issac, S., Girish Kumar, K., (2009). Voltammetric determination of sulfamethoxazole at a multiwalled carbon nanotube modified glassy carbon sensor and its application studies. *Drug Testing and Anal.*, **1(7)**: 350–354.
- Johnson, A. C., Keller, V., Dumont, E., Sumpter, J. P., (2015). Assessing the concentrations and risks of toxicity from the antibiotics ciprofloxacin, sulfamethoxazole, trimethoprim and erythromycin in European rivers. *Sci. Total Environ.*, **511**:747–755.
- Jović-Jovičić, N. P., Milutinović-Nikolić, A. D., Žunić, M. J., Mojović, Z. D., Banković, P. T., Gržetić, I. A., Jovanović, D. M., (2013). Synergic adsorption of Pb<sup>2+</sup> and reactive dye—RB5 on two series of organomodified bentonites. *J. Contam. Hydrol.*, **150**: 1–11.
- Karim, M., (2000). Arsenic in Groundwater and Health Problems in Bangladesh. *Water Res.*, **34**:304–310.
- Kim, J.-Y., Kim, K.-H., Yoon, S.-B., Kim, H.-K., Park, S.-H., Kim, K.-B., (2013). In situ chemical synthesis of ruthenium oxide/reduced graphene oxide

- nanocomposites for electrochemical capacitor applications. *Nanoscale*, **5**: 6804-6811.
- Kokoszka, K., Wilk, J., Felis, E., Bajkacz, S., (2021). Application of UHPLC-MS/MS method to study occurrence and fate of sulfonamide antibiotics and their transformation products in surface water in highly urbanized areas. *Chemosphere*, 131189.
- Kumar, A., Rahman, M. S., Ali, M., Niraj, P. K., Anand, G., Kumar, P., Ghosh, A. K., (2016). Ground water arsenic contamination: a local survey in India. *IJPM* **7**:100
- Kumar, B., Cumbal, L. (2016). UV-Vis, FTIR and antioxidant study of *Persea americana* (Avocado) leaf and fruit: A comparison. *Revista de La Facultad de Ciencias Químicas, January-April* (**10**): 13–20.
- Kumar, S., Bhanjana, G., Dilbaghi, N., Kumar, R., Umar, A., (2015). Fabrication and characterization of highly sensitive and selective arsenic sensor based on ultra-thin graphene oxide nanosheets. *Sens. Actuators B: Chem.*, **227**.
- Kwarciak-Kozłowska, A., (2019). Removal of pharmaceuticals and personal care products by ozonation, advance oxidation processes, and membrane separation. *Pharmaceutical Personal Care Products: Waste Management and Treatment Technology*, 151–171.
- Lakhe, M., Rohom, A., Londhe, P., Bhand, G., Chaure, N., (2018). Study of photoelectrochemical conductivity mechanism and electrochemical impedance spectroscopy of bulk CuInTe<sub>2</sub> – Electrolyte interface. *Surf. Interfaces*, **12**.
- Lalhmunsiam, L., Tiwari, D., Lee, S., (2012). Activated carbon and manganese coated activated carbon precursor to dead biomass in the remediation of arsenic contaminated water. *Environ. Eng. Res.*, **17**: 41–48.
- Lalliansanga, Tiwari, A., Shukla, A., Tiwari, D., Lee, S. M., (2018). Nanocomposite Au NP/TiO<sub>2</sub> thin film in the efficient remediation of aqueous solutions contaminated with emerging micro-pollutants. *Environ. Sci. Pollut. Res.*, **25(20)**: 20125–20140.

- Lalliansanga, Tiwari, D., Tiwari, A., Shukla, A., Shim, M. J., Lee, S.-M., (2020). Facile synthesis and characterization of Ag(NP)/TiO<sub>2</sub> nanocomposite: Photocatalytic efficiency of catalyst for oxidative removal of Alizarin Yellow. *Catalysis Today*, S0920586120306490.
- Lalmalsawmi, J., Zirliannngura., Tiwari, D., Lee, S.-M., (2020a). Low cost, highly sensitive and selective electrochemical detection of arsenic(III) using silane grafted based nanocomposite, *Environ. Eng. Res.* **24**:579-587.
- Lalmalsawmi, J., Tiwari, D., Kim, D. J. (2020b). Role of nanocomposite materials in the development of electrochemical sensors for arsenic: Past, present and future. *J. Electroanal. Chem.*, **877**:114630.
- Larsbo, M., Fenner, K., Stoob, K., Burkhardt, M., Abbaspour, K., Stamm, C., (2008). Simulating Sulfadimidine Transport in Surface Runoff and Soil at the Microplot and Field Scale. *J. Environ. Qual.*, **37**(3):788–797.
- Laverman, A. M., Cazier, T., Yan, C., Roose-Amsaleg, C., Petit, F., Garnier, J., Berthe, T. (2015). Exposure to vancomycin causes a shift in the microbial community structure without affecting nitrate reduction rates in river sediments. *Environ. Sci. Pollut. Res. Int.*, **22**(18): 13702–13709.
- Lazanas, A. C., Tsirka, K., Paipetis, A. S., Prodromidis, M. I., (2020). 2D bismuthene/graphene modified electrodes for the ultra-sensitive stripping voltammetric determination of lead and cadmium. *Electrochim. Acta*, **336**: 135726.
- Lee, P. M., Wang, Z., Liu, X., Chen, Z., Liu, E., (2015). Glassy carbon electrode modified by graphene-gold nanocomposite coating for detection of trace lead ions in acetate buffer solution. *Thin Solid Films*, **584**.
- Lee, S. M., Tiwari, D., (2012). Organo and inorgano-organo-modified clays in the remediation of aqueous solutions: An overview. *Appl. Clay Sci.*, **59–60**:84–102.

- Lee, S.-M., Lalhmunsiam, L., Thanhmingliana, Tiwari, D., (2015). Porous hybrid materials in the remediation of water contaminated with As(III) and As(V). *Chem. Eng. J.*, **270**: 496–507.
- Lee, S.-M., Zirlianggura, Anjudikkal, J., Tiwari, D., (2016). Electrochemical sensor for trace determination of cadmium(II) from aqueous solutions: Use of hybrid materials precursors to natural clays. *Int. J. Environ. Anal. Chem.*, **96**:1–15.
- Levy, S., Marshall, B., (2005). Antibacterial resistance worldwide: Causes, challenges and responses. *Nature Medicine*, **10**:S122-9.
- Li, D., Li, J., Jia, X., Han, Y., Wang, E., (2012). Electrochemical determination of arsenic(III) on mercaptoethylamine modified Au electrode in neutral media. *Anal. Chim. Acta*, **733**:23–27.
- Li, J., Zhang, S., Zhang, L., Zhang, Y., Zhang, H., Zhang, C., Xuan, X., Wang, M., Zhang, J., Yuan, Y., (2021). A Novel Graphene-Based Nanomaterial Modified Electrochemical Sensor for the Detection of Cardiac Troponin I. *Front. Chem.*, **9**: 339.
- Li, M., Gou, H., Al-Ogaidi, I., Wu, N., (2013). Nanostructured Sensors for Detection of Heavy Metals: A Review. *ACS Sustainable Chem. Eng.*, **1**:713–723.
- Li, Y.-H., Wang, S., Wei, J., Zhang, X., Xu, C., Luan, Z., Wu, A., Wei, B., (2002). Lead Adsorption on Carbon Nanotubes. *Chem. Phys. Lett.*, **357**:263–266.
- Lin, J.-L., Lin-Tan, D.-T., Hsu, K.-H., Yu, C.-C., (2003). Environmental lead exposure and progression of chronic renal diseases in patients without diabetes. *New England J. Med.*, **348**(4): 277–286.
- Link, S., El-Sayed, M. A., (1999). Size and Temperature Dependence of the Plasmon Absorption of Colloidal Gold Nanoparticles. *J. Phys. Chem. B*, **103**(21):4212–4217.
- Liu, N., Huang, W., Li, Z., Shao, H., Wu, M., Lei, J., Tang, L., (2018). Radiolytic decomposition of sulfonamide antibiotics: Implications to the kinetics, mechanisms and toxicity. *Sep. Purif. Technol.*, **202**:259–265.

- Liu, Y., Huang, Z., Xie, Q., Sun, L., Gu, T., Li, Z., Bu, L., Yao, S., Tu, X., Luo, X., Luo, S. (2013). Electrodeposition of electroreduced graphene oxide-Au nanoparticles composite film at glassy carbon electrode for anodic stripping voltammetric analysis of trace arsenic(III). *Sens. Actuators B: Chem.*, **188**:894–901.
- Liu, Y., Li, T., Ling, C., Chen, Z., Deng, Y., He, N., (2019). Electrochemical sensor for Cd<sup>2+</sup> and Pb<sup>2+</sup> detection based on nano-porous pseudo carbon paste electrode. *Chinese Chem. Lett.*, **30**(12): 2211–2215.
- Liu, Y., Wei, W., (2008). Jointly modified single-walled carbon nanotubes on low resistance monolayer modified electrode for arsenic(III) detection. *J. Electroanal. Chem.*, **624**(1–2):299–304.
- Liu, Z., Cai, L., Liu, Y., Chen, W., Wang, Q., (2019). Association between prenatal cadmium exposure and cognitive development of offspring: A systematic review. *Environ. Pollut.*, B, **254**:113081.
- Lormphongs, S., Miyashita, K., Morioka, I., Chaikittiporn, C., Miyai, N., Yamamoto, H., (2003). Lead exposure and blood lead level of workers in a battery manufacturing plant in Thailand. *Ind. Health*, **41**(4):348–353.
- Loučka, T., (1973). The adsorption, oxidation and reduction of arsenious acid on gold and platinum electrodes. *J. Electroanal. Chem. Interfacial Electrochem.*, **47**(1): 103–108.
- Lu, Z., Zhao, W., Wu, L., He, J., Dai, W., Zhou, C., Du, H., Ye, J., (2021). Tunable electrochemical of electrosynthesized layer-by-layer multilayer films based on multi-walled carbon nanotubes and metal-organic framework as high-performance electrochemical sensor for simultaneous determination cadmium and lead. *Sens. Actuators B: Chem.*, **326**: 128957.
- Luis, G., Rubio, C., Revert, C., Espinosa, A., González-Weller, D., Gutiérrez, A.J., Hardisson, A., (2015). Dietary intake of metals from yogurts analyzed by inductively coupled plasma optical emission spectrometry (ICP-OES), *J. Food Compos. Anal.*, **39**: 48–54.

- Luong, J. H. T., Lam, E., Male, K. B., (2014). Recent advances in electrochemical detection of arsenic in drinking and ground waters. *Anal. Methods*, **6**(16):6157–6169.
- Lv, M., Wang, X., Li, J., Yang, X., Zhang, C., Yang, J., Hu, H., (2013). Cyclodextrin-reduced graphene oxide hybrid nanosheets for the simultaneous determination of lead(II) and cadmium(II) using square wave anodic stripping voltammetry. *Electrochim. Acta*, **108**: 412–420.
- Maghear, A., Tertis, M., Luminita, F., Marian, I., Indrea, E., Walcarius, A., Sandulescu, R., (2014). Tetrabutylammonium-modified clay film electrodes: Characterization and application to the detection of metal ions. *Talanta*, **125**:36–44.
- Mahaffey, K. R., (1990). Environmental lead toxicity: Nutrition as a component of intervention. *Environ. Health Perspect.*, **89**:75–78.
- Marschner, K., Musil, S., Dedina, J., (2016). Achieving 100% efficient post column hydride generation for As speciation analysis by atomic fluorescence spectrometry. *Anal. Chem.*, **88**: 4041–4047.
- Mbouguen, J. C. K., Kenfack, I. T., Walcarius, A., Ngameni, E., (2011). Electrochemical response of ascorbic and uric acids at organoclay film modified glassy carbon electrodes and sensing applications. *Talanta*, **85**(1): 754–762.
- Mezynska, M., Brzóska, M. M., (2018). Environmental exposure to cadmium-a risk for health of the general population in industrialized countries and preventive strategies. *Environ. Sci. Pollut. Res. Int.*, **25**(4): 3211–3232.
- Mhammedi, M. A. E., Achak, M., Hbid, M., Bakasse, M., Hbid, T., Chtaini, A., (2009). Electrochemical determination of cadmium(II) at platinum electrode modified with kaolin by square wave voltammetry. *J. Hazard. Mater.*, **170**(2): 590–594.

- Miao, P., Wang, B., Han, K., Tang, Y., (2014). Electrochemical impedance spectroscopy study of proteolysis using unmodified gold nanoparticles. *Electrochem. Commun.*, **47**:21–24.
- Mie, G., (1908). A contribution to the optics of turbid media, especially colloidal metallic suspensions. *Annalen Phys.*, **330**(3): 377–445.
- Mohamed Ameen, H., Kunsági-Máté, S., Szente, L., Lemli, B., (2020). Encapsulation of sulfamethazine by native and randomly methylated  $\beta$ -cyclodextrins: The role of the dipole properties of guests. *Spectrochim. Acta, Part A: Molecul. Biomolecul. Spec.*, **225**: 117475.
- Mohan, D., Pittman, C., (2007). Arsenic removal from water/wastewater using adsorbents—A critical review. *J. Hazard. Mater.*, **142**:1–53.
- Mourya, A., Sinha, S. K., Mazumdar, B., (2019). Glassy carbon electrode modified with blast furnace slag for electrochemical investigation of  $\text{Cu}^{2+}$  and  $\text{Pb}^{2+}$  metal ions. *Microchem. J.* **147**: 707–716.
- Mousty, C., (2004). Sensors and biosensors based on clay-modified electrodes?new trends. *Appl. Clay Sci.*, **27**(3–4): 159–177.
- Muniyandi, R., Soundappan, T., Chen, S.-M., (2011). Electrochemical Detection of Arsenic in Various Water Samples. *Int. J. Electrochem. Sci.*, **6**.
- Murphy, C. J., Jana, N. R., (2002). Controlling the Aspect Ratio of Inorganic Nanorods and Nanowires. *Adv. Mater.*, **14**(1): 80–82.
- Navrátilová, Z., Kula, P., (2003). Clay Modified Electrodes: Present Applications and Prospects. *Electroanalysis*, **15**:837–846.
- Ndlovu, T., Arotiba, O., Sampath, S., Krause, R., Mamba, B., (2012). Electroanalysis of copper as a heavy metal pollutant in water using cobalt oxide modified exfoliated graphite electrode. *Phys.Chem. Earth.*, **50–52**:127–131.
- Ndlovu, T., Mamba, B. B., Sampath, S., Krause, R. W., Arotiba, O. A. (2014). Voltammetric detection of arsenic on a bismuth modified exfoliated graphite electrode. *Electrochim. Acta*, **128**(SI): 48–53.



- Negreanu, Y., Pasternak, Z., Jurkevitch, E., Cytryn, E., (2012). Impact of Treated Wastewater Irrigation on Antibiotic Resistance in Agricultural Soils. *Environ. Sci. Technol.*, **46**:4800–4808.
- Nielsen, L., Bandosz, T. J., (2016). Analysis of sulfamethoxazole and trimethoprim adsorption on sewage sludge and fish waste derived adsorbents. *Microporous Mesoporous Mater.*, **220**: 58–72.
- Ns, A. K., S, A., Malingappa, P., (2018). Nano zinc ferrite modified electrode as a novel electrochemical sensing platform in simultaneous measurement of trace level lead and cadmium. *J. Environ. Chem. Eng.*, **6(6)**: 6939–6946.
- Obouayeba, A. P., Diarrassouba, M., Soumahin, E. F., Kouakou, H., (2015). Phytochemical Analysis, Purification and Identification of Hibiscus Anthocyanins. *J. Pharm. Chem. Biol. Sci.*, **3(2)**:156–168.
- Özkorucuklu, S. P., Şahin, Y., Alsancak, G., (2008). Voltammetric Behaviour of Sulfamethoxazole on Electropolymerized-Molecularly Imprinted Overoxidized Polypyrrole. *Sensors*, **8(12)**: 8463–8478.
- Oztekin, Y., Ramanaviciene, A., Ryskevicius, N., Yazicigil, Z., Üstündağ, Z., Solak, A.O., Ramanavicius, A., (2011). 1,10-Phenanthroline modified glassy carbon electrode for voltammetric determination of cadmium(II) ions. *Sens. Actuators B: Chem.*, **157**:146–153 (2011).
- Pandey, P. K., Sharma, S. K., Sami, S. S., (2015). Removal of lead(II) from waste water on zeolite-NaX. *J. Environ. Chem. Eng.*, **3(4)**:2604–2610.
- Park, Y., Ayoko, G. A., Frost, R. L., (2011). Characterisation of organoclays and adsorption of p-nitrophenol: Environmental application. *J. Colloid Interface Sci.*, **360(2)**: 440–456.
- Patrolecco, L., Rauseo, J., Ademollo, N., Grenni, P., Cardoni, M., Levantesi, C., Luprano, M. L., Caracciolo, A. B., (2018). Persistence of the antibiotic sulfamethoxazole in river water alone or in the co-presence of ciprofloxacin. *Sci. Total Environ.*, **640–641**:1438–1446.

- Petrie, B., Barden, R., Kasprzyk-Hordern, B., (2015). A review on emerging contaminants in wastewaters and the environment: Current knowledge, understudied areas and recommendations for future monitoring. *Water Res.*, **72**:3–27.
- Pizarro, J., Segura, R., Tapia, D., Navarro, F., Fuenzalida, F., Jesús Aguirre, M., (2020). Inexpensive and green electrochemical sensor for the determination of Cd(II) and Pb(II) by square wave anodic stripping voltammetry in bivalve mollusks. *Food Chem.*, **321**: 126682.
- Pohl, P., (2009). Determination of metal content in honey by atomic absorption and emission spectrometries. *TrAC Trends in Anal.Chem.*, **28(1)**: 117–128.
- Poirier, L. A., Doerge, D. R., Gaylor, D. W., Miller, M. A., Lorentzen, R. J., Casciano, D. A., Kadlubar, F. F., Schwetz, B. A. (1999). An FDA Review of Sulfamethazine Toxicity. *Regul. Toxicol. Pharm.*, **30(3)**: 217–222.
- Premarathne, J. M. K. J. K., Satharasinghe, D. A., Gunasena, A. R. C., Munasinghe, D. M. S., Abeynayake, P., (2017). Establishment of a method to detect sulfonamide residues in chicken meat and eggs by high-performance liquid chromatography. *Food Control*, **72**: 276–282.
- Promphet, N., Rattanarat, P., Rangkupan, R., Chailapakul, O., Rodthongkum, N., (2015). An electrochemical sensor based on graphene/polyaniline/polystyrene nanoporous fibers modified electrode for simultaneous determination of lead and cadmium. *Sens. Actuators B: Chem.*, **207**:526–534.
- Punrat, E., Chuanuwatanakul, S., Kaneta, T., Motomizu, S., Chailapakul, O., (2013). Method development for the determination of arsenic by sequential injection/anodic stripping voltammetry using long-lasting gold-modified screen-printed carbon electrode. *Talanta*, **116**: 1018–1025.
- Quesada, H. B., Baptista, A. T. A., Cusioli, L. F., Seibert, D., de Oliveira Bezerra, C., Bergamasco, R., (2019). Surface water pollution by pharmaceuticals and an alternative of removal by low-cost adsorbents: A review. *Chemosphere*, **222**: 766–780.

- Radhakrishnan, H., Rajapan, D., Zaharia, S., Jeyakumar, D., R, R., (2015). Arsenic (III) Sensor Development and Analysis of Electro deposition of Gold nanoparticles on Glassy carbon modified electrodes. *Int. J. Emerging Technol. Comp. Sci. Electron.*, **13(4)**:353–361.
- Radke, M., Lauwigi, C., Heinkele, G., Mürdter, T.E., Letzel, M., (2009). Fate of the antibiotic sulfamethoxazole and its two major human metabolites in a water sediment test. *Environ. Sci. Technol.* **43 (9)**: 3135–314.
- Radović, T., Grujić, S., Petković, A., Dimkić, M., Laušević, M., (2015). Determination of pharmaceuticals and pesticides in river sediments and corresponding surface and ground water in the Danube River and tributaries in Serbia. *Environ. Monit. Assess.*, **187(1)**: 4092.
- Rafati Rahimzadeh, M., Rafati Rahimzadeh, M., Kazemi, S., Moghadamnia, A.-A., (2017). Cadmium toxicity and treatment: An update. *Caspian J. Internal Medicine*, **8(3)**: 135–145.
- Rahman, N., Utami Dewi, N., Bohari (2018). Phytochemical and Antioxidant Activity of Avocado Leaf Extract (*Persea americana* Mill.). *Asian J. Scientific Res.*, **11(3)**: 357–363.
- Ramesha, G. K., & Sampath, S., (2011). In-situ formation of graphene–lead oxide composite and its use in trace arsenic detection. *Sens. Actuators B: Chem.* **160**: 306-311.
- Rao, T. N., Sarada, B. V., Tryk, D. A., Fujishima, A., (2000). Electroanalytical study of sulfa drugs at diamond electrodes and their determination by HPLC with amperometric detection. *J. Electroanal. Chem.*, **491(1–2)**: 175–181.
- Raril, C., Manjunatha, J. G., (2020). Fabrication of novel polymer-modified graphene-based electrochemical sensor for the determination of mercury and lead ions in water and biological samples. *J. Anal. Sci. Technol.*, **11(1)**: 3.
- Richards, R. M. E., Taylor, R. B., Zhu, Z. Y., (2011). Mechanism for Synergism between Sulphonamides and Trimethoprim Clarified. *J. Pharm. Pharmacol.*, **48(9)**: 981–984.

- Ritchie, H., and Roser, M., (2017). "Water Use and Stress". *Published online at OurWorldInData.org*. Retrieved from: 'https://ourworldindata.org/water-use-stress'
- Rizzo, L., Manaia, C. M., Merlin, C., Schwartz, T., Dagot, C., Ploy, M.-C., Michael, I., Fatta-Kassinos, D., (2013). Urban Wastewater Treatment Plants as Hotspots for Antibiotic Resistant Bacteria and Genes Spread into the Environment: A Review. *Sci. Total Environ.*, **447C**: 345–360.
- Roy, E., Patra, S., Madhuri, R., Sharma, P. K., (2016). Europium doped magnetic graphene oxide-MWCNT nanohybrid for estimation and removal of arsenate and arsenite from real water samples. *Chem. Eng. J.*, **299**: 244-254.
- Rubin, R., Strayer, D. S., Rubin, E., McDonald (M.D.), J. M., (2008). Rubin's Pathology: Clinicopathologic Foundations of Medicine. *Lippincott Williams & Wilkins*.
- Sacco, A., (2017). Electrochemical impedance spectroscopy: Fundamentals and application in dye-sensitized solar cells. *Renew. Sust. Energy Rev.*, **79**:814–829.
- Saha, J., Datta Roy, A., Dey, D., Nath, J., Bhattacharjee, D., Hussain, S. A., (2016). Development of arsenic(v) Sensor based on Fluorescence Resonance Energy Transfer. *Sens. Actuators B: Chem.*, **241**.
- Salihu, S., Yusof, N. A., Mohammad, F., Abdullah, J., Al-Lohedan, H. A., (2019). Nickel Nanoparticle-Modified Electrode for the Electrochemical Sensory Detection of Penicillin G in Bovine Milk Samples. *J. Nanomater.*, 1–11.
- Salimi, A., Mamkhezri, H., Hallaj, R., & Soltanian, S., (2008). Electrochemical detection of trace amount of arsenic(III) at glassy carbon electrode modified with cobalt oxide nanoparticles. *Sens. Actuators B: Chem.*, **129(1)**:246–254.
- Sanghani, Y., (2017). Handbook of chemistry lab reagent.
- Satarug, S., (2018). Dietary Cadmium Intake and Its Effects on Kidneys. *Toxics*, **6(1)**.

- Segura, R., Pizarro, J., Díaz, K., Placencio, A., Godoy, F., Pino, E., Recio, F., (2015). Development of electrochemical sensors for the determination of selenium using gold nanoparticles modified electrodes. *Sens. Actuators B: Chem.*, **220**: 263–269.
- Sengupta, P., Pramanik, K., Sarkar, P., (2021). Simultaneous detection of trace Pb(II), Cd(II) and Hg(II) by anodic stripping analyses with glassy carbon electrode modified by solid phase synthesized iron-aluminate nano particles. *Sens. Actuators B: Chem.*, **329**:129052.
- Shams, N., Lim, H. N., Hajian, R., Yusof, N. A., Abdullah, J., Sulaiman, Y., Ibrahim, I., Huang, N. M., (2016). Electrochemical sensor based on gold nanoparticles/ethylenediamine-reduced graphene oxide for trace determination of fenitrothion in water. *RSC Advances*, **6(92)**: 89430–89439.
- Shrivastava, A., Gupta, V., (2011). Methods for the determination of limit of detection and limit of quantitation of the analytical methods. *Chron. Young Scientists*, **2(1)**:21.
- Sigdel, A., Park, J., Kwak, H., Park, P.-K., (2016). Arsenic removal from aqueous solutions by adsorption onto hydrous iron oxide-impregnated alginate beads. *J. Ind. Eng. Chem.*, **35**: 277–286.
- Simon, A., Price, W., Nghiem, L. D., (2011). Implications of membrane fouling toward the removal of the pharmaceutical sulfamethoxazole by nanofiltration processes. *J. Zhejiang University-SCIENCE A*, **12(8)**:575–582.
- Sinicropi, M. S., Amantea, D., Caruso, A., Saturnino, C., (2010). Chemical and biological properties of toxic metals and use of chelating agents for the pharmacological treatment of metal poisoning. *Archives Toxicol.*, **84(7)**: 501–520.
- Sokol, R. Z., Berman, N., (1991). The effect of age of exposure on lead-induced testicular toxicity. *Toxicol.*, **69(3)**: 269–278.

- Song, Y., Swain, G. M., (2007). Total inorganic arsenic detection in real water samples using anodic stripping voltammetry and a gold-coated diamond thin-film electrode. *Anal. Chim. Acta*, **593**(1): 7–12.
- Souza, C. D., Braga, O. C., Vieira, I. C., Spinelli, A., (2008). Electroanalytical determination of sulfadiazine and sulfamethoxazole in pharmaceuticals using a boron-doped diamond electrode. *Sens. Actuators B: Chem.*, **135**(1):66–73.
- Stetter, J. R., Penrose, W. R., Yao, S., (2003). Sensors, Chemical Sensors, Electrochemical Sensors, and ECS. *J. Electrochem. Soc.*, **150**(2): S11.
- Swetha, P., Chen, J., Kumar, A. S., Feng, S.-P., (2020). High index facets-Ag nanoflower enabled efficient electrochemical detection of lead in blood serum and cosmetics. *J. Electroanal. Chem.*, **878**:114657.
- Tang, J., Wang, J., (2019). MOF-derived three-dimensional flower-like FeCu@C composite as an efficient Fenton-like catalyst for sulfamethazine degradation. *Chem. Eng. J.*, **375**:122007.
- Tang, W.-W., Zeng, G.-M., Gong, J.-L., Liang, J., Xu, P., Zhang, C., Huang, B.-B., (2014). Impact of humic/fulvic acid on the removal of heavy metals from aqueous solutions using nanomaterials: A review. *Sci. Total Environ.*, **468–469**:1014–1027.
- Tangaraj, V., Janot, J.-M., Jaber, M., Bechelany, M., Balme, S., (2017). Adsorption and photophysical properties of fluorescent dyes over montmorillonite and saponite modified by surfactant. *Chemosphere*, **184**: 1355–1361.
- Teixeira, M. C., Tavares, E. de F. L., Saczk, A. A., Okumura, L. L., Cardoso, M. das G., Magriotis, Z. M., de Oliveira, M. F., (2014). Cathodic stripping voltammetric determination of arsenic in sugarcane brandy at a modified carbon nanotube paste electrode. *Food Chem.*, **154**: 38–43.
- Teshima, D., Hino, B., Itoh, Y., Oishi, R., (2003). Simple and simultaneous determination of sulphapyridine and acetylsulphapyridine in human serum by column-switching high-performance liquid chromatography. *J. Clin. Pharm. Ther.*, **27**:403–8.

- Thanhmingliana, Lalhriatpuia, C., Tiwari, D., Lee, S., (2016). Efficient removal of 17 $\beta$ -estradiol using hybrid clay materials: Batch and column studies. *Environ. Eng. Res.*, **21**: 203–210.
- Thanhmingliana, T., Lee, S.-M., Tiwari, D., Prasad, S., (2015a). Efficient attenuation of 17 $\alpha$ -ethynylestradiol (EE2) and tetracycline using novel hybrid materials: Batch and column reactor studies. *RSC Adv.*, **5**:46834-46842.
- Thanhmingliana, Tiwari, D., (2015b). Efficient use of hybrid materials in the remediation of aquatic environment contaminated with micro-pollutant diclofenac sodium. *Chem. Eng. J.*, **263**:364–373.
- Tinkov, A. A., Gritsenko, V. A., Skalnaya, M. G., Cherkasov, S. V., Aaseth, J., Skalny, A. V. (2018). Gut as a target for cadmium toxicity. *Environ. Pollut.*, **235**:429–434.
- Tiwari, A., Shukla, A., Lalliansanga, Tiwari, D., Lee, S. M., (2019a). Synthesis and characterization of Ag<sup>0</sup> (NPs)/TiO<sub>2</sub> nanocomposite: Insight studies of triclosan removal from aqueous solutions. *Environ. Technol.*, **41(26)**: 3500–3514.
- Tiwari, A., Shukla, A., Lalliansanga, Tiwari, D., Lee, S.-M., (2019b). Au-nanoparticle/nanopillars TiO<sub>2</sub> meso-porous thin films in the degradation of tetracycline using UV-A light. *J. Ind. Eng. Chem.*, **69**:141–152.
- Tiwari, D., Jamsheera, A., Zirliannurga, Lee, S., (2017). Use of hybrid materials in the trace determination of As(V) from aqueous solutions: An electrochemical study. *Environ. Eng. Res.*, **22**:186–192.
- Tiwari, D., Lee, S.-M., (2012). Novel hybrid materials in the remediation of ground waters contaminated with As(III) and As(V). *Chem. Eng. J.*, **204–206**: 23–31.
- Tiwari, D., Zirliannurga, Lee, S., (2016). Fabrication of efficient and selective total arsenic sensor using the hybrid materials modified carbon paste electrodes. *J. Electroanal. Chem.*, **784**:109-114.

- Toor, S., Sharma, P., Bansod, B., (2015). Electrochemical Detection of Trace Amount of Arsenic (III) at Glassy Carbon Electrode Modified with Au/Fe<sub>3</sub>O<sub>4</sub> Nanocomposites. *Aquat. Procedia*, **4**: 1107–1113.
- Tsuji, T., Iryo, K., Watanabe, N., Tsuji, M., (2002). Preparation of silver nanoparticles by laser ablation in solution: Influence of laser wavelength on particle size. *Appl. Surface Sci.*, **202**(1):80–85.
- Turco, A., Corvaglia, S., Pompa, P.P., Malitesta, C., (2021). An innovative and simple all electrochemical approach to functionalize electrodes with a carbon nanotubes/polypyrrole molecularly imprinted nanocomposite and its application for sulfamethoxazole analysis. *J. Colloid and Interface Sci.*, **599**: 676–685.
- UN-Water, United Nations. Quality and Wastewater. *UN-Water*. Retrieved June 15, 2021, from <https://www.unwater.org/water-facts/quality-and-wastewater/>
- Vieno, N., Hallgren, P., Wallberg, P., (2017). Pharmaceuticals in the aquatic environment of the Baltic Sea region: A status report. *International Initiative on Water Quality*. <https://unesdoc.unesco.org/ark:/48223/pf0000247889>
- W.H.O(World Health Organisation),(1971). International standards for drinking-water. <https://apps.who.int/iris/handle/10665/39989>.
- Wagheu, J., Forano, C., Besse-Hoggan, P., Kenfack, I., Ngameni, E., Mousty, C., (2013). Electrochemical determination of mesotrione at organoclay modified glassy carbon electrodes. *Talanta*, **103**:337–343.
- Wang, Q., Xue, Q., Chen, T., Li, J., Liu, Y., Shan, X., Liu, F., Jia, J., (2021). Recent advances in electrochemical sensors for antibiotics and their applications. *Chinese Chem. Lett.*, **32**(2): 609–619.
- Wang, Y., Fan, D., Zhao, G., Feng, J., Wei, D., Zhang, N., Cao, W., Du, B., Wei, Q., (2018). Ultrasensitive photoelectrochemical immunosensor for the detection of amyloid  $\beta$ -protein based on SnO<sub>2</sub>/SnS<sub>2</sub>/Ag<sub>2</sub>S nanocomposites. *Biosens .Bioelectron.*, **120**: 1–7.



- Wang, Y., Ge, H., Wu, Y., Ye, G., Chen, H., Hu, X., (2014). Construction of an electrochemical sensor based on amino-functionalized metal-organic frameworks for differential pulse anodic stripping voltammetric determination of lead. *Talanta*, **129**:100–105.
- Wani, A. L., Ara, A., Usmani, J. A., (2015). Lead toxicity: A review. *Interdisciplinary Toxicol.*, **8(2)**: 55–64.
- Wegst-Uhrich, S. R., Navarro, D. A., Zimmerman, L., Aga, D. S., (2014). Assessing antibiotic sorption in soil: A literature review and new case studies on sulfonamides and macrolides. *Chem. Central J.*, **8(1)**: 5.
- (2018). Accelerated degradation of sulfamethazine in water by VUV/UV photo-Fenton process: Impact of sulfamethazine concentration on reaction mechanism. *J. Hazard. Mater.*, **344**: 1181–1187.
- Wen, S.-H., Zhong, X.-L., Wu, Y.-D., Liang, R.-P., Zhang, L., Qiu, J.-D., (2019). Colorimetric assay conversion to highly sensitive electrochemical assay for bimodal detection of arsenate based on cobalt oxyhydroxide nanozyme via arsenate absorption. *Anal. Chem.*, **91**:6487-6497.
- World Water Assessment Programme, UNESCO (2017). Wastewater, The Untapped Resource. United Nations Educational, Scientific and Cultural Organization (UNESCO).
- Wu, L., Fu, X., Liu, H., Li, J., Song, Y., (2014). Comparative study of graphene nanosheet- and multiwall carbon nanotube-based electrochemical sensor for the sensitive detection of cadmium. *Anal. Chim. Acta*, **851**:43–48.
- Wu, S., Li, K., Dai, X., Zhang, Z., Ding, F., Li, S., (2020). An ultrasensitive electrochemical platform based on imprinted chitosan/gold nanoparticles/graphene nanocomposite for sensing cadmium (II) ions. *Microchem. J.*, **155**, 104710.
- Xiao, L., Wildgoose, G., Compton, R., (2008). Sensitive electrochemical detection of arsenic (III) using gold nanoparticle modified carbon nanotubes via anodic stripping voltammetry. *Anal. Chim. Acta*, **620**: 44–49.

- Xu, W., Zhang, G., Zou, S., Li, X., Liu, Y., (2007). Determination of selected antibiotics in the Victoria Harbour and the Pearl River, South China using high-performance liquid chromatography-electrospray ionization tandem mass spectrometry. *Environ. Pollut.*, **145**(3): 672–679.
- Xu, X., Niu, X., Li, X., Li, Z., Du, D., Lin, Y., (2020). Nanomaterial-based sensors and biosensors for enhanced inorganic arsenic detection: A functional perspective. *Sens. Actuators B: Chem.*, **315**: 128100.
- Xu, Z., Fan, X., Ma, Q., Tang, B., Lu, Z., Zhang, J., Mo, G., Ye, J., Ye, J., (2019). A sensitive electrochemical sensor for simultaneous voltammetric sensing of cadmium and lead based on Fe<sub>3</sub>O<sub>4</sub>/multiwalled carbon nanotube/laser scribed graphene composites functionalized with chitosan modified electrode. *Mater. Chem. Phys.*, **238**:121877.
- Yang, M., Wu, X., Hu, X., Wang, K., Zhang, C., Gyimah, E., Yakubu, S., Zhang, Z., (2019). Electrochemical immunosensor based on Ag<sup>+</sup>-dependent CTAB-AuNPs for ultrasensitive detection of sulfamethazine. *Biosens. Bioelectron.*, **144**: 111643.
- Yang, S., Liu, P., Wang, Y., Guo, Z., Tan, R., Qu, L., (2020). Electrochemical sensor using poly-(L-cysteine) functionalized CuO nanoneedles/N-doped reduced graphene oxide for detection of lead ions. *RSC Advances*, **10**(31): 18526–18532.
- Yang, X., Xu, J., Tang, X., Liu, H., Tian, D., (2010). A novel electrochemical DNAzyme sensor for the amplified detection of Pb<sup>2+</sup> ions. *Chem. Commun.*, **46**(18):3107–3109.
- Yari, A., Shams, A., (2018). Silver-filled MWCNT nanocomposite as a sensing element for voltammetric determination of sulfamethoxazole. *Anal. Chim. Acta*, **1039**: 51–58.
- Yola, M. L., Eren, T., Atar, N., (2015). A sensitive molecular imprinted electrochemical sensor based on gold nanoparticles decorated graphene oxide:

- Application to selective determination of tyrosine in milk. *Sens. Actuators B: Chem.*, **210**: 149–157.
- Yue, X., Li, Z., Zhao, S., (2020). A new electrochemical sensor for simultaneous detection of sulfamethoxazole and trimethoprim antibiotics based on graphene and ZnO nanorods modified glassy carbon electrode. *Microchem. J.*, **159**:105440.
- Zahed, F.M., Hatamluyi, B., Lorestani, F., Es'haghi, Z., (2018). Silver nanoparticles decorated polyaniline nanocomposite based electrochemical sensor for the determination of anticancer drug 5-fluorouracil. *J Pharm Biomed Anal.* **161**:12-19.
- Zaib, M., Athar, M. M., Saeed, A., & Farooq, U. (2015). Electrochemical determination of inorganic mercury and arsenic—A review. *Biosens. Bioelectron.*, **74**:895–908.
- Zazouli, M. A., Shokrzadeh, M., Izanloo, H., Fathi, S., (2008). Cadmium content in rice and its daily intake in Ghaemshahr region of Iran. *African J. Biotechnol.*, **7(20)**: 20.
- Zen, J.-M., Kumar, A. S., (2004). The prospects of clay mineral electrodes. *Anal. Chem.*, **76(11)**: 205A-211A.
- Zhang, L., Li, W., Shi, M., Kong, J., (2006). Probing trace Pb<sup>2+</sup> using electrodeposited N,N'-(o-phenylene)-bis-benzenesulfonamide polymer as a novel selective ion capturing film. *Talanta*, **70**: 432–436.
- Zhang, Y., Li, C., Su, Y., Mu, W., Han, X., (2020). Simultaneous detection of trace Cd(II) and Pb(II) by differential pulse anodic stripping voltammetry using a bismuth oxycarbide/nafion electrode. *Inorg. Chem. Commun.*, **111**:107672.
- Zhou, S., Han, X., Fan, H., Liu, Y., (2016). Electrochemical Sensing toward Trace As(III) Based on Mesoporous MnFe<sub>2</sub>O<sub>4</sub>/Au Hybrid Nanospheres Modified Glass Carbon Electrode. *Sensors*, **16**: 935.

- Zhu, W., Sun, F., Goei, R., (2017). Facile fabrication of RGO-WO<sub>3</sub> composites for effective visible light photocatalytic degradation of sulfamethoxazole. *Appl. Catal. B: Environ.*, **207**:93-102.
- Zhu, Z.L., Zhang, S.C., Lv, Y., Zhang, X.R., (2006). Atomization of hydride with a low-temperature, atmospheric pressure dielectric barrier discharge and its application to arsenic speciation with atomic absorption spectrometry. *Anal. Chem.* **78**: 865–872.

## BIO-DATA

- 1. NAME** : J. Lalmalsawmi
- 2. DATE OF BIRTH** : 24<sup>th</sup> September, 1990.
- 3. FATHER'S NAME** : J. Zothansanga
- 4. PERMANENT ADDRESS** : D-3/1, Hlimen, Aizawl, 796005.
- 5. EDUCATIONAL QUALIFICATIONS :**

Qualification	Year of Passing	Board/University	Subjects	% of Marks	Division
HSLC	2007	Mizoram Board of School Education	English, Mizo, Mathematics, Science, Social sciences	82.2	Distinction
HSSLC	2009	Mizoram Board of School Education	English, Biology, Physics, Chemistry, Mathematics	60	First
B.Sc (Chemisty)	2012	Mizoram University	Chemistry, Botany, Zoology	67.87	First
M.Sc (Chemistry)	2014	Mizoram University	Inorganic Chemistry (specialization), Physical Chemistry, Organic Chemistry, Analytical Chemistry	83.3	Distinction

## **PARTICULARS OF THE CANDIDATE**

**NAME OF THE CANDIDATE** : J. Lalmalsawmi  
**DEGREE** : Doctor of Philosophy (Ph.D)  
**DEPARTMENT** : Department of Chemistry  
**TITLE OF THESIS** : Nano-Particles Modified Glassy Carbon  
Electrodes in the Trace Detection of  
Arsenic and Some Micropollutants.  
**DATE OF ADMISSION** : 15<sup>th</sup> August, 2015

### **APPROVAL OF RESEARCH PROPOSAL:**

**1. BOS** : 13<sup>th</sup> April, 2016  
**2. SCHOOL BOARD** : 21<sup>st</sup> April, 2016  
**3. MZU REGN. NO.** : 3992 of 2009-10  
**4. Ph.D REGISTRATION NO.**  
**& DATE** : MZU/Ph.D/846 of 21.04.2016  
**5. EXTENSION** : Extension period 21.04.2021 to  
21.04.2022  
(No.16-2/MZU(Acad)20/391-393)

Head

Department of Chemistry

## List of Publications

### A. Journals

1. **Jongte Lalmalsawmi**, Zirlianngura, Diwakar Tiwari, Seung Mok Lee (2020). Low cost, highly sensitive and selective electrochemical detection of arsenic (III) using silane grafted based nanocomposite. *Environmental Engineering Research*, 25(4), 579–587.
2. **Jongte Lalmalsawmi**, Diwakar Tiwari, Dong Jin Kim (2020). Role of nanocomposite materials in the development of electrochemical sensors for arsenic: Past, present and future. *Journal of Electroanalytical Chemistry*, 877, 114630.
3. Diwakar Tiwari and **Jongte Lalmalsawmi**. Book Chapter: Arsenic Detection in an Aquatic Environment: Advancements in Electrochemical Sensors. Handbook of Smart Materials, Technologies, and Devices: Applications of Industry 4.0 (*Springer*).
4. **Jongte Lalmalsawmi**, Zirlianngura, Diwakar Tiwari, Seung-Mok Lee, Dong-Jin Kim (2021). Indigenously synthesized nanocomposite materials: Use of nanocomposite as novel sensing platform for trace detection of  $\text{Pb}^{2+}$ . *Journal of Electroanalytical Chemistry* **897**, 115578.
5. **Jongte Lalmalsawmi** and Diwakar Tiwari (2021). Facile Synthesized Novel Nanocomposites Modified Electrodes in the Trace Detection of Sulfamethoxazole. *Journal of Electrochemical Society* **168**, 126504
6. **Jongte Lalmalsawmi** and Diwakar Tiwari (2021). Simultaneous detection of  $\text{Cd}^{2+}$  and  $\text{Pb}^{2+}$  by anodic stripping differential pulse voltammetry: Use of highly efficient novel nanocomposite materials. *Journal of Environmental Chemical Engineering* (**Communicated**).
7. **Jongte Lalmalsawmi**, Diwakar Tiwari, Seung-Mok Lee and Dong-Jin Kim (2021). Efficient electrochemical sensor for trace detection of sulfamethazine spiked spring water: Use of novel nanocomposite material decorated with Ag/or Au nanoparticles. *Microchemical Journal* (**Communicated**).

## **B. Conference/Seminar**

1. Presented “Ultra-Trace Detection of Arsenic (III) Using Nano-composite Modified Carbon Paste Electrode” at International Conference on Chemistry & Environmental Sustainability (ICCES-2019) on 19<sup>th</sup> to 22<sup>nd</sup> February, 2019 which was organized by Department of Chemistry, Mizoram university Aizawl, Mizoram, India.
2. Presented “Electrochemical Detection of Emerging Water Contaminants: Voltammetric Determination of Sulfamethoxazole on Nano-composite Modified Glassy Carbon Electrode” at NCFMA- 2019) held on 22<sup>nd</sup> to 23<sup>rd</sup> November 2019, organized by Department of BS&HSS (Physics), National Institute of Technology, Aizawl, Mizoram, India.
3. Presented “Electrochemical Sensor for Low Level Determination of Lead Using Nanocomposite Modified Glassy Carbon Electrode: A Greener Method” at 2<sup>nd</sup> Annual Convention of North East (India) Academy of Science and Technology (NEAST) & International Seminar on Recent Advances in Science and Technology (ISRAST), 16<sup>th</sup> -18<sup>th</sup> November 2020, Organized by NEAST, Mizoram University, Aizawl, Mizoram, India.





# Low cost, highly sensitive and selective electrochemical detection of arsenic (III) using silane grafted based nanocomposite

Jongte Lalmalsawmi<sup>1</sup>, Zirliannigura<sup>1</sup>, Diwakar Tiwari<sup>1†</sup>, Seung-Mok Lee<sup>2†</sup>

<sup>1</sup>Department of Chemistry, School of Physical Science, Mizoram University, Aizawl-796004, India

<sup>2</sup>Department of Environmental Engineering, Catholic Kwandong University, Gangneung 25601, Republic of Korea

## ABSTRACT

Novel silane grafted bentonite was obtained using the natural bentonite as precursor material. The material which is termed as nanocomposite was characterized by the Fourier Transform Infra-red (FT-IR) and X-ray diffraction (XRD) methods. The surface imaging and elemental mapping was performed using Scanning Electron Microscopic (SEM/EDX) technique. The electroanalytical studies were performed using the nanocomposite electrode. The electroactive surface area of nanocomposite electrode was significantly increased than the pristine bentonite or bare carbon paste based working electrode. The impedance spectroscopic studies were conducted to simulate the equivalent circuit and Nyquist plots were drawn for the carbon paste electrode and nanocomposite electrodes. A single step oxidation/reduction process occurred for As(III) having  $\Delta E$  value 0.36 V at pH 2.0. The anodic stripping voltammetry was performed for concentration dependence studies of As(III) (0.5 to 20.0  $\mu\text{g/L}$ ) and reasonably a good linear relationship was obtained. The detection limit of the As(III) detection was calculated as  $0.00360 \pm 0.00002 \mu\text{g/L}$  having with observed relative standard deviations (RSD) less than 4%. The presence of several cations and anions has not affected the detection of As(III) however, the presence of Cu(II) and Mn(II) affected the detection of As(III). The selectivity of As(III) was achieved using the Tlawng river water sample spiked with As(III).

**Keywords:** As(III), Detection limit, Electrochemical sensor, Interfering ions, Nanocomposite, Tlawng river water

## 1. Introduction

The technological advancement greatly supported the healthcare sector. The devices developed for the efficient and selective detection of several medically important species is profoundly witnessed in improved quality of human life globally [1-3]. In a line the miniaturization of low-cost and robust detection devices are in greater demand for various healthcare units [4-5]. Further, variety of contaminants that enters into the biosystem through the aquatic environment is a serious concern for the developed or the developing nations. A suitable detection system could help in proper remediation of these contaminants from aquatic environment.

Arsenic is ubiquitous, naturally occurring, heavy metal and it is widely distributed in soil, sediment, water, aerosol, rain, aquatics and vegetations [6]. Arsenic is highly toxic and found carcinogenic and showed serious endanger to the human being exposed to it. Arsenic enters into the human body by two different possible pathways viz., by drinking arsenic contaminated water or by the consumption of plants that are cultivated in the arsenic contaminated

soils [7]. It was reported previously that arsenic was detected in ground water in many countries around the globe and more than 200 million people are directly or indirectly exposed to it [8]. The hyperkeratosis on the palm or feet, bladder cancer and mutagenic effects is often occurs with arsenic consumption in humans [9-10]. Therefore, because of its acute toxicity, the U.S. Environmental Protection Agency (EPA) and World Health Organization (WHO) has recommended the maximum contaminant level (MCL) of arsenic is 10 ppb (130 nM) in drinking water [11-12]. Therefore, this compels to introduce newer analytical techniques having adequate reliability, extremely low detection limit and importantly robust in on-site detection of arsenic. This eventually, helps in safeguarding the human population living around this contaminated area and bound to consume the arsenic contaminated ground/fresh water. Several analytical methods were proposed in literature for the detection of low level of arsenic [12]. The surface plasmon resonance materials are found useful in the low level colorimetric detection of arsenic [13-15]. In this regard, the electrochemical methods are found prominent in the arsenic detection because of its reliability,



This is an Open Access article distributed under the terms of the Creative Commons Attribution-NonCommercial License (<http://creativecommons.org/licenses/by-nc/3.0/>) which permits unrestricted non-commercial use, distribution, and reproduction in any medium, provided the original work is properly cited.

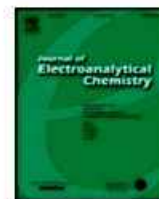
Copyright © 2020 Korean Society of Environmental Engineers

Received June 12, 2019 Accepted August 12, 2019

<sup>†</sup> Corresponding author

Email: diw\_tiwari@yahoo.com, leesm@cku.ac.kr

Tel: +91-9862323015, +82-33-649-7535



## Review

# Role of nanocomposite materials in the development of electrochemical sensors for arsenic: Past, present and future



Jongte Lalmalsawmi<sup>a</sup>, Diwakar Tiwari<sup>a,\*</sup>, Dong Jin Kim<sup>b</sup>

<sup>a</sup> Department of Chemistry, School of Physical Sciences, Mizoram University, Aizawl 796004, India

<sup>b</sup> Department of Environmental Science & Biotechnology, Hallym University, Chuncheon 24252, Republic of Korea

## ARTICLE INFO

## Article history:

Received 28 May 2020

Received in revised form 27 August 2020

Accepted 27 August 2020

Available online 02 September 2020

## Keywords:

Arsenic

Electrochemical sensor

Aptasensor

Advanced materials

Ultra-trace

Glassy carbon electrodes

## ABSTRACT

The specific aim of this review is to discuss the recent advances in the area of electrochemical sensor development for the ultra-trace detection of inorganic arsenic both in +3 or +5 oxidation states or the total arsenic. The role of advanced materials including the hybrid materials, nanocomposites or bio-nanocomposites have innumerable applications and are hence, found to be emerging next generation alternatives for its implications in the sensor development. Therefore, the review critically emphasizes upon the applications of advanced materials in sensor development with specific aim of its mechanism or insight of field implications. The use of these materials perhaps entails, several challenges while bringing technology from the laboratory to the field. Hence, the review possibly adds to the existing understanding of the sensors in terms of arsenic detection.

## Contents

1. Introduction . . . . .	1
2. Electrochemical detection methods . . . . .	2
3. Use of Nano-materials, nanocomposites in arsenic detection . . . . .	3
3.1. Nano-materials . . . . .	3
3.1.1. Metal nanoparticles . . . . .	3
3.1.2. Metal oxide nanoparticles . . . . .	5
3.1.3. Au-based bimetallic nanoparticles . . . . .	7
3.1.4. Carbon-based nanostructures . . . . .	8
3.1.5. Other polymeric materials . . . . .	10
3.2. Biomaterials . . . . .	10
3.2.1. Aptamer, DNA and protein based biomaterials . . . . .	10
3.2.2. Biopolymer-based biomaterials . . . . .	13
3.3. Metal ions . . . . .	14
3.4. Detection of As(V) . . . . .	14
4. Conclusion and future perspective . . . . .	16
Acknowledgement . . . . .	16
References . . . . .	16


\* Corresponding author.

E-mail address: [diw.tiwari@yahoo.com](mailto:diw.tiwari@yahoo.com). (D. Tiwari).





# Handbook of Smart Materials, Technologies, and Devices: Applications of Industry 4.0

About My Tasks My Chapters Table of Contents



Show Filter

Title	Due Date	Status
<p>Advanced Materials in the Detection of Arsenic from Aquatic Environment: Advancements in Electrochemical Sensors</p> <p>by Tiwari, D.   'Industry 4.0: Concept of Smart, Intelligent &amp; Sustainable Society'</p>		<div>In Production</div>

1 - 1 of 1

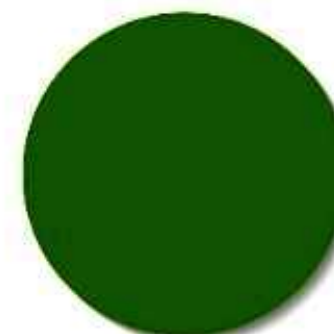
<

Page 1

of 1

>

## Project overview



In Production  
1 chapters, 100%



# Indigenously synthesized nanocomposite materials: Use of nanocomposite as novel sensing platform for trace detection of $\text{Pb}^{2+}$

Jongte Lalmalsawmi<sup>a</sup>, Zirliannigura<sup>a</sup>, Diwakar Tiwari<sup>a,\*</sup>, Seung-Mok Lee<sup>b</sup>, Dong-Jin Kim<sup>c</sup>

<sup>a</sup> Department of Chemistry, School of Physical Sciences, Mizoram University, Aizawl 796004, India

<sup>b</sup> Department of Health & Environmental, Catholic Kwandong University, 24, Beomil-ro 579 beon-gil, Gangneung 210-701, Republic of Korea

<sup>c</sup> Department of Environmental Sciences and Biotechnology & Institute of Energy and Environment, Hallym University, 1 Okcheon, Chuncheon, Gangwon 24252, Republic of Korea

## ARTICLE INFO

### Keywords:

Biosynthesis of nanoparticles  
Differential pulse anodic stripping  
voltammetry  
Real matrix analysis  
trace detection of  $\text{Pb}^{2+}$   
Efficient highly selectivity

## ABSTRACT

Indigenously low-cost, eco-friendly and efficient nanocomposite material Au(NP)/TCODS/BN (trichloro(octadecyl) silane grafted bentonite impregnated with biosynthesized gold nanoparticle) was synthesized. The nanocomposite material was characterized by the SEM/EDAX, TEM and FT-IR analyses. Further, the working electrode was fabricated using the Au(NP)/TCODS/BN material and intended for efficient sensing of  $\text{Pb}^{2+}$  in aqueous media. Electrochemical behaviour of indigenously fabricated electrodes was studied extensively using various electrochemical methods. Cyclic voltammetric results indicated that the nanocomposite fabricated electrode showed a significantly enhanced electroactive surface area. Similarly, the  $R_{ct}$  (charge transfer resistance) value is significantly decreased using the nanocomposite material. The differential pulse anodic stripping voltammetry (DPASV) is employed as a sensing method to detect the  $\text{Pb}^{2+}$  and a good calibration line was obtained within the  $\text{Pb}^{2+}$  concentration range (1.00–60.0  $\mu\text{g/L}$ ) having the calibration line equation  $I(\mu\text{A}) = 0.031(\mu\text{g/L}) + 0.611(\mu\text{A})$  ( $R^2 = 0.984$ ) at optimized experimental condition. Moreover, the reproducibility tests reveal that the RSD values are obtained below 3%. The estimated LOD and LOQ are 0.81  $\mu\text{g/L}$  and 2.70  $\mu\text{g/L}$ , respectively. The detection of lead is almost unaffected in presence of several co-existing cations and interestingly the real matrix analysis showed that reasonably a good recovery is achieved using  $\text{Pb}^{2+}$  spiked river or spring water samples utilizing the nanocomposite electrode.

## 1. Introduction

Lead is a ubiquitous element on the earth's crust and highly toxic. Additionally, the industrial input has further enhanced its contamination in different fragments of the environment including the water bodies. It has serious health impacts for both humans and animals [1,2]. It accumulates readily in bones and the kidney which severely affect the nervous system and renal mechanism [3,4]. Because of its acute toxicity, the World Health Organisation (WHO) and United States Environmental Protection Agency (US EPA) mandated a maximum acceptable concentration in drinking water as low as 10 ppb and 15 ppb, respectively [5]. This enforced the regulatory bodies to monitor efficient lead concentrations in contaminated water. Further, the commonly employed techniques such as ICP-OES/MS (Inductively Coupled Plasma-Optical Emission Spectrometry/Mass Spectrometry), AAS (Atomic Absorption Spectrometry), HPLC (High Performance Liquid Chromatography) etc., are found to be highly efficient in the low level detection of lead. However, these techniques suffer major draw-

backs such as high instrumentation cost, expertise operation and most importantly only *off-site* operation is possible. Therefore, the newer, efficient and selective detection techniques are quite inevitable which could allow us to detect the pollutants *on-site* as well.

Electrochemical techniques are formidable for trace measurement of several toxic ions. These methods are primarily simple in operation, provide fair reliability and low detection limit with high selectivity [6]. The introduction of newer materials opens the way for efficient electrode fabrication which significantly enhances the sensitivity and selectivity of detection [7]. In a line, the nanostructured or advanced materials exhibit catalytic action in the efficient detection of analytes [8–11]. Trace detection of lead (II) and arsenic (III) was efficiently performed using carbon paste electrodes catalysed by advanced materials precursor to bentonite and HDTMA (hexadecyltrimethylammonium bromide) [12,13]. Similarly, the silane grafted bentonite was introduced in the carbon paste electrode for sensing the arsenic (III). The results showed that an extremely low LOD (0.0036  $\mu\text{g/L}$ ) for arsenic (III) was achieved using the silane grafted bentonite [14].

\* Corresponding author.

E-mail address: [diw\\_tiwari@yahoo.com](mailto:diw_tiwari@yahoo.com) (D. Tiwari).





## Facile Synthesized Novel Nanocomposites Modified Electrodes in the Trace Detection of Sulfamethoxazole

Jongte Lalmalsawmi and Diwakar Tiwari<sup>2</sup>

Department of Chemistry, School of Physical Sciences Mizoram University, Aizawl-796004, India

Micro-pollutants, especially antibiotics contamination in water bodies, are a serious concern, and their detection at a low level is important for human health and even aquatic life at large. The present investigation aims to obtain the novel nanocomposite material precursor to clay and silane. The nanocomposite material is decorated with Ag or Au nanoparticles as obtained indigenously by a green route using natural phytochemicals. The materials were extensively characterized by advanced analytical methods. The nanocomposite materials (Ag(NP)/TCBN and Au(NP)/TCBN) are employed in the selective and efficient trace measurement of sulfamethoxazole (SMZ) in aqueous solutions using the differential pulse anodic stripping voltammetry. The cyclic voltammetric and electrochemical impedance spectroscopic methods showed an increased electroactive surface area as well as faster electron transfer reactions compared to the glassy carbon electrode (GCE). The DPASV measurements at the concentration range of 0.25 mg l<sup>-1</sup> to 30.0 mg/l showed that the novel nanocomposites provide the LOD of 0.022 and 0.036 mg l<sup>-1</sup>, respectively, for the Ag(NP)/TCBN/GCE and Au(NP)/TCBN/GCE for sulfamethoxazole. Further, the application of the method for the detection of sulfamethoxazole in real water samples resulted in an acceptable recovery percentage of 93.08 to 103.7. © 2021 The Electrochemical Society ("ECS"). Published on behalf of ECS by IOP Publishing Limited. [DOI: 10.1149/1945-7111/ac3ab5]

Manuscript submitted September 8, 2021; revised manuscript received October 12, 2021. Published December 2, 2021.

Supplementary material for this article is available [online](#)

The contamination of water bodies due to rising human activities has led to a crisis of safe drinking water supplies across countries.<sup>1</sup> Pharmaceuticals such as antibiotics, antimicrobials, etc. are often used medications for treating infectious diseases in humans, as well as in livestock or even as growth promoters in agricultural sectors.<sup>2</sup> According to a recent report, the annual usage of non-prescribed drugs in the UK and Poland alone are 152 and 83 tons, respectively.<sup>3</sup> A substantial portion, reaching 95% of the administered veterinary and human antibiotics is not metabolized fully and hence expelled in the original or active forms.<sup>4</sup> The discharged residues from the wastewater effluents from hospitals, agricultural sites, and veterinary farms make their way into the surface waters, causing dilution and deterioration of the water qualities.<sup>5</sup> Moreover, most of the pharmaceuticals including antibiotic compounds have high persistence and are not entirely removed in the wastewater treatment plants, hence enter into the environment polluting the surface and groundwater, sewage sludge, and soil.<sup>6-8</sup> This persistent nature imposed high risks of bioaccumulation and even contributed to microbial antibiotic resistance. Sulfamethoxazole (SMX) is one such contaminant that has been detected in groundwater, surface water, wastewater sludge, and streams.<sup>2,9,10</sup> Sulphonamide drugs are used as antibiotics/antimicrobials to treat various infections in the urinary tract and respiratory systems.<sup>11</sup> It tops the US Geological Survey list of 30 most frequently perceived pharmaceuticals in wastewater.<sup>12</sup> Sulfamethoxazole detected in various water bodies is well documented and according to United Nations Educational, Scientific and Cultural Organisation (UNESCO) and Helsinki Commission (HELCOM) reports, concentrations reaching 10 mg l<sup>-1</sup> were detected in the samples collected from river water in Germany.<sup>13</sup> Because of its persistency, the toxic consequences caused by sulfamethoxazole are more chronic than being fatal. It is reported that antibiotic resistance among microbial populations is stimulated within the time frame of sulfamethoxazole degradation in the natural environment.<sup>14,15</sup> Furthermore, the excessive application of antibiotics in agriculture can disturb the mediation of nitrogen among microbes in soil and some antibiotics including sulphonamides can inhibit the denitrification process in wastewater treatment plants.<sup>16</sup> Hence the emergence of pharmaceuticals and other synthetic residues in the natural environment urges the development of accurate, sensitive, and fast analytical procedures. Mostly, chromatographic techniques like LC-MS, HPLC-MS, GC-MS, LC-MS/MS,

etc., and other methods including electrophoresis, chemiluminescence, fluorometric and photometric methods are employed for analysis of sulphonamides.<sup>17-20</sup> However, these conventional methods are limited by expensive instrumentation, high maintenance cost, time consumption, and exhaustive sample pre-treatment steps. Compared to these methods, the electrochemical technique based on the employment of various electrode sensors has received greater attention due to low cost, user-friendly, simplicity in operations, and more rapid response, and more importantly on-site detection is performed with high precision.<sup>21-24</sup> Therefore, electrochemical methods are promising alternatives to the traditional methods towards more facile and on-site measurements of environmental pollutants.<sup>25</sup>

The sensitivity as well as selectivity of detection through electrochemical methods is primarily dependent on the electrode material hence, numerous advances took place introducing newer and advanced materials, during a couple of decades, to intensify the detection signal as well as to improve the selectivity towards the target analyte.<sup>26-29</sup> The recent reports on the electrochemical detection of sulfamethoxazole used advanced materials such as modified carbon nanotubes, metal nanoparticles, polymers (eg. Poly-1,5-Diaminonaphthalene, polypyrrole, etc.), graphene, etc. in the fabrication of chemically modified electrodes to improve sensing of sulfamethoxazole.<sup>30-32</sup> Nanoparticles are reported to possess excellent electrocatalytic properties since they offer a large surface area having enhanced active sites at the electrode surface.<sup>33,34</sup> ZnO and CeO<sub>2</sub> nanoparticles are utilized for the development of nanostructured materials for the effective detection of sulfamethoxazole. The developed sensors, Fe doped ZnO carbon paste electrode, and CeO<sub>2</sub>/Chitosan nanocomposite glassy carbon electrodes are efficiently applied for sensing the sulfamethoxazole having a detection limit of 30x10<sup>-9</sup> M and 1.28x10<sup>-9</sup> M.<sup>35,36</sup> Similarly, several works documented the decoration of noble metal nanoparticles with other substrates for the synthesis of nanocomposites suitable for electrochemical sensing applications. Silver and gold nanoparticles are often exploited for sensing applications of various pollutant species including several heavy metal ions (As, Pb, Cd, Zn, etc.) and some pharmaceutical compounds.<sup>37</sup> But reports on their application in antibiotics, particularly sulfamethoxazole detection is scanty. Therefore, the challenges lie in developing a sensing platform for sulfamethoxazole utilizing novel and advanced materials. Furthermore, the desire to synthesize materials with lower input cost and toxicity has prompted the development of numerous greener synthesis of materials and implications in device developments.

<sup>2</sup>E-mail: diw\_tiwari@yahoo.com

**ABSTRACT**

**NANO-PARTICLES MODIFIED GLASSY CARBON  
ELECTRODES IN THE TRACE DETECTION OF ARSENIC AND  
SOME MICROPOLLUTANTS**

**A THESIS SUBMITTED IN PARTIAL FULFILLMENT OF THE  
REQUIREMENTS FOR THE DEGREE OF DOCTOR OF  
PHILOSOPHY**

**J. LALMALSAWMI**

**MZU REGISTRATION NUMBER : 3992 OF 2009-10**

**PH.D REGISTRATION NUMBER : MZU/PH.D/846 OF 21.04.2016**



**DEPARTMENT OF CHEMISTRY  
SCHOOL OF PHYSICAL SCIENCES  
SEPTEMBER, 2021**

**ABSTRACT**  
**NANO-PARTICLES MODIFIED GLASSY CARBON ELECTRODES IN THE**  
**TRACE DETECTION OF ARSENIC AND SOME**  
**MICROPOLLUTANTS**

**BY**  
**J. LALMALSAWMI**  
**Department of Chemistry**

**Under the supervision of**  
**Prof. Diwakar Tiwari**

**Submitted**  
**In partial fulfillment of the requirement of the Degree of Doctor of Philosophy**  
**in Chemistry of Mizoram University, Aizawl.**

## ABSTRACT

The contamination of water bodies due to rising human activities has led to a crisis of safe drinking water supplies across countries. Many manufacturing industries are responsible for contamination of various heavy metal toxic ions in water bodies. Although many heavy metals are reported to be essential at trace concentrations, however, an elevated amount of intake resulted a negative effect on living organisms. The non-essential heavy metal ions such as As, Pb, Cd, Hg, etc. are highly toxic, and non-biodegradable causing major hazards to the environment. These toxic ions are readily accumulated in the tissues of the body and cause serious health problems affecting the nervous system, skin, liver, kidneys, bones, etc. Because of their acute toxicity, World Health Organization (WHO) have mandated the maximum acceptable concentration of As, Pb and Cd in drinking water as 10 µg/L, 10 µg/L and 5 µg/L, respectively. Wastes from metal plating, mining operations, tanneries, and other industrial effluents are particularly responsible for heavy metal pollution to water bodies. The agricultural sector is also a big contributor to water pollution. An excessive use of fertilizers in farmlands can also lead to the accumulation of various toxic chemicals, which eventually contaminating the soil and aquatic environment. Moreover, in recent years, there is a tremendous increase in the use of synthetic chemicals such as hormones, pharmaceuticals, and personal care products, which are known to be emerging water pollutants since these chemicals are very persistent and the municipal waste contains high levels of these pollutants. This persistent nature imposed high risks of bioaccumulation and even contributed to microbial antibiotic resistance. Sulfamethoxazole (SMX) and sulfamethazine (SMZ) are examples of such contaminant that has been detected in groundwater, surface water, wastewater sludge, and streams. Many of the pharmaceuticals are used in animal husbandry, and the overexploitation of these chemicals, particularly the antibiotics lead to serious environmental impacts.

In most cities, wastewater is collected and treated, however, the treatment efficiency varies depending on the system used. It is known that most of the potential water pollutants are quite persistent and tend to escape from the conventional treatment



plants and enter into the natural aquatic systems which may further enter back to the food chain. Therefore, new challenges arise for proper waste treatments and proper monitoring of the water qualities. The regulatory bodies are enforced to monitor efficiently the pollutant concentrations in contaminated water. Although the advanced detection techniques *viz.*, inductively coupled plasma mass spectrometry or optical emission spectrometry (ICP-OES/MS), atomic absorption spectrometry (AAS), high performance liquid chromatography (HPLC), etc. are highly efficient, major drawbacks of these techniques include high instrumentation cost, expertise operation and most importantly *off-site* operation only be conducted. Therefore, the newer efficient and elective detection techniques are quite inevitable which could allow us to detect the pollutants *on-site*. Compared to the conventional methods, the electrochemical technique based on the employment of various electrode sensors has received greater attention due to low cost, user-friendly, simplicity in operations, and more rapid response, and more importantly on-site detection is performed with high precision.

The introduction of newer materials opens the way for efficient electrodes fabrication which enhances significantly the sensitivity and selectivity of detection. The sensitivity as well as selectivity of detection through electrochemical methods primarily dependent on the electrode material hence, numerous advances took place introducing newer and advanced materials, during a couple of decades, to intensify the detection signal as well as to improve the selectivity towards target analyte. In a line, the nanostructured or advanced materials exhibit catalytic action in the efficient detection of analytes. These are mainly composed of two or more types of materials so as to produce more stable and sensitive nanostructured surface that can offer synergistic effect for enhanced electrochemical detection. Hence, this area of research has received much attention during the last couple of decades and introduced variety of novel materials ranging from metal nanoparticles, nanocomposites, polymers to biological composites obtained from DNA, enzymes, proteins, chitosan etc.

Further, the urge for the synthesis of materials with minimum cost and toxicity has instigated many green/clean pathways of reaction mechanisms and processes. The recent research efforts are directed towards biocompatible, non-toxic, simple and

greener methods for material synthesis. Therefore, utilizing the phytochemicals as reducing and stabilizing agents received greater attention. This involves the natured chemistry for material synthesis. The biosynthetic method of nanoparticle synthesis is one such example that utilizes green chemicals (phytochemicals) as a reducing and stabilizing agent. The phytochemicals in the leaf extract are potentially active to reduce the metal precursor ions to zerovalent metals while acting as stabilizing and capping agents to prevent the aggregation of the synthesized nanoparticles. Hence, they function as green chemical alternative to the toxic and reactive compounds used in the conventional synthesis method of nanoparticles. Further, in terms of cost-effectiveness and environmental safety, clays are often used in material preparation since they are easily available and non-toxic. The role of clay materials is unique due to its wide variety of intriguing features (physical and chemical stability, high ion exchange capacity in a micro-structured environment, hydrophilic character, etc.), possibly be useful electrochemical interface materials to be explored for efficient and selective detection of several trace analytes in aqueous wastes. Clays might thus be utilized in constructing electrochemically active nanostructured materials with greater sensitivity to the target pollutant species due to its ease of modification and accurate functionalization with desirable components.

Therefore, the potential applicability of the bentonite (BN) clay modified with silane and further decorated with nanoparticle for trace detection of heavy metals and some micro-pollutants from aqueous solutions is presented in this work. Leaf extract of *Persea americana* was utilized for synthesis of silver and gold nanoparticles (Ag(NP) and Au(NP)). The UV-Vis spectra for the colloidal solution of Ag(NP) and Au(NP) showed the surface plasmon resonance (SPR) peaks occurring at 414 nm and 550 nm, respectively. Various phytochemicals are present in the leaf extract which are potentially active to reduce the  $\text{Ag}^+/\text{Au}^{3+}$  to zerovalent  $\text{Ag}^0/\text{Au}^0$  as well as to stabilize aggregation of nanoparticles by capping. Hence, the leaf extract of *P. americana* was studied for different phytochemical tests which confirmed the presence of saponins, alkaloids, flavonoids, tannins, polyphenols, glycosides and polysaccharides. The biosynthesized nanoparticles were further used to decorate the silane grafted bentonite. The silane modified bentonite and nanoparticles modified nanocomposites were labelled as TCBN, Ag(NP)/TCBN and Au(NP)/TCBN,

respectively. The structure/morphology of the nanocomposite materials were characterized by Scanning Electron Microscopy/Energy Dispersive X-ray (SEM/EDX), Fourier Transform Infrared (FT-IR), Transmission Electron Microscopy (TEM), and X-ray Photoelectron Spectroscopy (XPS). The TCBN material was then used for fabricating carbon paste electrode (TCBN/CPE) and employed in As(III) detection. Ag(NP)/TCBN and Au(NP)/TCBN were utilized for surface modification of glassy carbon electrode (named as Ag(NP)/TCBN/GCE and Au(NP)/TCBN/GCE) and used for efficient detection of pollutants (lead, cadmium, SMX and SMZ). The fabricated electrodes were electrochemically characterized using cyclic voltammetry (CV) and electrochemical impedance spectrometry (EIS) techniques using the  $\text{Fe}(\text{CN})_6^{3-}/\text{Fe}(\text{CN})_6^{4-}$  (prepared in 0.1 mol/L KCl) redox probe. Further, the electrochemical detection of the selected pollutants – As(III), Pb(II), Cd(II), SMX and SMZ were performed using CV, linear sweep voltammetry (LSV) and differential pulse anodic stripping voltammetry (DPASV) techniques. Extensive parametric studies *viz.*, pH, depositional potential, and time, potentially interfering ions, as well as applicability in real water samples were studied for each pollutant.

From CV studies at different scan rate, a plot of oxidative peak current against the square root of scan rate was recorded for each electrode. The plots showed diffusion-controlled system behavior and the line obtained was utilized for calculating the electroactive surface area using the Randles-Sevcik equation. The estimated areas were  $0.244 \times 10^{-3} \text{ cm}^2$ ,  $0.503 \times 10^{-3} \text{ cm}^2$ ,  $1.19 \times 10^{-3} \text{ cm}^2$ ,  $0.269 \times 10^{-3} \text{ cm}^2$ ,  $0.404 \times 10^{-3} \text{ cm}^2$ ,  $0.418 \times 10^{-3} \text{ cm}^2$ ,  $0.539 \times 10^{-3} \text{ cm}^2$  and  $0.674 \times 10^{-3} \text{ cm}^2$  for CPE, BN/CPE, TCBN/CPE, GCE, TCBN/GCE, Ag(NP)/TCBN/GCE and Au(NP)/TCBN/GCE, respectively. Further, EIS studies showed that interfacial charge transfer resistance ( $R_{ct}$ ) was significantly decreased using the TCBN nanocomposite compared to the bare CPE i.e., 3.00 k $\Omega$  to 6.34 k $\Omega$ . Similarly, the bare GCE's high  $R_{ct}$  value (16.5 k $\Omega$ ) was dropped significantly to 6.21 k $\Omega$  and 5.28 k $\Omega$  for the BN and TCODS/BN modified GCEs, respectively. Further, the  $R_{ct}$  value obtained for Ag(NP)/TCBN/GCE and Au(NP)/TCBN/GCE showed further and remarkable decrease i.e., 3.20 k $\Omega$  and 3.13 k $\Omega$ , respectively.

Comparison of electrochemical response of As(III) was investigated using the carbon paste electrodes (CPE), BN/CPE and TCBN/CPE showed that increased

response was achieved with the TCBN/CPE. The concentration dependent studies of As(III) (0.5 to 20.0  $\mu\text{g/L}$ ) using the linear sweep voltammetry showed reasonably good linearity between the concentration of As(III) and anodic peak current values and detection of limit (LOD) for As(III) was determined to be 0.0036  $\mu\text{g/L}$ . Similarly, the electrochemical detection of Pb(II) conducted with Au(NP)/TCBN/GCE showed using DPASV at optimized preconcentration conditions (pH 4.5, deposition potential -1.2 V and deposition time of 180 s) show very low detection limit of 0.817  $\mu\text{g/L}$  throughout a large linear calibration range of 1.0-60.0  $\mu\text{g/L}$ . Moreover, the simultaneous detection of Pb(II) with Cd(II) was performed with Ag(NP)/TCBN/GCE within the concentration range of 5.0-60.0  $\mu\text{g/L}$  and LOD of 0.79  $\mu\text{g/L}$  for Cd(II) and 0.88  $\mu\text{g/L}$  for Pb(II) was achieved. In addition to the heavy metal toxic ions, the micro-pollutants, SMX and SMZ were detected using Ag(NP)/TCBN/GCE and Au(NP)/TCBN/GCE. For DPASV measurements, the optimized pH, deposition potential, and time was found to be 4.0, -1.2 V, and 210 s (for SMX) and 180 s (for SMZ), respectively. Detection limit for SMX was obtained as 0.022 mg/L and 0.036 mg/L for Ag(NP)/TCBN/GCE and Au(NP)/TCBN/GCE, respectively. Similarly, for SMZ, the LOD were found to be 0.027 mg/L and 0.035 mg/L using Ag(NP)/TCBN/GCE and Au(NP)/TCBN/GCE, respectively.

The detection of the pollutants was studied in presence of high concentrations of several co-existing ions, which may be potentially interfere with the detection of the target analyte at the fabricated electrodes. The presence of some cations and anions could not affect the detection of As(III). However, the presence of Cu(II) and Mn(II) impacted the detection of As(III). In presence of several metal cations viz., Cu(II), Fe(II), Ca(II), Mn(II), Hg(II), Zn(II) and Cd(II), the nanocomposite sensing platform could efficiently detect Pb(II). Similarly, these co-existing ions appear to have no effect on the detection of Pb(II) and Cd(II) simultaneously. The presence of Zn(II), however, revealed an extra and well-separated oxidative peak. However, the studies on effects of high concentrations of electroactive metal ions on SMX and SMZ determination, showed that the presence of Cu(II) and Zn(II) affected the detection of these micro-pollutants. These interferences are primarily due to the competition of analytes and interferent towards the surface-active sites on the electrode surface.

Moreover, proximity of the oxidation potential of the analytes and interferent within the operating potential window could also affect the detection.

Finally, to assess the practical applicability of fabricated electrodes for sensitive and efficient measurement of the pollutants, investigation of the electrochemical experiments was performed in real water samples. The water samples were collected from river, spring, and surface run-off waters in different localities of Aizawl City, Mizoram, India. Before electrochemical measurements, samples were filtered and physico-chemical parametric studies were like pH, conductivity, resistivity, salinity, oxidation-reduction potential, and total dissolved solids, NPOC (Non-purgeable Organic Carbon) and IC (inorganic carbon) were conducted for these water samples. The samples were also analyzed for various elements present as impurity using the AAS. The water samples were then spiked with known concentrations of the pollutant solutions. The selectivity of As(III) was successfully accomplished using a water sample from the Tlawng river spiked with As (III). Similarly, the actual matrix and spiked concentration analysis of Pb(II) using river and spring water using Au(NP)/TCBN/GCE revealed that Pb(II) recovery varied from 91.6 to 98.2%. The detection technique using Ag(NP)/TCBN/GCE in the simultaneous detection of Cd(II) and Pb(II) in spring water samples also show a cadmium detection recovery of 93 to 108% and a lead detection recovery of 99 to 113% . Surface run-off water spiked SMX studies revealed that SMX detection recovery was within 93.08 - 103.7%. Similarly, the SMZ detection was investigated in spring water spiked with 0.5 mg/L, 5.0 mg/L and 10.0 mg/L which gave an apparent recovery between 92.47 and 106.65%. These results further indicated that the detection of As(III), Pb(II), Cd(II), SMX and SMZ is not noticeably affected in the real water samples hence, this proved the practical applicability of the proposed method in the detection of these pollutants in real-world samples.